UNIVERSITÀ DEGLI STUDI DI NAPOLI FEDERICO II

FACOLTÀ DI FARMACIA

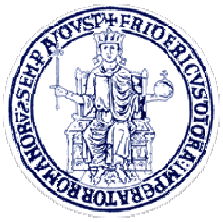

DOTTORATO DI RICERCA IN

"SCIENZA DEL FARMACO"

XXIII CICLO 2007/2010

Secondary metabolites from natural sources: chemical and pharmacological characterization.

Dott.ssa Carmen Festa

Tutor

Prof. F. Zollo

Coordinatore

Prof. ssa M.V. D'Auria

In everything I seek to grasp
The fundamental:
The daily choice, the daily task,
The sentimental.
To plumb the essence of the past,
The first foundations,
The crux, the roots, the inmost hearts,
The explanations.
And, puzzling out the weave of fate,
Events observer,
To live, feel, love and meditate
And to discover.

In ogni cosa ho voglia di arrivare
sino alla sostanza.
Nel lavoro, cercando la mia strada,
nel tumulto del cuore.
Sino all'essenza dei giorni passati,
sino alla loro ragione,
sino ai motivi, sino alle radici,
sino al midollo.
Eternamente aggrappandomi al filo
dei destini, degli avvenimenti,
sentire, amare, vivere, pensare
effettuare scoperte.

Boris L. Pasternak

INDEX

ABSTRACT

Natural products have long been a source of bioactive metabolites utilized for the treatment of human disease. In spite the impressive progress of new competing methodologies, as for example, combinatorial chemistry and high-throughput screening or genetic engineering, natural products remain a valuable source of bioactive compounds with therapeutic potential.

In recent years, the marine environment has been seen as a vast resource for the discovery of structurally unique bioactive secondary metabolites, some belonging to totally novel chemical classes. In particular the Porifera have developed an arsenal of new compounds.

Part of my research work is collocated within this area and concerns the investigation of the natural products deriving from marine sponges. In the frame of the project *C.R.I.S.P.* (Coral Reef Initiative of South Pacific), directed to the chemical investigation and valorisation of the marine invertebrates of South Pacific, particular attention was paid to two sponges: *Theonella swinhoei* and *Coscinoderma mathewsi*.

From these sponges, several structurally interesting bioactive molecules have been isolated with promising biological activities. Worthy of note are perthamides, a family of cyclic octapeptides, encompassing majority of non-proteogenic amino acids, and solomonamides which represent a new class of cyclic peptides, featuring a potent *in vivo* anti-inflammatory activity. Solomonsterols have been demonstrated the first examples of sulfated sterols with a truncated side chain from a marine source endowed with a PXR agonistic activity.

The structure elucidation of these new molecules was performed using the most modern sophisticated spectroscopic techniques (2D-NMR and MS).

The main interest in these compounds is related to their strong biological activity, that had led to pharmacological investigations on biomolecular target, the mechanism of action and the pharmacophore useful in the identification of new leads for developing a new generation of drugs. The detailed pharmacological investigation has in some cases required the access to adeguate amount of natural products or of semisynthetic derivatives through chemical synthesis, an issue addressed in a research parallel to the present work.

The stereochemical novelty and complexity of some amino acid units of cyclopeptides have required a tailored integrated approach which combined NMR methods, stereoselective synthesis and LC/MS

The second part of my research has been employed and addressed on the analysis of plants of Mediterranean area and used as foodstuff and as drugs in the folk medicine, to isolate the active principles with biological activity and nutraceutical property. In this respect, my research objectives have been to identify the chemical constituents from three plants *Cucumis melo*, *Borrago officialis* and *Ruscus aculeatus.*

It is clear that Nature continues to be a major source not only of potential chemotherapeutic agents but also of lead compounds that have provided the basis and inspiration for the semisynthesis or total synthesis of effective new drugs; natural product chemistry has enriched both organic chemistry and medicine in a myriad of different ways.

PRESENTAZIONE DEL LAVORO SVOLTO

La maggioranza degli agenti terapeutici attualmente in commercio deriva direttamente oppure indirettamente da molecole organiche naturali provenienti da organismi sia terrestri che marini. L'interesse della ricerca verso la chimica delle sostanze naturali è, quindi, collegato in particolare alla grande opportunità di scoprire molecole da usare come lead compound per lo sviluppo di nuove classi di farmaci. La diversità chimica che caratterizza le molecole naturali rende l'esplorazione delle loro caratteristiche biologiche, non solo una delle principali fonti di nuovi composti potenzialmente utilizzabili per la realizzazione di nuovi farmaci, ma anche un utile strumento per la scoperta di nuovi meccanismi d'azione.

E' per tale motivo che le piante hanno da sempre suscitato l'interesse per i chimici delle sostanze naturali. Negli ultimi decenni, invece, il progresso di alcune tecnologie ha reso possibile l'estensione della ricerca anche agli organismi marini e ciò ha portato all'isolamento di migliaia di nuove molecole con strutture del tutto inusuali mai trovate nel mondo terrestre e dotate di una vasta gamma di attività farmacologiche. In particolare, i Poriferi, più comunemente noti come spugne, rappresentano una fonte inesauribile di nuovi composti.

All'interno di questo ambito si colloca il mio dottorato che si è focalizzato su due linee di ricerca, finalizzate allo studio di metaboliti secondari farmacologicamente attivi isolati da poriferi e da piante dell'area mediterranea. Tutte le strutture sono state caratterizzate con l'ausilio di tecniche spettroscopiche, in particolare la spettroscopia di risonanza magnetica nucleare e la spettrometria di massa.

La prima linea di ricerca rientra nell'ambito del progetto C.R.I.S.P. (Coral Reef Initiative of South Pacific) ed ha riguardato lo studio di spugne provenienti dal Sud Pacifico. Tale lavoro ha condotto all'isolamento di numerosi metaboliti caratterizzati da insolite strutture e significative attività biologiche.

Lo scopo del progetto di ricerca non è tanto volto all'utilizzo terapeutico dei composti naturali in quanto tali, ma è per lo più indirizzato verso un loro impiego come composti modello (*lead compounds*) per la progettazione di nuovi farmaci. Tale ricerca prevede un approfondito studio sulla natura delle interazioni molecolari fra la sostanza bioattiva ed il *target* biologico, al fine di ottenere indicazioni sulla porzione della molecola responsabile dell'attività; ciò ha richiesto la messa a punto di strategie sintetiche o semisintetiche, condotte in un lavoro di ricerca parallelo a quello descritto in questa tesi.

Lo studio della spugna *Coscinoderma mathewsi* ha portato all'isolamento di due nuovi sesterterpeni con lo scheletro del cheilantano, il coscinolattame A e B, e di un composto già noto, la suvanina. Questi tre composti, assieme a due derivati semisintetici della suvanina, hanno mostrato una moderata attività antinfiammatoria, inibendo la produzione di PGE_2 e NO.

La seconda spugna studiata è stata la *Theonella swinhoei*, dalla quale sono stati isolati nuovi metaboliti secondari, appartenenti a diverse classi biogenetiche, confermando la ricchezza biologica di tale spugna.

L'estratto butanolico ha portato all'isolamento di una famiglia di ottapeptidi ciclici, denominati pertammidi C-K caratterizzati dalla presenza di diversi residui amminoacidici non proteogenici; tra tali peptidi la pertammide C è risultata essere il principale metabolita.

La caratterizzazione della struttura primaria di questi nuovi ciclopeptidi è avvenuta grazie all'utilizzo di tecniche spettroscopiche, quali la risonanza magnetica nucleare, nei suoi esperimenti mono e bidimensionali, e la spettrometria di massa. Un ulteriore sforzo è stato effettuato per la definizione della stereochimica dei residui amminoacidici presenti, che ha previsto l'uso combinato di tecniche NMR, sintesi stereoselettiva delle unità non ribosomiali, degradazione chimica e l'applicazione del metodo di Marfey combinato ad analisi LC/MS.

La pertammide C ha mostrato un'interessante attività antinfiammatoria *in vivo*, riducendo significativamente l'edema della zampa di topo indotto da carragenina. Peptidi ciclici di origine marina dotati di attività antiinfiammatoria sono molto poco comuni, per cui l'attività mostrata dalla pertammide C risulta molto singolare e sicuramente meritevole di ulteriori indagini sulle origini di tale attività e sull'identificazione del target biologico su cui agisce. L'isolamento di una piccola library di analoghi strutturali della pertammide C, insieme alla natura modulare di tale peptide ed il facile accesso chimico, consentirà di effettuare dettagliati studi al fine di stabilire le porzioni farmacoforiche utili nell'individuazione di nuovi lead per lo sviluppo di una nuova classe di farmaci antinfiammatori.

Dalla stessa spugna sono stati isolati anche altri due nuovi peptidi ciclici, strutturalmente non correlati alla pertammide C, denominati solomonammide A e B, caratterizzati dalla presenza di un'unità non amminoacidica senza precedenti e dotati anche essi di attività antinfiammatoria *in vivo*.

Dagli estratti più polari della stessa spugna sono stati isolati due steroli solfatati, denominati solomonsterolo A e B, che non sono relazionati agli steroli

precedentemente isolati dal genere *Theonella*. Questi rappresentano il primo esempio di steroli con nucleo 5*α*-colano e 24-nor-5*α*-colano da organismi marini, in grado di legare e attivare i recettori nucleari PXR. L'attivazione dei recettori X del Pregnano è responsabile dell'attività immunomodulante di entrambi i composti, attraverso l'inibizione dell'accumulo di Interleuchina-1*β*.

Infine, l'analisi dell'estratto cloroformico della *Theonella swinhoei* ha portato all'isolamento di un nuovo macrolide, correlato strutturalmente allo swinolide A; quest'ultimo è noto per la sua capacità di legarsi specificamente al sistema dell'actina intracellulare.

La seconda linea di studio si è inserita in un più ampio progetto di ricerca volto all'isolamento di metaboliti da piante dell'area mediterranea utilizzate a scopo alimentare e nella medicina tradizionale. Tale linea di ricerca è in atto già da diversi anni presso il gruppo in cui ho svolto il lavoro di dottorato, ed è volta all'isolamento di metaboliti secondari di interesse nutraceutico e farmacologico. In questo ambito la mia attenzione si è focalizzata sullo studio di tre piante tipiche del bacino mediterraneo: il *Cucumis melo*, la *Borrago officinalis* e il *Ruscus aculeatus*. In seguito allo studio di queste piante sono stati isolati vari metaboliti secondari.

Dal *Cucumis melo* è stato isolato, assieme ad altri composti già noti ma mai isolati in tale pianta, un nuovo glicoside, formato da una catena disaccaridica, costituita da un'unità di glucosio ed una di apiosio unite mediante un legame interglicosidico β-(1''→2') e da un aglicone costituito dall'alcol (*E*)-4-idrossicinnamilico.

Lo studio della *Borrago officinalis* ha portato all'isolamento di un nuovo benzilglucoside, che è risultato particolarmente interessante in quanto presenta

l'ossidrile in 6' dell'unità di glucosio esterificato con l'acido 3-idrossi-3-metilglutarico (HMGA).

Infine, lo studio dell'estratto polare dei rizomi del *Ruscus aculeatus* ha portato all'isolamento di tre nuove saponine furostaniche. Particolarmente interessanti risultano due saponine caratterizzate dalla presenza di un gruppo solfato legato al C-1. Infatti, saponine contenenti unità monosaccaridiche solfatate di solito sono abbastanza frequenti nelle piante, mentre risulta poco comune l'esterificazione con un gruppo solfato nella porzione agliconica.

In conclusione, la Natura è, e continua ad essere, la maggiore fonte di ispirazione di nuovi classi di farmaci, da utilizzare come *lead* per la progettazione di nuovi composti ottenibili per via sintetica.

Dunque, la chimica delle sostanze naturali offre ancora entusiasmanti prospettive.

INTRODUCTION

Drug discovery and development has a long history and dates back to the early days of human civilization. In those ancient times, drugs were entirely of natural origin and composed of herbs, animal products and inorganic materials. However, through trial and error, humans have discovered that some plants or parts of these (seeds, leaves, flowers, roots...) can have medical effects and humans have learnt to use them to reduce pain and suffering.

Those treatments, that were effective, were subsequently recorded and documented, leading to the early Herbals. The development of pharmacognosy provided a disciplined and scientific description of natural products destined in medicine use. As chemical techniques improved, more and more drugs, isolated from natural sources, were discovered, structurally characterized, tested and, in due course, many were synthesized in the laboratory. Nowadays, many of today's medicines are obtained directly or indirectly from natural sources. These compounds, pharmacologically active, are known as secondary metabolites.

In contrast to primary metabolic pathways, which synthesize, degrade, and generally interconvert compounds commonly encountered in all organisms, secondary metabolites have a much more limited distribution in nature, which are characteristic of specific species or specific taxa and they are not necessarily produced under all condition. For years, these compounds have been considered waste or products of primary overflow, but now it is well recognized that they play some vital role for the well-being of the producer, although the vast majority of cases the function of these compounds and their benefit to the organism is not yet known. Some are undoubtedly produced for easily appreciated reason, e.g. as

toxic materials providing defence against predators and the growth of neighboring species (allelopathy), as volatile attractants towards the same or other species, as coloring agents to attract or warn other species, or as photoprotective agents for the protection from ultraviolet radiation. In practice, the secondary metabolites are involved in the interactions within or between species and environment and they are produced to preserve and improve the life of the producing organism.

These secondary metabolites has evolved in nature in response to needs and challenges of the natural environment. The diversity of secondary compounds reflects that Nature apparently optimizes certain compounds through many centuries of evolution and Nature has been continually carrying out its own version of combinatorial chemistry for the over 3 billion years. During that time, there has been an evolutionary process going on in which producers of secondary metabolites evolved according to their local environments. Combinatorial chemistry practiced by Nature is much more sophisticated than that in the laboratory, yielding elaborate structures rich in stereochemistry, concatenated rings and reactive functional groups. As a result, an amazing number of products have been found in nature, with peculiar structures and biological activities.

Nowadays, although the increasing of synthesized drugs, it is estimated that over 40% of medicines have their origins in these secondary metabolites, used as lead compounds. These molecules provide the source or inspiration for the majority of FDA-approved agents and continue to be one of the major sources of inspiration for drug discovery, presenting important structural motifs and pharcophores. They can be used as drugs in themselves, or they can be optimize via semi-synthesis or by total synthesis of analogues of the active principles, to yield drugs with improved properties. In the last decades, the natural products chemistry is grown,

not only to find new compounds to use as drugs but also to understand their mechanism of action.

In 2009, Newman and Cragg published[1] an analysis of the sources of drugs, covering the period from 01/1981 to the middle of October 2008 and 1024 small molecule drugs (Figure 1). The analysis demonstrated the continuing and valuable contributions of Nature as a source not only of potential chemotherapeutic agents but also of lead compounds that have provided the basis and inspiration for the semisynthesis or total synthesis of effective new drugs. In this analysis, the drugs were classified as N (an unmodified natural product); ND (a modified natural product); S (a synthetic compound with no natural product conception); S/NM (a synthetic compound showing competitive inhibition of the natural product substrate); S* (a synthetic compound with a natural product pharmacophore); and S*/NM (a synthetic compound with a natural product pharmacophore showing competitive inhibition of the natural product substrate).

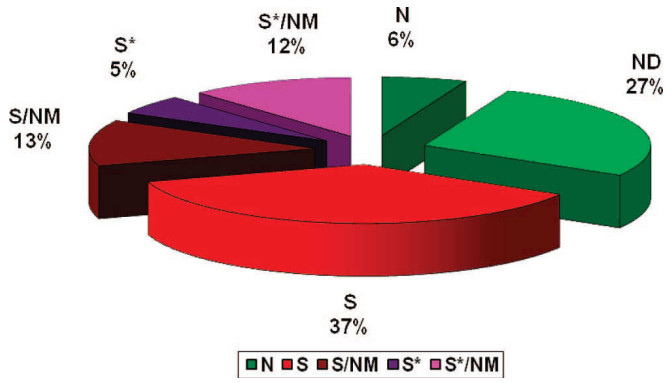

Figure 1. Analysis of the source of drugs carried out by Newman and Cragg in 2009.[1]

This analysis underlined that the proportion of truly synthetic (i.e., devoid of natural product inspiration and coded as S) is at 37% and 68.3% of compounds were classified as naturally derived or inspired.

Plants, in particular, have played a dominant role in the development of sophisticated traditional medicine systems, and for centuries they have been the only source of drugs known by humans. Among the innumerable examples of drugs, which have been developed from natural compounds, we can remember anti-inflammatory compounds (salicylic acid), decongestant drugs (ephedrine), analgesic agents (morphine), anesthetic compounds (cocaine), and so on. Clinically useful drugs which have been recently isolated from plants include the anticancer agent paclitaxel (Taxol) from the yew tree, and the antimalarial agent artemisinin from *Artemisia annua*.

In recent years, there has been a great interest in finding new lead compounds from marine sources. The progress in some technologies and the wider availability of diving equipment made it possible to extend this research to marine organisms for the study of natural products chemistry.

The greater part of earth surface is covered by seas and oceans which contains a larger number of organisms and less genetic homogeneity between separate populations of the same species than the terrestrial environment. There are over 200,000 invertebrate and algal species. Other types of marine organisms include sponges (Porifera), cnidarians or coelenterates (corals, octocorals, hydroids and sea anemones), nemerteans (worms), ascidians (including sea squirts), mollusks (sea snails and sea slugs) and echinoderms (brittlestars, sea urchins, starfish and sea cucumbers). The molecular variety associated with this biodiversity represents a challenge for drug discovery.

The study of marine organism as a source of biologically active compounds is considered a very promising field for the discovery of pharmacological tools and new medicines. In fact, since the natural products chemists diverted their attention

to exploit the vast researches of marine flora and animal world, numerous novel compounds have been isolated from these marine organisms during the second half of 20th century and many of these compounds have shown very promising biological activities and are already at advanced stages of clinical trials, mostly for the treatment of cancer, or have been selected as promising candidates for extended preclinical evaluation.

Among marine organisms, the chance of finding bioactive compounds is remarkably higher in some invertebrates, like corals, tunicates, and porifera. Presently, more than 35% of useful medical compounds from the sea are isolated from porifera, well known as sponges.

The harsh marine environment which they inhabit, together with their lack of physical defences has required these organisms to develop chemical deterrents in order to survive. For these reason these metabolites show often antiviral, antifungal, antimicrobial, anti-inflammatory, antitumor, cytotoxic properties.

Recent findings have proved that much of the unique chemistry isolated from marine invertebrates, such as sponges and tunicates, is also of bacterial origins. The symbiotic microorganisms constitute up to 40% of the biomass of some sponges and they are sources of various natural products; in fact metabolites previously ascribed to sponges have recently been demonstrated to be biosynthesized by symbionts. So, on one hand sponges offer nourishment and a safe habitat to their symbionts; on the other hand, symbiotic microorganisms help in the nutritional process, and participate in the host's chemical defense system against predators, producing secondary metabolites.

Although natural compounds isolated from marine organism show interesting and specific pharmacological activities, they rarely raise the interest of

pharmaceuticals companies, because they are difficult to obtain in sufficient amounts for clinical use. Such compounds can only be harvested from their natural source: a process which can be tedious, time consuming, and expensive, as well as being wasteful on the natural resource. Total synthesis is a possible way to overcome this problem, but this is usually prevented by the complex structure of most natural products, often including many chiral centers, which makes this option economically unfeasible. Alternative approaches have therefore been proposed, such as the cultivation of the organism of interest under controlled conditions (aquaculture), and the laboratory production of metabolites in bioreactors from cell cultures. A more recent approach is the study of the metabolic processes leading to the synthesis of secondary metabolites. With the advent of genetic techniques that permit the isolation and expression of biosynthetic cassettes, microbes and their marine invertebrate hosts may be the new frontier for natural products lead discovery.

In conclusion, it is clear that Nature will continue to be a major source of new drug leads. For these reasons effective utilization of these resources will require advances in technologies and the opening of new frontiers in science, understanding the importance of multidisciplinary teamwork, embracing natural product lead discovery and optimization through the application of total and semi synthesis and biochemistry, combined with good biology.

CHAPTER 1

RESEARCH STEPS

For the discovery of new compounds from natural source it is important a constant need to separate both large and small quantities of mixture efficiently and then it is necessary to characterize these new compound in a non-destructive way, with submilligram samples.

The study of natural compounds consists on some steps:

1. Isolation and purification of new compounds from biologic material;
2. Structural determination of new compounds isolated;
3. Determination of absolute and relative stereochemistry of new compounds.

1.1 ISOLATION PROCEDURE OF NEW COMPOUNDS

The isolation of natural products from natural sources poses numerous problems, because these compounds may only be present in infinitesimal quantities. When one considers, for example, that plants may have thousands of constituents, the difficulties in separating out one particular component can be appreciated.

The nature of the separation problem varies considerably, from the isolation of small quantities (milligrams or less) for structure determination purposes to the isolation of very much larger amounts (hundred milligram to gram quantities) for comprehensive biological testing, for semi-synthetic work or even for production of therapeutic agents. For these purposes, a good selection of different techniques and approaches is essential. The problem of separation and isolation of new metabolites from natural sources was solved with the development of refined

techniques, such as the various analytical and preparative chromatographic methods. We have successfully performed a procedure of purification.

First of all, the biological materials is extracted with an organic solvent, such as methanol. Then the crude extract is partitioned, utilizing modified Kupchan's partitioning methodology,[2] in which the composition of aqueous phase is adjusted sequentially as follows (Scheme 1).

- The methanol extract is dissolved in a mixture of 10% H_2O/MeOH and partitioned against *n*-hexane; the so obtained hexane extract is rich in lipophilic compounds.
- The water content (% v/v) of the MeOH extract is adjusted to 30% and partitioned against $CHCl_3$; in this extract compounds with medium polarity (peptides, macrolides, polyfuntionalized sterols, and so on) were usually found.
- The aqueous phase is concentrated to remove MeOH and then extracted with *n*-BuOH; this extract contains polar compounds and salts.

The so obtained four extracts (*n*-hexane, $CHCl_3$, *n*-BuOH and H_2O extracts) are tested trough preliminary bioassay to establish a potentially interesting activity.

The most promising crude extracts are further fractioned trough sequential chromatographic techniques. The initial stages of a separation procedure involve methods with a high loading capacity and cheap stationary phases - these have traditionally been column chromatography with silica gel or liquid-liquid methods. Subsequent steps employ techniques which require smaller samples - HPLC, for example.

Scheme 1. Modified Kupchan's partitioning methodology.

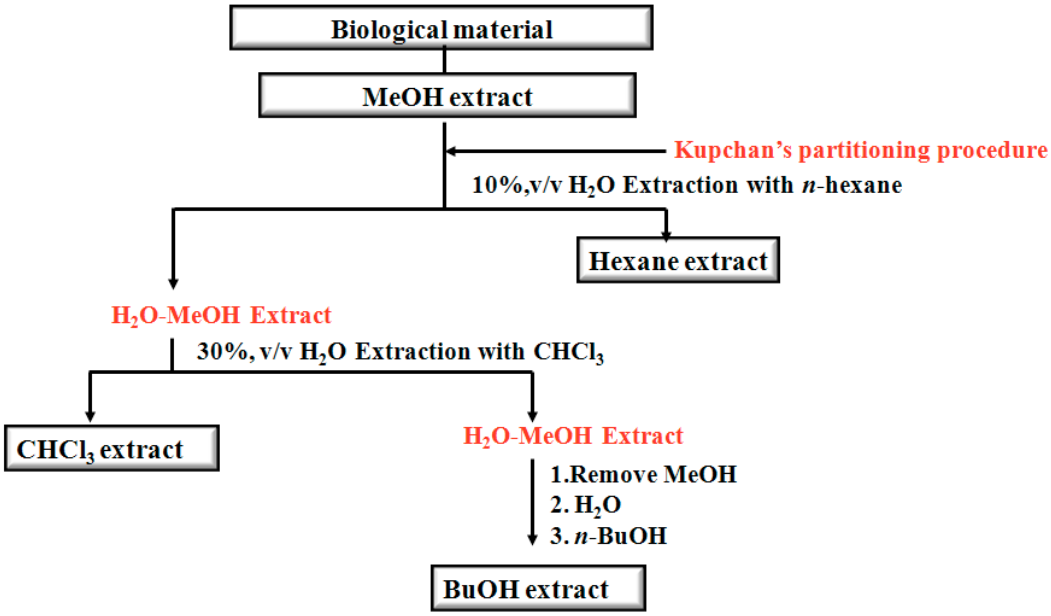

DCCC (droplet countercurrent chromatography) is a preparative method usually used in our laboratories. In spite of a number of advantage (such as total recovery of the introduced sample, no irreversible adsorption, and so on), this method doesn't have a large development, but in my work it represents an useful tool for the separation of mixture of compounds. It is a liquid-liquid separation method which does not require a sorbent; it relies on the passage of droplets of a mobile phase through an immiscible stationary liquid phase for the continuous partition of a solute between the two phases. A typical DCCC instrument consists of 200-600 vertical glass columns interconnected in series by capillary Teflon tubes.[3] These columns are first filled with the stationary phase of biphasic solvent system and the sample is injected. The mobile phase is then pumped into the first of the columns, forming a stream of droplets in the immiscible stationary phase. Depending on the choice of solvents for the mobile and stationary phases, droplets are made either to ascend ("ascending mode") or descend ("descending mode") through the columns (Figure 2). The choice of a two-phase solvent system is

crucial to the success of DCCC separations. Binary systems are impractical for the formation of suitable droplets because of the large difference in polarity between the two components, and ternary (or quaternary) systems are required, such that the addition of the third (or fourth) component, miscible with the other components, diminishes the difference in polarity between the two phases. The selectivity of the system is thus increased, allowing the separation of closely related substances. In my work I usually used the ternary biphasic *n*-BuOH/Me_2CO/H_2O (3:1:5) in the descending mode or $CHCl_3$/MeOH/H_2O (7:13:8) in the ascending mode.

The fractions, collected, are combined on the basis of their similar TLC retention factors.

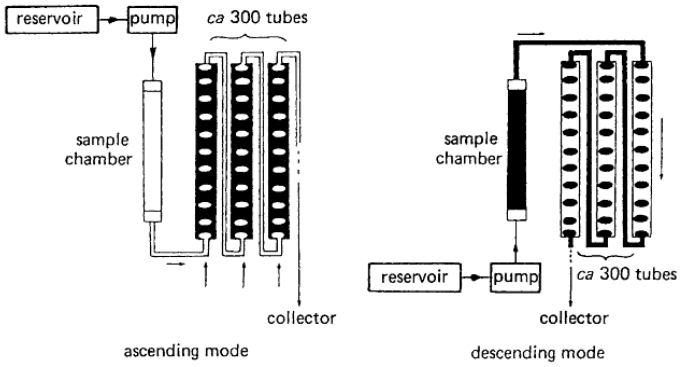

Figure 2. The principle of DCCC.

Another preparative chromatographic technique used in my work is the MPLC (Medium Pressure Liquid chromatography). It is a liquid-solid chromatography, in which the liquid mobile phase is forced through the solid stationary phase at medium pressure. MPLC is more efficient in resolution than the open-column and flash chromatography methods and the separation involves a considerable gain in time. The solid stationary phase can be a normal phase, like silica gel (used in my work), or bonded phase (RP-8, RP-18). The technique makes use of pressures of

ca. 5-40 bar and can easily accommodate much larger sample loads (100 mg-100 g) than are generally applied in other separations. As far as separating power is concerned, MPLC lies somewhere between flash chromatography and semi-preparative HPLC.

High Performance (or High Pressure) Liquid Chromatography (HPLC) , both normal-phase and reverse-phase, is the most widely used chromatographic method, and finds application in the preparative separation of samples to "pilot" the preparative isolation of natural products (optimization of the experimental conditions, checking of the different fractions throughout the separation). On the whole, however, HPLC is commonly applied as the last step in purification processes affording pure compounds in high yields, and, in this respect, the quantities involved tend to be at the lower end of the scale.

Finally the compounds, so isolated, are structurally characterized and are submitted to pharmacological assays.

1.2 STRUCTURAL DETERMINATION METHODS

Structural characterization of new compounds surely is the most interesting work of the natural products chemist. It is possible to determine complex organic structures completely in a non-destructive way, with submilligram samples through the combined use of all spectroscopic techniques. Structural determination described in this thesis is largely based on mostly mass spectrometry (MS) and nuclear magnetic resonance (NMR).

1.2.1 Mass Spectrometry

Mass spectrometry is an analytical technique that is used to determine the molecular mass of a compound on the basis of the mass-to-charge ratio (*m*/*z* ratio)

of ions produced from the molecules. A very accurate measurement of the molecular mass (high resolution mass spectrometry) can also provide the molecular formula of the molecule under study.

A mass spectrometer converts sample molecules into ions in the gas phase (*source*), separates them according to their mass to charge ratio *m/z* (*analyzer*) and sequentially records the individual ion current intensities at each mass (*detector*), giving the mass spectrum. There are many different types of sources, as well as of analyzers.

More information on the structure of the molecule under examination are given by the fragmentation of the ion produced in source. The ions may fragment by themselves, or they may be induced to fragment by letting them collide with gas molecules. In this case, a second analyzer is used to measure the mass of the fragments. This is known as tandem mass spectrometry or MS/MS.

Most of compounds described in the following sections were analyzed by ESI mass spectrometry. The ESI source is especially useful in producing ions from polar compounds or macromolecules. The sample is dissolved in a volatile solvent like H_2O, MeOH, and CH_3CN; volatile acids, bases or buffers are often added to the solution.

This solution passes through the electrospray needle that has a high potential difference applied to it (Figure 3). This forces the spraying of charged droplets from the needle with a surface charge of the same polarity to the charge on the needle. The droplets are repelled from the needle towards the source sampling cone on the counter electrode. As the solvent

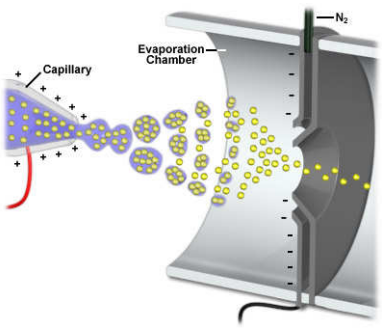

Figure 3. Source electrospray

evaporation occurs, the droplet shrinks until it reaches the point that the surface tension can no longer sustain the charge (the Rayleigh limit) at which point a "Coulombic explosion" occurs and the droplet is ripped apart. This produces smaller droplets that can repeat the process until the ionized analyte molecules can escape from the droplet by electrostatic repulsion. For molecules with a high molecular weight, the ions may take more than one proton (up to some tens), and therefore may have multiple charge. Formation of multiply charged ions allows the analysis of high molecular weight molecules such as proteins, because it reduces the *m/z* ratio of the ions, which is therefore easier to measure.

This is a very soft method of ionization as very little residual energy is retained by the analyte upon ionization. The major disadvantage of the technique is that very little (usually no) fragmentation is produced. For structural elucidation studies, this leads to the requirement for tandem mass spectrometry where the analyte molecules can be fragmented.

1.2.2 Nuclear Magnetic Resonance spectroscopy

Nuclear magnetic resonance spectroscopy, most commonly known as NMR spectroscopy, is the most important spectroscopic technique used for structure elucidation of the isolated secondary metabolites. This technique is not destructive compared to mass spectrometry. In addition to standard ^{1}H and ^{13}C NMR spectra, a large use of 2D NMR experiments was made, resolving overlapping multiplet patterns and allowing interpretation of more first-order-like spectra.

COSY (COrrelated SpectroscopY) is an homonuclear 2D experiment. It allows to determinate the connectivity of a molecule by identifying which protons are scalarly coupled. This method is very useful when the multiplets overlap or when extensive second order coupling complicates the 1D spectrum.

TOCSY (TOtal Correlated SpectroscopY also known as HOHAHA–HOmonuclear HArtmann HAhn) is very useful in the analysis of molecules composed of many separate spin systems. It shows the correlations between all protons within a given spin system, not just between geminal or vicinal protons as in COSY. Correlations are seen between distant protons as long as there are couplings between every intervening proton. This is extremely useful for identifying protons on sugar rings in oligosaccharides or amino acids in peptides: all protons on a given sugar ring will have a correlation with all other protons on the same ring but not with protons on different rings.

ROESY (Rotating frame Overhauser Effect SpectroscopY) is useful for determining which signals arise from protons that are close to each other in space even if they are not bonded, detecting ROEs (Rotating-frame Overhauser Effect). ROESY also detects chemical and conformational exchange. ROE is similar to NOE (Nuclear Overhauser Effect), being related to dipolar coupling between nuclei, and depending on the geometric distance between the nuclei. While NOE is positive for small molecules and negative for macromolecules, ROE is always positive. Therefore, the ROESY experiment is particularly useful for medium-size molecules, which would show a NOE close to zero.

The HSQC (Heteronuclear Single Quantum Correlation) is a 2D NMR heteronuclear correlation experiment, in which only one-bond proton-carbon couplings ($^{1}J_{CH}$) are observed. Instead HMBC (Heteronuclear Multiple Bond Correlation) is an experiment that identifies proton nuclei with carbon nuclei that are separated by more than one bond ($^{2,3}J_{CH}$).

1.3 DETERMINATION OF STEREOCHEMISTRY

The determination of absolute and relative stereochemistry is a key step for the characterization of natural products. The stereochemistry involves the study of the relative spatial arrangement of atoms within molecules, their three-dimentional disposition in the space. The stereochemistry of a molecule is a concept of fundamental importance and is inseparably linked with molecular recognition, in fact the biological activity of a molecule is strictly related not only to its planar structure, but also to its sterical arrangement. It is now widely recognized that enantiomeric drugs may give to different interactions in the human system, thus behaving very differently in their activity, toxicology, adsorption, metabolism, pharmacokinetics and bioavailability.[4] So, the knowledge of the three-dimentional disposition of a molecule is important to understand the biological activity, the interaction drug-receptor, but also to synthesize the natural products or its improved analogues.

The majority of natural products have one or more chiral centers. Usually, in a step-by-step structural elucidation, the first goal is the identification of relative stereochemistry of chiral centers. Then, after the elucidation of absolute stereochemistry even at a single stereogenic carbon, it will be possible to deduce the absolute configuration of the total structure. Unluckily, when the relative stereochemistry of different chiral centers cannot be correlated, the absolute configuration must be assigned independently.

1.3.1 Scalar and spatial NMR couplings

NMR spectroscopy gives a lot of information about molecular three-dimensional structure. Structural information from NMR experiments come primarily from the

chemical shift of a nucleus that is sensitive to the environment, from through-magnetization transfer between pairs of protons.

J couplings between pairs of protons separated by three or fewer covalent bonds can be measured. The value of a three-bond *J* coupling constant contains information about the intervening torsion angle (θ). This is called the *Karplus relationship*[5] and has the form:

$$^{3}J = A \cos \theta^{2} + B \cos \theta + C$$

where A, B, and C are empirically derived constants for each type of coupling constant. The magnitude of these couplings are generally smallest when the torsion angle is close to 90° ($^{3}J_{H\text{-}H}$ ~0-1.5 Hz) and largest at angles of 0° and 180° (generally $J_{180°} > J_{0°}$). Thus, it is possible to discriminate easily an axial-axial relation between two protons within a six membered ring, $^{3}J_{a\text{-}a}$~7-9 Hz, and an axial- equatorial or equatorial-equatorial correlation, $^{3}J_{a\text{-}e} \sim {}^{3}J_{e\text{-}e}$~2,5 Hz. It is also possible to discriminate between *cis* and *trans* relationship of two double bond protons ($^{3}J_{cis}$~6-12 Hz, $^{3}J_{trans}$~14-20 Hz).

The other major source of structural information comes from through space dipole-dipole coupling between two protons called the NOE (Nuclear Overahauser Effect).[6] This effect can be observed upon irradiation, during the acquisition of the spectra, on a specific signal. In this way, the relaxation times of all the protons surrounding the irradiated proton (distance < 2.5 Å), even though not belonging to the same spin system, are influenced and thus, their height changes. The intensity of a NOE is proportional to the inverse of the sixth power of the distance separating the two protons. Thus the NOE is a sensitive probe of short intramolecular distances.

NOEs are categorized according to the location of the two protons involved in the interaction. Intraresidual NOEs are between protons within the same residue, whereas sequential, medium, and long range NOEs are between protons on residues sequentially adjacent, separated by 1, 2 or 3 residues, and separated by four or more residues in the polypeptide sequence.

The NOE effect establishes a spatial relationship between substituents of fixed molecules, but this effect is dependent from the dimensions of the molecule. Indeed, NOE effects cannot be evidenced for large molecules. To overcome this limitation, a two-dimensional homonuclear experiment, the ROESY experiment (Rotating-frame Overhauser Effect SpettroscopY), can be used.[7]

1.3.2 Murata's method

NMR is certainly one of the most powerful instrumental techniques for the analysis of the relative stereochemistry of organic compounds. Even more, the application of NMR techniques to the problem of determining the relative spatial orientation of substituents has became a routine task in modern organic chemistry laboratories.

Cyclic compounds with small (three to six memberered) rings display a predicable conformation behavior that allows the knowledge of their configuration to be extracted from simple NMR parameters, such as proton-proton *J*-coupling values and NOE intensities. A much more challenging task is the assignment of relative (and absolute) configuration in the case of flexible system, such as open (polysubstituted) chain and/or macrocyclic compounds for which a clear-cut, definite stereochemical strategy is not yet available.

In acyclic system all coupling constants are observed as a weighted average of each conformer, and for this reason, the dihedral angles obtained from these data provide a much more reliable constraint information regarding the major conformer than NOE data. However, the use of the sole homonuclear coupling constants ($^{3}J_{H\text{-}H}$) for relative stereochemistry assignments in flexible system is not feasible since they don't allow to distinguish between all the spatial arrangements of the substituents linked to a two-carbon fragments, as it would be needed for the identification of the rotamer with the correct configuration (Figure 4).

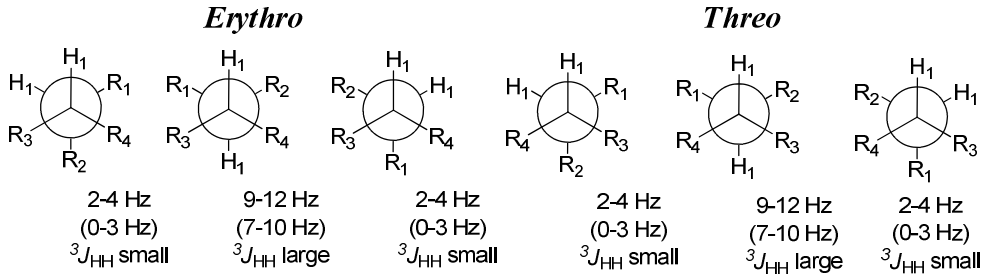

Figure 4. Values of $^{3}J_{HH}$ coupling for the six staggered rotamers corresponding to two different diastereomers *erythro* and *threo*

In other words, even if we restrict our attention just to staggered conformations, in absence of additional information on the geometry of the system, one angular constraint for each C2 segment is not sufficient to solve the problem, since more solutions are consistent with the experimental data. The situation change dramatically, though, when additional angular information on a stereochemically undetermined C2 fragment is provided from heteronuclear coupling costant ($^{2,3}J_{C\text{-}H}$). Along these lines, Murata et al.[8] have lately reported a method for the assignment of the relative configuration of acyclic compounds based on the combined use of homonuclear proton-proton coupling constants $^{3}J_{H\text{-}H}$, heteronuclear proton-carbon coupling constants $^{2,3}J_{H\text{-}C}$ and NOE data.

This model is basically applicable to acyclic structures having stereogenic carbons bearing hydroxyl, alkoxy or methyl substituents. Every chiral molecule containing consecutive or alternate streochemical centers can be ideally divided in two-carbon fragment. This simplification allows to determinate, for each single fragment, the predominant rotamer with the exact configuration, among the six possible staggered conformers through the use of the *J*-based NMR approach, see Scheme 2. For the sake of simplicity, let us compare every single couple of vicinal asymmetric carbons to those belonging to a 2,3-disubstituted butane system. The strategy followed for a 2,3-disubstituted butane can then be applied to a large variety of natural and synthetic products in which the substituents are methoxy, hydroxy and methyl groups. A 2,3-disubstituted butane can have two relative diastereomeric configurations, named *syn* (or *threo*) and *anti* (or *erythro*). Each of these two configurations can be arranged in three staggered rotamers, for a total of six possible conformers, as shown in Scheme 2 (A1, A2, A3, B1, B2, B3). Every single rotamer shows its own homonuclear and heteronuclear coupling constant pattern. Assuming that we have a sufficient number of experimental coupling constraints, these ${}^{3}J_{\text{H-H}}$ and ${}^{2,3}J_{\text{C-H}}$ will allow to univocally identify four of the six rotamers, namely A1, A3, B1, B3. The two rotamers A2 and B2, characterized by an *anti* position of the two vicinal protons, have to be distinguished on the basis of NOE (or ROE) data because they show the same coupling constant pattern.

The first step in the determination of the relative configuration of two vicinal methines consists in the evaluation of the homonuclear proton-proton coupling constant of the C_2 fragment of interest (Scheme 2), in order to assess whether or not it exists in a predominant conformation.

Scheme 2. Identification of the single conformer with a correct configuration from the staggered rotamers with threo (syn) and erytro (anti) arrangements through the combined use of measured $^{3}J_{HH}$ and $^{2,3}J_{CH}$ values.

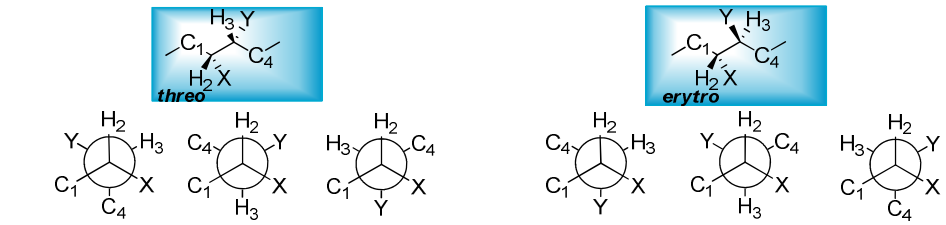

	A1	A2	A3	B1	B2	B3
$^{3}J_{H2-H3}$	small	large	small	small	large	small
$^{3}J_{H2-C4}$	large	small	small	small	small	large
$^{3}J_{H3-C1}$	large	small	small	large	small	small
X=Me, Y=OR				**X=Me, Y=OR**		
$^{3}J_{CX-H3}$	small	small	large	small	small	large
$^{2}J_{C3-H2}$	large	large	small	small	large	large
X=OR, Y=OR				**X=OR, Y=OR**		
$^{2}J_{C2-H3}$	large	large	small	large	large	small
$^{2}J_{C3-H2}$	large	large	small	small	large	large

Small $^{3}J_{H\text{-}H}$ (0-4 Hz) will indicate a *gauche* arrangement of H2 and H3 protons. In this case the relative configuration can be safely obtained from three or four additional angular constraints deriving from the heteronuclear coupling constants values. These $^{2,3}J_{C\text{-}H}$ values, indeed, will allow to establish the arrangement (*gauche* or *anti*) of H2 with regard to substituent Y and C4 and the arrangement of H3 with regard to substituent X and C1 and will therefore allow to choose the correct *gauche* rotamer among A1, A3 (*threo*), B1 and B3 (*erythro*) (Schemes 2 and 3).

Large $^{3}J_{H\text{-}H}$ values (8-12 Hz) indicate *anti* disposition of the protons. Nevertheless the $^{2,3}J_{C\text{-}H}$ values are the same for both rotamers A2 (*threo*) and B2 (*erythro*) (Schemes 2 and 3) and so they don't allow to distinguish them. In this case it is necessary to use NOE data regarding protons on carbons C1 and C4 and possibly protons on substituents Y and X. An NOE effect between protons on C1 and C4 and/or an NOE effect between protons on Y and X suggest the rotamer A2 in

Scheme 2, while an NOE between protons on C1 and on Y and/or an NOE between protons on C4 and on X are suggestive of the rotamer B2. Intermediate values of $^{3}J_{H\text{-}H}$ (4-8 Hz) are usually indicative of an interconversion between two or more conformers that is fast on the NMR scale. In this case, it would be still possible to identify the alternating conformers on the basis of the homonuclear and heteronuclear coupling constant value and to assign the relative configuration, but the methodology is being pushed to the limit and therefore much more care has to be put in its application. In addition, the registration of NMR spectra at a low temperature can be of help in case of complex conformational equilibria, due to the population increase of the most stable conformer.

Scheme 3. General *J*-coupling procedure.

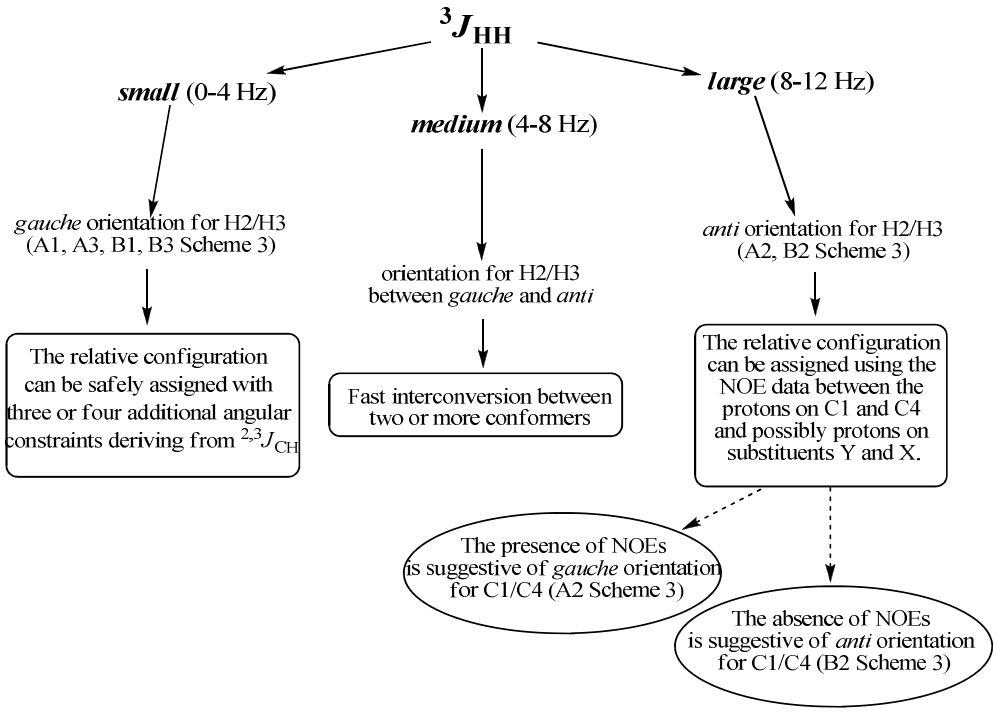

For small molecules, the homonuclear $^{3}J_{H\text{-}H}$ can be easily determined through the analysis of a 1D proton spectrum. Nevertheless, the use of more sophisticated 2D NMR techniques, such as E.COSY[9] or P.E.COSY[10], is mandatory when the direct

measurement of the *J* values in the proton spectra of medium and high molecular weight products is prevented by severe signal overcrowding.

Heteronuclear long range $^{2,3}J_{C\text{-}H}$ values have become widely available after the introduction of inverse detection NMR techniques[11] and the implementation of pulse-field-gradient (PFG) hardware in commercial NMR spectrometers. These values are determined, in the original method proposed by Murata, by 2D hetero half-filtered TOCSY (HETLOC),[12-13] phase sensitive HMBC (PS-HMBC) [14-17] experiments and, in a recent application of the methodology, HSQC-TOCSY spectra have also been used for this purpose.

However, the extensive use of $J_{C\text{-}H}$ couplings in the analysis of the relative configuration has been hampered due to the difficulties arising from the need to make reliable judgments on the size (*large, medium* or *small*) of a given heteronuclear *J* coupling value in the absence of a desirable wealth of literature data and of efficient empirical rules, unlike the case of $^{1}H\text{-}^{1}H$ *J* values, and due to the impossibility to deal with cases in which the dominant conformation of the C2 fragment under investigation is represented by an anti arrangement between protons. Indeed, in this particular instance, the sole pattern, however extensive, of homo- and heteronuclear *J*-couplings does not allow us to distinguish between the two possible relative configurations (*erythro* and *threo*).

These limitations were overcame utilizing a recent method, performed by the research group of Riccio-Gomez-Bifulco-Bassarello, of University of Salerno.[18]

This method represents a strategy for configurational analysis of flexible organic compounds, based on the use of QM calculations at DFT (density functional theory) level,[19,20] to accurately predict *J* coupling values and to subsequently compare them against their corresponding experimental counterparts. Indeed, QM

methods[21,22] have lately proved to be invaluable tools for computing faithfully a number of atomic and molecular properties, including relevant NMR parameters, such as chemical shifts and coupling constants. [23-25]

QM method calculates, quantitatively and not qualitatively (not more *small*, *medium* or *large*), homo- and heteronuclear coupling constant values for each of the six main staggered rotamers in which any given two-carbon (chiral) fragment can be ideally represented (Figure 4). It is based on the dissection of the full molecular system into a series of simplified fragments which, in most cases, are nothing else than suitable versions of each pair of stereocenters in which the molecule can be ideally divided.

Once the simplified C2 fragments of the molecule under investigation have been selected, all six staggered rotamers of a given C2 fragment are first subjected to a high-level geometry optimization, and then *J* coupling values are computed for all optimized rotamers. The so-obtained data sets of *J* coupling values can then be analyzed against the experimental values, allowing to draw conclusions on the relative configuration of the examined C2 molecular fragment. Then, the same approach is repeated for all the other C2 fragments of the system. For only one of the six arrangements are the *J* values in agreement with the experimental ones.

1.3.3 Marfey's method

Indirect methods, to determinate the absolute configuaration, involve the formation of covalent diastereomeric derivates by reacting the enantiomers with a chiral derivatizing agent (CDA). Thus the diastereomeric derivatives may be resolved by using conventional achiral columns in HPLC, both normal and reversed phase.

The most widely used method to determinate the absolute stereochemistry of ribosomial amino acids is the Marfey's method.[26] This method consists of the derivatization of amino acid residues, belonging to complete acid hydrolysis of peptide, with a chiral agent FDAA (1-fluoro-2,4-dinitrophenyl-L-alaninamide, Figure 5) and then the comparison of retention times of these derivates from parent peptide with the retention time of appropriate standards D and L through HPLC.

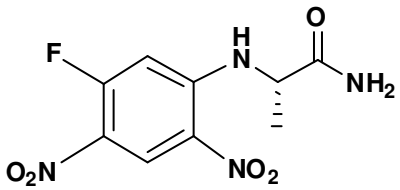

Figure 5. Structure of L-FDAA

This method is enough easy for ribosomial amino acids, commercially available, and consist of four phases:

1. Hydrolysis of parent peptide with HCl 6 N;
2. Derivatization of the hydrolyzed with L-FDAA;
3. Derivatization of both standards, D and L, with L-FDAA. If the D-standard isn't commercially available or is too expensive, it is possible to derivatize L-amino acid with D-FDAA.
4. Analysis through HPLC of retention times.

However, it is difficult to apply this chromatographic method to a peptide containing unusual amino acids without having their standard samples. Another limitation is the possibility to make mistake valuing the t_R of the derivates in HPLC. The last problem can be solved using LC-MS that allowed to identify the peak through the ratio *m/z*.

Recently a new method was developed, known as advanced Marfey's method.[27]

It is useful to determinate the absolute stereochemistry of non conventional amino acid, not commercially available, and is based on the elution time of amino acids derivatized wih L-FDAA. This method was tested on a number of proteogenic or not amino acids and showed the L-amino acid-L-FDAA derivate is eluted from the column before its corresponding D-isomer.

Now it is well recognized, according to the NMR and UV measurement, that D and L-amino acid-L-FDAA derivatives can be resolved due to the difference in their hydrophobicity which is derived from the *cis* or *trans* type arrangement of two more hydrophobic substituents at both α-carbons of an introduced amino acid and L-FDAA. In fact the D-isomer (with a *cis* type arrangement) interacts more strongly with RP silica gel and has the longer retention time compared to the less hydrophobic L-amino acid-L-FDAA, which has a *trans* type arrangement (Figure 6).

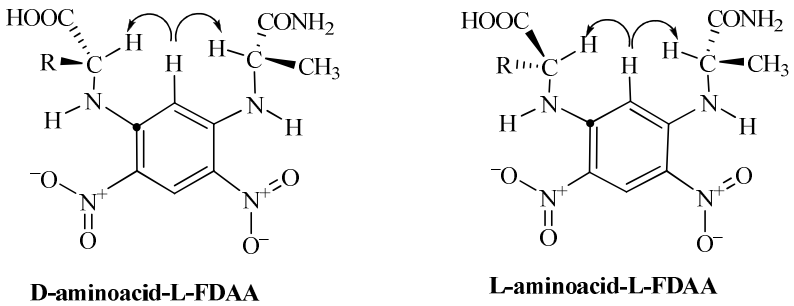

Figure 6. Structures of D and L amino acids-L-FDAA derivatives

The advanced Marfey's method is an useful tool to determinate the absolute configuration of non ribosomial amino acids. It consists of four steps:

1. The amino acid obtained from hydrolysis of the peptide is divided into two portions;
2. Derivatization of amino acid with L-FDAA;
3. Derivatization of amino acid with D-FDAA;

4. Analysis of t_R through LC-MS.

The peaks of any amino acids in peptides are identified without a standard sample using mass spectrometry, and the absolute configuration of a desired amino acid is deduced from its corresponding enantiomer.

This method is applicable to determinate the absolute configuration of the α chiral center of α-amino acid and to determine the absolute configuration of α-amino acid with more chiral centers, only if the relative configuaration is known.

The method cannot be used:

a) for β or γ-amino acids ;

b) for amino acids with more chiral centers, if it isn't known the relative configuration.

The advanced Marfey's method is a nonempirical one, but it has some draw-backs, since it relies on the eluition order of amino acid derivative with L-FDAA to determine its absolute configuration. It is clear that the nature of the amino acid side-chain is responsible for this behavior. So some amino acid don't follow the eluition order in column and the isomer L-amino acid-L-FDAA has a longer ritention time compared to the D-amino acid-L-FDAA, or the two derivatives have t_R too similar (see Table 1). The amino acids with ionizable side-chain, like Asp and Glu, have problem of derivatization. Amino acids like tyrosine and histidine or containing two amino groups such as ornithine and lysine can form both mono- and di-substituted Marfey's derivatives thus doubling the number of peaks in a chromatogram for these amino acids.

Table 1. Analysis of amino acid derivtized with L and D-FDAA.

Amino acid	L-FDAA t_R (min)	D-FDAA t_R (min)
β-*threo*-hydrossiapartic acid	3.8	3.7
β-*erythro*-hydrossiacpartic acid	6.9	6.1
Ornithine (mono-α-FDAA)	9.4	8.5
Ornithine (di-FDAA)	28.5	26.0
Hystidine (mono-α-FDAA)	6.7	6.0
Citruline	10.7	10.0
N-Me aspartic acid	11.4	11.0
Serine	9.2	9.3
Glutamine	8.8	8.9
Asparagine	6.7	7.3
Lysine	10.6	10.8

CHAPTER 2

PORIFERA

Sponges, which constitute *phylum* Porifera, are the most primitive of the multicellular animals. Neither true tissues nor organs are present and the cells display a considerable degree of independence. All the members of the phylum are sessile and exhibit little detectable movement. This combination of characteristic convinced Aristotele, Pliny and other ancient naturalist that sponges were plants.

They are aquatic sessile filter feeders and live permanently attached to a location in the water. Sponges can be found in nearly all aquatic environment (marine and fresh water; shallow and deep; tropical and Antarctic), wherever there are substrata for sponge attachment and growth. There are over 9000 presently known species of sponges and as many species not yet described.[28]

They can show a variety of sizes, colors, and shapes, including arboresecent (tree-like), flabellate (fan-shaped), caliculate (cup shaped), tubular (tube shaped) and amorphous (shapeless) (Figure 6).

Figure 6. Some examples of Porifera.

The closest to a tissue in a sponge is the outer dermal membrane composed of two cell layers of specialized cells called pynacocytes, which digest food particles too large to enter the ostia. The body wall is approximately two cell layers thick with a gel like substance called the mesohyl, the gelatinous matrix within the sponge made of collagen. The body wall is perforated by many pores and channels (ostia), through which water enters the animal, passing into the spongocoel, and exiting it through a large opening, the osculum (Figure 7). The interior cells are called choanocytes and contain a central flagellum surrounded by a collar of microvilli which are connected by a thin membrane. By cooperatively moving their flagella, choanocytes generate a flow of water through the sponges pores, into the spongocoel, and out through the osculum. This improves both respiratory and digestive functions for the sponge, pulling in oxygen and nutrients and allowing a rapid expulsion of carbon dioxide and other waste products.

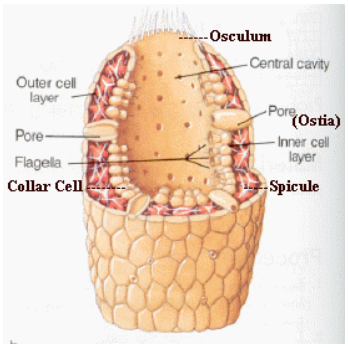

Figure 7. A sponge body structure.

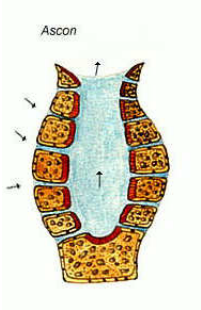

Body plans range from simple through to complex, produced by varying degrees of infolding of the body wall and complexity of water canals throughout the sponge. The simplest body structure in sponges is a tube or vase shape known as asconoid. This refers to a sessile tubular structure. Water, along with particulate matter, flows through small pores. The ostia lead to flagellated coanoderm which

pick up particulate matter, while the water is pushed up and out of the tube at the osculum.

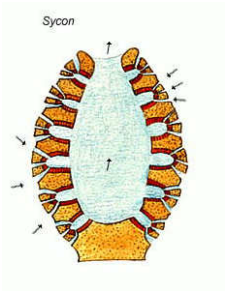

Syncanoids also take on tubular structure but have an internal tissue which generates a much greater surface area for the absorption of nutrients. Folds in the internal tissue create a sort of zigzag pattern in which the internal openings are referred to as choanocyte chambers. The external openings are incurrent canals. However this is not a typical zigzag pattern as the internal and external chambers are connected by small canals called prosopyles. As such, the water flow enters the ostia, moves through the incurrent canals, through the prosopyle, into the coanoderm chamber, through the atrium and out the osculum.

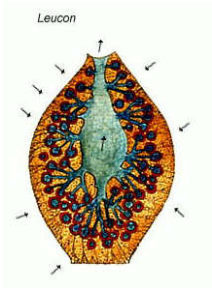

The most derived form of sponges takes on leucanoid design. Leucanoids differ from Syncanoids in that they have spherical choanocyte chambers and often several osculum. These sponges minimize the amount of water which is pumped through the body and maximize the number of choanocytes.

The body of the sponges is reinforced by the skeleton, collagen fibers and spicules (Figure 8). Sponges use various materials to reinforce their mesohyl and in some cases to produce skeletons and this form the main basis for classifying sponges. Sponges produce spicules made of calcium carbonate.

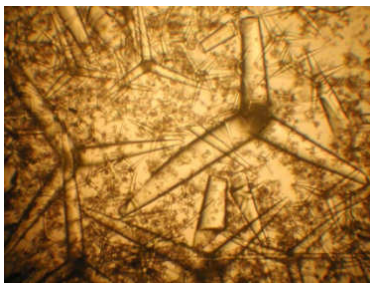

Figure 8. Spicules seen at microscope.

Demosponges reinforce the mesohyl with fibers of a special form of collagen called spongin, most also produce spicules of silica, and a few secrete massive external frameworks of calcium carbonate. Although glass sponges also produce spicules made of silica, their bodies mainly consist of syncytia that in some ways behave like many cells sharing a single external membrane, and in others like individual cells with multiple nuclei.

Probably because of their variety of construction methods, demosponges constitute about 90% of all known sponge species, including all freshwater ones, and have the widest range of habitats. Calcareous sponges are restricted to relatively shallow marine waters where production of calcium carbonate is easiest. The fragile Hexactinellida (glass sponges) are restricted to polar regions and the ocean depths where predators are rare, and their feeding systems very efficiently harvest what little food is available.

Sponges, lacking any nervous, digestive, circulatory, muscular systems or any physical defence from their predators, produce secondary metabolites, involved in their chemical defence, which is essential for their survival. In fact many species contain toxic substances, probably to discourage predators. The chemicals also probably play a role in competition among sponges and other organisms, as they are released by sponges to insure themselves space in the marine ecosystem. Some of these chemicals have been found to have beneficial pharmaceutical effects for humans, including compounds with respiratory, cardiovascular, gastrointestinal, anti-inflammatory, antitumor, and antibiotic activities.

Sponges also provide a home for a number of small marine plants, which live in and around their pore systems. Symbiotic relationships with bacteria and algae

have also been reported. It is well recognized that the symbiontic bacteria are the real producer of many secondary metabolites with biological activities.

Sponges are very fertile host animals for diverse symbiotic microorganisms and various microorganisms have been found in sponges. They include a diverse range of archaea, heterotrophic bacteria, cyanobacteria, green algae, red algae, cryptophytes, dinoflagellates and diatoms.

One host sponge can possess diverse symbionts. For example, sponge *Theonella swinhoei* supports unicellular heterotrophic bacteria, unicellular cyanobacteria and filamentous heterotrophic bacteria at the same time.[29]

The symbionts locate both intra- and extra cellularly (Figure 9), and each symbiotic microorganism seems to have a specific habitat in the host sponge. Extracellular symbionts are present on the outer layers of sponges as exosymbionts, or in the mesohyl as endosymbionts. Intracellular or intranuclear symbionts permanently reside in host cells or nuclei. In the case of the sponge *Theonella swinhoei*, all populations of symbiotic bacteria are located extracellularly.

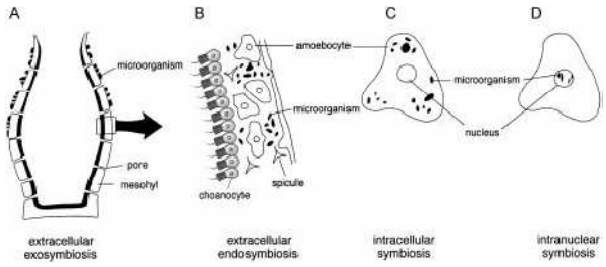

Figure 9. Schematic diagram of symbiotic relationships between sponges and microorganisms. A, extracellular exosymbiosis; B, extracellular endosymbiosis; C, intracellular symbiosis; and D, intranuclear symbiosis.

The amount of symbiotic microorganisms residing in sponges varies between host species. While bacteria constitute up to 60% of the biomass of some sponges, others contain only a small number of bacteria inside their tissue.

Then why do symbiotic microorganisms inhabit sponges? The surfaces or internal spaces of marine sponges are more nutrient-rich than seawater and sediments; therefore sponges offer nourishment and a safe habitat to their symbionts. On the other hand, symbiotic microorganisms help in the nutritional process, either by intracellular digestion or by translocation of metabolites including nitrogen fixation, nitrification and photosynthesis. Microorganisms also stabilize the sponge skeleton and participate in the host's chemical defense system against predators and biofouling. Bacteria collected from sponges have allowed isolation of antimicrobioal compounds, which suggests that these bacteria may play a role in the defence mechanism of these invertebrates.

2.1 METABOLITES ISOLATED FROM SPONGES

A number of promising compounds have been identified from marine sponges that possess pronounced biological activity and are already at advanced stages of clinical trials, mostly for the treatment of cancer, or have been selected as promising candidates for extended preclinical evaluation.[30] The types of compounds characterized from marine organisms are diverse and represent many different classes, structurally complex with unique functionalities, including:

- **Macrolides** are a group of compounds that stems from the presence of a macrolide ring, a large macrocyclic lactone ring to which one or more sugars may be attached.
- **Terpenes** are a large and varied class of natural compounds, structurally different each other. They derive from C5 isoprene units linked together head to tail. Several modes of cyclization are conceivable and lead to various skeletons just like the cyclization of polyketide chains. The

terpenes are classified according to the number of C5 units: monoterpenes, C10; sesquiterpenes C15; diterpenes, C20; sesterterpenes, C25; triterpenes, C30; and tetraterpenes C40.

- **Steroids** have a tetracyclic ring system and comprise a large number of ubiquitous compounds which are divided into subgroups, chiefly according to side chain functionality: sterols, sapogenins, cardiac aglycones, bile acids, adrenal steroids and sex hormones, all of vital importance for life. The most common sterol of animal origin is cholesterol.
- **Cyclic Peptides** are polypeptide chains whose amino and carboxyl terminus are themselves linked together with a peptide bond that forms a circular chain. They are often characterized for the presence of unusual amino acids.

2.1.1 Macrolides

Marine macrolides provide a fascinating range of structural and functional diversity, which may find application as specific molecular probes for the investigation of the cytoskeleton and cell cycle events. In fact, many macrolides isolated from sponges disrupt the organization of microfilaments, interacting with actin in the cell cytoskeleton, and represent a promising mechanism of action for developing novel anticancer drugs.

The latrunculins are 2-thiazolidinone-containing macrolides, isolated from the Red Sea sponge *Latrunculia magnifica*.[31] Latrunculin A is the most potent of the class and affects different components of the actin-based cytoskeleton.

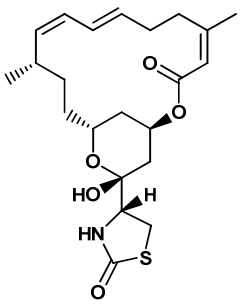

latrunculin A

The sphinxolides and reidispongiolides are 26-membered lactones isolated from two New Caledonian marine sponges *Neosiphonia superstes* and *Reidispongia coerulea*.[32-36] They exhibit an extraordinary *in vitro* activity against various human tumor cell lines and a potent actin-depolimerizating activity.

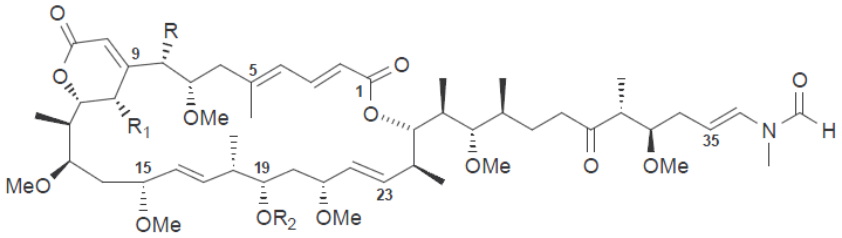

Sphinxolide	R=OMe, R_1=OH, R_2=H
Sphinxolide B	R=H, R_1=OH, R_2=H
Sphinxolide C	R=OMe, R_1=OH, R_2=Me
Sphinxolide D	R=H, R_1=OH, R_2=Me
Reidispongiolide A	R=H, R_1=H, R_2=Me
Reidispongiolide B	R=H, R_1=H, R_2=H

Other macrolides that are becoming important as molecular tools are the macrolide swinholide A[37] and its analogue misakinolide,[38] which bind specifically to the intracellular actin network and represent useful tools in investigations of actin organization, dynamics and function.

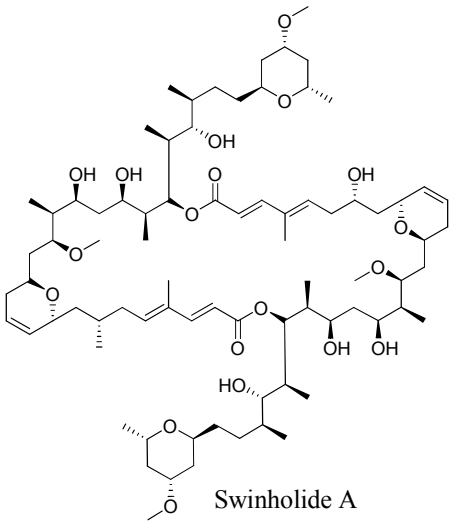

Swinholide A

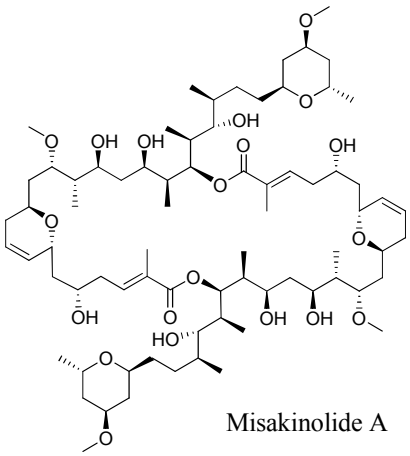

Misakinolide A

2.1.2 Terpenes

Marine organisms produce a wide array of fascinating terpenoid structures distinguished by characteristic structural features. Especially striking is the frequent occurrence of sesterterpenes in marine organisms, and sponges must be considered as one of the prime sources of these C25 terpenoid compounds. In most cases however, these structural features are not strictly unique for marine natural products. The prominent biological activity of marine terpenes is evident in their ecological role in the marine environment, and makes them interesting as potential drugs.

Examples are: curcuphenol, that is a sesquiterpene phenol isolated from different marine sponges belonging to the genus *Didiscus*, that inhibts growth of several cell lines and exhibits *in vitro* antimalarial activity;[39] spongiadiol and epispongiadiol, furanoditerpenes with cytotoxic and antiviral activity, isolated from a Caribbean deep water marine sponge, *Spongia* sp.[40]

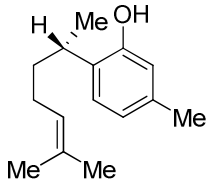

Curcuphenol

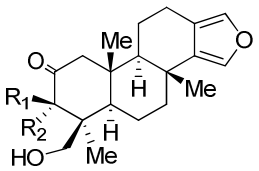

R1=H R2=OH Spongiadiol
R1=OH R2=H Epispongiadiol

A number of cytotoxic furanosesterterpenes have been obtained from a variety of sponges, such as palominin from a Caribbean *Ircinia* sp. and cacospongionolide from the marine sponge *Cacospongia mollior.*[41,42]

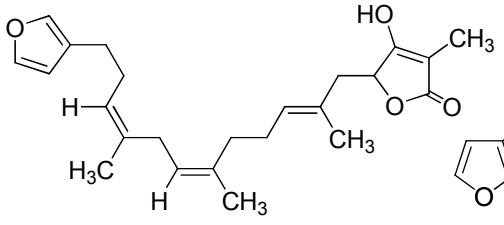

Palominin

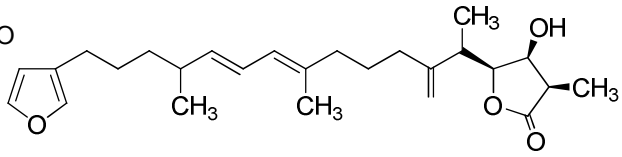

Cacospongionolide

2.1.3 Sterols

In the last 30 years many sterols with unprecedented structures have been isolated from marine sources. For many years the known carbon skeleton of sterols ranged from C27 to C29, and the carbon variation occurred exclusively in the side chain at C24.[43] After the discovery of the C26-sterols, first detected in 1970 from the mollusk *Placopecten magellanicus*[44] and later found widespread in marine invertebrates and also in a marine phytoplankton,[45] a number of "nonconventional" sterols have been reported.

Unconventional steroids often co-occur with conventional ones and are sometimes present in small amounts; however, many exceptions are reported for some sponges that are found with unusual structures as the predominant steroids rather than cholesterol or the conventional 3β-hydroxy sterols.[46-48] It is, therefore, particularly interesting when a sponge contains unusual steroids in large quantities, as these very likely play a functional (rather than metabolic) role in maintaining the integrity of membranous structures. It has been hypothesized and, to some extent, documented that the uniqueness of sterols in cell membranes of sponges is related to the other membrane components, particularly the phospholipids. These latter compounds seem to have head groups and fatty acids very different from those of higher animals; therefore, the structural modifications exhibited by the sponge sterols may be a sort of structural adjustments for a better fit with other membrane components.[49-52]

The sterols isolated from sponges are sometimes very complex mixtures of highly functionalized compounds, many of which have no terrestrial counterpart. These include sterols having side chains modified by the apparent loss of carbon atoms or by the addition of extra carbon atoms at biogenetically unprecedented positions

of a normal Cα side chain, as well sterols with unusual nuclei, containing a variety of oxygenated functionalities such as polyhydroxy, epoxide, epidioxy, and mono or polyenone systems.

The highly functionalized steroids have attracted considerable attention because of their biological and pharmacological activities. Remarkable example is the 9,11-secosterol herbasterol, isolated from the sponge *Dysidea herbacea*, which is ichthyotoxic. [53]

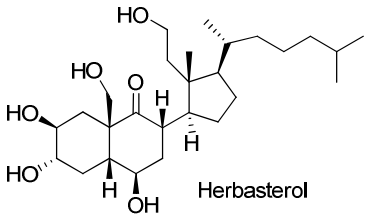

Herbasterol

Contignasterol represents the first marine steroid found to have a *cis* C/D ring junction as well as a cyclic hemiacetal functionality at C-29 in the side-chain and it is a potent inhibitor of histamine release from rat mast cells induced by anti-IgE.[54]

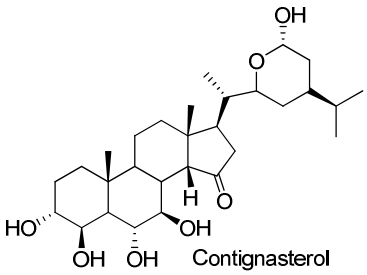

Contignasterol

Other examples of sterols with unconventional nuclei are theonellasterone and bistheonellasterone, isolated from the Okinawan *Theonella swinhoei*; the last one represents a dimeric steroid, considered to be biosynthesized through a Diels-Alder cycloaddition of theonellasterone and its Δ^4-isomer.

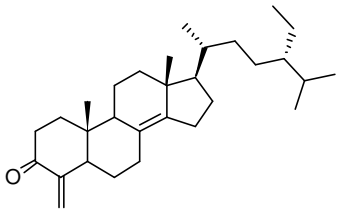

Theonellasterone

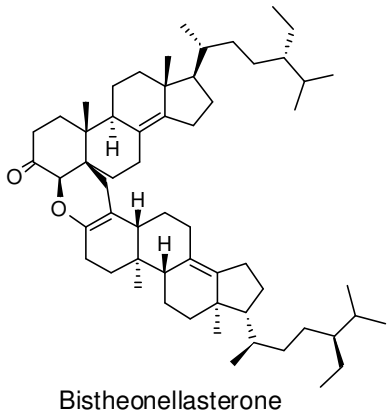

Bistheonellasterone

Another unusual structural features of these sterols are associated with their side chains. Sterol side chains have been isolated with such unusual features as

quaternary alkyl groups, cyclopropane and cyclopropene rings, allenes, and acetylenes (Figure 10). Biosynthetic studies have been performed on mechanism and scope of sterol side-chain dealkylation in sponges [55], and a detailed review has been published as a comprehensive summary of biosynthesis of sterol side-chain in marine organisms. [56]

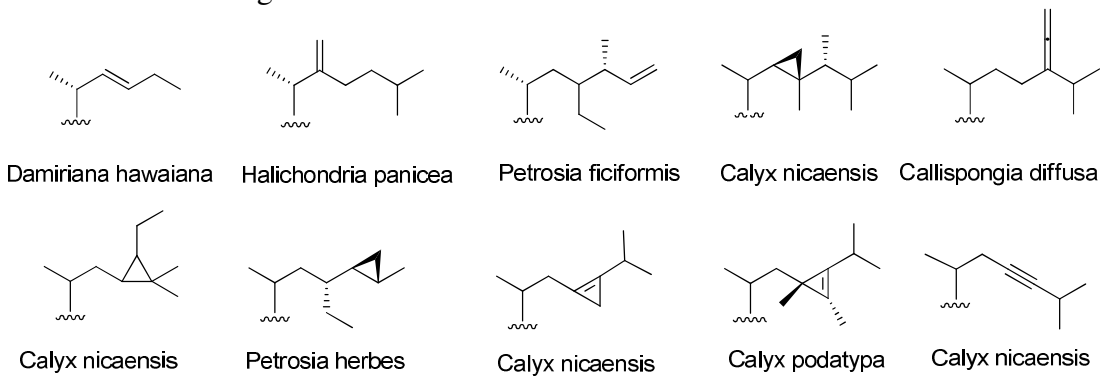

Figure 10. Examples of nonconventional side chains of sponge monohydroxysterols.

Finally, the discovery of the interesting properties of sulfated polyhydroxysterols has increased interest in these compounds. Most of these natural products are characterized by the 2β,3α,6α-tri-O-sulfate functions together with additional alkylation in the side chain. These steroids are of interest not only because of their structures but also because of their physiological activities, which include an anti-human immunodeficiency virus (HIV) effect and a high inhibitory action on some enzymes.

Halistanol sulfate, present in *Halichondriidae* sponges and characterized by the 2β,3α,6α-trisulfoxy functionalities, is the first example of sulfated sterol isolated from *Porifera*, with a potent anti-HIV activity.[57] Successively, several new sulfate sterols have been reported.

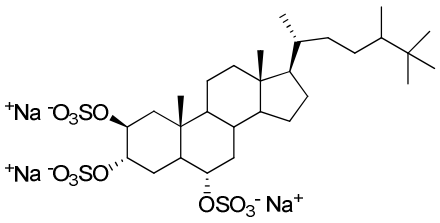

Halistanol Sulfate

2.1.4 Cyclic peptides

Cyclic peptides are an unusual class of compounds in which a carboxyl function is linked with an amine group to form a ring. They represent the most interesting class of secondary metabolites isolated from sponges.

The unusual properties of cyclic peptides are due both to their circular structure and their unusual mode of biosynthesis, which frequently incorporates uncommon amino acids. For instance, they can contain D amino acids, β-hydroxyamino acids, and N-alkylated amino acids. As result, the presence of non-ribosomial amino acids produces pronounced effects on the pharmacological activities of these metabolites. For example, N-alkylation and the lack of N and C termini enhance the hydrophobicity, thus determining a more facile crossing of biological membranes and an improved stability to enzymatic degradation. In addition N-alkyl residues exhibit reduced preferences to form the *trans* conformation of the amide bond leading to biologically important β-*turns* structures. Cyclization reduces peptide conformational flexibility that results in a higher receptor affinity and often offers the possibility to determine their three dimensional structures. All these features make cyclopeptides promising lead compounds in drug discovery; thus these compounds are undergoing very active investigation as potential new sources of drugs and antibiotics. They are much more resistant to proteases than a linear peptide chain. This resistance to proteolysis means that they tend to survive the human digestive process. They can also bind proteins in the cell where traditional drugs cannot.

Cyclic depsipeptides are cyclic peptides in which one or more of the peptide (amide) bonds are replaced by other bonds. Other functional groups, different

from the usual amino and carboxyl group, are linked together, closing the polypeptide chain, including ester, lactone, thioester bonds.

The biosynthesis of natural cyclic peptides is interesting to biologists, since it frequently involves *non-ribosomal peptide synthetases*. Most peptides are made by bacteria. Some microorganisms have large enzyme complexes composed of modules that they use to assemble the cyclic peptides and they do not use ribosomes or mRNA.

Nonribosomal peptide synthetases (NRPSs) and polyketide synthases (PKSs) are multi-enzymatic, multi-domain megasynthases involved in the biosynthesis of nonribosomal peptides and polyketides.[58-60]

Nonribosomal peptides are biosynthesized by sequential condensation of amino acid monomers, whereas polyketides are made from repetitive addition of carbon ketide units derived from thioesters of acetate or other short carboxylic acids. NRPSs and modular PKSs are comprised of so-called modules, which are sets of distinct active sites for catalysing each condensation and chain elongation step (Figure 11). Each module in an NRPS or PKS consists of certain obligatory or core domains for addition of each peptide or ketide unit and a variable number of optional domains responsible for modification of the peptide/ketide backbone. The minimal core module in the case of an NRPS consists of an adenylation (A) domain for selection and activation of amino acid monomers, a condensation (C) domain for catalysing the formation of peptide bonds and a thiolation or peptidyl carrier protein (T or PCP) domain with a swinging phosphopantetheine group for transferring the monomers/growing chain to various catalytic sites. During the biosynthesis, the growing chain remains covalently attached to the enzyme and upon reaching its full length, a thioesterase (TE) domain catalyses the release of

the NRPS and PKS products, forming linear, cyclic, or branched cyclic products. The number of modules in such PKSs or NRPSs correlates directly with the number of chain elongation steps during biosynthesis, and the domains present in each module dictate the chemical moiety which the given module would add to a growing chain.

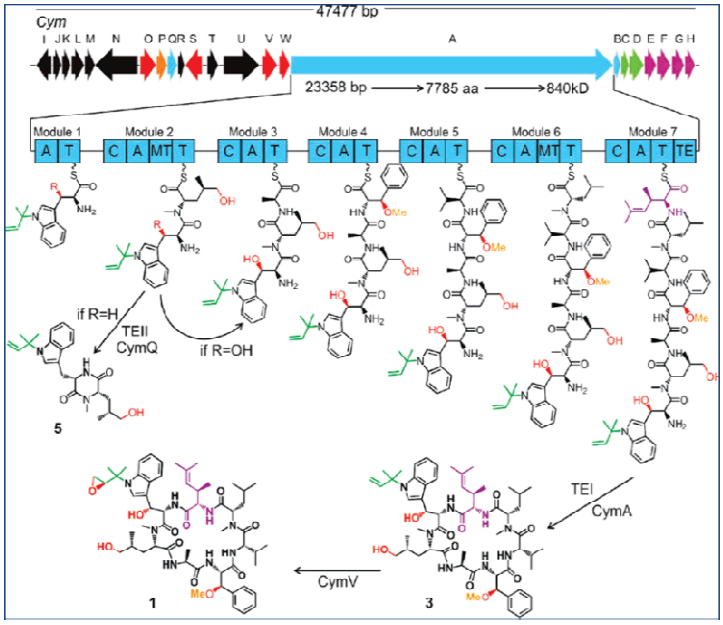

Figure 11. Biosynthetic gene cluster of CYM and proposed biosynthesis of cyclomarin A (1) and cyclomarzaine A (5).

The first bioactive peptide isolated from sponges is the discodermin A, obtained from *Discodermia kiiensis*.[61] It shows various activities, the most important one is the ability to inhibit the tumor grown, induced by okadaic acid.

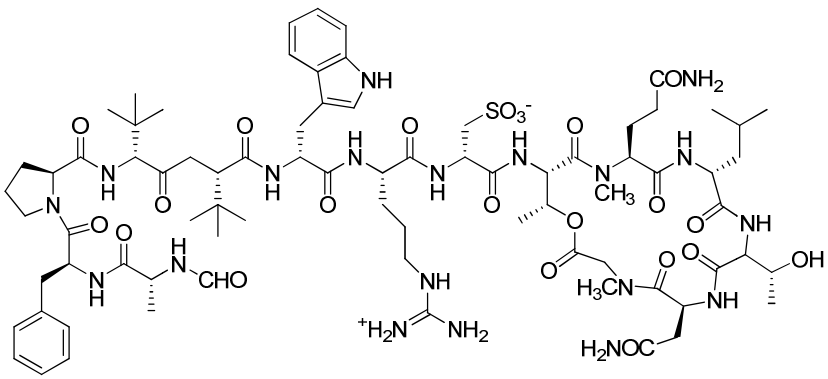

Discodermin A

Interesting examples of cyclodepsipeptides are the family of callipeltins, which show a potent antiviral activity. The first compounds of this family is callipeltin A, isolated in the 1996 from the sponge *Callipelta sp.*[62-64]

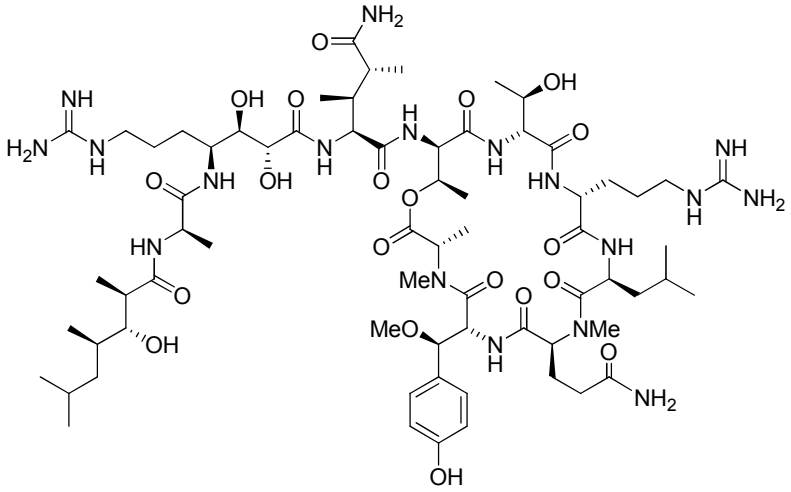

Callipeltin A

CHAPTER 3

COSCINODERMA MATHEWSI

In the course of a project directed to the chemical investigation and evaluation of the marine invertebrates of South Pacific (*C.R.I.S.P.*, Coral Reef Initiative Sud Pacific), I had the opportunity to study various marine sponges, analyzing their chemical composition and biological activities of the secondary metabolites.

In the frame of this project, I had the opportunity to examine a specimen of *Coscinoderma mathewsi*, collected along the coasts of Solomon Island.

Coscinoderma mathewsi

The sponge *Coscinoderma mathewsi* Lendenfield belongs to the order of Dyctioceratida, family Spongiidae and has been a source of various terpenoid compounds,[65-67] as have other members of this family.[68-71] Recently, many sulfated steroids were isolated from marine sponges of the *Coscinoderma* genus, often characterized by unusual biological effects.

As examples halisulfates 1[72] and 7[73] were isolated from a Micronesia collection of the sponge. Halisulfate 7 is an inhibitor of the catalytic subunits of the mammalian Ser/Thr protein phosphatases calcineurin, PP-1, and PP-2A,[74] whereas halisulfate 1 is a potent isocitrate lyase inhibitor.[75,76]

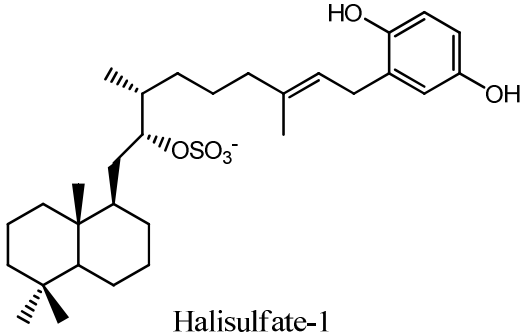

Halisulfate-1

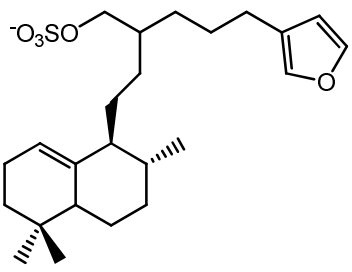

Halisulfate-7

Coscinosulfate, a sesquiterpene sulphate from the New Caledonian sponge *Coscinoderma mathewsi,* displays significant inhibitory activity towards CDC25A phosphatase. [77]

The tricyclic sesterterpene suvanine[78,79] is a thrombin and trypsin inhibitor and shows moderate antimycobacterial activity. [80]

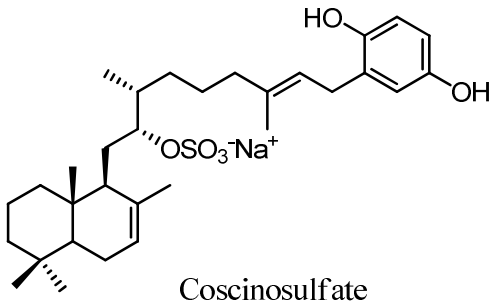

Coscinosulfate

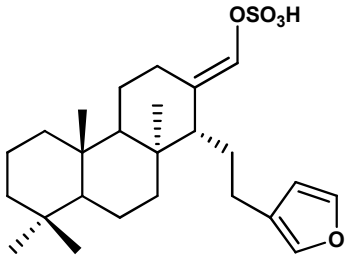

Suvanine

Investigation of the marine sponge *Coscinoderma mathewsi* led to the isolation of two novel nitrogen-containing cheilanthane sesterterpenoids, coscinolactams A and B, together with known suvanine.[81]

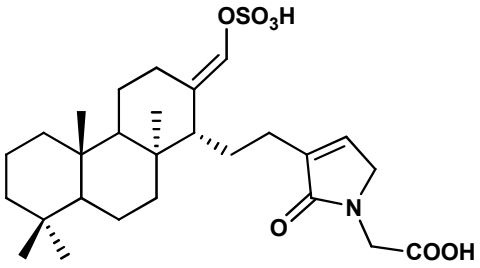

Coscinolactam A

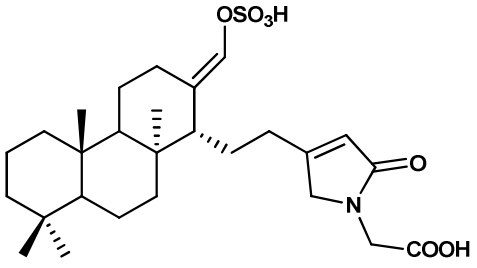

Coscinolactam B

Cheilanthanes represent a relatively new class of sesterterpenoids with the "triterpene-type" ring-closure. The name "cheilanthane" is derived from the name of the fern *Cheilanthes farinose*- the source of the first representative of this class of compounds, namely cheilanthatriol, isolated in 1971 by

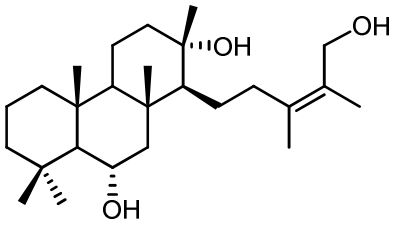

Cheilanthatriol

Indian researchers.[82] Numerous cheilanthanic sesterterpenoids have been isolated later on from other plant sources, marine organisms and fossil sediments.

Today, there are more than 50 known cheilanthanes. The interest in these compounds is first of all due to their strong biological activity. This aspect has also inspired synthetic chemists to develop several synthetic routes to cheilanthane sesterterpenoids.

3.1 ISOLATION OF COSCINOLACTAMS A AND B

Samples of *Coscinoderma mathewsi* Lendenfield (order Dictyoceratida, family Spongiidae) were collected on the barrier reef of Vangunu Island (Solomon Islands), immediately frozen and lyophilized. The crude ethanolic extract exhibited an anti-PLA_2 activity (72% inhibition at 400 μg/mL).

The specimens of lyophilized sponge were extracted three times with methanol at room temperature. The combined extracts were fractionated according to the Kupchan partitioning procedure, obtaining four extacts.[2]

The bioactive chloroform extract was purified by DCCC ($CHCl_3$:MeOH:H_2O ascending mode), followed by reverse-phase HPLC (MeOH aqueous 65%) to give suvanine (**3**).

The more polar coscinolactams A (**1**) and B (**2**) were obtained from the butanol extract chromatographed by DCCC ($CHCl_3$:MeOH:H_2O ascending mode) and reverse-phase HPLC (MeOH acqueous 45%).

3.2 STRUCTURE DETERMINATION OF COSCINOLACTAM A

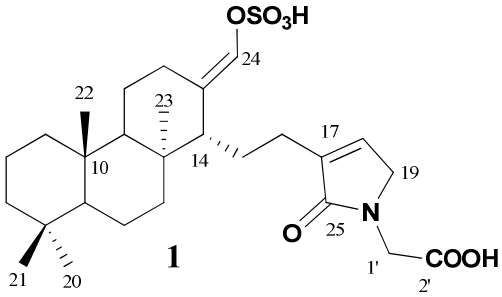

The molecular formula of coscinolactam A (**1**) was determined to be $C_{27}H_{41}NO_7S$ by HR-ESIMS (*m/z* 522.2547 $[M - H]^-$). The gross structure was deduced from detailed analysis of the ^1H and ^{13}C NMR spectroscopic data (Table 2), aided by 2D NMR experiments (^1H-^1H COSY, TOCSY, HSQC and HMBC).

The NMR spectroscopic data showed the signals for two acyl carbons at δ_C 176.3 and 173.7, two trisubstituted double bonds [δ_C 125.2 (s), 140.5(s), 133.9 (d), 137.8 (d); δ_H 6.89 (1H, s) and 6.36 (1H, s)], and two diasterotopic methylenes linked to a nitrogen atom [δ_H 4.00 (1H, d, J = 15.9 Hz)-4.12 (1H, d, J = 15.9 Hz), δ_C 52.8 and δ_H 3.89 (1H, d, J = 16.9 Hz)-4.15 (1H, d, J = 16.9 Hz), δ_C 46.8]. The remaining signals are at higher field and correspond to four methyls on quaternary carbons, nine methylenes, three methines and three quaternary carbons. Comparison with the NMR spectroscopic data of suvanine clearly indicated that coscinolactam A possesses the same tricyclic spongiane-like framework of suvanine. The enol sulphate functionality at C-13, characteristic of suvanine, was also present, as evidenced by ^{13}C NMR spectroscopic data and by the presence of the diagnostic ^1H NMR signal at δ_H 6.36 relative to H-24.

COSY and HMBC data revealed the linkage of the C-14 to the methylene at C-15 (δ_H 1.47, 1.91, δ_C 23.6) and the allylic methylene C-16 (δ_H 2.22, 2.51, δ_C 25.9).

HMBC correlations of H-18 to C-17 (δ_C 140.5), C-19 (δ_C 52.8) and C-25 (δ_C 173.7) and the chemical shift of C-19 (δ_C 52.8) revealed the presence of an α,β-unsaturated γ-lactam ring. The linkage between C-16 and C-17 was inferred by key HMBC correlation H-18 to C-16, and H_2-16 to C-25. The remaining set of resonances, a methylene (δ_H 3.89 and 4.15, δ_C 46.8) and an acyl carbonyl (δ_C 176.3) was easily assigned to a glycine residue (C-1' to C2'). The linkage of this latter unit to N-25 was evidenced by HMBC correlations H_2-1' to C-19 and C-25 (Figure 12).

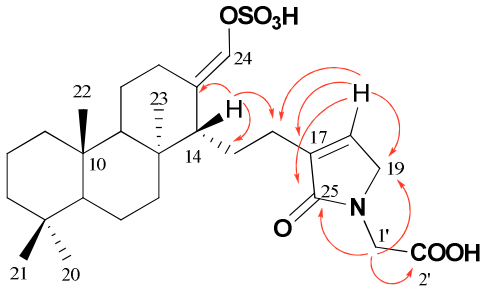

Figure 12. Key HMBC cross peaks detected for coscinolactam A.

The relative stereochemistry of the tricyclic system was determined by NOESY correlations. In particular, intense NOESY cross-peaks between CH_3-22 and CH_3-21, H-12 and H-14 suggested a tricyclic system with a AB *trans*, BC *cis* stereochemistry (Figure 13). The stereochemistry of the exocyclic double bond was established as *E* on the basis of the observed NOE contact between H-24 (δ_H 6.36) and one of the protons belonging to diasterotopic methylene at C-15 (δ_H 1.47). The good match with the ^1H and ^{13}C NMR resonances of coscinolactam A with the corresponding resonances of the tricyclic portion of suvanine indirectly confirmed the proposed structure.

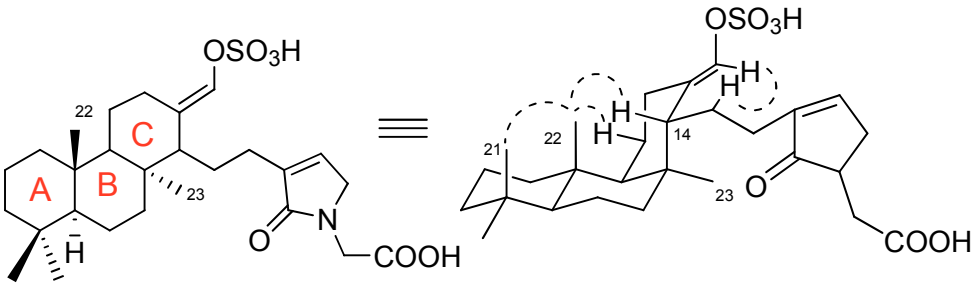

Figure 13. NOESY correlation of coscinolactam A.

3.3 STRUCTURAL DETERMINATION OF COSCINOLACTAM B

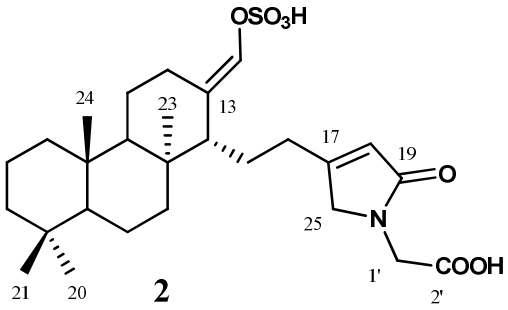

The mass spectrum of coscinolactam B (2) showed the same ion peak of coscinolactam A (*m/z* 522.2509 $[M–H]^-$), suggesting that coscinolactam B was isomeric with coscinolactam A. Also ^1H and ^{13}C NMR spectra of coscinolactam B were very similar to those of coscinolactam A except for the signals relative to the α,β-unsaturated γ-lactam ring.

In particular the upfield shift of the olefinic proton (δ_H 5.85 in coscinolactam B *vs.* 6.89 in coscinolactam A) and the downfield shift of the γ-carbon (δ_C 56.3 in coscinolactam B *vs.* 52.8 in coscinolactam A) suggested the presence of a β-substituted α,β-unsaturated γ-lactam ring. The linkage of the β-carbon of the lactam ring to C-16 was also confirmed by the diagnostic HMBC correlation between H_2-16 and C-25 (Figure 14).

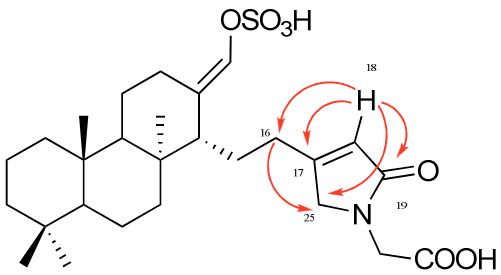

Figure 14. Key HMBC cross peaks detected for coscinolactm B.

Whereas lactam systems are quite unusual in natural products, a similar system consisting of a aminoacyl-derived unit fused with a terpenoid system was found in echinophyllins A and D clerodane diterpenoids from the brazilian medicinal plant *Echinodorus macrophyllus*.[83,84] ^{1}H and ^{13}C NMR spectroscopic data of coscinolactams A and B match very well with those of echinophyllins A and D relative to the isomeric γ-lactam ring subunits. A glycine-derived lactam system was found in spongolactam C, a diterpene derivative isolated from the Okinawan marine sponge *Spongia* sp.[85]

Biogenetically the isomeric coscinolactams A and B may be derived from suvanine, through oxidation to isomeric γ-hydroxybutenolide derivatives, condensation with glycine and reduction to γ-lactam which has been chemically explored in the semisynthesis of spongolactam C from the corresponding furanoterpene (Scheme 4).[85]

Scheme 4. Biogenesis of coscinlactams A and B.

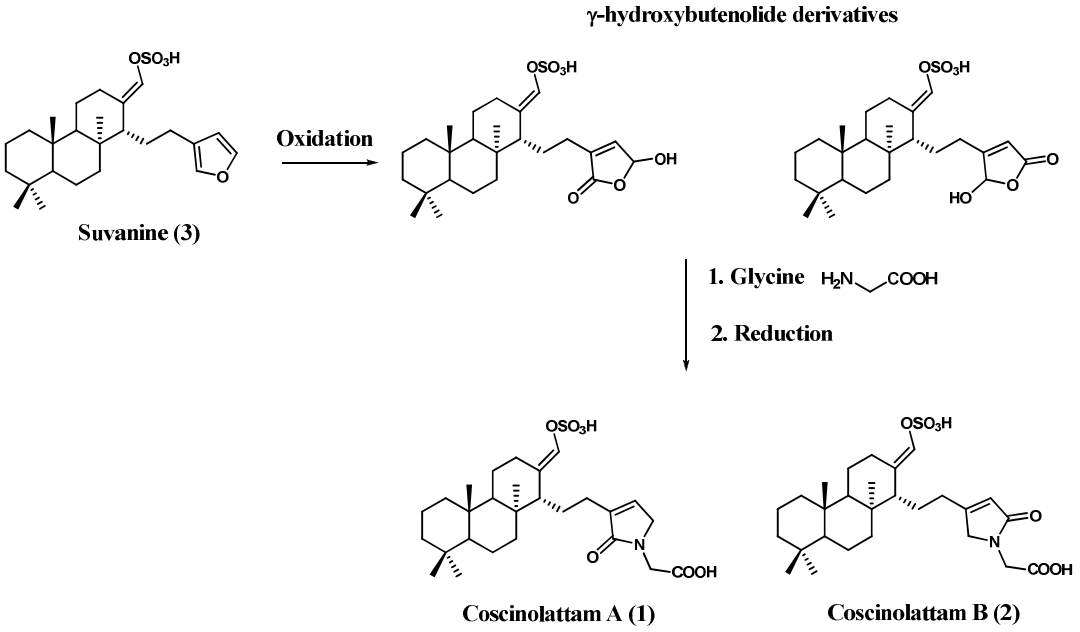

3.4 PHARMACOLOGICAL ACTIVITY

To investigate the role of the sulphate group on the pharmacological profile of these natural compounds, major suvanine was subjected to hydrolytic and reductive transformations, obtaining two semisynthetic derivates depicted in Scheme 5.

Suvanine was desulfated with pyridine and dioxane, obtaining the aldehyde derivate (**4**); this one was reduced with $NaBH_4$ to give the alcohol derivate (**5**).

Scheme 5. a) dioxane-pyridine, 180 °C; b) $NaBH_4$, MeOH, r.t.

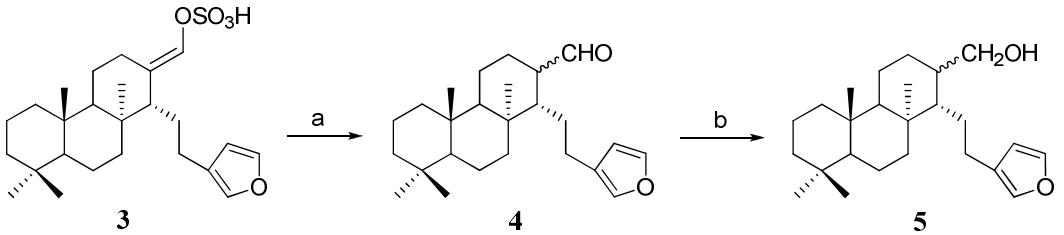

Il coscinolactam A, suvanine and the derivatives **4** and **5** were tested against four different secretory PLA2 belonging to groups IA, IB, IIB and III) (Table 3). LY311727, a well known inhibitor of group IIA sPLA2, was used as a reference tool.[86] Despite the good activity previously exhibited by the crude extract, only suvanine showed a moderate activity against human synovial sPLA2-IIA and bee venom sPLA2-III. In addition, all compounds were devoid of significant cytotoxic effects on RAW 264.7 at concentrations up to 10 mM, as assessed by the mitochondrial-dependent reduction of 3-(4,5-dimethylthiazol-2-yl)-2,5-diphenyltetrazolium bromide (MTT) to formazan (data not shown). Their ability to inhibit PGE2 and NO production on RAW 264.7 cells stimulated with LPS was also investigated (Table 4). Interestingly, the suvanine aldehyde derivative **4** showed an improved capability to inhibit NO production and to a lesser extent PGE2, whereas the suvanine alcoholic derivative **5** was proved to be almost inactive in all experiments. Compound **4** inhibited dose-dependently the production of NO, showing an IC_{50} value of 7.3-2.3 mM. The NO reduction was the consequence of the inhibition of the expression of inducible NO synthase (Figure 14), exactly as the dexamethasone control drug did. This suvanine aldehyde derivative **4**, which can mainly reduce NO and PGE2 production by affecting the expression of the inducible NO synthase enzyme, could be an interesting strategy to obtain promising anti-inflammatory agents.

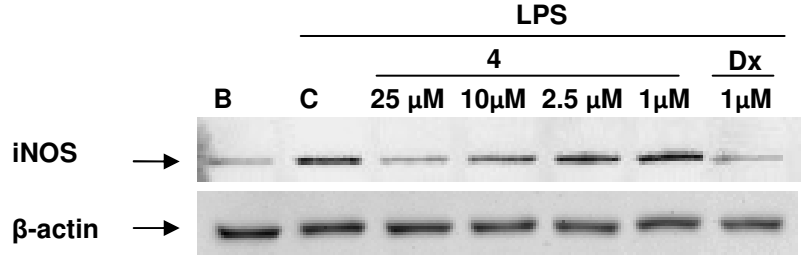

Figure 14. Effect of compound **4** on iNOS expression in LPS-stimulated RAW264.7 cells.
The figure is representative of two similar experiments. B: normal cells. C: LPS-stimulated cells. Dx= Dexamethasone

Table 2. ^{1}H and ^{13}C NMR spectroscopic data (700 MHz, CD_3OD) for coscinolactams A and B.

	Coscinolactam A (1)			Coscinolactam B (2)		
	δ_H[a]	δ_C	HMBC	δ_H[a]	δ_C	HMBC
1	1.86 ovl, 0.87 dd (14.0, 7.4)	43. 2		1.86 ovl, 0.87	43. 1	
2	1.63 ovl, 1.40 ovl	19.7		1.62 ovl, 1.40 ovl	19. 6	
3	1.40 ovl, 1.16 m	43.0		1.40 ovl, 1.16 m	43.0	
4	-	34. 3		-	34.0	
5	1.06 dd (9.0, 4.4)	54. 2	C1, C4, C6, C10, C21,	1.08 dd (11.2, 4.6)	54.1	C1, C4, C6, C21
6	1.54 m, 1.33 ovl	19. 3		1.60 ovl, 1.34 ovl	19. 3	
7	1.90 ovl, 1.33 ovl	36. 3	C5, C6, C8, C9, C23	1.90 ovl, 1.37 ovl	36. 1	
8	-	39. 9		-	39. 7	
9	0.91 t (7.6)	58. 6	C1, C8, C11, C12, C22, C23,	0.92 t (6.0)	58. 3	C1, C8, C11, C12, C22, C23
10	-	40. 2		-	40. 1	
11	1.70 m, 1.61 ovl	20. 9		1.71 m, 1.62 ovl	20. 9	
12	2.60 dt (15.9, 6.1), 2.18 m	25. 4	C9, C11, C13, C14, C24	2.59 m, 2.18 dt (16.2, 8.5)	25. 2	C9, C11, C13, C14, C24
13	-	125. 2		-	124. 9	
14	2.35 d (10.4)	43. 9	C8, C13, C15, C16, C24, C23,	2.33 d (10.4)	43. 9	C8, C13, C15, C16, C23, C24
15	1.91 ovl, 1.47 m	23. 6		1.89 ovl, 1.57 ovl	23. 7	
16	2.51 m, 2.22 m	25. 9	C14, C15, C17, C18, C25	2.62 m, 2.36 dt (16.1, 8.1)	29. 1	C14, C15, C17, C18, C25
17	-	140. 5		-	164. 2	
18	6.89 s	137.8	C16, C17, C19, C25	5.85 s	121. 3	C16, C17, C19, C25
19	4.12 d (15.9), 4.00 d (15.9)	52. 8	C17, C18	-	174.0	
20	0.86 s	33. 7	C3, C4, C5, C21	0.87 s	33. 8	C3, C4, C5, C21
21	0.89 s	22. 2	C3, C4, C5, C20	0.89 s	22.1	C3, C4, C5, C20
22	1.05 s	18. 5	C1, C5, C9, C10	1.05 s	18. 5	C1, C5, C9, C10
23	0.84 s	26. 5	C7, C8, C9, C14	0.86 s	26. 5	C7, C8, C9, C14
24	6.36 s	133. 9	C12, C13, C14	6.27 s	133. 3	C12, C13, C14
25	-	173. 7		4.18 d (16.8)	56.3	C17, C18, C19,
1’	4.15 d (16.9), 3.89 d (16.9)	46. 8	C19, C25, C2’	3.82 d (17.1)	39.5	C19, C25
2’	-	176.03.00		-	n.o	

Ovl: overlapped.
a Coupling constants are in parentheses and given in hertz. ^{1}H and ^{13}C assignments aided by COSY, TOCSY, HSQC and HMBC experiments.

Table 3. Inhibitory activity (% I) of compounds **1**, **3**-**5** at 10 μM on different $sPLA_2$ belonging to the groups IIA, IA (*Naja naja* venom), IB (porcine pancreatic enzyme), and III (bee venom enzyme).

Compound (10 μM)	**GroupIIA-$sPLA_2$ % I**	**GroupIA-$sPLA_2$ % I**	**GroupIB-$sPLA_2$ % I**	**GroupIII-$sPLA_2$ % I**
1	6.7 ± 1.6	0.0 ± 0.0	0.0 ± 0.0	0.0 ± 0.0
3	32.8 ± 1.3**	0.0 ± 0.0	0.0 ± 0.0	29.4 ± 3.0**
4	10.6 ± 5.3	0.0 ± 0.0	0.0 ± 0.0	0.0 ± 0.0
5	7.6 ± 4.0	0.0 ± 0.0	0.0 ± 0.0	0.0 ± 0.0
LY311727	96.3 ± 1.7**	7.9 ± 5.6	36.9 ± 11.0**	2.4 ± 1.8

Results show mean_S.E.M. (n=6). Statistical significances: **p<0.01, with respect to the corresponding enzyme control group (IIA sPLA2=12,129±384 cpm; IA sPLA2=10,973±350 cpm; IB sPLA2¼8008_47 cpm; III sPLA2¼14,854_1054 cpm). Enzyme control group contains the vehicle (ethanol 1%). LY311727 used as control.

Table 4. Inhibitory activity of compounds 1 and 3–5 at 10 μM on the production of PGE2 and NO in LPS-stimulated RAW 264.7 cells

	PGE_2	**NO**
Compound (10 μM)	**% Inhibition**	**% Inhibition**
1	48.5 ± 3.0**	31.8 ± 4.0**
3	41.6 ± 4.6**	21.0 ± 5.7
4	49.2 ± 4.1**	60.0 ± 8.1**
5	14.9 ± 2.1**	31.9 ± 2.8**
Dexamethasone 1 μM	78.7 ± 5.4**	96.6 ± 1.4**

Results show mean_SEM (n=6). Statistical significances: **p<0.01, with respect to the LPS-stimulated control group (contains the vehicle ethanol 1%). PGE2 (non stimulated cells=0.6±0.2 ng/mL; LPS-stimulated cells=16.0±1.6 ng/mL). Nitrite (non-stimulated cells=48.8±3.6 ng/mL; LPS-stimulated cells=414.1±16.4 ng/mL). Dexamethasone used as control.

CHAPTER 4
THEONELLA SWINHOEI

Theonella swinhoei

Sponges of the order Lithistida are an evolutionary ancient lineage that is typically found in deeper waters and caves of tropical oceans. Lithistid sponges have a structurally massive, rigid or "rock-like" morphology. This polyphyletic order is grouped together because their skeletons consist of fused or interlocked spicules, colled desmas.

Over half of the compounds reported for litisthid sponges were isolated from *Theonella* (family Theonellidae). *Theonella* species have been reported to contain a wide variety of diverse secondary metabolites with intriguing structures and promising biological activities, which have been calculated to represent more than nine biosynthetic classes.[87] In particular, *Theonella swinhoei* represents one of the most prolific source of innovative and bioactive metabolites, which include complex polyketides as swinholide A and misakinolide A,[37,38] that had shown a potent cytotoxic activity, disrupting the actine cytoskeleton; tetramic acid glycosides as antifungal aurantosides,[88] innumerable sterols (theonellasterols, swinhosterols).[89,90] Hovewer, among bioactive metabolites found from worldwide collections of *Theonella swinhoei*, surely the peptides represent the most significant group. The diverse array of Theonella derived peptides range from acyclic peptides such as polytheonamides,[91-94] koshikamides A1 and A2;[95,96] cyclic peptides, exemplified by cyclotheonamides,[97,98] kombamide,[99] orbiculamide,[100] keramamides,[101-105] cupolamide,[106] oriamide;[107] large-ring

bicyclic peptides, such as theonellamides[108]; depsipetides headed by theonellapeptolides,[109-111] koshikamides A and B,[112,113] nagahamide;[114] and glycopeptides.[115,116] As for other peptides of marine origin, the most striking feature of these metabolites is the preponderance of non-ribosomial amino acids, including the D configured, N-methylated and alkylated.

The exceptional chemical diversity found in the metabolites of Theonella sponges may in part be due to the biosynthetic capacity of bacteria that they host.[117] This hypothesis has been convincingly supported in the case of swinholide A, omnamides and theopederins. In 2005, Gerwich[118] reported the direct isolation of swinholide A and related derivatives from two different cyanobacteria, thus unequivocally demonstrating that marine cyanobacteria possess the metabolic capacity to produce this skeletal class. As concerning omnamides and theopederins, from the highly complex metagenome of *Theonella swinhoei*, was identified a prokaryotic gene cluster,[119] likely responsible for the biosynthesis of these two metabolites. [120,121]

In the course of a search for novel metabolites from marine sponges belonging to Lithistida order, I had the opportunity to study the sponge *Theonella swinhoei*. The analysis of this sponge afforded to the isolation of new compounds, belonging to different chemical classes. The variety of compounds isolated reaffirms the biological richness of *Theonella swinhoei*, that may be considered a cornucopia of metabolites.

4.1 ISOLATION AND PURIFICATION

A specimen of sponge *Theonella swinhoei* was collected on the barrier reef of Vangunu Island, Solomon Islands, in July 2004.

The samples were frozen immediately after collection and lyophilized to yield 207 g of dry mass. Taxonomic identification was performed by Prof. John Hooper of Queensland Museum, Brisbane, Australia, and reference specimens are on file (R3170) at the ORSTOM Centre of Noumea.

The lyophilized material was extracted with methanol; and the crude methanolic extract was subjected to a modified Kupchan's partitioning procedure (Scheme 6).[2]

The study of the polar extracts afforded the isolation of two new sulphated sterols, solomonsterols A and B, the first example of C-24 and C-23 sulfated sterols from a marine source endowed with a PXR agonistic activity; nine peptides named perthamides C-K, endowed with a potent anti-inflammatory and immunosuppressive activities; other two minor peptides, solomonamides A and B with an interesting anti-inflammatory activity and an unprecedented skeleton.

The chloroform extract gave the cytotoxic macrolide swinholide A together with a minor new structural analogue.

Scheme 6. Modified Kupchan's partitioning methodology applied to the sponge *Theonella swinhoei*.

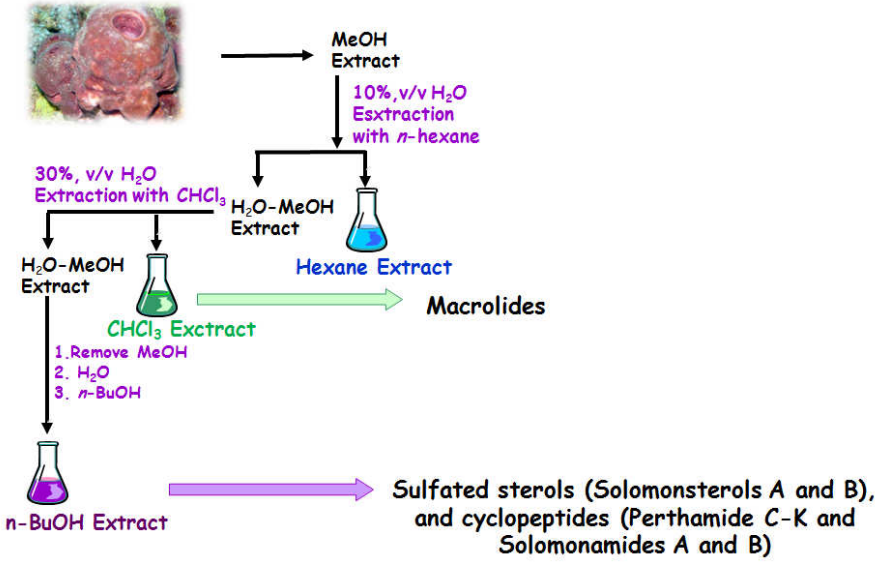

4.2 SOLOMONSTEROLS

The purification of the most polar fractions of *n*-BuOH extract of the sponge afforded two new sulfated sterols with a 5-α-cholane and 24-nor-5-α-cholane skeleton**,** named solomonsterols A and B.

Sulfated steroids are a family of secondary metabolites often found in sponges and echinoderms. Since the isolation of halistanol from *Halichondriidae* sponges,[57] several sulfated polyhydroxysterols have been isolated from sponges. Most of them are characterized by the 2β,3α,6α-tri-*O*-sulfate functions with different pattern of alkylation in the side chain, whereas some show unprecedented structural features.

Recent examples are pregnane ptilosterols from *Ptilocaulis spiculifer*,[122] geodisterol sulfate[123] and iodinated and chlorinated topsentiasterol sulfates[124] from the sponge *Topsentia*, eurysterols[125] from an unclassificated sponge of the genus *Euryspongia*. Steroidal sulphates are of interest not only due to their structures, but also because they often exhibited a variety of biological activities including anti-viral,[126,127] antifungal,[128] antifouling,[129] and action on specific enzymatic targets.[130-133]

4.2.1 Solomonsterol A

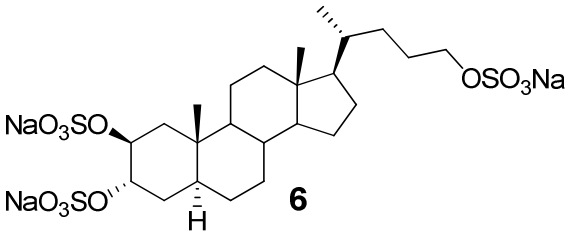

Solomonsterol A (**6**) was isolated as a colourless amorphous solid. The ^{1}H NMR spectrum showed signals typical of a sterol: two upfield Me singlets at δ_H 0.69 and δ_H 1.00 and one methyl doublet at δ_H 0.95 (J = 6.5 Hz). The negative ion HR ESIMS spectrum gave a predominant pseudomolecular ion at m/z 661.1415 [M-Na^+]$^-$ corresponding to a molecular formula of $C_{24}H_{39}Na_3O_{12}S_3$. The ESI and MS/MS spectra showed pseudomolecular and fragment ions compatible with the presence of sulfate groups: 617 (M^- in hydrogen form), 308.3 (double charged species), 559 [M - $NaSO_3$]$^-$, 541 [M -$NaHSO_4$ - Na^+]$^-$, 439 [M - 2$NaHSO_4$ - Na^+]$^-$. ^{1}H and ^{13}C NMR spectra, together with mass data, evidenced the presence in the molecule of two secondary (δ_H 4.74, q, J = 2.9 Hz, δ_C 76.1, CH; δ_H 4.70, q, J = 2.9 Hz, δ_C 75.8, CH) and one primary sulfoxy groups (δ_H 3.96, t, J = 6.6 Hz, δ_C 69.3, CH_2). The location of two secondary sulfoxy groups at C2 and C3 of the steroidal nucleus was determined by interpretation of ^{1}H NMR, COSY, HSQC, and HMBC spectra (Figure 15). In fact, following the spin system -CH_2-CH(O^-)-CH(O^-)-CH_2 the two solfoxy group had to be on C2 and C3.

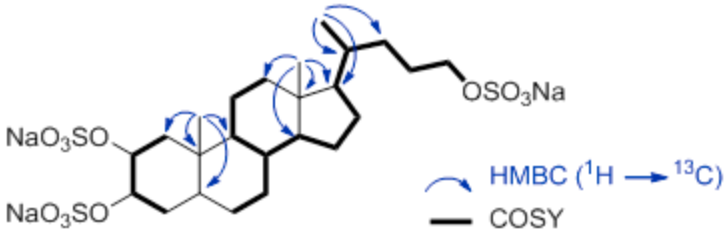

Figure 15. Key skeletal connectivities for solomonsterol A (**1**), as deduced from COSY and HMBC spectra.

The 2β,3α-disulfoxy configuration was assigned on the basis of the coupling pattern of H-2 (q) and H-3 (q). Both signals were observed as "sharp" quartet with a *J*= 2.0 Hz, suggesting the absence of any axial coupling costants (*J*= 10-15 Hz); therefore the H-2 and H-3 were equatorial, and because the rigidity of the steroidal skeleton, the two solfoxy group are axial, 2α,3β .

The tetracyclic steroidal skeleton was considered to adopt an all-*trans* arrangement as evidenced by ROESY analysis (Figure 16). The ROESY correlations observed from H_3-19 and H_3-18 to H-8 and H-11β, from H-5 to H-9 and from H-9 to H-14 indicated the relative configuration for each ring junction to be *trans*. The constitution and configuration of steroidal nucleus was also supported by ^{1}H and ^{13}C NMR data in agreement with those of all-*trans* 2β,3α-disulfoxy steroids reported from sponges[134] and ophiuroids.[135]

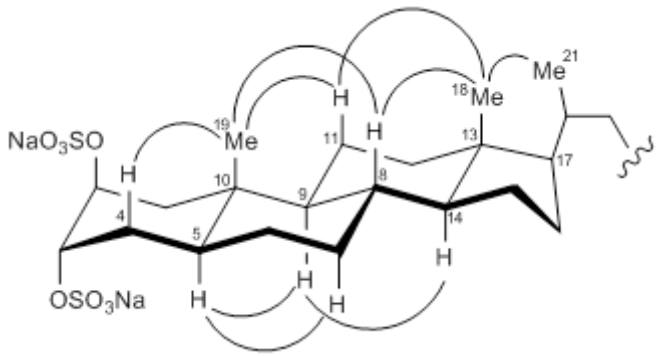

Figure16. ROE correlations supporting the relative configuration of solomonsterol A.

The COSY spectrum revealed useful information concerning the side chain. Starting from the methine proton at δ_H 1.13 (H-17), COSY correlations could be observed to the methine proton at δ_H 1.43 (H-20), which in turn was coupled to both of the methyl protons at δ_H 0.95 (H_3-21) and the methylene protons at δ_H 1.10-1.54 (H_2-22). These latter protons were coupled to the methylene protons at δ_H 1.55-1.75 (H_2-23), which in turn were coupled to the methylene protons at δ_H 3.96 (H_2-24), suggesting a 24-sulfoxy-C24 side chain.

Hence, the new sulfated steroid, solomonsterol A, was established as 5α-cholan-2β,3α,24-tryl-2,3,24-sodium sulphate.

4.2.2 Solomonsterol B

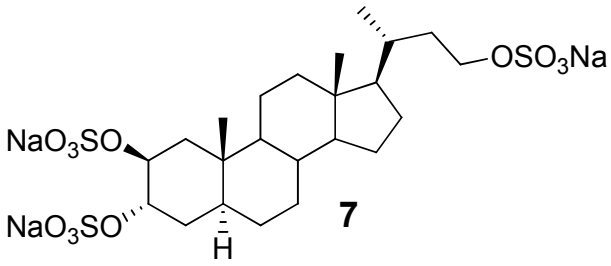

7

The molecular formula of the solomosterol B was established as $C_{23}H_{37}Na_3O_{12}S_3$ through NMR (Table 5) and HR ESIMS data. The analysis of ESIMS, ^{1}H and ^{13}C NMR data suggested a close analogy between solomonsterols A and B. In particular, the resonances relative to the steroid nucleus of solomonsterol B (**7**) were almost superimposable to those of solomonsterol A, indicating a common 2β-3α disulfoxy substitution.

A shortened side chain, also suggested by MS data, was easily determined by the interpretation of 2D NMR spectra. Two downfield signals relative to a diasterotopic carbinol methylene, at δ_H 4.00 and 4.05 observed in the ^{1}H NMR spectrum were assigned to H_2-23 on the basis of key HMBC correlations H_2-23/C20, H_2-22/C23 and H_2-22/C20 (Figure 17). Therefore the structure of new steroid sulfate solomonsterol B was defined as 24-nor-5α-cholan-2β,3α,24-tryl-2,3,23-sodium sulfate.

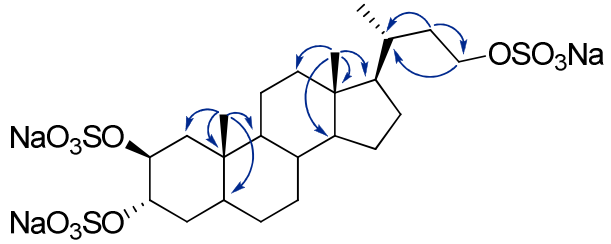

Figure 17. Key HMBC correlations of solomonsterol B.

The tetracyclic steroidal skeleton was considered to adopt an all-*trans* arrangement as evidenced by ROESY analysis, similarly to solomonsterol A.

Few examples of steroidal derivatives with a truncated side chain have been so far reported from marine organisms. They include pregnane derivatives isolated from octocorals,[136-139] and sponges;[140-143] androstanes from a *Cliona* sponge,[144] and ergostane geodisterol, again from a sponge.[145] Whereas bile acid derivatives have been isolated from a bacterium associated to a sponge,[146] in the literature the occurrence of C23 and C22 steroids is limited to 3β-hydroxy-24-norchol-5-en-23-oic acid, isolated from *Euryspongia* n. sp.[147] and to 23,24-dinor-5α-cholane from an *Haliclona* sponge.[140]

4.2.3 Pharmcological activity

Because there is evidence that sponge-derived steroids could be antiinflammatory and several compounds derived from exploitation of marine sponge chemistry are used to treat a variety of human diseases ranging from inflammation to cancer,[148] we have investigated whether solomonsterols A and B exert any effect on cells of innate immunity, the first line and the most ancient line of defence of mammalians against bacteria and viruses.[149] For this purposes RAW264.7 cells, a murine macrophage cell line, were used. In these experiments, cells were incubated with solomonsterols A and B at the concentration of 10 and 50 μM and expression of mRNA encoding for pro-inflammatory mediators measured by Real-Time (RT) polymerase chain reaction (PCR). As illustrated in Figure 18, solomonsterols A and B effectively inhibited induction of the expression of interleukin-(IL)-1β mRNA induced by challenging RAW264.7 cells with lipopolysaccharide (LPS) a tool like receptor (TLR)-4 ligand. At the concentration of 50 μM both compounds reduced the expression of IL-1β mRNA by 50% (Figure 18, panel A; N=4; $P<0.05$

versus LPS alone). In contrast with their effect on IL-1β, both compounds exerted no effect on expression of TNFα (tumor necrosis factor) mRNA (Figure 18, panel B).

At the end of the experiment cell viability was valued using the trypan blue (a diazo dye used to selectively colour dead tissues or cells blue). In fact both compounds had no effect on cell viability measured by the trypan blue excluding test (viability was greater than 95%) excluding that inhibition of IL-1β production was due to a cytotoxic effect.

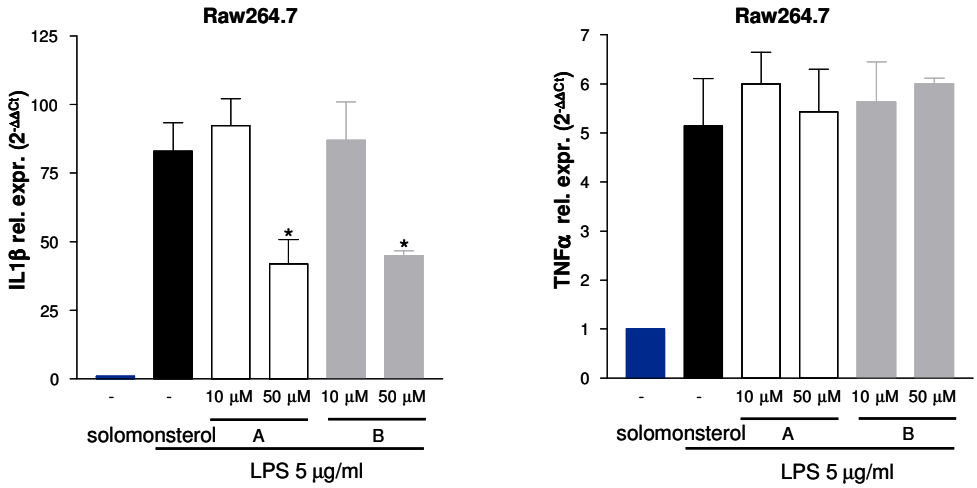

Figure 18. Relative mRNA expression of IL-1β and TNFα in RAW264.7 macrophages treated with LPS alone or with LPS in combination with **1** and **2**.

The pharmacological screening demonstrated that both solomonsterols A and B are endowed with an immunomodulatory potential. Because IL-1β is a key cytokine and high in the hierarchy that drives innate immune response, these results highlight the potential for the use of solomonsterols in clinical conditions characterized by a dysregulation of innate immunity.

4.2.4 PXR agonism

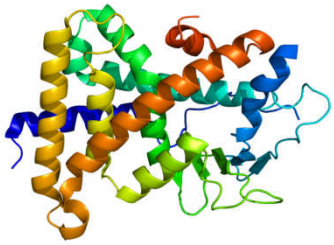

Pregnane-X-receptor

In the search for a molecular target(s) and to identify the mechanism of action of solomonsterols A and B we speculated on the possibility that they could be potential ligands for nuclear receptors. The results of these studies demonstrated that while solomonsterols A and B do not activate the farnesoid-X-receptor (FXR, data not shown), both agents were effective ligands for PXR, an evolutionary conserved nuclear receptor.

PXR (pregnane-X-receptor), also known as NR1I2 (nuclear receptor subfamily 1, group I, member 2), is a master gene orchestrating the expression of a wide family of genes involved in uptake, metabolism and disposal of a number of endo- and xeno-biotics, including drugs, bile acids, steroid hormones and metabolic intermediates in mammalian cells.[149] Following ligand binding, PXR forms an heterodimer with the retinoid-X-receptor (RXR) that binds to specific PXR response elements (PXREs), located in the 5′-flanking regions of PXR target genes, resulting in their transcriptional activation.[150 -152]

PXR is mainly associated with the cellular response to xenobiotics, including induction of enzymes involved in drug oxidation and conjugation, as well as induction of xenobiotic and endobiotic transporters. These include the phase I enzymes such as cytochrome P450, CYP2B6, CYP2B9, CYP2C8, CYP2C9, CYP3A4 and CYP3A7, the phase II enzymes such as the glutathione-*S*-transferases (GSTs), UDP-glucuronosyltransferases (UGTs) and sulfotransferases (SULTs); and the transporters, such as multidrug resistance protein 1 (MDR1), MDR2, multidrug resistance-associated protein 2 (MRP2) and the organic anion transporter polypeptide 2 (OATP2).[151] Rifaximin, a non absorbable antibiotic, is a

human PXR agonist and has been known as an immunosuppressant modulating humoral and cellular immunological responses, and its immunosuppressive role has also been well-documented in humans.[152]

A transactivation experiment was performed in HepG2 cells, a human hepatocarcinoma cell line. To investigate their PXR-activating properties, solomonsterols A and B were tested in a cell based luciferase assay. Since PXR functions as an heterodimer with the retinoid-X-receptor (RXR), HepG2 cells were transfected with a PXR and RXR expressing vectors (pSG5-PXR and pSG5-RXR), with a reporter vector containing the PXR target gene promoter (CYP3A4 gene promoter) cloned upstream of the luciferase gene (pCYP3A4promoter-TKLuc) and with a β-galactosidase expressing vector as internal control of transfection efficiency (pCMV-β-gal). 24 hours post transfection the cells were stimulated 18 hours with the PXR ligand rifaximin 10 μM (as positive internal control) and with 50 μM of solomonsterols A and B**.** 5 μL of cell lysate was incubated with a substrate of luciferase gene (luciferase assay substrate - Promega) and the Relative Luciferase Units (RLU) were measured with the Glomax 20/20 luminometer (Promega). Luciferase activities were normalized for transfection efficiencies by dividing the relative light units by β-galactosidase activity expressed from cotransfected pCMV-βgal plasmid (RLU/β-gal).

As illustrated in Figure 19, both compounds were potent inducers of PXR transactivation boosting the receptor activity by 4-5 folds (n=4; $P<0.05$ versus untreated) and were at least as potent of rifaximin. In addition both agents effectively stimulated the expression of two PXR target genes, CYP3A4 and MDR1 in the same cell line (figure 19 B and C; n=4; $P< 0.05$).

These data indicate that solomonsterols A and B exert immune-modulatory activity and are ligands for the human PXR.

Recent studies have shown that activation of PXR ameliorates inflammation in rodent models of inflammatory bowel disease via inhibition of the expression of NF-kB target gene and a recent report identified PXR as a gene strongly associated with the susceptibility to inflammatory bowel diseases in humans, highlighting a possible role of solomonsterols in counter-regulating dysregulated immunity in human diseases.[153]

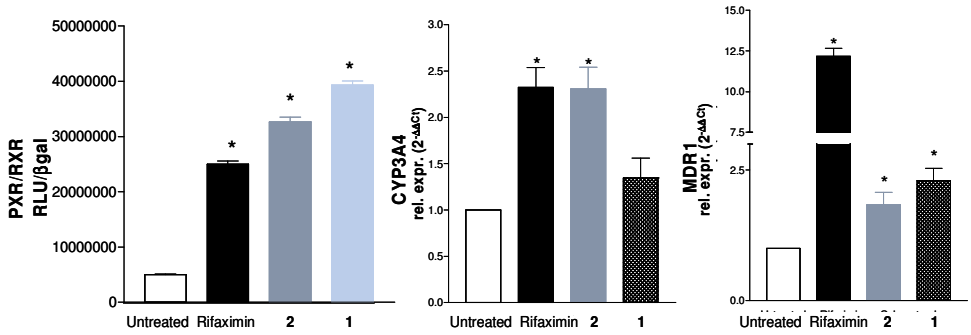

Figure 19. *Panel A*. Transactivation of PXR by compounds 1 and 2 in HepG2 cells. *Panel B and C*. Compounds 1 and 2 effectively increased the expression of CYP3A4 and MDR1, two PXR regulated genes in HepG2 cells. Expression of target genes was measured by RT-PCR.

4.2.5 Docking studies

To have details for what concerns the binding mode of solomonsterols A and B to PXR at atomic level, molecular docking studies were performed on **1** with PXR using Autodock Vina 1.0.3 software.[154] The docking results positioned solomonsterol A within the PXR binding pocket, and among the 9 docked conformations generated, the lowest binding energy displayed an affinity of -10.0 Kcal/mol (Figure 20). In this model, the steroidal nucleus shows hydrophobic interactions with LEU206, LEU209, VAL211, ILE236, LEU239, LEU240, MET243, MET246, confirming the binding mode already reported for a set of analogous compounds.[155] Moreover, the sulfate groups exert hydrogen bonds with

SER247 (3-*O*-sulfate), HIS407 (2-*O*sulfate), and LYS210 (24-*O*-sulfate, also protruding toward the solvent), providing the complex with an increased predicted stability fully compatible with the experimental biological assays.

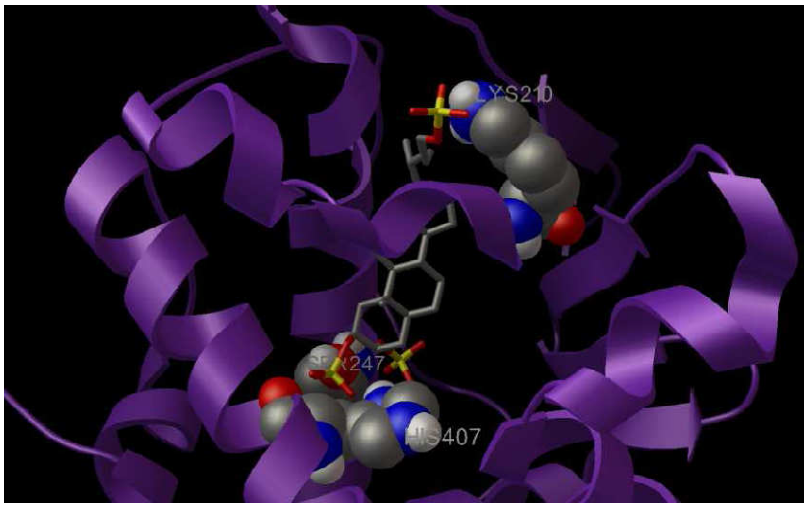

Figure 20. Docked model of solomonterol A bound to PXR model (pdb code: 1M13, displayed as purple ribbon); solomonsterol A is displayed as sticks coloured by atom type, while HIS407, SER247, and LYS210 are depicted as atom type coloured CPK models.

In conclusion, solomonsterols A and B are a novel class of PXR agonsts, isolated from *Theonella swinhoei*; such compounds could be potentially used for the treatment of human disorders characterized by dysregulation of innate immunity and with inflammation, and, in light of our molecular modelling results, they can inspire the synthesis of new compounds able to target PXR. Furthermore the discovery of solomonsterols provides insight into the mechanism of ligand recognition by PXR and reaffirms the utility of examining natural product libraries for identifying novel receptor ligands.

Table 5. ^{1}H and ^{13}C NMR spectroscopic data (700 MHz, CD_3OD) for solomonsterols A and B.

	solomonsterol A (**1**)		solomonsterol B (**2**)	
position	δ_c, mult.	δ_H (*J* in Hz)	δ_C, mult.	δ_H (*J* in Hz)
1α	38.8, CH_2	1.40, ovl	38.8, CH_2	1.40, ovl
1β		2.10 br, dd (14.4, 2.9)		2.10, br dd (14.4, 2.9)
2	76.1, CH	4.74, q (2.9)	76.0, CH	4.73, q (2.9)
3	75.8, CH	4.70, q (2.9)	75.7, CH	4.70, q (2.9)
4α	30.1, CH_2	1.63, ovl	30.1, CH_2	1.63, ovl
4β		1.81, dt (13.0, 2.9)		1.80,dt (14.1, 2.9)
5	39.9, CH	1.60, ovl	39.9, CH	1.60, ovl
6α	28.8, CH_2	1.27, m	28.9, CH_2	1.25, m
6β		1.29, m		1.29, ovl
7α	32.9, CH_2	1.68, m	32.9, CH_2	1.68, m
7β		0.95, m		0.94, m
8	36.3, CH	1.44, ovl	35.9, CH	1.42, ovl
9	56.2, CH	0.71, m	56.1, CH	0.72, m
10	36.3, C	-	36.1, C	-
11α	21.7, CH_2	1.53, ovl	21.9, CH_2	1.53, m
11β		1.33, ovl		1.33, ovl
12α	41.1, CH_2	1.15, m	41.2, CH_2	1.15, m
12β		2.00, dt (12.6, 2.9)		2.01, dt (12.6, 3.2)
13	43.5, C	-	43.7, C	-
14	57.5, CH	1.04, m	57.6, CH	1.04, m
15α	24.9, CH_2	1.59, ovl	24.9, CH_2	1.60, ovl
15β		1.07, m		1.07, m
16α	28.9, CH_2	1.87, m	28.8, CH_2	1.88, ovl
16β		1.30, ovl		1.31, ovl
17	57.3, CH	1.13, m	57.6, CH	1.13, m
18	12.2, CH_3	0.69, s	12.2, CH_3	0.70, s
19	14.1, CH_3	1.00, s	14.2, CH_3	1.00, s
20	36.6, CH	1.43, ovl	33.9, CH	1.59, ovl
21	18.7, CH_3	0.95, d (6.5)	18.9, CH_3	0.98, d (6.5)
22	32.8, CH_2	1.10, m 1.54, ovl	36.2, CH_2	1.29, ovl 1.87, ovl
23	26.9, CH_2	1.55, ovl 1.75, m	66.9, CH_2	4.00, m 4.05, m
24	69.3, CH_2	3.96, t (6.6)		

4.3 THE FAMILY OF PERTHAMIDES

Pursuing the study of the polar n-BuOH extract of *Theonella swinhoei* some new cyclic peptides were isolated. They are 8-residue cyclic peptides related to perthamide B, a cytotoxic peptide isolated from an Australian collection of a *Theonella swinhoei* sponge,[156] which we named perthamides C-K. Their structures were determined using extensive 2D NMR, ESI-MS/MS experiments; and stereochemical determination of conventional and unusual amino acid units was based on an integrated approach which combined NMR methods, stereoselective synthesis, chemical degradation and LC/MS analysis.

Perthamide C is the major component of the buthanol extract of the sponge, isolated on gram scale (1.2 g).[157] From a chemical point of view, it is characterized by a 25-membered structure with several non conventional amino acids. The other perthamides isolated from this sponge are correlated to perthamide C and differ in the amino acid residues.

4.3.1 Perhamide C

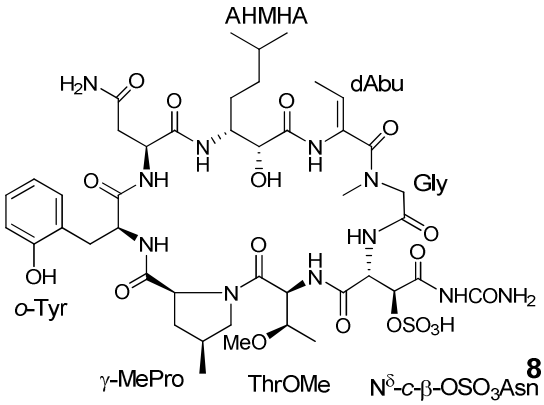

8

The HR-ESIMS spectrum of perthamide C (**8**) showed a pseudomolecular ion peak at *m/z* 1066.4106 $[M-H]^-$, corresponding to a molecular formula of $C_{44}H_{65}N_{11}O_{18}S$; when we run the mass spectrum in positive ion mode we observed that the pseudomolecular ion peak was absent and the major observed

ion peak at *m/z* 945.4652 $[M + H]^+$ was due to the loss, in source, of both the sulphate and the carbamoyl groups.

The ^{1}H NMR spectrum in DMSO-d_6 showed signals ascribable to exchangeable NH protons from δ_H 6.00 to 9.02, a signal corresponding to a methyl amide at δ_H 2.71 (3H, s), suggesting a peptidic structure for perthamide C, confirmed by the presence of acyl carbons (δ_C 167.1-172.5) in the ^{13}C NMR spectrum.

Extensive analysis of the ^{1}H and ^{13}C NMR data of perthamide C, including ^{1}H-^{1}H COSY, HSQC, HMBC spectra (Table 6), by comparison with those of perthamide B, established the presence of the 2-amino-2-butenoic acid (dAbu), *O*-methylthreonine (ThrOMe), and γ-methylproline (γMePro), along with one *N*-methylglycine and one asparagine residue (figure 21).

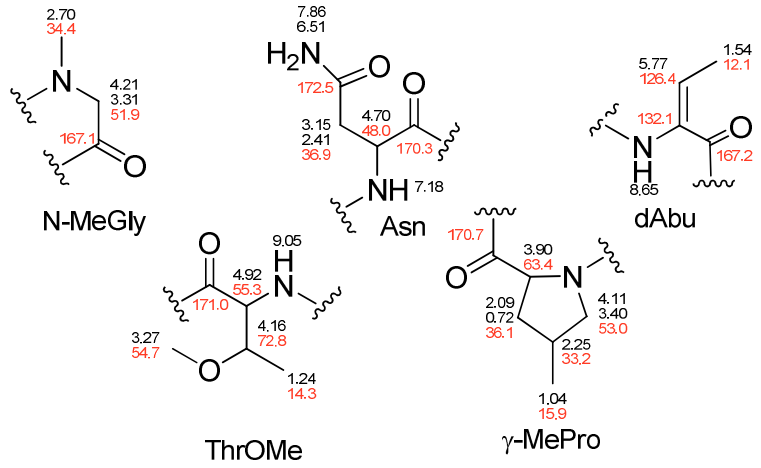

Figure 21. N-MeGly, Asn, dAbu, ThrOMe, γ-MePro units in perthamide C.

The ^{1}H NMR spectra also suggested the presence of a *o*-substituted phenolic ring, a downfield pair of doublets at δ_H 7.16 (1H, d, J = 7.4 Hz) and 6.88 (1H, d, J = 7.8 Hz) together with a downfield pair of triplets at δ_H 7.11 (1H, t, J = 7.8 Hz) and 6.80 (1H, t, J = 7.4 Hz), that on the basis of HMBC data was assigned to an *o*-tyrosine subunit. In particular diagnostic HMBC correlations are from the α-amino acyl proton at δ_H 4.12 (H-2*o*-Tyr) to the carbon resonances at δ_C 170.6 (C-1

o-Tyr) and 124.0 (C-1' *o*-Tyr), and from the β-methylene protons at δ_H 2.95 and 2.86 (H_2-3 *o*-Tyr) to the carbon resonances at δ_C 170.6, 124.0, 154.4 (C-2' *o*-Tyr), and 130.3 (C-6' *o*-Tyr), and from the exchangeable proton OH at δ_H 10.2 to the C-2' *o*-Tyr and C-1' *o*-Tyr (Figure 22).

o-Tyrosine is well known as product of the oxidation of phenylalanine residue in proteins and is reported to be an endogenous biomarker of oxidative damage.[158,159] To the best of our knowledge this residue is unprecedented in marine natural products.

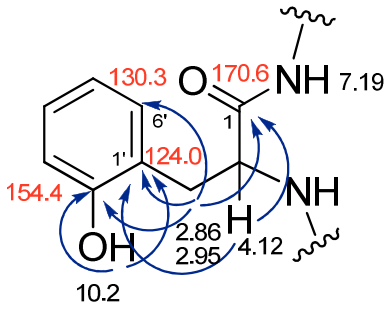

Figure 22. Key HMBC correlations of *o*-Tyr unit of pethamide C.

A spin system was identified as the unusual amino acid residue 3-amino-2-hydroxy-6-methylheptanoic acid (AHMHA) which is also unprecedented in natural peptides. The complete spin system was easily inferred from COSY and TOCSY data. An acyl group was placed at C1 on the basis of HMBC cross peak between the hydroxymethine proton at C2 (δ_H 4.14) with a carbonyl at δ 169.7 ppm (Figure 23).

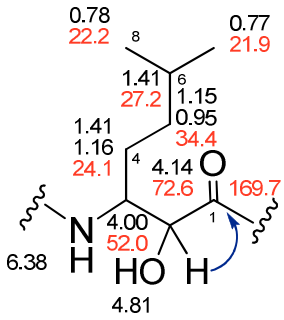

Figure 23. *AHMHA* residue in pethamide C.

The remaining spin system corresponded to a modified β-hydroxyasparagine (β-OHAsn) unit (Figure 24). However this residue bore a sole downfield NH-4 proton at δ_H 8.90 (1H, s) that suggested substitution of the N^{δ} atom. Although no HMBC correlations were observed for this exchangeable proton; correlations with

an unassigned pair of NH_2 protons at δ 7.51 (1H, br s) and 7.31 (1H, br s) were observed in TOCSY and ROESY experiments. Together with the loss of 59 Da in the MS/MS spectrum, these data supported addition of a carbamoyl moiety[160] linked to the δ-amide of β-OHAsn. Finally sulfation of the β-hydroxyl group was apparent from the downfield chemical shifts of the hydroxymethine signal (δ_H 4.59, δC 74.9). This appears to be the first example where a β-OHAsn residue is further modified by an N^{δ}-carbamoyl moiety and *O*-sulfation (N^{δ}-c-β-OSO_3Asn).

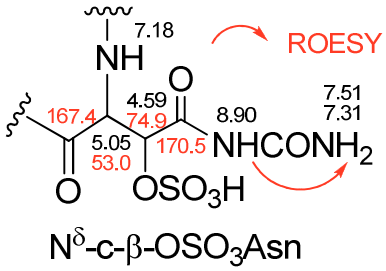

Figure 24. N^{δ}-c-β-OSO_3Asn unit in perthamide C.

The complete cyclic amino acid sequence of perthamide C was secured from the inter-residue NOE NH/CHα and NCH_3/CHα interactions and HMBC correlations acquired in DMSO-d_6 (Figure 25). Particularly long-range correlations between NH/NCH_3 protons to carbonyl carbons of adjacent amino acids allowed us to establish the following sequences: AHMHA-Asn-*o*Tyr-γMePro-ThrOMe-N^{δ}-c-β-OSO_3Asn and NMeGly-dAbu. Moreover, connectivity of the N^{δ}-c-β-OSO_3Asn unit to NMeGly residue was indicated from an ROESY correlation between exchangeable amidic proton NH^{β} of N^{δ}-c-β-OSO_3Asn (δ_H 7.18) and one of the γMePro-δ-methylene protons (δ_H 4.23). The ROESY cross peak between the NH at δ_H 8.65 of dAbu unit with the hydroxymethine proton at δ_H 4.14 of AHMHA suggested the connectivity of the dAbu residue to β-amino-α-hydroxy-amino acid unit.

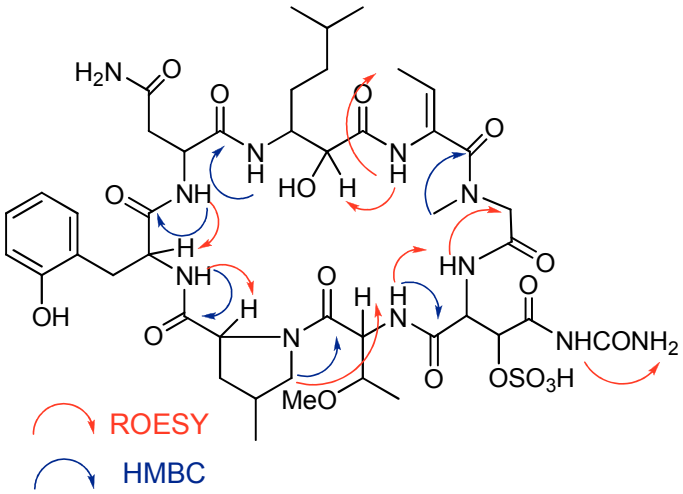

Figure 25. Inter residue ROESY (red) and HMBC (blue) correlations of perthamide C.

This sequence was consistent with the fragmentation pattern obtained from ESI-MS/MS experiments. In addition to the major ion peak at *m/z* 945.81 $[M + H]^+$, the ESI Q-TOF MS/MS spectrum provided several fragment ion peaks. The detailed interpretation of the fragmentation pattern confirmed the sequence of amino acids. In the first instance, the pseudomolecular ion lossed the sulphate group and the carbamoyl moiety. The major peaks corresponded also to *C*-terminus fragments derived from a homogeneous ring opening between the dehydrated threonine (dAbu) and the *N*-methylglicine residue.

In particular, the signal at *m/z* 744.55 corresponding to the loss of 201.26 uma from the major ion was indicative of the presence of *N*-methylglicine and β-hydroxy aspartic acid residues. Subsequently, the loss of 114.99 amu from the pseudo ion was attributed to the lack of ThrOMe (*m/z* at 629.56) residue, and the further losses of 111.30 from pseudo ion and 163.07 uma from pseudo ion were indicative of the presence of γ-methylproline and *o*-tyrosine.

Besides, several internal fragments have been detected; the peak at 275.21 uma has been attributed to the dipeptide unit γ-methylproline/*o*-tyrosine; the fragment at 389.30 uma was ascribed to the tripeptide γMePrO-*o*-Tyr-Asn and the peak at

546.51 to the previous tripeptide increased by AHMHA unit. Finally, the peak at 629.88 uma supported the presence of the dAbu residue.

At this point it was evident that the amino acid sequence of perthamide C was related to that perthamide B. These two peptides differed by three residues, where perthamide B contained *m*-bromotyrosine, β-hydroxyasparagine, and 3-amino-2-hydroxy-6-methyloctanoic acid residues, versus perthamide C that contained *o*-Tyr, N^{δ}-c-β-OSO_3Asn, and AHMHA residues.

Once the planar structure was established, the next step was the determination of the configurations of the chiral centers, that were secured through an integrated multiparametric approach which combined NMR analysis, chemical degradation, stereoselective synthesis and LC/MS analysis.

The absolute stereochemistry of the sole ribosomial amino acid residue (Asn) was determined by complete acid hydrolysis of perthamide C and Marfey's analysis, establishing the presence of L-Asn.

The Marfey's method was used also to determinate the absolute stereochemistry of ThrOMe residue. The two possible diastereoisomeric ThrOMe standards have been already prepared in our laboratory by etherification of suitable protected L-Thr and L-*allo*Thr.[161] The Marfey's analysis revealed the L-configuration for ThrOMe.

A NOE between the NH (δ 8.65) and vinyl methyl (δ 1.54) signals established a *Z* geometry for the dAbu residue (Figure 26).

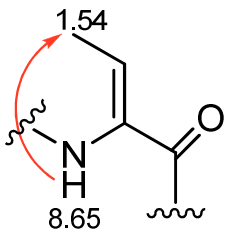

Figure 26. NOE correlation in dAbu unit.

The relative configuration of γ-methylproline was determined on the isolated amino acid residue obtained by acidic hydrolysis of the parent peptide followed by HPLC separation.

Recently a stereoselective access to all stereoisomers of γ-methylproline residue has been published together with relevant physical data.[162] The two diastereoisomers can be differentiated on the basis of ^{1}H NMR data in CD_3OD. Particular diagnostic are the chemical shifts of H-3 diasterotopic methylene protons observed at δ_H 2.52 and 1.64 in the *cis* isomer and at δ_H 1.94 and 2.25-2.38 in the *trans* isomer, and the coupling constant pattern of one of the H-5 protons observed as a broad triplet (δ_H 2.87, *J* 10.6) in the *cis* isomer and as double doublet (δ_H 2.83, *J* 11.5 and 8.6 Hz) in the *trans* isomer (Figure 27).

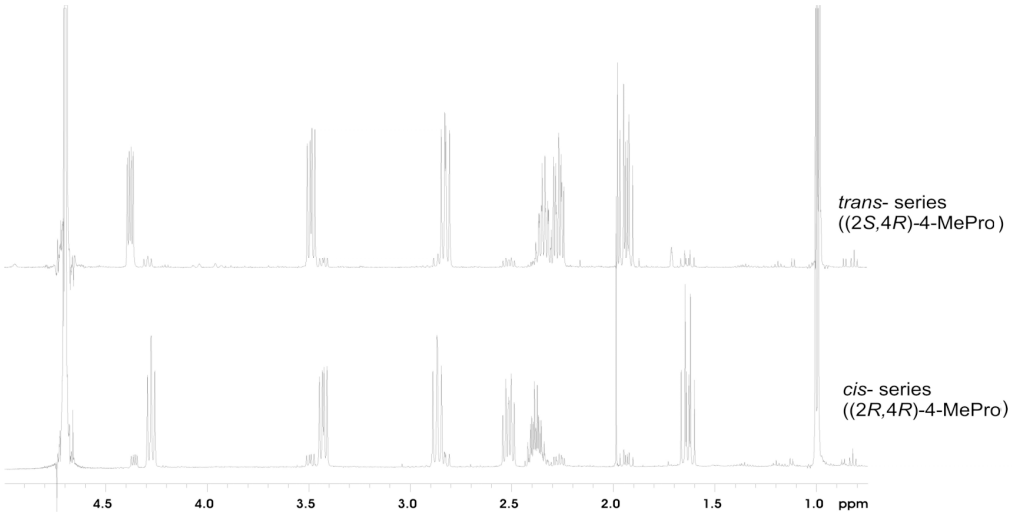

Figure 27. ^{1}H NMR (500 MHz, D_2O) spectra of the two diastomeric 4-methylproline hydrochloride standards by synthesis.

The ^{1}H NMR spectral data of γ-methylproline isolated from parent perthamide C are consistent with the *cis* stereochemistry (Figure 28).

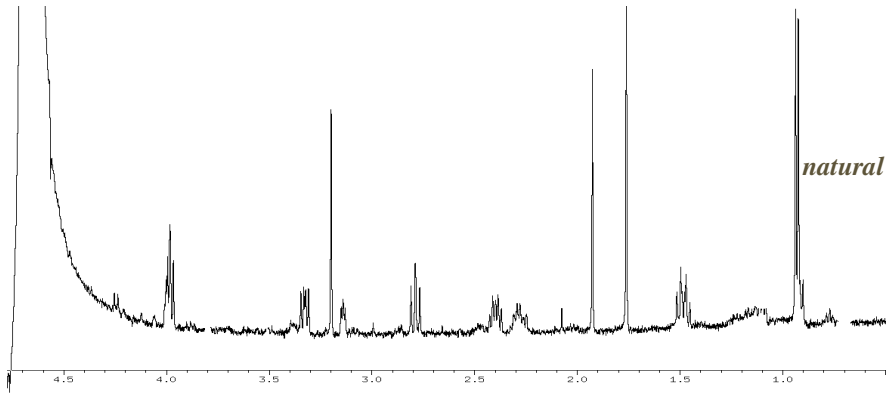

olated from

The absolute configuration of the γ-methylproline residue was determined by application of the advanced Marfey's method.[27] The Marfey's derivatives of all stereoisomers of γ-methylproline has been prepared and characterized, and it was found that they follow the usual elution order, namely the L-amino acid FDAA derivative is eluted from a C-18 column before its corresponding D-isomer.[162] Thus a small sample of perthamide C was hydrolysed and derivatised with both enantiomers of the Marfey's reagent. By monitoring for FDAA-γ-methylproline at *m/z* 382, the 2S configuration was assigned, therefore we assign the *cis*-4-methyl-L-proline stereostucture to this subunit.

The absolute configuration of the new *o*-Tyr residue was assigned after transformation of the residue, isolated from the acidic hydrolysis of perthamide C followed by HPLC separation, to aspartate by ozonolysis followed by oxidative work-up (Figure 29). The presence of a peak corresponding to L-Asp was observed by ion-selective monitoring for FDAA-Asp (*m/z* 386) indicating that *o*-Tyr had a L-configuration.

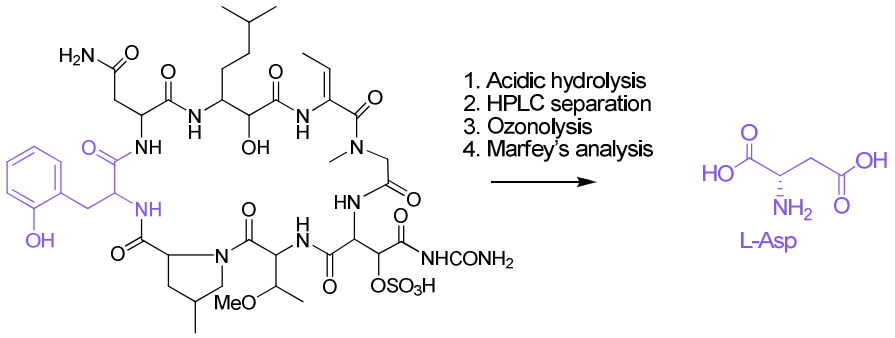

Figure 29. Determination of absolute stereochemistry of *o*-Tyr unit in perthamide C.

To determine the relative configuration of N^{δ}-c-β-OSO_3Asn was used *J*-based NMR configurational analysis method (Figure 30). A small coupling constant between H-2 and H-3 (1.0 Hz) suggested that they were gauche. H-2 exhibited a small ^{3}J coupling constant with C-4 and a small ^{2}J coupling constant with C3, whereas H-3 displayed a large ^{2}J coupling constant with C-2 supported an *anti* relative configuration.

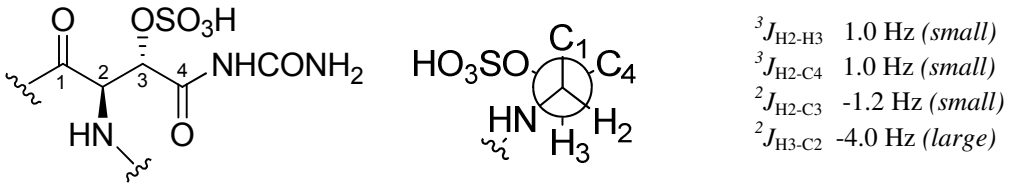

Figure 30. Relative configuration for N^{δ}-c-β-OSO_3Asn residues in perthamide C.

Because the acidic hydrolysis of perthamide C to obtain this residue afforded β-hydroxy aspartate, to support the assignment of the relative configuration and to assign the absolute stereochemistry, all stereoisomers of β-hydroxy aspartate were prepared by ozonolysis of the corresponding β-hydroxy-phenylalanine stereoisomers (Figure 31).[163] The so obtained β-hydroxy aspartatic acids were used as standards in the Marfey's analysis, that evidenced the presence of (2*R*,3*S*)-N^{δ}-c-β-OSO_3Asn residue in perthamide C.

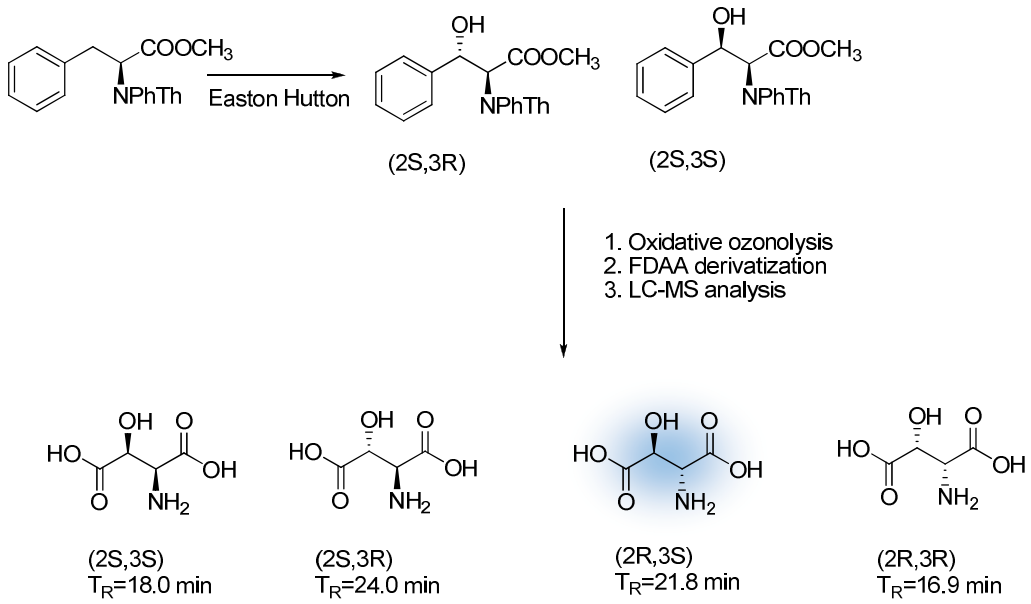

Figure 31. Synthesis of all steroisomers β-OHAsn and t_R in LC/MS

The remaining stereochemical uncertainty of perthamide C concerns the configuration of the two stereogenic centres in the AHMHA unit. We tentatively proposed a *threo* relative disposition of the hydroxyl and the amino group on the α and β-position, respectively, on the basis of the *J* coupling analysis. A small coupling constant between H-2 and H-3 (0.8 Hz) suggested that they were gauche. H-2 exhibited a small ^3J coupling constant with C-4, and H-3 displayed a small ^3J coupling constant with C-1, indicating that H-2/C-4 and H-3/C-1 were gauche, pointing for a *threo* configuration.

The issue of stereochemistries of AHMHA residue was unambiguously solved in a parallel study by my research group.[164] All steroisomers were prepared by asymmetric synthesis, and the (2R,3R) configuration for the AHMHA residue was established by comparison of spectral data and by pre-column derivatition method (Marfey's analysis).

4.3.2 Perthamide D

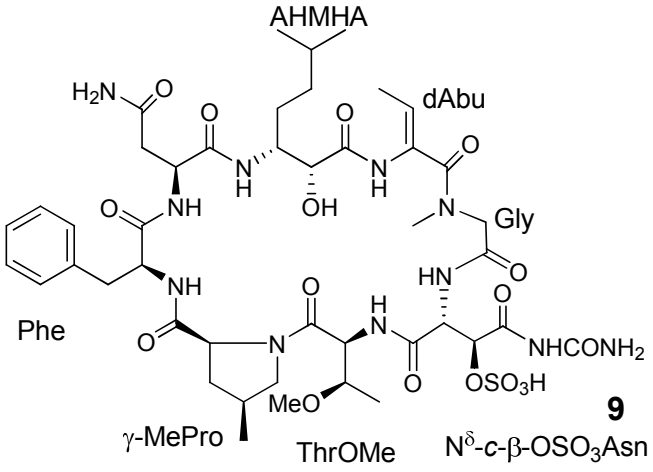

The HR-ESIMS of perthamide D (**9**) showed a major ion peak at *m/z* 1050.4302 $[M-H]^-$ corresponding to a molecular formula of $C_{44}H_{65}N_{11}O_{17}S$, that was 16 mass units (one oxygen atom) smaller than that of perthamide C (**8**). The ^1H NMR spectrum is very similar to that of perthamide C, suggesting it is an analogue of the major cyclopeptide. This spectrum clearly evidenced the presence of a monosubstituted phenyl ring and the lack of a downfield exchangeable phenolyc proton, suggesting the replacement of *o*-tyrosine residue in perthamide D with a phenylalanine residue (Figure 32).

Interpretation of 2D NMR data, including COSY, HSQC, HMBC and ROESY data led to the planar structure of perthamide D, that is almost superimposable with that of perthamide C.

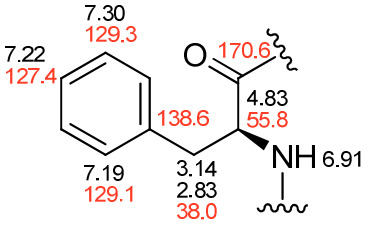

Figure 32. Phe unit in perthamide D.

The complete agreement of chemical shifts and coupling constant patterns of γ-methylproline and dAbu residues suggested the same relative configuration. Application of the Marfey's method enable us to determine the chirality of the residue as L-Asn, L-Phe, L-ThrOMe and (2*R*,3*S*)- N^{δ}-c-β-OSO_3Asn.

4.3.3 Perthamide E and its analogue perthamide F

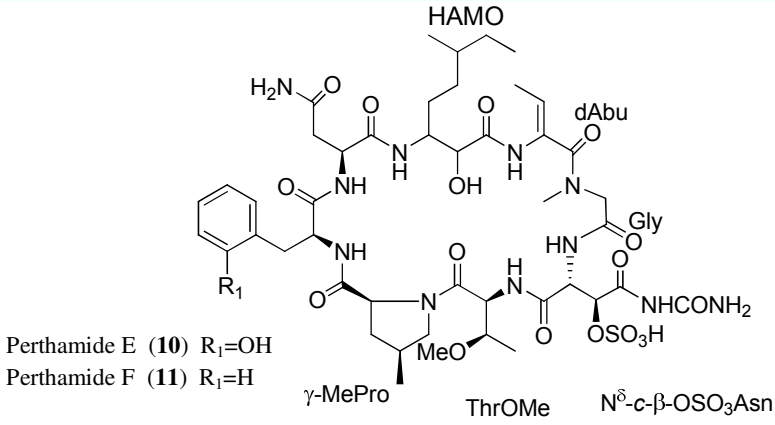

Perthamide E (**10**) R_1=OH
Perthamide F (**11**) R_1=H

The structural analysis of perthamide E (**10**) began with the HR-ESIMS *m/z* 1080.4394 $[M-H]^-$ corresponding to a molecular formula of $C_{45}H_{67}N_{11}O_{18}S$. Compared with the molecular formula of perthamide C, there was the gain of 14 u.m.a., as well as one additional methylene group. ^{1}H NMR spectra indicated that perthamide E differed to perthamide C in the AHMHA unit. This spectrum showed the presence of two additional methylene proton signals at δ_H 1.03 and 1.22 and the two methyl group were found slightly shifted at δ_H 0.76 and 0.74 (0.77 and 0.78 in perthamide C).

As inferred from a careful analysis of COSY, HSQC and HMBC spectra, the resonances relative to other portion of the molecule were almost superimposable with that found in the perthamide C (Table 6).

As regards the modified residue, the analysis of bidimensional NMR experiments indicated that perthamide E possessed a residue of 3-hydroxy-3-amino-6-methyloctanoic acid (HAMO) rather than AHMHA. The complete spin system of this residue was easily assigned by the analysis of the COSY, TOCSY and HMBC spectra (Figure 33).

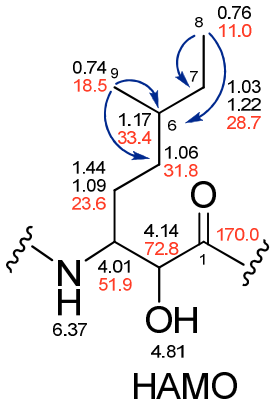

Figure 33. *HAMO* unit in pethamide E.

The peptidic sequence of perthamide E and the placement of HAMO unit were assigned from the analysis of HMBC and ROESY correlations reported in Figure 34 and was superimposable to perthamide C.

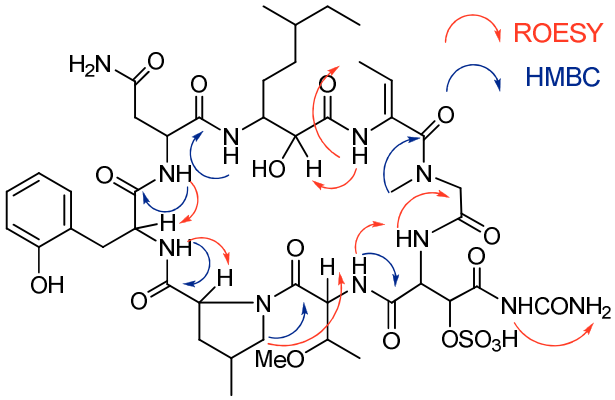

Figure 34. Inter residue ROESY (red) and HMBC (blue) correlations of perthamide *E*.

The determination of stereochemistry of HAMO unit, that presents an additional chiral center compared to AHMHA unit in perthamide C, is currently in progress in our laboratory. The complete agreement of chemical shifts and coupling constant patterns of remaining amino acid residues suggest the same relative configurations than perthamide C.

The molecular formula of perthamide F (**11**), $C_{45}H_{67}N_{11}O_{17}S$, was deduced by HR-ESIMS, *m/z* 1064.4473 $[M-H]^-$. The NMR data suggested that this compound had the HAMO residue, like perthamide E; in fact, the spectra of perthamide F were almost superimposable with the corresponding signals in perthamide E, except for the aromatic ring. The mass data indicated that perthamide F was 16 u.m.a. (one atom of oxygen) smaller than perthamide E. The ^1H NMR spectrum showed the presence of a monosubstituted phenyl ring, confirmed also by the lack of a downfield exchangeable phenolyc proton, suggesting the replacement of *o*-tyrosine residue in perthamide F with a phenylalanine residue (Figure 35).

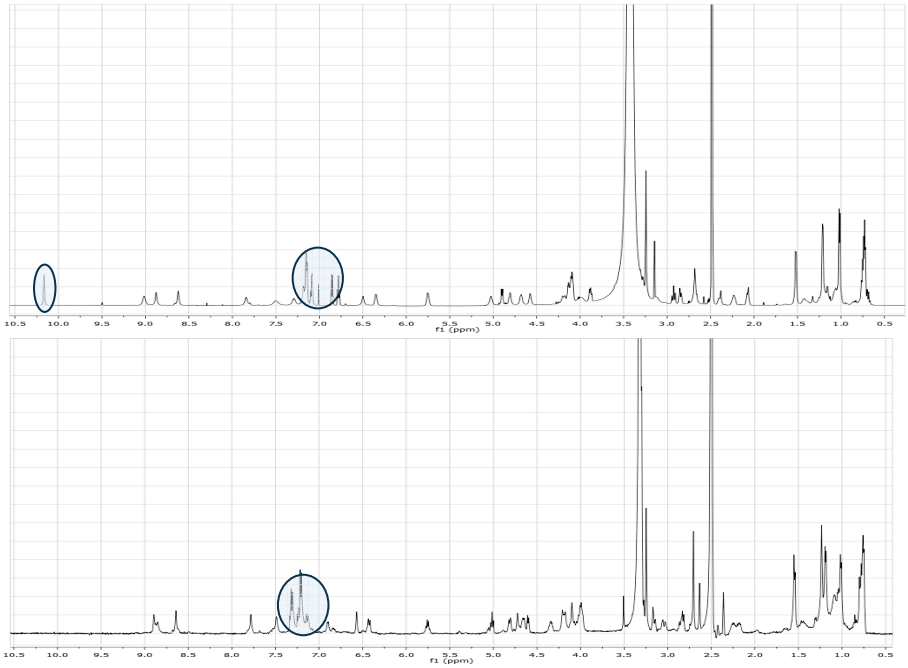

Figure 35. Comparison of ^{1}H NMR spectra of perthamides E and F.

4.3.4 Perthamide G

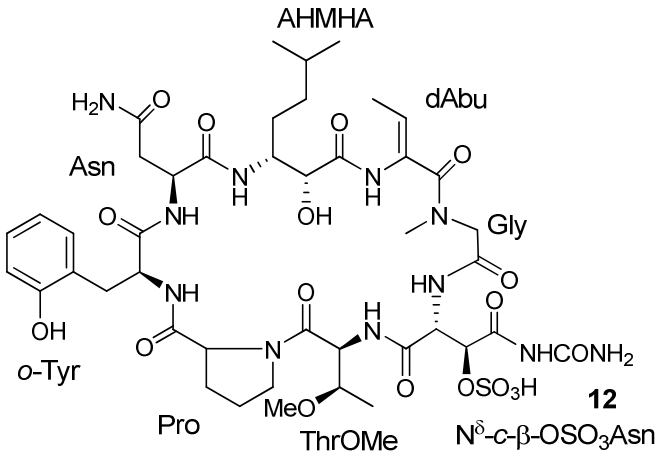

The HR-ESIMS spectrum of perthamide G (**12**) showed a major ion peak at *m/z* 1052.4237 $[M-H]^-$ corresponding to a molecular formula of $C_{43}H_{63}N_{11}O_{18}S$, that was 14 u.m.a. smaller than that of perthamide C (**8**).

^{1}H NMR spectrum suggested that perthamide I differed from perthamide C in the γ-MePro unit. This spectrum showed just few differecences, includig the absence of the methyl group at δ_H 1.04 and the presence of two additional methylene proton signals at δ_H 1.84 and δ_H 1.93, suggesting the replacement of a γ-MePro unit with Pro unit (Figures 36 and 37).

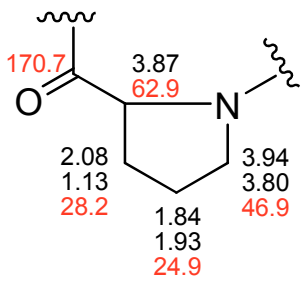

Figure 36. Pro unit in perthamide G.

The peptidic sequence of perthamide E and placement of Pro residue were assigned from the analysis of HMBC and ROESY correlations.

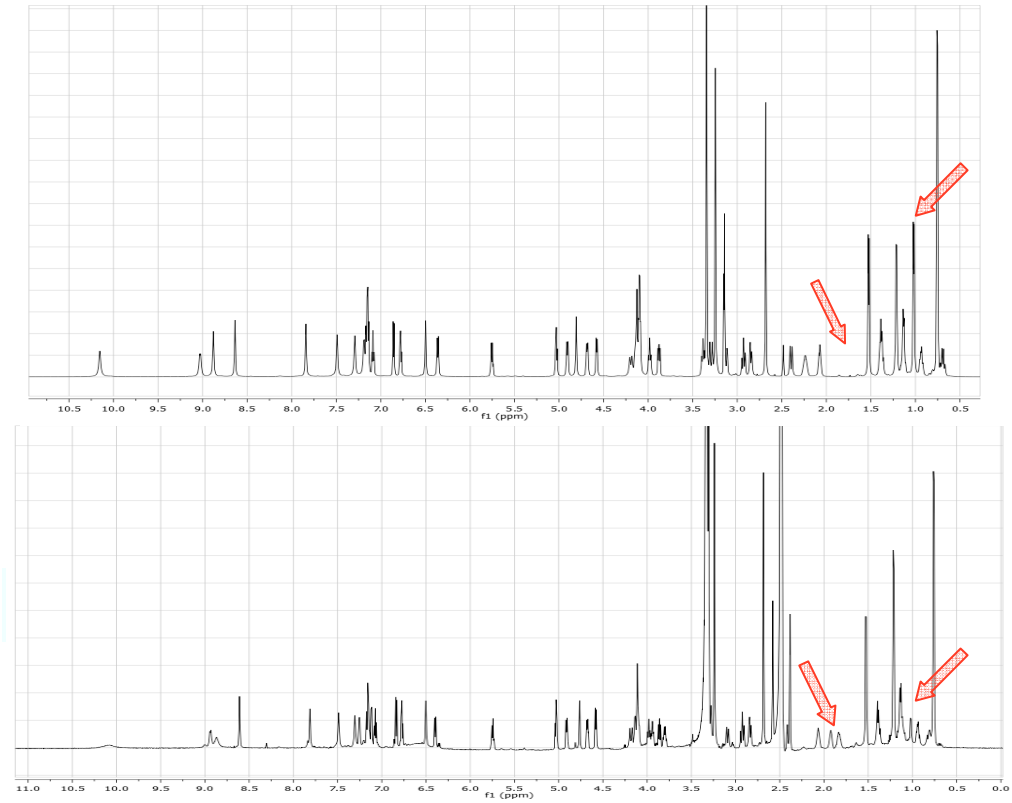

Figure 37. ^{1}H NMR spectra of perthamides C and G in DMSO-d_6 at 700 MHz.

4.3.5 Perthamides H and I

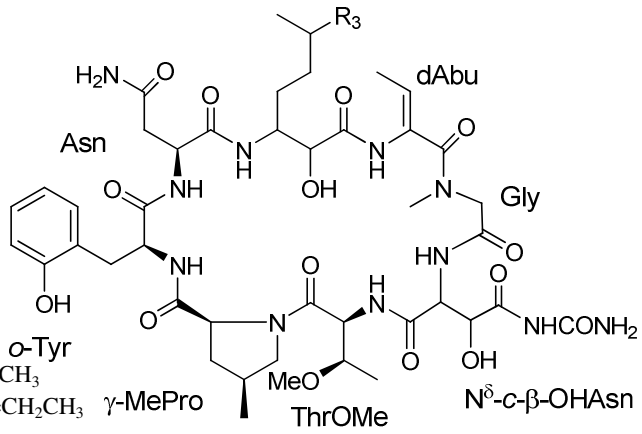

Perthamide H (**13**) R_3=CH_3
Perthamide I (**14**) R_3=CH_2CH_3

The HR-ESIMS of perthamide H (**13**) showed a major ion peak at *m/z* 986.4804 $[M-H]^-$ corresponding to a molecular formula of $C_{44}H_{65}N_{11}O_{15}$, that was 80 mass units (a sulphate group) smaller than perthamide C (**8**), suggesting the lack of the sulphate group. The structure of the peptide H was performed through extensive application of NMR techniques and MS experiments.

The perturbation in the N^{δ}-c-β-OSO_3Asn residue was confirmed also by ^{1}H NMR spectrum. In fact, the β-hydroxymethine proton of this residue was found slightly upfield shifted at δ_H 4.12 compared to the one in perthamide C (δ_H 4.59). The ^{1}H NMR showed also the gain of an exchangeable OH proton at δ 6.16 and the downfield shift of the NH^{δ} at 9.52, while the proton α was found slightly upfield at δ 4.82 vs 5.05 of major peptide (Figure 38). The remaining part of the molecule was almost superimposable with that of perthamides C.

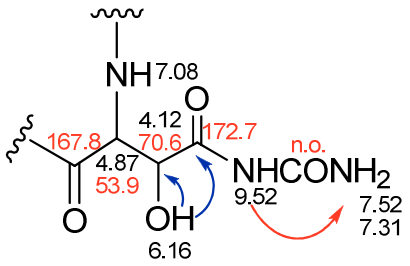

Figure 38. N^{δ}-c-Asn residue in perthamide H and I.

The molecular formula of perthamides I (**14**), $C_{45}H_{67}N_{11}O_{15}$, deduced by HR-ESIMS, was 14 u.m.a. larger than that of perthamide H, suggesting the gain of a methylene group. The comparison of the ^1H NMR of the two peptides clearly showed that perthamide H and I differed each other in the portion reguarding the β-amino acid residue: in fact, while perthamide H had the AHMHA residue, perthamide I posseded the HAMO unit, like perthamide E.

As inferred from a careful analysis of COSY, HSQC and HMBC spectra, the resonances relative to other portion of the molecula were almost superimposable with that found in the perthamide H.

4.3.6 Perthamides J and K

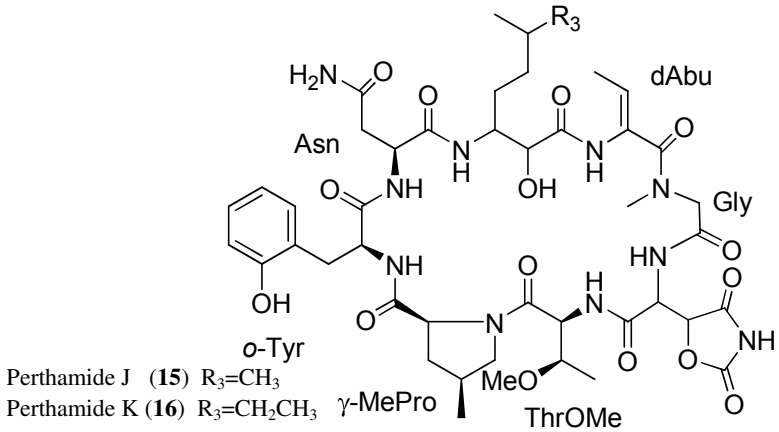

Perthamide J (**15**) $R_3=CH_3$
Perthamide K (**16**) $R_3=CH_2CH_3$

The HR-ESIMS spectrum of perthamide J (**15**) showed a pseudomolecular ion peak at m/z 970.4405 $[M-H]^-$, corresponding to a molecular formula of $C_{44}H_{62}N_{10}O_{15}$, which is 97 u.m.a. less than the perthamide C. NMR data of perthamide J were almost superimposable to those of parent peptide, whereas only a perturbation in N^{δ}-c-β-OSO_3Asn residue was observed.

In particular in the ^1H NMR the signals regarding the -NH_2 group of the δ-carbamoil moiety and the –OH exchangeable proton in position β were absent.

The downfield shift experienced by both proton and carbon in position β (at δ_H 5.22 vs 4.59 in perthamide C; δ_C 79.0 vs 74.9) was indicative of an acylation shift. Also the signal of the NH^{δ} appeared downfield shifted at δ_H 12.2 vs 8.90 in perthamides C; this exanchageable proton, in the HMBC spectrum, correlated only with the C3 (δ_C 79.0) and C4 (δ_C 154.9) (Figure 39). Even if any long-range correlation could be traced from H-3 proton, mass data and chemical shift consideration clearly suggested a cyclization between the β-OH group and the carbamoil moiety to form a cyclic oxazolidin-2,4-dione.

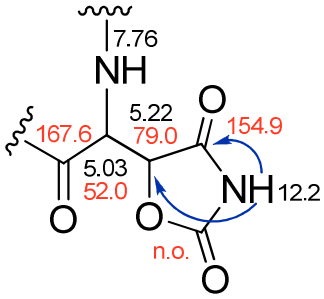

Figure 39. The modified β-OHAsn residue in perthamide J.

The peptidic sequence of perthamide L and placement of the modified β-OHAsn residue were assigned from the analysis of HMBC and ROESY correlations, affording the planar structure of the clyclic peptide.

The molecular formula of perthamide K (**16**), $C_{45}H_{64}N_{10}O_{15}$, was deduced by HR-ESIMS, *m/z* 984.4635 $[M-H]^-$. The NMR data suggested that perthamide K had the same perturbation in the N^{δ}-c-β-OSO_3Asn residue like perthamide J, whereas differed in the portion reguarding the β-amino acid residue. The gain of 14 u.m.a. in mass spectrum, as well as one additional methylene group, together the comparison of NMR data, suggested the replacement in perthamide M of AHMHA unit with the HAMO residue.

Interpretation of 2D NMR data, including COSY, HSQC, HMBC and ROESY data led to the planar structure of perthamide K, that is almost superimposable with that of perthamide J.

4.3.7 Pharmaological activity of perthamide C

Perthamides C and D did not show antiproliferative activity on KB cell line up to a dose of 10 µg/ml, in spite of the anti-KB activity showed by the crude extract. However, when tested in a well characterised model of inflammation in vivo i.e. mouse paw oedema,[165] perthamide C significantly reduced carrageenan-induced paw oedema both in the early phase (0-6 h) and in the late phase (24-96 h) as shown in Figure 40. In particular perthamide C displayed a dose-dependent (0.1, 0.3 and 1 mg/kg) anti inflammatory activity causing about 60% reduction of oedema in mice at the dose of 300 µg/kg (i.p.). Also perthamide D showed an anti inflammatory activity in both phases of oedema; however due to the scarcity of natural compound available, it was tested only in a single dose (0.3 mg/kg) where caused a 46% oedema inhibition. These data if compared with the ED_{50} of one of the most common NSAID sold in the market, *e.g.* naproxen (ED_{50} 40 mg/kg) clearly indicate that perthamide C is about 100 times more potent. Furthermore the activity observed implies that the peptide is bioavailable and able to access the site of inflammation.

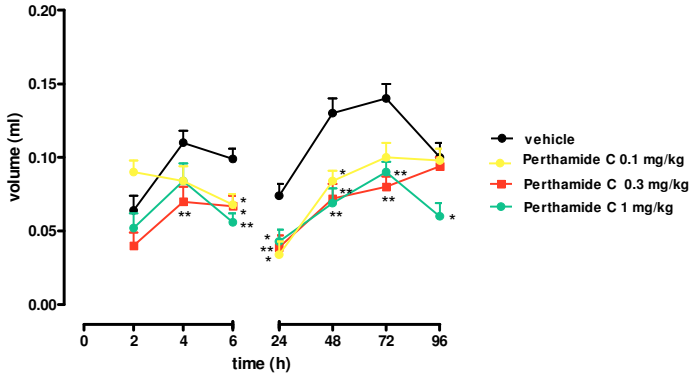

Figure 40. Dose-dependent inhibition on first (A) and second (B) phase of carrageenan-induced paw oedema by perthamide C (**8**).

Perthemide C showed also an immunosuppressive activity, this activity is shown by its ability to significantly reduce the Concanavalin A- induced proliferation of murine splenocytes obtained from mice injected with carrageenin into the paw and receiving perthamide intraperitoneally. The immunosuppressive activity of pertahmide is comparable with dexamethasone used as control (Figure 41).

Anti inflammatory marine cyclic peptide are rare, with the exception of cyclomarins,[1660] salinamides[167,168] and halipeptins;[169] the discovery that perthamides are potent and, in a way, unexpected anti-inflammatory agents deserves further investigations on the origin of their activity.

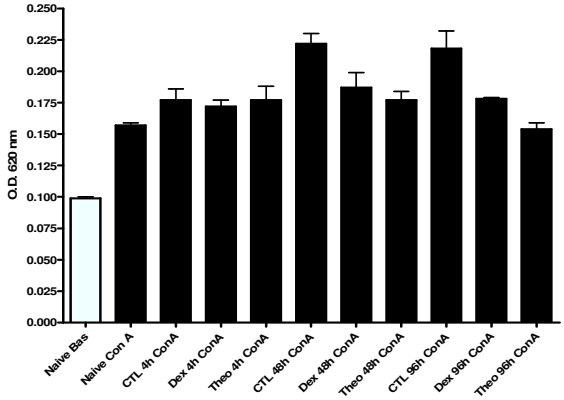

Figure 41. Reduction of the Concanavalin A- induced proliferation of murine splenocytes by perthamide C (**8**).

Detailed pharmacological investigations to clarify the biomolecular target and therefore the mechanism of action at the molecular level are currently in progress in our laboratory. Target-discovery studies through chemical proteomics approaches will be performed, and it will try to identify the macromolecular partners of perthamide showing, in preliminary pharmacological assays immunoregulating and anti-inflammatory activities. Finally, global proteomics studies will be pursued in order to evaluate the quantitative modifications of cell proteomes when treated with perthamide.

Indeed the modular peptidic nature and the quite easily chemical access to perthamide C may open the possibility to investigate new pharmacophores useful in the identification of new leads for developing a new generation of anti-inflammatory drugs.

Moreover the isolation of small library of natural analogues will allowed for a detailed SAR study to determine the pharmacophores of the peptide.

Table 6. NMR Spectroscopic Data (700 MHz, DMSO-d_6) for Perthamide C (**8**) and Perthamide E (**10**).

	Perthamide C (**8**)		Perthamide E (**10**)	
Position	δ_H (*J* in Hz)	δ_C	δ_H (*J* in Hz)	δ_C
ThrOMe				
1	-	171.0	-	171.2
2	4.92 d (9.5)	55.3	4.91 d (9.5)	55.4
3	4.16 m	72.8	4.16 m	72.9
4	1.24 d (5.8)	14.3	1.23 d (5.9)	14.3
OMe	3.27 s	54.7	3.26 s	54.7
NH	9.05 d (8.8)		9.01 d (9.1)	
γMePro				
1	-	170.7	-	171.0
2	3.90 dd (11.0, 6.7)	63.4	3.89 dd (11.1, 6.6)	63.4
3	0.72 m, 2.09 m	36.1	0.71 m, 2.09 m	36.2
4	2.25 m	33.2	2.25 m	33.2
5	3.40 t (10.8) 4.11 ovl	53.0	3.39 ovl, 4.11 ovl	53.2
6	1.04 d (6.1)	15.9	1.03 d (5.8)	15.8
oTyr				
1	-	170.6	-	170.8
2	4.12 ovl	56.3	4.11 ovl	56.4
3	2.86 dd (13.2, 3.2), 2.95 t (13.2)	30.6	2.86 dd (13.2, 3.2), 2.93 t (13.2)	30.7
1’	-	124.0	-	124.3
2’	-	154.4	-	154.6
3’	6.88 d (7.8)	114.5	6.87 d (7.8)	114.5
4’	7.11 t (7.8)	127.9	7.10 t (7.8)	128.0
5’	6.80 t (7.4)	119.7	6.80 t (7.3)	119.9
6’	7.16 d (7.4)	130.3	7.16 ovl	130.5
NH	7.19 ovl		7.20 ovl	
OH	10.2 s		10.1 s	
Asn				
1	-	170.3	-	170.5
2	4.70 m	48.0	4.69 m	48.0
3	2.41 dd (16.9, 2.2), 3.15 d (16.9)	36.9	2.41 d (16.3), 3.14 dd (16.3, 4.7)	36.8
4	-	172.5	-	172.6
NH	7.18		7.19 ovl	
NH_2	6.51 br s, 7.86 br s		6.52 br s, 7.83 br s	
AHMHA				
1	-	169.7	-	170.0
2	4.14 br s	72.6	4.14 ovl	72.8
3	4.00 t (9.9)	52.0	4.01 t (9.9)	51.9
4	1.16 m, 1.41 m	24.1	1.44 m, 1.09 m	23.6
5	0.95 m, 1.15 m	34.4	1.06 m	31.8
6	1.41 m	27.2	1.17 m	33.4
7	0.77 d (6.4)	21.9	1.03 m, 1.22 m	28.7
8	0.78 d (6.4)	22.2	0.76 t (7.0)	11.0
9			0.74 d (6.2)	18.5
NH	6.38 d (9.1)		6.37 d (9.1)	
OH	4.81 br s		4.81 br s	

dAbu				
1	-	167.2	-	167.5
2	-	132.1	-	132.3
3	5.77 q (6.9)	126.4	5.77 q (6.8)	126.5
4	1.54 d (6.9)	12.1	1.54 d (6.8)	12.0
NH	8.65 s		8.62 s	
NMeGly				
1	-	167.1	-	n.o
2	3.31 d (17.9) 4.21 d (17.9)	51.4	3.31 d (17.5), 4.19 d (17.5)	51.5
NMe	2.70 s	34.4	2.70 s	34.6
N^{δ}-c-β-OSO_3Asn				
1	-	167.4	-	167.5
2	5.05 t (7.4)	53.0	5.04 t (7.3)	53.0
3	4.59 d (7.1)	74.9	4.59 d (7.1)	74.9
4	-	170.5	-	172.7
βNH	7.18 ovl		7.16 ovl	
NH	8.90 s		8.89 s	
CO	-	n.o	-	n.o
NH_2	7.31 br s, 7.51 br s		7.29 br s, 7.51 br s	

Ovl: overlapped; n.o: not observed.
^{1}H and ^{13}C assignments aided by COSY, TOCSY, HSQC and HMBC experiments.

4.4 SOLOMONAMIDES

Pursuing the chemical investigation of the polar extracts of the sponge *Theonella* we isolated two minor cyclopeptide derivatives unrelated to cyclopeptides previously described, which we named solomonamides A and B, endowed of anti-inflammatory activity.

4.4.1 Solomonamide A

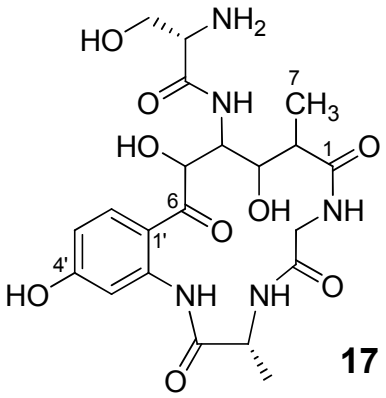

17

Solomonamide A (**17**) was isolated as minor peptide component as optical active amorphous solid. A molecular formula of $C_{21}H_{29}N_5O_9$ was established by high resolution ESIMS mass spectrometry.

The ^{1}H NMR spectrum contained four exchangeable amide NH protons between δ_H 11.5 and 7.49, disclosing the peptide nature of the compound, also corroborated by four ^{13}C NMR resonances (δ_C 167.5, 169.2, 170.7 and 173.6) relative to the acyl carbonyls.

The presence of three conventional amino acid residues, alanine, glycine, serine were easily deduced by interpretation of 2D NMR data obtained by ^{1}H-^{1}H COSY, HSQC, HMBC experiments (Figure 42, Table 7). A signal at δ 8.10, integrating for two protons, was assigned as α-amino group of the serine residue, indicating that the above residue is the N-terminus.

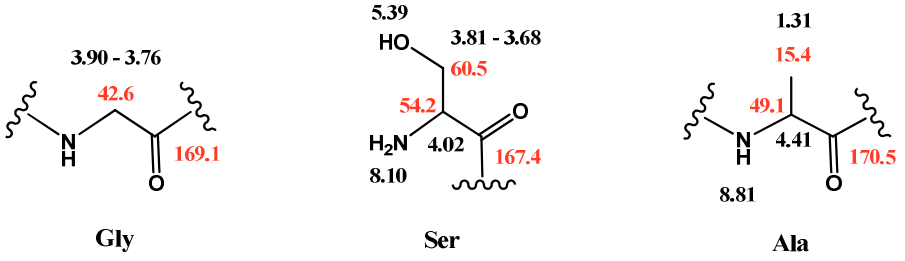

Figure 42. Gly, Ser and Ala units in solomonamide A

Two spin systems, one comprising a CH-CH_3 group (δ_H 2.31, δ_C 44.4,C2; δ_H 0.94, δ_C 13.6, C7) and a sequential CH-OH (δ_H 3.13, δ_C 70.3, C3); and a second formed by a CH-NH (δ_H 4.51, δ_C 53.3, C4) and a sequential CH-OH (δ_H 4.72, δ_C 70.5, C5), were disclosed from COSY and HSQC data.

Even if no COSY correlation was observed between the protons at δ_H 3.13 and δ_H 4.51 the connection between C3 and C4 was deduced by HMBC data (Table 7, Figure 43). The linkage of an acyl carbonyl with the CH(2)-CH_3 group at δ_H 2.31 was deduced from the diagnostic heteronuclear long range correlations between the protons at C2; C3 and C7 with the carbon resonance at δ_C 173.6 (C1). Moreover a ketone carbonyl group was placed at C6 of the spin system on the basis of ^3J heteronuclear coupling between CH(4)-NH (δ_H 4.54) with a carbonyl group at δ_C 201.2 (C6).

In addition, the ^{1}H NMR together with COSY, HSQC and HMBC data showed the presence of a 1,2,4 trisubstituted phenyl ring. The ketonic carbonyl at C6 of the abovementioned spin system was placed at C1' of the phenyl ring on the basis of the HMBC cross peaks between the C6' aromatic proton at δ 7.86 with the signal at δ 201.2.

One phenolic hydroxy and one aromatic amido groups deduced by mass and ^{13}C NMR data were also evidenced by two downfield signals, observed in the ^{1}H

NMR spectrum at δ 10.7 and 11.5 respectively, and in the ^{13}C NMR spectrum at δ 162.7 and 141.7. The relative regiochemistry of oxygenated and nitrogen functionalities on the phenyl ring was secured by diagnostic long-range heteronuclear couplings showed in Figure 43.

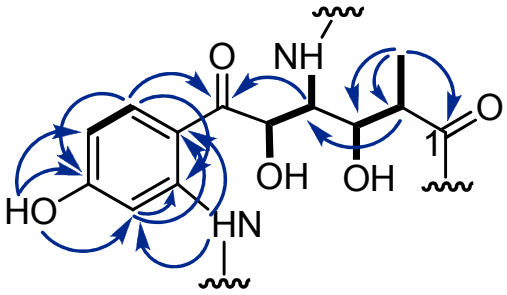

Figure 43. New subunit of solomonamide A (**17**) with COSY/TOCSY connectivities (bold bonds) and key HMBC correlations (blue arrows).

Therefore the new unit in solomonamide A was defined as 4-amino-(2'-amino-4'-hydroxyphenyl)-3,5-dihydroxy-2-methyl-6-oxohexanoic acid (ADMOA), which is unprecedented in natural products.

A plausible biogenetic origin of this unit could be drawn. 5-hydroxytryptophan could undergo to two well known processes of tryptophan catabolism, *i.e* β-hydroxylation[170] and oxidative scission of the indole ring to afford a hydroxykynurenine unit.

Reduction of the carboxy group to aldehyde, followed by a Claisen-type condensation with a propionate C3 unit (Scheme 7) would eventually afford the 4-amino-3,5-dihydroxy-2-methyl-6-oxa-6-(2'-amino-4'-hydroxyphenyl)hexanoic acid residue.

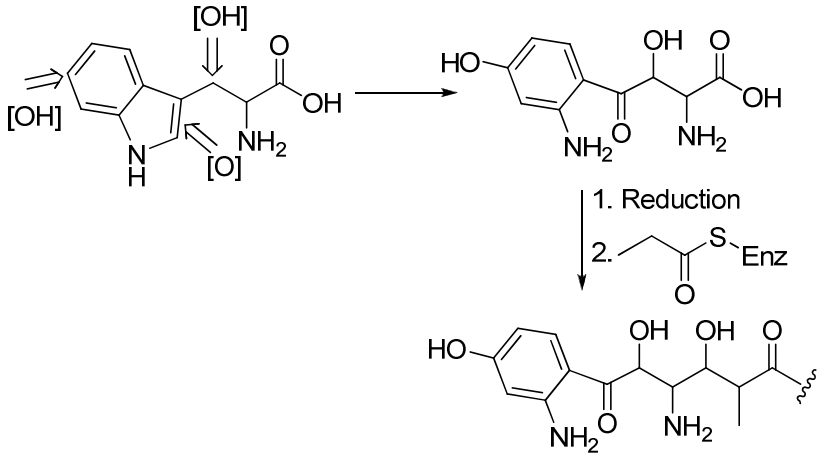

Scheme 7. Plausible biogenesis for ADMOHA unit in solomonamide A.

The amino acid sequence of solomonamide A could be established from interpretation of the HMBC experiment where long-range correlations between protons on α-carbon and on α-amido groups and carbonyl carbons belonging to adjacent amino acids provided the partial sequence ADMOA-Gly-Ala (Table 1). Cyclization between the C-terminal alanine and the ADMOA 2'-amino group was apparent from HMBC correlations between 2'-amino proton of ADMOA (δ_H 11.5) and the carbonyl resonance at δ 170.7 (C-1 Ala). The linkage of γ-CHNH of ADMOHA residue to acyl group of N-terminal seine residue was determined by long-range correlations between protons at δ 7.89 (NH -4) and δ 4.54 (C4) to C1 Ser (δ_C 167.5). Several inter-residue ROESY correlations confirmed the proposed sequence (Figure 44).

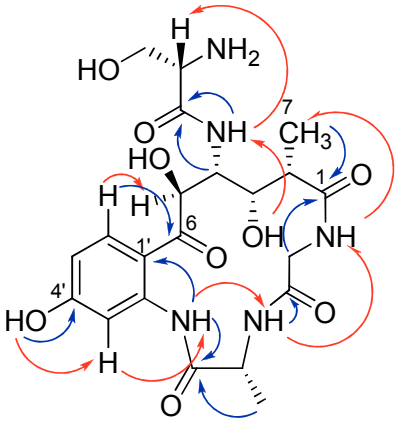

Figure 44. Inter residue ROESY (red) and HMBC (blue) correlations of solomoamide A.

Definitive confirmation of the sample structure was derived from ESI MS/MS analysis. In addition to the pseudomolecular ion at *m/z* 496.2 $[M + H]^+$, the ESI Q-TOF MS/MS spectrum provided some fragment ion peaks, in agreement with the proposed sequence (Scheme 8). The major peak at *m/z* 374 corresponds to the simultaneous dehydratation at C2 and eliminative loss of terminal serine residue. Further MS3 fragmentation of the daughter ion at *m/z* 374 gave C-terminus ion fragments at *m/z* 303 $[374 - Ala]^+$and *m/z* 386 $[374\text{-}Ala\text{-}Gly]^+$.

Scheme 8. Fragment ions in ESI Q-TOF MS/MS.

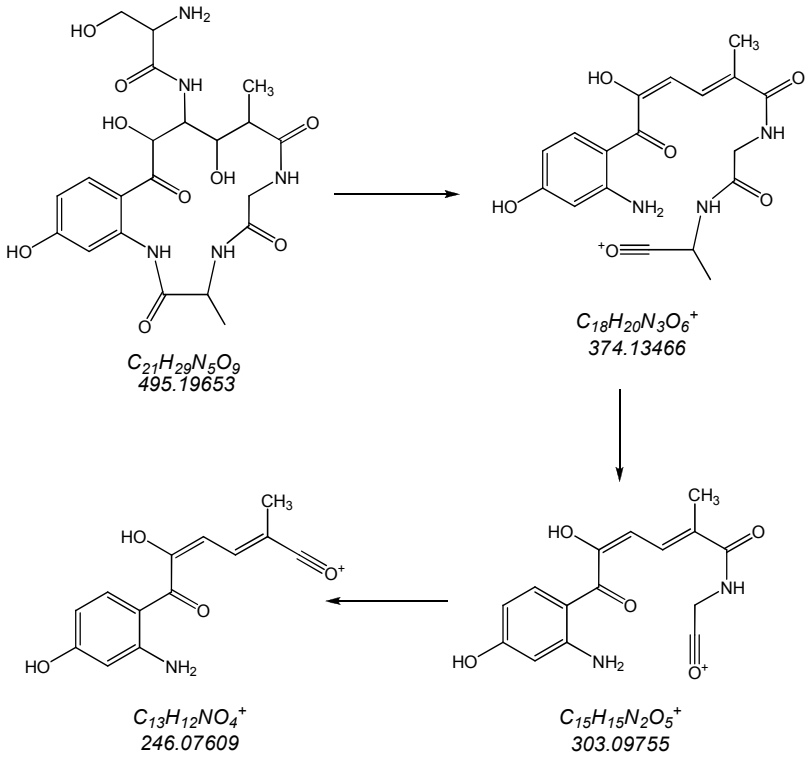

The absolute stereochemistry of Ala and Ser residues was determined by complete acid hydrolysis of solomonamide A (6N HCl, 110°C, 12h) and Marfey's analysis. The acid hydrolysate was derivatised with (1-fluoro-2,4-dinitrophenyl)-5-L-alaninamide (L-FDAA), and then LC-MS comparison of the derivatives from parent peptide with the FDAA derivatives of appropriate standards established the presence of D-Ala and L-Ser.

The configurational assignment of ADMOA residue was proved quite difficult. The fortuitous anti arrangement of H2/H3 and H4/5 and the absence of diagnostic ROE effects hampered the application of *J*-based analysis. Moreover solomonamide A showed an high instability towards chemical derivatization. The determination of the absolute stereochemistries of the ADMOA residue is in progress through the use of a computational method, relying on DFT calculation of ^{13}C chemical shift values of all the possible stereoisomers.

4.4.2 Solomonamide B

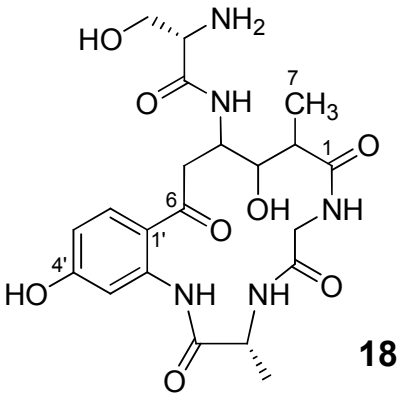

18

Solomonamide B (**18**) was isolated as very minor peptide component as optical active white amorphous solid. The HR-ESIMS of solomonamide B showed a major ion peak at *m/z* 480.2094 $[M + H]^+$ ($C_{21}H_{29}N_5O_8$, calcd for $C_{21}H_{30}N_5O_8$, 480.2094), 16 mass units lower than that of solomonamide A.

Comparison of 2D NMR data of solomonamide B with those of solomonamide A (Table 8) clearly evidenced a close analogy between two compounds and a perturbation in the ADMOA residue. The signal assigned to H-4 hydroxymethine of the above residue in solomonamide A was replaced by signals relative to a diasterotopic allyl methylene (δ_H = 3.34 and 2.87; δ_C 41.2) in solomonamde B. In this way it was easy establish the structure of 4-amino-6-(2'-amino-4'-

hydroxyphenyl)-3-hydroxy-2-methyl-6-oxohexanoic acid residue (AHMOA) instead of ADMOA residue.

Interpretation of 2D NMR data, including COSY, HSQC, HMBC and ROESY data led to the planar structure of solomonamide B, that is almost superimposable with that of solomonamide A.

The presence of D-Ala and L-Ser was established by Marfey method as described before. The determination of the absolute stereochemistries of the AHMOA residue is in progress through the use of a computational method.

4.4.3 Pharmacological activity of solomonamide A

Because the perthamides isolated from the same sponge showed a potent anti-inflammatory activity, we have investigated whether solomonamide A have the same property.

Solomonamide A displayed a dose-dependent anti-inflammatory activity causing about 60% reduction (Figure 45) of oedema in mice at the dose of 100 μg/kg (ip). The scarcity of the material humpered the evaluation of anti-inflammatory activity for solomonamide B.

In conclusion, solomonamide A is representative of a new class of anti-inflammatory compounds.

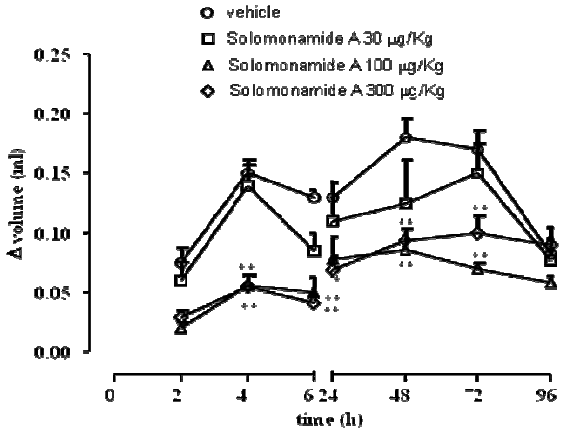

Figure 45. Dose-dependent inhibition on first (A) and second (B) phase of carrageenan-induced paw oedema by solomonamide A (**17**).

Table 7. NMR Spectroscopic Data for Solomonamide A (**17**) (DMSO-d_6, 700 MHz).

	δ_C[a]	δ_H[b]	HMBC[c]	ROESY[d]
Gly				
1	169.2			
2a	42.6	3.90 dd (15.3, 6.6)	1, 1_{ADMOA}	
2b		3.76 dd (15.3, 4.7)	1, 1_{ADMOA}	NH_{Ala}
NH		7.49 br t (5.5)	2, 1_{ADMOA}	2a e 2b, NH_{Ala}, 2_{ADMOA}, 3_{ADMOA}, 4_{ADMOA}, 7_{ADMOA}
Ala				
1	170.7			
2	49.1	4.41 quint (7.6)	1, 3, 1_{Gly}	NH-2'$_{ADMOA}$
3	15.5	1.31 d (7.0)	1, 2	
NH		8.77 d (7.9)	2, 3, 1_{Gly}	$2b_{Gly}$, $NH_{Gly,}$ NH-2'$_{ADMOA}$
Ser				
1	167.5			
2	54.2	4.02 m	1, 3	NH-4_{ADMOA}
3a	60.5	3.81 dd (11.4, 4.6)	1	NH-4_{ADMOA}
3b		3.68 dd (11.4, 6.9)	1, 2	NH-4_{ADMOA}
NH		8.10 br d (4.3)	1, 2, 3	
OH		5.39 br s		
ADMOA				
1	173.6			
2	44.3	2.34 m	1, 7, 3, 4	4, 5, NH_{Gly},
3	70.3	3.15 ovl	1, 2	4, 5, NH_{Gly}
4	53.3	4.54 t (9.5)	2, 3, 6, 1_{Ser}	2, 3, 6', NH_{Gly},
5	70.4	4.75 d (9.5)	4	2, 3, NH-4, 6'
6	201.2			
7	13.7	0.98 d (7.1)	1, 2, 3	NH_{Gly}
OH-3		5.26 br s		NH-4
OH-5		5.53 br s		
NH-4		7.89 d (9.5)	1_{Ser}, 3	5, 2_{Ser}
1'	115.3			
2'	141.8			
3'	106.0	8.02 d (2.3)	1', 2', 4', 5'	NH-2', OH-4'
4'	162.8	-		
5'	109.6	6.57 dd (8.7, 2.3)	1', 3', 4'	OH-4'
6'	133.4	7.86 d (8.7)	6_{ADMOA}, 2', 4'	5
OH		10.7 s	3', 4', 5'	3', 5'
NH-2'		11.5 s	1', 3', 1_{Ala}	3', $2_{Ala,}$ NH_{-Ala}

[a]Recorded at 175 MHz; referenced to residual DMSO-*d*6 at δ 39.51 ppm.
[b]Recorded at 700 MHz; referenced to residual DMSO-*d*6 at δ 2.50 ppm.
[c]Proton showing HMBC correlation to indicated carbon.
[d]Proton showing ROESY correlation to indicated proton.

Table 8. NMR Spectroscopic Data for Solomonamide B (**18**) (DMSO-d_6, 700 MHz).

	δ_C [a]	δ_H [b]	HMBC [c]
Gly			
1	169.0		
2a	42.4	4.19 dd (15.7, 7.1)	1, 1_{AHMOA}
2b		3.78 dd (15.7, 3.4)	1, 1_{AHMOA}
NH		7.30 br dd (7.0, 3.4)	
Ala			
1	171.2		
2	49.7	4.29 quint (7.1)	1, 3, 1_{Gly}
Me-2	16.0	1.36 d (7.2)	1, 2
NH		8.79 d (7.2)	2, 1_{Gly}
Ser			
1	166.7		
2	53.6	3.98 m	
3	60.3	3.69 br s	1
NH_2		8.08 br d (4.4)	1, 2, 3
OH		5.46 br s	
AHMOA			
1	173.2		
2	45.4	2.35 m	1, 3
3	72.2	3.39 ovl	
4	48.0	4.52 br dt (9.5, 1.7)	1_{Ser}
5a	41.2	3.34 ovl	3, 4, 6
5b		2.87 br dd (17.6, 1.7)	3, 4, 6
6	201.1		
7	13.6	1.08 d (7.2)	1, 2, 3
OH-3		5.53 br d (5.3)	2
NH-4		7.98 d (9.5)	1_{Ser}
1’	115.8		
2’	141.3		
3’	106.1	7.92 d (2.1)	1’, 2’, 4’, 5’
4’	162.9	-	
5’	110.0	6.57 dd (8.8, 2.1)	1’, 3’
6’	132.9	7.77 d (8.8)	2’, 4’, 6_{AHMOA}
OH		10.7 s	3’, 4’, 5’
NH-2’		11.5 s	

[a]Recorded at 175 MHz; referenced to residual DMSO-*d*6 at δ 39.51 ppm.
[b]Recorded at 700 MHz; referenced to residual DMSO-*d*6 at δ 2.50 ppm.
[c]Proton showing HMBC correlation to indicated carbon.
[d]Proton showing ROESY correlation to indicated proton.

3.4 MACROLIDES FROM *THEONELLA SWINHOEI*

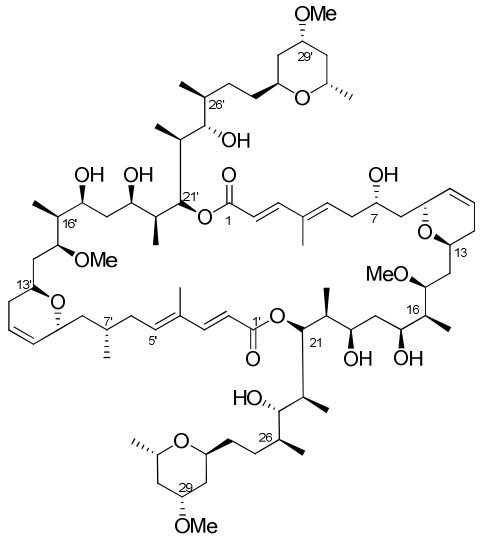

Swinholide A

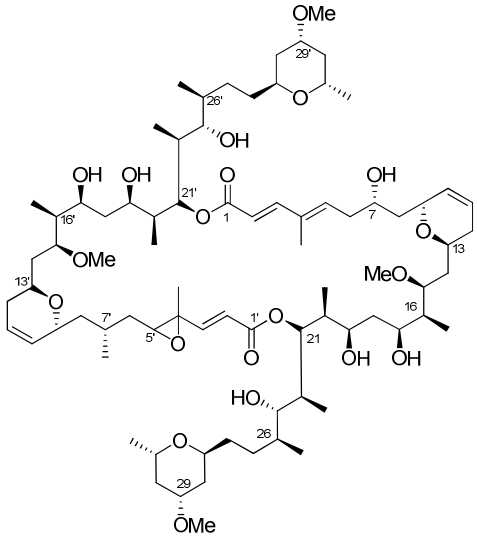

Compound 19

The chloroform extract of *Theonella* sponge afforded to the isolation of a new dimeric macrolide (compound **19),** togheter with the known major macrolide, swinholide A.

Compound **19** showed a chemical lability in $CDCl_3$; therefore all spectra were acquired in CD_3OD. In order to compare the new macrolide with parent compound, all resonances of swinholide A were reassigned in CD_3OD by careful analysis of 2D-NMR data and comparison of the data in $CDCl_3$ reported in literature (Table 9).

Compound **19** displayed a molecular formula of $C_{79}H_{134}O_{20}$, 16 mass units higher than that of swinholide A.

The ^{1}H and ^{13}C NMR spectra appeared more complicated than those of swinholide A, which suggested a dimeric structure comprising two non-identical units. In particular, the NMR data showed a perturbation in one of two dienone substructures in the dimeric molecule. The assignment of the complete structure,

as well as the assignment of ^{1}H and ^{13}C NMR resonances, were supported by extensive study of ^{1}H, ^{13}C NMR, COSY, HSQC, HMBC spectra (Table 9).

The ^{13}C NMR spectrum of swinholide A showed six signals in the region between 152.3 and 115.6 ppm, corresponding to six pair of equivalent carbons of C-2/C-2' (δ_C 115.6, CH), C-3/C-3' (δ_C 152.3, CH), C-4/C-4' (δ_C 135.3, qC), C-5/C-5' (δ_C 140.5, CH), C10-C-10' (δ_C 130.9, CH), and C-11/C-11' (δ_C 124.9, CH), together with the lactone signal of C1/C1' at δ_C 170.6. In comparison to swinholide A, the downfield region of ^{13}C NMR spectrum of compound **19** showed 10 resonances for olefinic carbons in the region 152.5-115.9 ppm instead of six signals, together with two resonances at δ_C 170.2 and 168.7 for the lactone carbons C-1 and C-1', respectively. The ^{1}H NMR spectrum of compound **19** showed resonances for nine non-equivalent protons in the region 7.46-5.67 ppm, instead of resonances of five pairs of equivalent protons (H2/H2', H-3/H-3', H-5/H-5', H-10/H-10', H-11/H-11') between 7.43 and 5.65 ppm in swinholide A. Additionally, this spectrum, in contrast to that of swinholide A, displayed an additional resonance at δ_H 3.22, that in the HSQC experiment was correlated with a carbon at δ_H 64.4. On the basis of the COSY spectrum, this proton was assignable to an oxygen-bearing methine at C5' and appeared upfield shifted compared to a hydroxymethine. This findings, together with the mass data and chemical shift consideretions, suggested the replacement of the C-4'/C-5' double-bond moiety with an epoxy group in half of the molecule, causing twinning of most of the ^{1}H and ^{13}C NMR signals in this portion of the molecule. In particular, diagnostic chemical shift differences were observed for the signals due to methyl protons at δ_H 1.42 (1.77 in swinholide A) at C4' and methylene protons at C6' (δ_H 1.63 and 1.81 vs 2.40 in swinholide A).

The placement of the epoxy group was unambiguously supported from HMBC cross-peaks of H-5'/C4', CH_3-4'/C6'(Figure 46).

The relative stereochemistry are proposed on the basis of the similarity of the J_{HH} values between compound **19** and swinholide A.

In conclution compound **19** was the first asymmetrical epoxidated version of swinholide A.

Since swinholide A is a potent microfilament disrupting toxin and represents an useful tool in investigations of actin organization, dynamics and function; pharmacological activity of compound **19** will be valued.

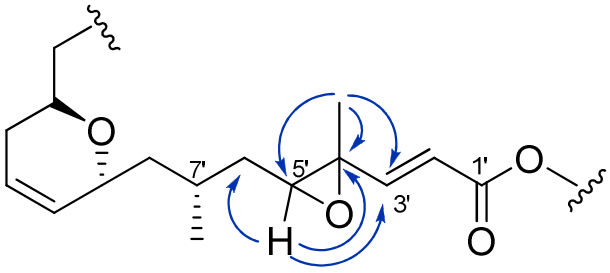

Figure 46. Key HMBC correlations in partial structure of compound **19**.

Table 9. NMR Spectroscopic Data (700 MHz, CD_3OD) for Swinholide A and compound **19.**

	Swinholide A		**Compound 19**	
position	$\delta_H/\delta_{H'}$ (*J* in Hz)	$\delta_C/\delta_{C'}$	$\delta_H/\delta_{H'}$ (*J* in Hz)	$\delta_C/\delta_{C'}$
1/1’	-	170.6	-	170.2/168.7
2/2’	5.84 d (15.6)	115.6	5.88 d (15.6)/6.15 d (15.7)	115.9/122.1
3/3’	7.43 d (15.6)	152.3	7.46 d (15.6)/6.81 d (15.7)	152.0/152.5
4/4’	-	135.3	-	135.5/59.7
4/4’-Me	1.77 s	12.3	1.85 s/1.42 s	12.7/15.5
5/5’	6.14 t (7.2)	140.5	6.16 t (7.2)/3.22 m	140.6/64.6
6/6’	2.40 t (6.9)	38.8	2.44 m/1.81 m, 1.63 m	38.7/37.9
7/7’	4.02 m	68.0	3.99 ovl/4.12 m	68.2/66.4
8/8’	1.28 m, 1.75 m	41.0	1.87 m, 1.37 m/1.37 m, 1.78 m	41.8/41.6
9/9’	4.48 br d (10.3)	70.4	4.48 br d (10.2)	70.4
10/10’	5.65 dd (1.8, 10.3)	130.9	5.67 br d (10.3)	130.8
11/11’	5.82 m	124.9	5.83 m	124.8
12/12’	1.94 m	32.2	1.96 m	32.2
13/13’	3.49 m	65.3	3.54 m	65.4
14/14’	1.58 m, 1.77 m	37.2	1.58 m, 1.82 m	36.9
15/15’	3.76 m	78.2	3.76 m/3.83 m	78.4/77.9
15/15’-OMe	3.32 s	56.8	3.34 s/3.35 s	56.9/57.2
16/16’	1.52 m	43.7	1.55 m	43.3
16/16’-Me	0.82 d (6.9)	8.8	0.83 d (7.0)/ 0.84 d (7.0)	9.2
17/17’	3.61	73.2	3.60 m	73.2
18/18’	1.63 m, 1.74 m	39.0	1.61 m, 1.75 m	39.2
19/19’	3.97 ovl	70.1	3.97 ovl/3.88 m	69.9/70.1
20/20’	1.93 m	39.4	1.94 m	39.4
20/20’-Me	0.90 d (7.0)	8.9	0.90 d (7.1)/0.91 d (7.1)	9.1
21/21’	5.47 d (10.5)	75.6	5.45 t (10.3)	75.7/76.3
22/22’	1.97 m	37.8	1.97 m	38.0
22/22’-Me	0.93 d (6.9)	9.6	0.92 d (7.0)/0.93 d (7.0)	9.7
23/23’	3.11 dd (1.9, 9.7)	77.4	3.09 m	77.3
24/24’	1.70 m	34.4	1.70 m	34.5
24/24’-Me	0.97 d (6.7)	17.7	0.97 d (6.7)/0.98 d (6.7)	17.9
25/25’	1.23 m, 1.42 m	25.1	1.23 m, 1.41 m	25.1
26/26’	1.27 m, 1.94 m	29.7	1.28 m, 1.94 m	29.8
27/27’	3.99 ovl	72.7	3.98 ovl	72.8
8/28’	1.52 m, 1.87 br d (12.5)	35.8	1.52 m, 1.87 br d (12.5)	35.8
29/29’	3.61 m	74.2	3.61 m	74.3
29/29’-OMe	3.34 s	55.3	3.34 s	55.3
30/30’	1.09 dd (10.4, 12.6), 2.02 br d (12.6)	39.7	1.09 dd (10.4, 12.6), 2.02 br d	39.7
31/31’	3.74 m	65.7	3.74 m	65.8
31/31’-Me	1.19 d (6.2)	21.7	1.19 d (6.2)	21.8

^{1}H and ^{13}C assignments aided by COSY, TOCSY, HSQC and HMBC experiments.

CHAPTER 5

PLANTS AS PHARMACY

Man's first interest in plants arose from his search for food, for fuel, and for fibre. He soon discovered that many plants had marked effects on his physiological functions, and consequently, since prehistoric times, plants and their extracts have been used for their healing properties and have played a dominant role in the development of sophisticated traditional medicine systems.

Some were successful. Ancient Egyptians, for example, chewed willow bark to relieve fever and headaches. Thousands of years later, scientists discovered that the bark contains salicylic acid, the active ingredient used to make aspirin.

Some were not so successful. Medieval doctors believed that baldness could be cured by rubbing an onion on the scalp.

Even today we are still using compounds derived from plants; so the plant kingdom represents an extraordinary reservoir of novel molecules.

Of the estimated 400,000-500,000 plant species around the globe, only a small percentage has been investigated phytochemically and the fraction submitted to biological or pharmacological screening is even lower. There is currently a resurgence of interest in the vegetable kingdom as a possible source of new lead compounds for introduction into therapeutical screening programmes. For this reason plants are still contributing to medicine; plants and plant products have provided a definitive stimulus for the development of natural product chemistry.

CHAPTER 6

CUCUMIS MELO

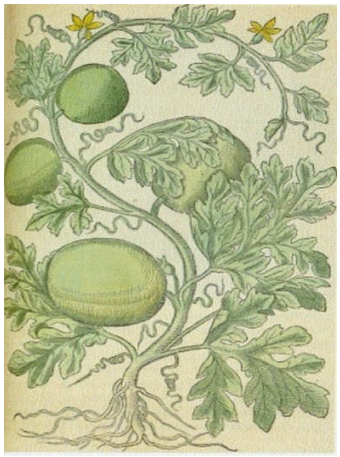

Melon (*Cucumis melo* L. var. *inodorus*, Cucurbitaceae) is one of the important horticultural crops worldwide and plays an important role in international trade. Different forms of melon are known that are morphologically different and have different uses.

Cucumis melo

Melons plants are procumbent vines that thrive on heat and sunshine and are grown in fields and gardens throughout the warmer and sunnier parts of the world. Melons rank high in economic value among vegetable crops. They are widely grown for their sweet, ripe fruits, which often fetch premium prices, but in some regions they are grown for the production of their immature fruits, which are reminiscent of cucumbers (*C. sativus* L.) in superficial appearance, taste, and usage.

The center of origin of melons is considered to be the eastern tropical Africa, south of the Sahara. But wild types are commonly found in the Sudano-Sahelian

area, while Asia from the Mediterranean to Japan is a secondary centre of diversity.

Of the species of cucurbis, *Cucumis melo* was probably the most ancient in cultivation as a food plant around the Mediterranean Sea. This is not surprising, given the greater geographical proximity of the center of origin of this species to the Mediterranean Sea.

The main plant organ used is the fruits, which are used both immature and mature as desserts and vegetables for salad. Fruits are usually consumed in the summer period and are popular because the pulp of the fruit is very refreshing and sweet, with pleasant aroma. Melon seeds may be eaten after being slightly roasted, or edible oil can be extracted from them.

Cucumis melo fruit

A number of studies have investigated the relationship between a range of physical and chemical parameters of melons and their sensory evaluation[171,172] and the compositional changes during ripening of fruits.[173]

The seeds of *Cucumis melo* L. are used in Chinese folk medicine as antitussive, digestive, febrifuge and vermifuge[174] and melon seeds extract can be used as an antidiabetic, and they are beneficial in chronic eczema.[175,176] Many Cucurbitaceae seeds are rich in oil and protein. More recent studies were largely focused on fatty acids, tocopherols, sterols and phenolic profiles of seed oil[177] and on physicochemical properties.[178] As our current interest involves the chemistry of biologically active natural products, we investigated the chemical constituents of the seeds of *C. melo* L.

6.1 EXTRACTION AND ISOLATION

Melon (*C. melo* var. *inodorus*) fruits were obtained from a local market in Napoli, Campania, Italy. The seeds were removed from their flesh and cleaned under running tap water. The whole seeds including the shell were finely ground using a blender. Fruits were identified in the Dipartimento di Scienze e Tecnologie per l'Ambiente e il Territorio (University of Molise) and a voucher specimen is deposited under N° ZZ-0743 in the Herbarium of University of Molise (Pesche, Isernia).

The powdered seeds were extract with MeOH at room temperature. The MeOH extract of powdered seeds of *Cucumis melo* was subjected to Kupchan's partitioning methodology to give four extracts: *n*-hexane, $CHCl_3$, *n*-BuOH and the aqueous residue.[2] The *n*-BuOH extract, after purification by droplet counter current chromatography (DCCC) and reversed phase HPLC, gave the new glycoside (**20**) and the known benzyl *O*-β-D-glucopyranoside (**21**). The $CHCl_3$ extract, purified by DCCC and HPLC, mainly contained multiflorane triterpene esters (**22**, **23**).[179]

4.2 STRUCTURAL CHARACTERIZATION OF COMPOUND 20

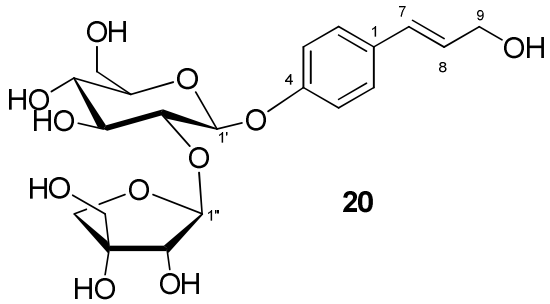

20

ESI-MS of compound **20** exhibited a quasi-molecular ion at *m/z* 467 $[M + Na]^+$, corresponding to a molecular formula $C_{20}H_{28}O_{11}$. This molecular formula was

determined by HR-ESI-MS ($C_{20}H_{28}O_{11}$) $[M + Na]^+$ at *m/z* 467.1602, (calcd. for $C_{20}H_{28}O_{11}Na$ 467.1529) and confirmed by ^1H and ^{13}C NMR experiments. The structure of compound **20** was elucidated by detailed analyses of ^1H and ^{13}C NMR chemical shift, and by COSY, HSQC, and HMBC experiments (Table 10).

The ^1H NMR spectrum of compound **20** showed a carbinyl methylene group at δ_H 4.20 (2H, d, *J* = 5.9 Hz), two trans olefinic protons as ABX_3 type signal [δ_H 6.26 (1H, dq, *J* = 5.9, 16.3 Hz) and 6.55 (1H, d, *J* = 16.3 Hz)], aromatic protons as an A_2B_2 type pattern signals at δ_H 7.02 (2H, d, *J* = 8.7 Hz) and 7.35 (2H, d, *J* = 8.7 Hz) and two anomeric protons [δ_H 4.96 (*J* = 7.4 Hz) and 5.47 (*J* = 1.4 Hz)].

Inspection of COSY and TOCSY spectra allowed to detect fuor distinct spin systems: two of them belonging to the aglycon moiety, and the remaining two belonging to two sugar units.

Concerning the aglycone moiety, the first spin system was ascrivable to a 1-4-disubstituted aromatic ring, as suggested by ^1H NMR; the second one corresponded to a chain including -CH=CH-CH_2OH.

Concerning the sugar portions of molecule, the first spin system started from the anomeric proton at δ_H 4.96 and arrived to the hydroxyl methylene at C-6', identifying a hexopyranose unit. When the anomeric proton at δ_H 5.47 was used as a starting point, a sequence of only one oxymethine was identified.

Acid hydrolysis of compound **20** afforded the two sugar units, which were identified as D-glucose and D-apiose by GC analysis.[180] The chemical shift and coupling constants of H-1' (δ_H 4.96 d, *J* = 7.4 Hz) and of H-1" (δ_H 5.47 d, *J* = 1.4 Hz) and the chemical shift of C-1' (δ_C 100.5) and C-1" (δ_C 110.4) supported a β-configuration for the anomeric carbons.[181]

In the apiofuranoside ring when H-1'' and H-2'' are *trans*, $^{3}J_{1,2}$ is usually close to 1 Hz, indicating that both oxygen atoms take up *quasi*-axial positions. The 2D-NOESY spectrum contains cross peaks between H-2'' and the protons of the hydroxymethyl group (δ_H 3.54). Similar NOE cross peaks was observed between H_2-5'' (δ_H 3.54) and H-4''b (δ_H 4.05) indicating that H-2'', H_2-5'' and H-4''b are found on the same face.

By HSQC and HMBC experiments (Table 10) a total of 20 carbon signals were detected, 11 signals assignable to glucopyranosyl and apiofuranosyl moieties. The low-field chemical shift of glucose C-2' (δ_C 78.2) suggests that the hydroxyl group at C-2 of glucose bears the apiose unit. The interglycosidic linkage was determined by the HMBC correlation evidenced between δ_H 3.64 (H-2' Glc) and δ_C 110.4 (C-1" Api). H-1" (δ_H 5.47) also displayed cross peaks with C-3" (δ_C 80.6) and C-4" (δ_C 75.2) by ^{3}J correlations to reveal an apiofuranoside. The attachment of the sugar chain at C-4 of the aromatic ring was supported by the HMBC correlation observed between δ_H 4.96 (H-1' Glc) and δ_C 157.4 (C-4) proving the C-4 glycosylation (Figure 47).

On the other hand, the HMBC correlation of the olefinic proton at δ_H 6.55 with C1 (δ_C 132.5) allowed to link the side chain to the aromatic ring (Figure 47).

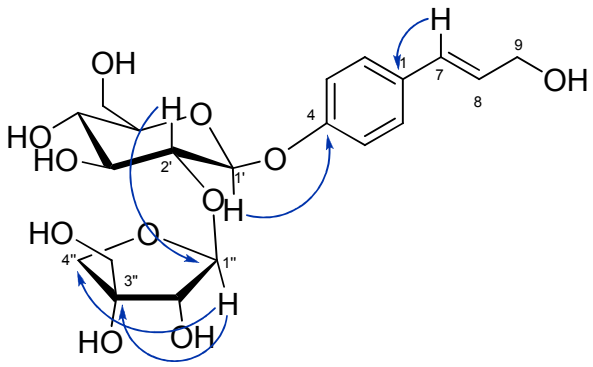

Figure 47. Key HMBC cross peaks of compound **20**.

E–geometry of C-7/C-8 double bond in the aglycone portion of the molecula was inferred by the *J*(H-7/H-8) value (16.3 Hz). Inspection of ^{1}H NMR spectrum indicated that all signals relative to aglycone moiety were superimposable to that of (*E*)-4-hydroxycinnamyl alcohol 4-*O*-β-D-glucopyranoside isolated from the leaves of *Lilium cordatum.*[182]

On the basis of the foregoing the structure of compound **20** was determined to be (*E*)-4-hydroxycinnamyl-4-*O*-(2'-*O*-β-D-apiofuranosyl)(1"→2')-β-D-glucopyranoside.

6.3 STRUCTURAL CHARACTERIZATION OF COMPOUND 21

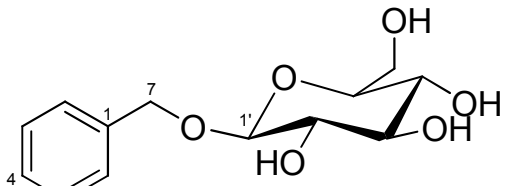

21

The molecular formula of compound **21** was deduced from its positive ion FAB-MS as $C_{13}H_{18}O_6$ which showed a $[M + Na]^+$ ion at *m/z* 293. The ^{1}H NMR spectrum of compound **21**, in addition to the signals due to the β-glucopyranosyl moiety (anomeric signals: δ_C 102.1 and δ_H 4.36, J = 7.7 Hz), showed a set of monosubstituted aromatic proton signals at δ_H 7.42, 7.33, 7.28 and a hydroxymethyl signal at δ_H 4.93 suggesting the presence of a benzyl alcohol moiety. The significant downfield shift of the H_2-7 (δ_H 4.93 and 4.67, each d, J = 11.9 Hz) and C-7 (δ_C 70.5) signals of compound **21** supported the location of glucosyl linkage also confirmed by the HMBC data. HMBC correlations were observed for H-7 (δ_H 4.93)/C-1' (δ_C 102.1 Glc), H-7/C-1 (δ_C 138.0), H-7/C-2(6)

(δ_C 128.0), proving that the glucose unit was linked to the benzyl carbon (Figure 48).

Thus the structure was defined as benzyl *O*-β-D-glucopyranoside. This compound was previously identified in *Vitis vinifera* grapes and has been described as the corresponding peracetylated derivative.[183]

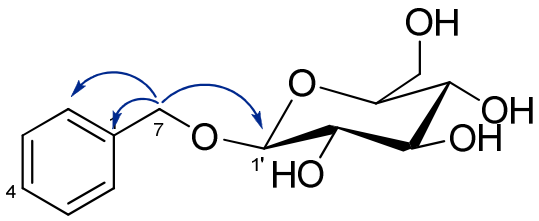

Figure 48. Key HMBC cross peaks of compound **21**.

6.4 OTHER METABOLITES ISOLATED

Compounds **22** and **23** were found to be known multiflorane triterpene esters. By spectroscopic analysis the structures of the two compounds were determined to be 3,29-*O*-dibenzoylmultiflor-8-en-3α,7β,29-triol (**22**) previously isolated from the seeds of *Trichosanthes kirilowii*[184] and 3-*O*-*p*-amino-benzoyl-29-*O*-benzoylmultiflor-8-en-3α,7β,29-triol (**23**) identified only from the seeds of pumpkin[185] and seeds of zucchini.[186]

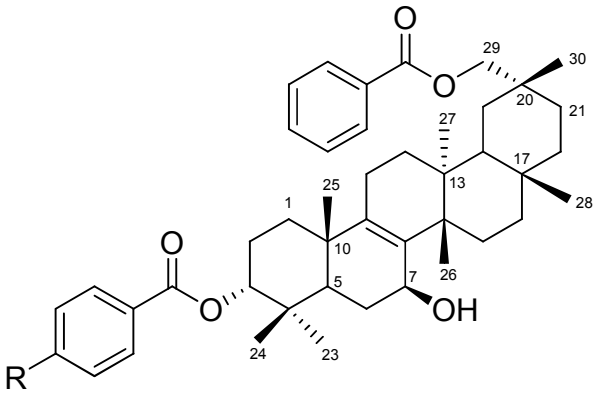

22 R=H (OBz)
23 R=NH2 (OPABA)

Table 10. ^{1}H and ^{13}C NMR (CD_3OD, 500 MHz) of compound **20.**

position	δ_H[a] (*J* in Hz)	δ_C[a]	HMBC[b]
1	-	132.5	
2,6	7.35 d (8.7)	128.3	4, 7,
3,5	7.02 d (8.7)	117.3	4, 1
4	-	157.4	
7	6.55 d (16.3)	130.9	2, 9
8	6.26 dq (5.9, 16.3)	128.3	1, 9
9	4.20 d (5.9)	63.4	7, 8
Glc			
1’	4.96 d (7.4)	100.5	4
2’	3.64 dd (7.4, 9.2)	78.2	1’, 1’’
3’	3.59 t (9.1)	78.4	
4’	3.39	71.1	
5’	3.43 m	77.7	
6’	3.69 dd (5.4, 11.9),	62.4	
Api			
1’’	5.47 d (1.4)	110.4	3’’, 5’’
2’’	3.95 d (1.4)	77.8	
3’’	-	80.6	
4’’	4.05 d (9.5),	75.2	
5’’	3.54 s	65.8	

[a] ^{1}H and ^{13}C assignments aided by COSY, TOCSY, HSQC and HMBC experiments.
[b] HMBC correlations, optimized for 8 Hz, are from proton(s) stated to the indicated carbon.

CHAPTER 7

BORRAGO OFFICINALIS

Borage, also known as a starflower, is an annual herb originating in Syria, but naturalized throughout the Mediterranean region, as well as Asia Minor, Europe, North Africa, and South America.

The name *borage* can, by way of French and Spanish, be traced back to Medieval Latin *borrago*. The latter name is generally accepted to have Arabic origin; it has been proposed to derive it from Andalusian Arabic *abu buraq* "father of sweat" (standard Arabic *abu araq*) or from *abu huras* "father of roughness". In the first case, the motive would be the use of borage leaves in diaphoretic medicines, in the second case the rough leaf surface.

Borrago officinalis

Borrago officinalis flower

It grows to a height of 60–100 cm (2.0–3.3 ft), and is bristly or hairy all over the stems and leaves; the leaves are alternate, simple, and 5–15 cm (2.0–5.9 in) long. The flowers are complete, perfect with five narrow, triangular-pointed petals. Flowers are most often blue in color, although pink flowers are sometimes observed. White flowered types are also cultivated. The flowers arise along scorpiod cymes to form large floral displays with multiple flowers blooming simultaneously, suggesting that borage has a high degree of geitonogamy. It has an indeterminate growth habit which may lead to prolific spreading. In milder climates, borage will bloom continuously for most of the year.

Traditionally borage was cultivated for culinary and medicinal uses, although today commercial cultivation is mainly as an oilseed. The seed oil is desired as source of γ-linolenic acid (GLA, 18:3, cis 6,9,12-octadecatrienoic acid), for which borage is the highest known plant-based source (17-28%).[187] This fatty acid is an intermediate of indispensable compounds in the body, such as prostaglandin E1 and its derivatives.[188] The seed oil content is between 26-38% and in addition to GLA contains the fatty acids palmitic acid (10-11%), stearic acid (3.5-4.5%), oleic acid (16-20%), linoleic acid (35-38%), eicosenoic acid (3.5-5.5%), erucic acid (1.5-3.5%), and nervonic acid (1.5%). The oil is often marketed as "starflower oil" or "borage oil" for uses as a GLA supplement, although healthy adults will typically produce ample GLA through dietary linoleic acid. The main constituents of the oil are vitamin C, saponins, tannins and minerals.

Borage production does include use as either a fresh vegetable or a dried herb. As a fresh vegetable, borage, with a cucumber like taste, is often used in salads or as

a garnish. The flower, which contains the non-toxic pyrrolizidine alkaloid thesinine,[189] has a sweet honey-like taste and as one of the few truly blue-colored edible things, is often used to decorate dessert.

It is notable that the leaves have been found to contain small amounts pyrrolizidine alkaloids: intermedine, lycopsamine, amabiline and supinine.[190,191] Pyrrolizidine alkaloids, which are extremely common in the Boraginaceae family, are powerful hepatotoxins that cause severe liver damage on chronic ingestion, often with lethal outcome. Although the total concentration in borage is extremely small (around 10 ppm in the dried herb), it has been argued that borage is an unsafe herb when used in folk medicine; the risks associated with casual culinary usage are probably negligible.

Borage is also traditionally used for its cosmetic properties, as cleanser and emollient mash and as a facial scrub.

Naturopathic practitioners use borage for regulation of metabolism and the hormonal system, and consider it to be a good remedy for premestrual syndrome and menopause symptoms, such as the hot flash. Borage is sometimes indicated to alleviate and heal colds, bronchitis, and respiratory infections, and in general for its anti-inflammatory, depurative, diuretic, purifier, regenerative, sudorific and balsamic properties. The flowers can be prepared in infusion to take advantage of its medicinal properties. The oleic and palmitic acid of borage may also confer a hypocholesterolemic effect.

In the book History of Plants, published in 1597, John Gerad quoted as “an old verse” the following sentence: “*Ego Borago gaudia simper ago*” (I, Borage, bring always courage), confirming the old bielef in the properties of the leaves and flowers of borage to take away sorrow and melanchony.[192]

7.1 EXTRACTION AND ISOLATION

The plants of Borrago officinalis were collected from natural population growing in the mountain areas of Avellino (Italy) in October 2008.

The flowers, deprived of stems, were crushed and subsequently extract with MeOH (1.5 L) at room temperature. The methanol extracts were then subjected to Kupchan's partitioning methodology to give four extracts. The butanol-soluble portions were separated by sequential chromatographic techniques, affording, as major metabolite, a new glucoside (compound **24**).

7.2 STRUCTURAL ELUCIDATION OF COMPOUND 24

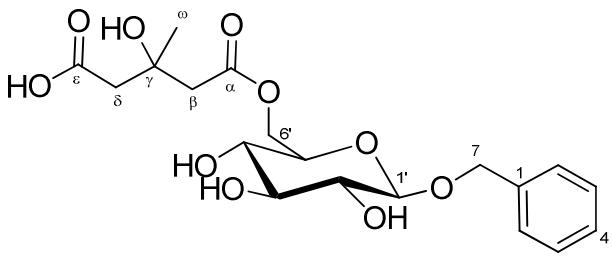

24

The molecular formula of compound **24** was determined as $C_{19}H_{26}O_{10}$ by HR-ESI $[M+H]^+$ (*m/z* 415.1534, calcd. 415.1526), which was consistent with ^{13}C NMR and HSQC data. The structure of compound **24** was elucidated by detailed analyses of ^{1}H and ^{13}C NMR chemical shift, and by COSY, HSQC, and HMBC experiments (Table 11).

The ^{1}H NMR spectrum clearly showed the presence of a methyl group at δ_H 1.35; an anomeric proton at δ_H 4.36 (d, *J*=7.8 MHz), with a large $^{3}J_{H1,H2}$ coupling constant indicating the β-anomeric configuration of the monosaccharide residue; a set of monosubstituted aromatic proton signals at δ_H 7.26 (t, *J*=7.2 Hz), 7.32 (t,

J=7.2 Hz), 7.40 (d, *J*=7.7 Hz) and hydroxymethylene signals at δ_H 4.63 and 4.88 suggesting the presence of a benzyl alcohol moiety.

The H_2-7 (δ_H 4.88 and 4.63) and C-7 (δ_C 71.6) signals of the benzyl alcohol residue appeared downfield shifted and suggested the position of a monosaccharide unit. HMBC correlations were observed for H-7/C-1' (δ_C 103.1), H-7/C-1 (δ_C 138.6), H-7/C-2(6) (δ_C 128.9), indicating that the monosaccaride unit was linked to the benzyl carbon C-7 (Figure 49).

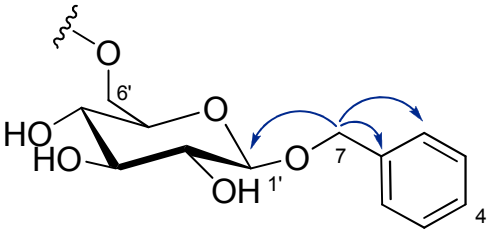

Figure 49. HMBC cross peaks of compound **24**.

Starting from the anomeric proton signal, the proton resonances of sugar moiety were assigned as reported in Table 11, by ^{1}H-^{1}H COSY and TOCSY experiments. The acid hydrolysis of compound **24** afforded D-glucose, which was identified after derivatization with L-cysteine methyl ester hydrochloride, followed by trimethylsilylation and GC analysis.[193,194]

The chemical shift and coupling constants of H-1' (δ_H 4.36 d, *J* = 7.4 Hz) and the chemical shift of C-1' (δ_C 100.5) supported a β-configuration for the anomeric carbon. The low-field chemical shift of H_2-6 (δ_H 3.84 dd and 4.06 dd) in the ^{1}H NMR spectrum, indicated that the hydroxyl group at C-6 of glucose was linked with a second residue.

The ^{13}C NMR data disclosed the presence of two downfield signals at δ_C 172.2 and 180.5, respectively assignable to an ester and a carboxylic function, a quaternary carbon at δ_C 70.9, two methylene carbon and a methyl group.

The HMBC correlations showed the presence of 3-hydroxy-3-methylglutaric acid (HMGA) chain (Figure 50).

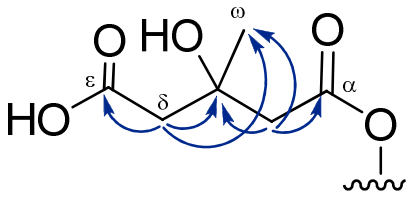

Figure 50. HMBC cross peaks of HMGA in compound **24**.

The connection of the 3-hydroxy-3-methylglutaric acid with the sugar residue was supported from the HMBC correlation observed between the protons at δ_H 4.47 and 4.22 (H_2-6' Glc) and the carbon at δ_C 172.2 (Cα). This data were indicative of an ester function formed between the hydroxyl group in 6' of glucose and the carboxylic group of 3-hydroxy-3-methilglutaric acid (Figure 51).

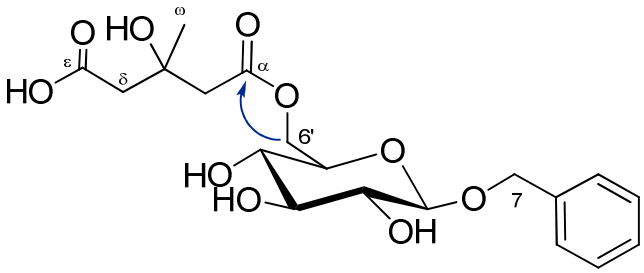

Figure 51. HMBC cross peaks of compound **24**.

Thus the structure of this compound was defined as a benzyl *O*-β-D-glucopyranoside ester-linked with a chain of 3-hydroxy-3-methylglutaric acid (HMGA). This compound was unprecedented in natural products.

There are few examples of natural compounds linked with HMGA. In flaxseed hulls the hydroxy-methyl-glutaric acid is the linker-molecule that connettes a glucosidated lignin with a second monosaccharide derivative to form macromolecules or oligomers.[195,196]

Table 11. ^{1}H and ^{13}C NMR (CD_3OD, 500 MHz) of compound **24.**

Position	δ_H[a] (*J* in Hz)	δ_C	HMBC[b] (H→C)
1	-	138.6	
2,6	7.40 d (7.7)	128.9	C4, C7
3,5	7.32 t (7.2)	128.9	C1
4	7.26 t (7.2)	128.5	C2,6
7	4.88 ovl, 4.63 d (11.8)	71.6	C1, C2,6, C1'
Glc			
1'	4.36 d (7.8)	103.1	C7
2'	3.26	74.9	C1', C3'
3'	3.35	77.7	
4'	3.35	71.4	C3'
5'	3.46	75.1	C4'
6'	4.47 dd (11.8,2.0) 4.22 dd (11.8, 5.6)	64.3	Cα, C4, C5
HMGA			
α	-	172.2	
β	2.63, s	46.8	Cγ, Cα, Cω, Cδ
γ	-	70.9	
δ	2.55 d (15.3)	47.5	Cε, Cγ, Cω, Cβ
δ	2.38 d (15.3)		
ε	-	180.5	
ω	1.35 s	27.5	Cγ, Cβ, Cδ

a ^{1}H and ^{13}C assignments aided by COSY, TOCSY, HSQC and HMBC experiments.
b HMBC correlations, optimized for 8 Hz, are from proton(s) stated to the indicated carbon.

CHAPTER 8

RUSCUS ACULEATUS

Ruscus aculeatus, Ruscaceae, (formerly in Liliaceae) is a low evergreen shrub that is native to the Mediterannean regions, but grows throughout Europe and elsewhere in woods and waste places.

Tough, green, erect, striated stems, which are destitute of bark, have in the upper part many short branches, plentifully furnished with very rigid leaves known as cladodes, which are really a mere expansion of the stem, and terminate each in a single sharp spine (Figure 52). The plant's true leaves are very small and appear at the center of cladodes. They are triangular or lanceolate, and are only a few millimeters long. The plant's greenish-white flowers are placed singly in the center of the cladodes (along with the true leaves), they have a casing made up of 6 petals and blossom in the early spring. The fertile flowers are succeeded by scarlet berries as large as cherries, containing 1-2 seeds, which are ripe in September, and remain attached to the plant all the winter and cause it often to be

picked for room decoration. The root or rhizome is thick, striking deep into the ground, that has no odour, but its taste is sweetish at first and then slightly acrid.

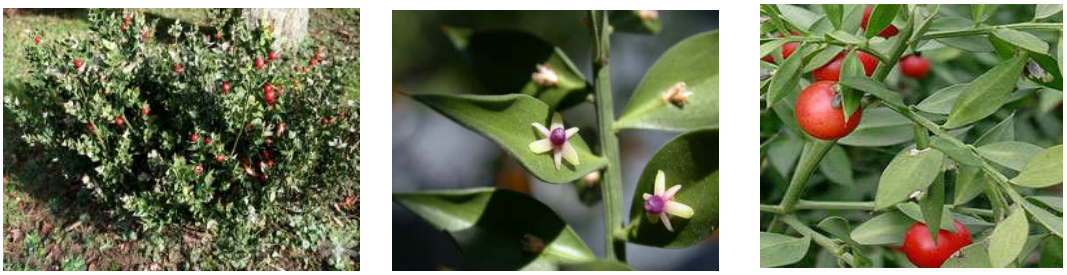

Figure 52. Ruscus aculeautus plant, leaves, flowers and barriers.

Ruscus aculeatus is known with various names. The common name, Knee Holly, is derived from the fact that it rises to a height of a man's knee. The name, *Butcher's Broom,* is derived from the fact that the dried plant was actually used as a broom (until the twentieth century!) throughout Europe, mostly by butchers who used it to whisk scraps from their cutting blocks.

The aerial parts and roots are used in herbal medicine. Ancient Mediterranean healers utilized the root for circulatory and inflammatory disorders, and Greek doctors reported curing swelling with its use, referring to Butcher's Broom as "the miracle herb." The first-century Roman scholar, Pliny, described its use as a cure for varicose veins in the first century, while Dioscorides highly recommended it as a diuretic and aperient (mild laxative), as well as a remedy for kidney stones and dropsy (edema). The herb was used regularly for many years to treat jaundice, gout and kidney and bladder stones.

Today, it is used in Europe for disorders involving the venous system, including venous fragility or varicose veins, and clinical data also revealed positive effects on circulation. In particular, the extracts of rhizomes are used in the prevention and treatment of venous insufficiency.[197-199] Moreover, because of their antielastase activity, they are components of drugs administered as

antiinflammatory and vasoconstrictor agents.[200] Their antiedematous effects have been also demonstrated.[201,202]

8.1 EXTRACTION AND ISOLATION

The plants of *Ruscus aculeatus* were collected from natural population growing in the hill areas of Pisa (Italy) in May 2009. The rhizomes were cleaned and kept frozen at -20°C until analyzed.

Rhizomes of *Ruscus aculeatus* were shaved and exhaustively extracted with MeOH. The MeOH extracts were partitioned according the modified Kupchan partitioning procedure, obtaining four extracts.[2]

The butanol-soluble portions were separated by sequential chromatographic techniques, affording, as major metabolites, three new furostanol saponins (compounds **25**, **26** and **27**).

8.2 SAPONINS

Saponins are terpenoid glycosides distributed widely in the plant kingdom. Saponins can be broadly divided into two groups based on whether the aglycone is of a triterpene or steroidal type. Triterpene saponins are the more widespread class, while steroidal saponins are mainly found in families of monocotyledons. Many medicinally important species are rich in these compounds; plant-derived saponins present a broad spectrum of biological uses, such as anti-cancer, anti-inflammatory, ion channel blocking, immune stimulating, antifungal, antitrombotic, and hypocholesterolemic properties.[203,204]

Rhizomes of *Ruscus aculeatus* are rich in saponins, that are considered to be the active principles of the extract since they induce a beneficial effect on venous insufficiency, especially in the haemorroidal crisis.[205-208]

Steroidal saponins isolated from *Ruscus* species are spirostane prosapogenins bearing a sugar chain linked to C-1 and furostanols carrying a sugar chain at C-1 and a D-glucose residue at C-26.[209-211]

8.3 STRUCTURAL CHARACTERIZATION OF COMPOUND 25

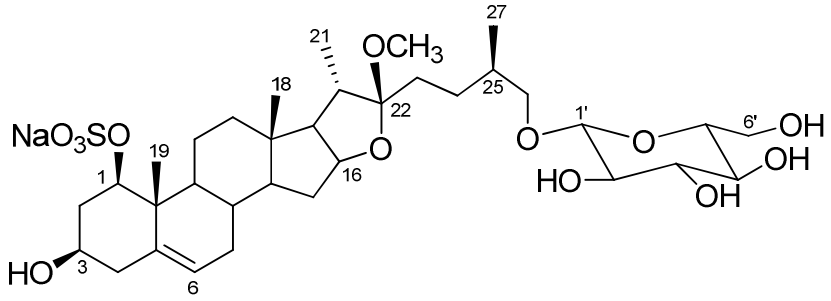

25

Compound **25** showed in the HR-ESIMS spectrum a pseudomelecular ion peak at *m/z* 703.3447 $[M-Na]^-$ corresponding to the molecular formula $C_{34}H_{55}NaO_{13}S$.

The ^1H NMR spectrum (Table 12) exhibited the signals of four distinct methyl groups (two singlets at δ_H 0.84 and 1.10 and two doublets at δ_H 0.95 and 0.99), a methoxyl signal at δ_H 3.14, an anomeric proton at δ_H 4.23 (d, *J*=7.7 MHz), a signal at δ_H 5.59 (br d, *J*=5.3 MHz), that was ascribable to a proton on sp^2 carbon, and a further signal at δ_H 4.01, that in the HSQC experiment was correlated to the carbon at δ_C 85.6, that was attributed to a proton on oxygenated bearing carbon esterificated with a sulfate group. This pattern of proton chemical shifts led us to initially suppose the glycoterpene nature of the compound. This was further corroborated by the ^{13}C NMR spectrum, which showed the resonance of an

anomeric carbon (δ_C 104.3); the presence of the semiketal carbon signal at δ_C 113.9, together with the carbinol at δ_C 82.2, suggested the furostanol nature of the aglycon. All the proton resonances were unambiguously associated with the relevant carbon atoms by using the HSQC spectrum.

Insepction of COSY and TOCSY spectra allowed us to detect four distinct spin systems: three of them belonging to the aglycon moiety and the remaining one belonging to a monosaccharide unit (Figure 53).

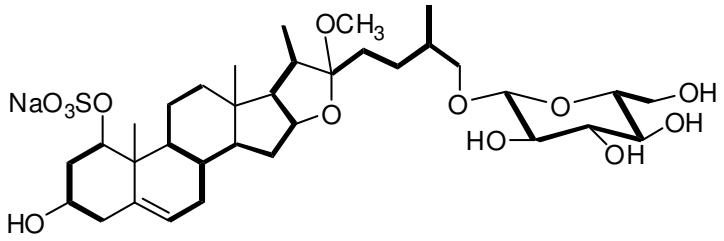

Figure 53. Four distinct spin systems deduced from COSY spectrum.

Concerning the aglycon moiety, the first spin system possessed two substituents at position 1 and 3, respectively a sulfated and an hydroxyl group; this spin system connected the sulfated carbon C-1 (δ_H 4.01, δ_C 85.6) with C-4, while the second one, starting from the sp^2 C-6 (δ_H 5.60, δ_C 126.4) and encompassing all the protonated carbons of rings B, C and D ran out with C-21. The last spin system of the aglycon was constituted by protons of the side chain, from C-23 to the oxygen-bearing C-26 (δ_H 3.38-3.73, δ_C 75.6), including CH_2-CH_2-$CH(CH_3)$-CH_2O-.

Concerning the sugar portion of the molecule, the last spin system started from the anomeric proton and arrived to the hydroxymethylene at C-6', identifying a hexopyranose unit. Comparing the ^1H and ^{13}C NMR values of this monosaccharide unit with the data reported in literature, a glucose was identified.

The chemical shift and the coupling constants of H-1' (δ_H 4.23, d, *J*=7.7 MHz) and the chemical shift of C-1' (δ_C 104.3) supported a β-configuration for the anomeric proton. To confirm the nature of the sugar and to determine its absolute configuration, compound **25** was subjected to acid hydrolysis (HCl 1N). The hydrolyzed was reacted with L-cysteine methyl ester hydrochloride; followed by trimethylsilylation and GC analysis in comparison with D- and L- glucose.[193] By this procedure the sugar was identified as D-glucose.

Data arising from HMBC experiment were used to interconnect the spatial structures (Figure 54). The following HMBC cross-peaks were particularly diagnostic to assemble the above structures: H_3-19 (δ_H 1.10) with C-1 (δ_C 85.6), C-5 (δ_C 138.7), C-9 (δ_C 50.7), and C-10 (δ_C 43.7); H_3-18 (δ_H 0.84) with C-12 (δ_C 40.8), C-13 (δ_C 41.4), C-14 (δ_C 57.5) and C-17 (δ_C 65.0); H_3-21 (δ_H 1.72) with C-17, C-20 (δ_C 41.0) and the ketal carbon C-22 (δ_C 113.9), and the methoxyl protons (δ_H 3.14) with C-22. So the three methyl groups were placed in positions 10, 13 and 20; and the methoxyl group was placed on the ketal carbon at C-22. The side chain was linked to C-22, because the presence of HMBC cross-peaks between H_2-23 (δ_H 1.72-1.63) and C-20 and C-22. A further methyl group was placed on the side chain at C-25 for the presence of the HMBC correlations of H_3-27 with C-24 (δ_C 28.7), C-25 (δ_C 34.7) and C-26 (δ_C 75.6). The total of this evidence allowed us to identify the aglycon moiety as a Δ^5-furostan-1,3,22,26-tetraol.

The β-D-glucose unit was placed at C-26 by interpretation of the key HMBC correlation peak between H-1' (δ_H 4.23) and C-26 (δ_H 75.6).

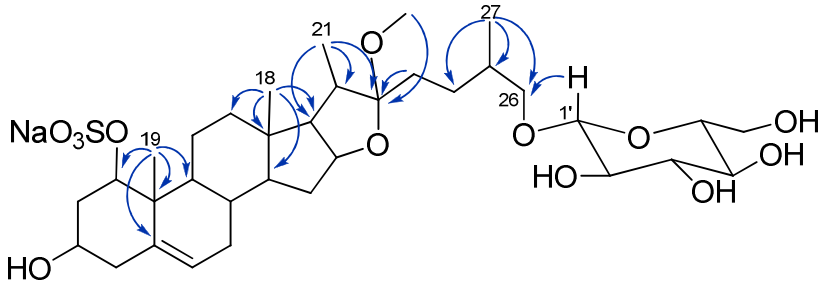

Figure 54. Key HMBC correlations of compound **25**.

The presence of the sulfate group was confirmed after solvolysis in a dioxane-pyridine mixture, that afforded a less polar desulfated derivative, which gave a pseudomolecular ion at *m/z* 623.5 $[M-H]^-$. The upfield shift of the H-1 signal from δ_H 4.01 to 3.34 ppm in the desulfate derivative established the location of the sulfate residue at C-1 of the aglycon. This placement was confirmed by ^{13}C NMR, in which the signal of C-1 was upfield shifted from δ_C 85.6 to 78.6 ppm.

The ROESY experiment allowed us to determinate the ring-junctions (Figure 55). In particular, the ROESY correlations H-11/H_3-19, H-11/H_3-18, H-9/H-14, H-14/H-16, H-16/H-17 and H-17/H_3-21 completed the relative stereochemistry of the saponin with the usual B/C *trans*, C/D *trans*, D/E *cis*, and C-20α stereochemistries.[212,213] The ROE effect between H-1 and H-3 indicated the *cis* orientation of the two substituents of ring A.

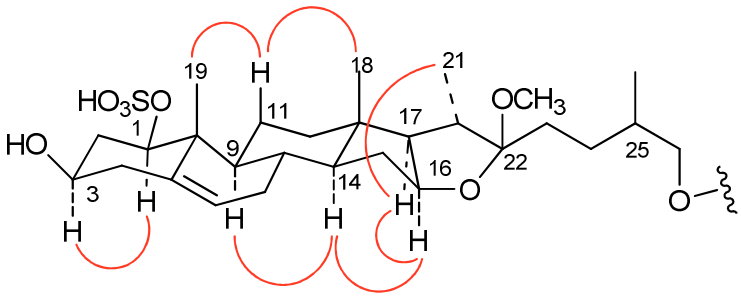

Figure 55. ROE correlations supporting the relative configuration of compound **25**.

The last step was the determination of the stereochemistries at C-22 and C-25.

We have assigned the 22β orientation on the basis of the chemical shift value of H-16. In fact when the methoxyl group is α, the signal of H-16 was downfield shifted, due to the deshielding effect of the *cis*-oriented OCH_3 group (H-16 δ_H 4.60 instead of 4.35).[214,215]

The 25*R* stereochemistry of the side chain was tentatively assigned by the resonances of the protons and carbons at C-25, C-26 and C-27 and by the vicinal couplings between H-25 and the two H-26, in comparison with the literature data.[216] To confirm this stereochemistry, we will derivatize with a chiral agent (MPTA, the Mosher reagent). This method allows determination of the absolute configuration of primary carbinols with a chiral center at C-2 by comparing ^{1}H-NMR spectra with those of 25-(R)- and 25-(S)-MPTA esters of model compounds.

8.4 STRUCTURAL CHARACTERIZATION OF COMPOUND 26

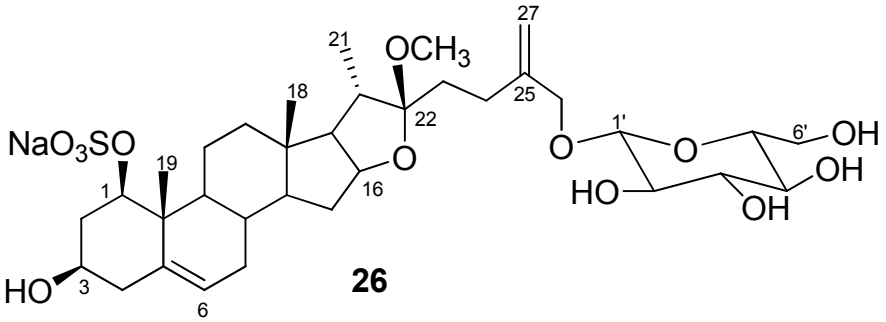

26

Compound **26** showed a pseudomolecular ion peak at *m/z* 701.4326 $[M-Na]^-$, corresponding to the molecular formula $C_{34}H_{53}NaO_{13}S$, indicating, as in compound **25,** the presence of a sulfate function. The ^{1}H NMR spectrum was very similar to that of compound **25**, concerning the steroidal portion, but it differs only for the side chain (Table 12). In particular the ^{1}H NMR spectrum clearly showed the loss

of the methyl group at C-25 and the gain of two signals [δ_H 5.10 and 4.94 (br s)], ascribable to protons on sp^2 carbon, suggesting the replacement of a methyl group with an exomethylene group. This function was placed in the side chain at C-25 for the presence of diagnostic HMBC cross-peaks between the two vynil portons with the C-24 (δ_C 28.5), C-25 (δ_C 147.0), and C-26 (δ_C 72.5) (Figure 56).

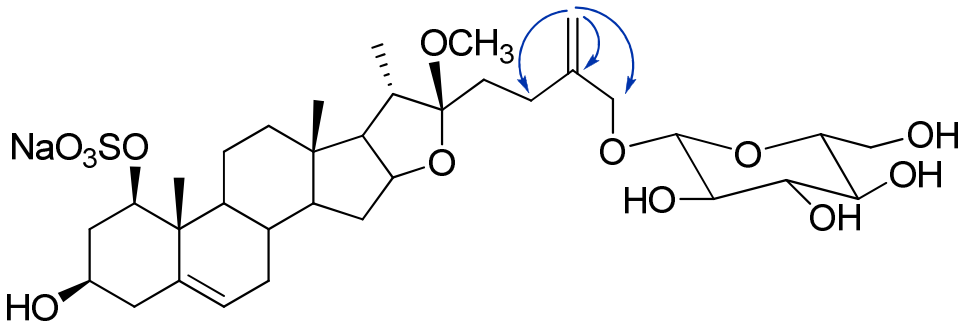

Figure 56. Key HMBC correlations of the side chain of compound **26**.

The steroidal saponin skeleton was considered to adopt the usual B/C trans, C/D trans, D/E cis arrangement, and the two substituents of ring A was considered to adopt a cis orientation as evidenced by ROESY analysis. The stereochemistry at C-22 and C-25 were established similarly to compound **25**.

Saponins containing sulphated sugar residues have frequently been identified,[217,218] but direct esterification of the aglycone by a sulphate function is much less common.[219]

8.5 STRUCTURAL CHARACTERIZATION OF COMPOUND 27

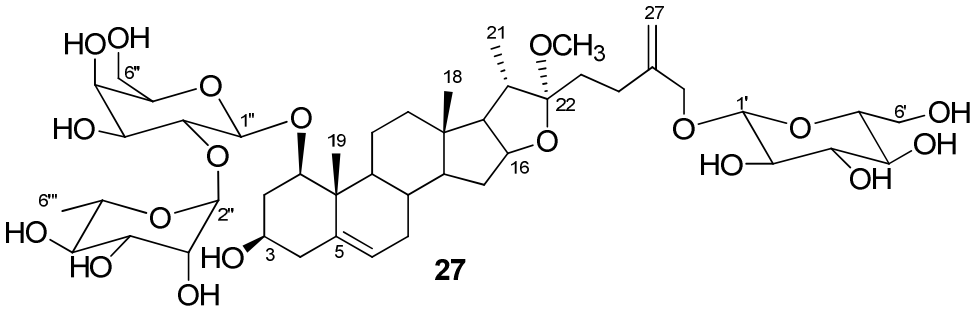

27

Compound **27** showed a pseudomolecular ion peak at *m/z* 929.5682 $[M-H]^-$, corresponding to the molecular formula $C_{46}H_{74}O_{19}$. The ^1H NMR spectrum of compound **27** was very similar to that of compound **26** concerning the side chain (Table 13 Hz). This spectrum clearly evidenced the gain of a methyl group at δ_H 1.24 (d, *J*=6.6); the loss of the proton at δ_H 4.03, suggesting the absence of the sulfate group, also confirmed by mass data; and a number of overlapped signals between δ_H 3.16 and 5.30, attributable to protons on oxygen-bearing carbons, indicating the presence of some sugar units. In particular there were three anomeric protons at δ_H 4.27 (d, *J*=7.5), 4.28 (d, *J*=7.6) and 5.29 (br s), indicating the presence of three sugar units. This was further corroborated by the ^{13}C NMR which showed the resonances of three anomeric carbons at δ_C 101.0, 101.6, 103.3. The interpretation of bidimentional NMR data showed that the aglycone moiety of compound **27** was superimposable to that of compound **26**, except for the replacement of the sulfate group at C-1 with a sugar moiety. In fact, the H-1 proton was upfield shifted from δ_H 4.03 to 3.37 ppm.

Analysis of homonuclear COSY and TOCSY experiments allowed the assignements of all the proton resonances of the three sugar moieties, whereas

evaluation of the coupling constants was used to elucidate the monosaccaride relative stereochemistry.

Hence, when the anomeric proton at δ_H 4.27 (H-1'') was used as a starting point, a sequence of only two oxymethines was identified from the TOCSY spectrum. The large coupling constants observed for H-1"/H-2" and H-2"/H-3" vicinal couplings, and the relatively small coupling constants of H-3"/H-4" and H-4"/H-5", indicated the β-galactopyranose nature of this sugar. The pattern of ^{13}C NMR resonances confirmed this assignment. The galactopyranose residue was linked to the C-1 of the aglycon, as indicated by the HMBC correlation peak between the anomeric proton H-1" at δ_H 4.27 to the C-1 at δ_C 84.2 (Figure 56).

The spin system starting with the anomeric proton at δ_H 5.29 (H-1'''), extended to four oxymethine and one methyl group. This sugar moiety was identified as a rhamnopyranose. The chemical shift of C-3''' (δ_C 72.1) and C-5''' (δ_C 69.7) indicated the α-anomeric configuration of this sugar, in accordance with data reported in literature.[220] The linkage of this monosaccharide at C-2" of the galactose unit was inferred on the basis of the HMBC cross-peaks between H-1''' (δ_H 5.29) and C2" (δ_C 75.6) (Figure 57).

On the other hand, the HMBC cross-peaks of H-1' (δ_H 4.28) with the C-26 (δ_C 72.5) allowed to identify this carbon as a further glycosidic linkage site. Starting from the H-1' (δ_H 4.28), we identified a sequence of four oxymethine and one oxymethylene protons. These data led to the assignment of this sugar as a β-glucopyranose linked at C-26 like in compound **26**.

The stereochemical series of the sugar units were defined as D for glucose and galactose and L for rhamnose, assuming that these monosaccharides belong to the most commonly found stereochemical series.

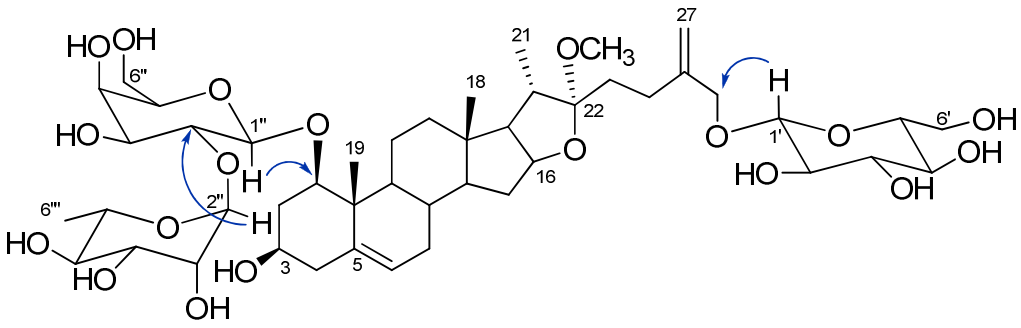

Figure 57. HMBC cross-peaks of the sugar units.

ROESY experiment showed the usual B/C *trans*, C/D *trans*, D/E *cis* arrangement, C-20α stereochemistry, and a *cis* orientation for the two substituents of ring A, similarly to compound **26**.

However, this compound differed from compound **26** in the stereochemistry of C-22. In fact ^{1}H and ^{13}C NMR spectra of these two compounds appeared to differ considerably in the resonances of atoms located close to C-22. We had tentatively assigned the 22α orientation to compound **27** on the basis of the ^{1}H NMR resonance of H-16, slightly downfield shifted (at δ_H 4.57 instead of 4.39) compared to compound **26**, suggesting that it was deshielded by the *cis*-orientation of the methoxyl group at C-22.

Table 12. ^{1}H and ^{13}C NMR (CD_3OD, 500 MHz) of compounds **25** and **26.**

	Compound 25		**Compound 26**	
Position	δ_H (*J* in Hz)	δ_C	δ_H (*J* in Hz)	δ_C
1	4.01 (dd, 11.7, 3.9)	85.6	4.03 (dd, 11.7, 3.89	84.6
2a	2.55 [a]	38.8	2.58 [a]	38.8
2b	1.67 [a]		1.72 [a]	
3	3.42 [a]	68.7	3.46 [a]	68.6
4a	2.21 [a]	42.8	2.26 [a]	42.7
4b				
5	-	138.7	-	137.9
6	5.60 (br d, 5.3)	126.4	5.61 (br d, 5.4)	126.5
7a	1.95 [a]	32.7	1.99 [a]	32.6
7b	1.54 [a]		1.51 [a]	
8	1.54 [a]	33.7	1.58 [a]	33.8
9	1.35[a]	50.7	1.38 [a]	50.8
10	-	43.7	-	43.7
11a	2.36[a]	24.0	2.39 [a]	23.8
11b			1.55 [a]	
12a	1.70[a]	40.8	1.74 [a]	40.9
12b	1.25[a]		1.29 [a]	
13	-	41.4	-	41.4
14	1.13[a]	57.5	1.19 [a]	57.4
15a	1.95[a]	32.6	2.00 [a]	32.7
15b	1.25[a]		1.32 [a]	
16	4.35 (m)	82.2	4.39 (m)	82.3
17	1.71[a]	65.0	1.75 [a]	65.0
18	0.84 s	16.7	0.87 s	16.7
19	1.10 s	14.5	1.13 s	14.5
20	2.17 [a]	41.0	2.23 [a]	41.1
21	0.99 (d, 6.8)	16.1	1.04 (d, 6.7)	15.9
22	-	113.9	-	112.7
23a	1.72 [a]		1.58 [a]	31.8
23b	1.63 [a]			
24a	1.57 [a]	28.7	2.22 [a]	28.5
24b	1.12 [a]		1.87 [a]	
25	1.72 [a]	34.7	-	147.0
26a	3.73 [a]	75.6	4.36	72.5
26b	3.38 [a]		4.12	
27	0.95 (d, 6.6)	17.1	5.10 (br s)	111.9
			4.94 (br s)	
OCH_3	3.14 s	47.4		
Glucose				
1’	4.23 (d, 7.7)	104.3	4.27 (d, 7.7)	103.0
2’	3.18 [a]	74.9	3.23 [a]	74.8
3’	3.35 [a]	77.9	3.35 [a]	77.8
4’	3.25 [a]	71.5	3.20 [a]	71.4
5’	3.26 [a]	77.9	3.26 [a]	77.6
6’	3.84 (br d, 11.7)	62.6	3.88 (br d, 11.8)	62.5
	3.64 (dd, 11.7, 5.1)		3.69 (dd, 11.8, 5.2)	

[a] Overlapped with other signals

Table 13. ^{1}H and ^{13}C NMR (CD_3OD, 500 MHz) of compounds **27.**

Position	δ_H (*J* in Hz)	δ_C
1	3.37 [a]	84.2
2a	2.09 [a]	36.9
2b	1.68 [a]	
3	3.34 [a]	68.9
4a	2.26 [a]	43.1
4b	2.22 [a]	
5	-	141.1
6	5.56 (br d, 5.3)	125.6
7a	1.97 [a]	32.7
7b	1.56 [a]	
8	1.55 [a]	33.7
9	1.24 [a]	51.1
10	-	43.1
11a	2.56 [a]	24.5
11b	1.44 [a]	
12a	1.69 [a]	40.9
12b	1.21 [a]	
13	-	41.2
14	1.44 [a]	57.5
15a	1.97 [a]	32.4
15b	1.28 [a]	
16	4.57 (m)	82.1
17	1.77 [a]	63.9
18	0.85 s	16.9
19	1.10 s	14.9
20	2.14 [a]	40.6
21	1.02 (d, 6.6)	15.7
22	-	111.1
23a	1.85 [a]	37.6
23b		
24a	2.28 [a]	28.2
24b		
25	-	147.0
26a	4.34	72.5
26b	4.12	
27	5.08 (br s)	111.9
	4.93 (br s)	
OCH_3	3.16 s	47.4

[a] Overlapped with other signals

Position	δ_H (*J* in Hz)	δ_C
Glucose		
1’	4.28 (d, 7.6)	103.3
2’	3.20 [a]	75.2
3’	3.35 [a]	78.1
4’	3.28 [a]	71.7
5’	3.26 [a]	77.9
6’	3.88 [a]	62.8
	3.65 [a]	
Galactose		
1’’	4.27 (d, 7.5)	101.0
2’’	3.69 [a]	75.6
3’’	3.67 [a]	72.2
4’’	3.63 [a]	76.0
5’’	3.73 [a]	70.9
6’’	3.85 (br d, 11.5)	67.4
	3.48 (br d, 11.5)	
Rhamnose		
1’’’	5.29 (br s)	101.6
2’’’	3.88 [a]	72.4
3’’’	3.69 [a]	72.1
4’’’	3.39 [a]	74.2
5’’’	4.08 [a]	69.7
6’’’	1.24 (d, 6.6)	18.4

[a] Overlapped with other signals

CONCLUSIONS

In conclusion, natural products have proven to be the most prolific source of new and effective drugs, and they have also provided insight into new mechanisms of action. Medicine would be immeasurably poorer without the insights and the compounds provided from Nature.

It is thus instructive to ask why it is that natural products have proved to be such a prolific source of bioactive agents. There are several reasons, but certainly one of the most important is that plants and marine organisms produce many biologically active substances for defense and other purposes, and so these substances are uniquely tailored to fit into a biological receptor of some kind. Natural products are often large molecules with built-in chirality and are thus uniquely suited to bind to complex proteins and other biological receptors. As a result of these considerations, there is a high correlation between the properties of drugs and those of natural products.

The focus of this phD Thesis was the investigation of bioactive secondary metabolites from different natural sources (plants and marine sponges) that has been successful in the discovery of new chemistry with potential pharmaceutical and biochemical applications. This thesis underlines that the marine sponges are a cornucopia of new bioactive compounds, and plants are still contributing to medicine. The interest in these compounds is first of all due to their strong biological activity. This aspect has also inspired synthetic study to develop several synthetic methodologies and strategies for new drugs.

In summary, the misconception that natural products research has not produced many drugs is laid: the future of natural products research remains bright.

EXPERIMENTAL SECTION

I. General Experimental Procedures.

Optical rotations ($CHCl_3$ or MeOH) were measured at 589 nm on a JASCO P-2000. High-resolution ESI-MS spectra were performed with a Micromass Q-TOF mass spectrometer. ESIMS experiments were performed on an Applied Biosystem API 2000 triple–quadrupole mass spectrometer. ^{1}H (500 and 700 MHz) and ^{13}C (125 and 175 MHz) NMR spectra were measured on Varian INOVA spectrometers. Chemical shifts were referenced to the residual solvent signal ($CHCl_3$: δ_H 7.26, δ_C 77.0; CD_2HOD: δ_H 3.30, δ_C 49.0; CD_2HSOCD_3: δ_H 2.50, δ_C 39.5). Homonuclear ^{1}H connectivities were determined by the COSY experiment; one-bond heteronuclear ^{1}H-^{13}C connectivities by the HSQC experiment; two- and three-bond ^{1}H-^{13}C connectivities by gradient-HMBC experiments optimized for a $^{2,3}J$ of 8 Hz .

DCCC was performed using a DCC-A (Rakakikai Co. Di Tokio) equipped with 250 columns (internal diameter 3 mm).

Medium pressure liquid chromatography was performed on a Büchi apparatus using a silica gel (230-400 mesh) column.

HPLC was performed using a Waters Model 510 pump equipped with Rheodine injector and a differential refractometer, Waters model 401.

II. Experimental Section of *Coscinoderma mathewsi*

Sponge material and separation of individual sesterpenoids. *Coscinoderma mathewsi* Lendenfield (order Dictyoceratida, family Spongiidae) was collected on the barrier reef of Vangunu Island, Solomon Islands, in July 2004. The samples were frozen immediately after collection and lyophilized to yield 322 g of dry mass. The sponge was identified by Dr John Hooper, Queensland Museum, Brisbane, Australia, where a voucher specimen is deposited under the accessing number G322695.

The lyophilized material (322 g) was extracted with methanol (3×3 L) at room temperature and the crude methanolic extract (72.6 g) was subjected to a modified Kupchan's partitioning procedure as follows. The methanol extract was dissolved in a mixture of MeOH/H_2O containing 10% H_2O and partitioned against *n*-hexane. The water content (% v/v) of the MeOH extract was adjusted to 30% and partitioned against $CHCl_3$. The aqueous phase was concentrated to remove MeOH and then extracted with *n*-BuOH. The hexane, chloroform and butanol extracts were tested against PLA_2 at 400 mg/mL dose showing 94, 93 and 59% inhibition, respectively.

The *n*-BuOH extract (4 g) was chromatographed in four runs by DCCC ($CHCl_3$/MeOH/H_2O, 7:13:8, ascending mode) and fractions of 6 mL were collected and combined on the basis of their similar TLC retention factors.

Fraction 7 (28.4 mg) was purified by HPLC on a Nucleodur C18 column (3μm, 150×4.60 mm, flow rate 1.0 mL/min) with 45% MeOH/H_2O as eluent to give 3.1 mg of coscinolactam A (**1**) (t_R=10 min) and 1.9 mg of coscinolactam B (**2**) (t_R=11 min).

The chloroform-soluble material (1.5 g), mainly containing suvanine, was chromatographed by DCCC using $CHCl_3$/MeOH/H_2O (7:13:8) in the ascending mode (the lower phase was the stationary phase); the flow rate was 18 mL/h; 6 mL fractions were collected and combined on the basis of their similar TLC retention factors.

Fraction 2 (262 mg) was purified by HPLC on a μ-Bondapack C18 column (10μm, 300×7.8 mm, flow rate 4.0 mL/min) with 65% MeOH/H_2O as eluent to give 240 mg of suvanine (t_R=8 min).

Characteristic data for each compound

Coscinolactam A: white amorphous solid; $[\alpha]_D^{25}$ +25.7 (*c* 0.07, methanol); ^1H and ^{13}C NMR data in CD_3OD given in Table 1; ESI-MS: *m/z* 522.3 $[M-H]^-$. HRMS (ESI): calcd. for $C_{27}H_{40}NO_7S$: 522.2525; found 522.2547 $[M-H]^-$.

Coscinolactam B: white amorphous solid; $[\alpha]_D^{25}$ +8.57 (*c* 0.07, methanol); ^1H and ^{13}C NMR data in CD_3OD given in Table 1; ESI-MS: *m/z* 522.3 $[M-H]^-$. HRMS (ESI): calcd. for $C_{27}H_{40}NO_7S$: 522.2525; found 522.2509 $[M-H]^-$.

Suvanine: white amorphous solid; $[\alpha]_D^{25}$ +12.2 (*c* 0.4, methanol); ESI-MS: *m/z* 522.3 $[M-H]^-$. HRMS (ESI): calcd. for $C_{25}H_{37}O_5S$: 449.2362; found 449.2387 $[M-H]^-$.

Synthetic Procedures

Aldehyde 4

A solution of suvanine **3** (15 mg, 0.033 mmol) in pyridine (0.5 ml) and dioxane (0.5 ml) was heated at 150°C for 2.5 h in a stoppered reaction vial. After the solution was cooled, the mixture was evaporated to dryness and then purified by HPLC on a μ-Bondapak C18 column (30 cm x 3.9 mm i.d.) with MeOH/H_2O

80:20, to give aldehyde **4** as a 9:1 mixture of two diasteroisomers (9.2 mg, 80%). ESIMS: 371.30 $[M+H]^+$; selected ^{1}H-NMR (500 MHz, $CDCl_3$) for major diasteroisomer: 9.48 (1H, s, -CHO), 7.39 (1H, s), 7.28 (1H, s), 6.33 (CH-18, s), 1.04 (3H, s), 0.87 (3H, s), 0.86 (3H, s), 0.84 (3H, s),.

Alcohol 5

$NaBH_4$ was added in one portion to a stirred solution of **4** (5.2 mg, 0.014 mmol) in MeOH at room temperature. The mixture was stirred for 1 h and then was concentrated *in vacuo* and then diluted with NH_4Cl and ethyl acetate. The aqueous phase was extracted with ethyl acetate and then the combined organic extracts were washed with brine, dried (Na_2SO_4) and concentrated *in vacuo* to yield alcohol **5** as a 9:1 mixture of two diasteroisomers (4.7 mg, 90%). ESIMS: 373.40 $[M+H]^+$; selected ^{1}H-NMR (500 MHz, $CDCl_3$) for major diasteroisomer: 7.39 (1H, s), 7.28 (1H, s), 6.33 (1H, s), 3.71 (d, J=11.3 Hz, H-24), 3.43 (dd, J=11.3, 4.5 Hz, H-24), 1.13 (3H, s), 0.90 (3H, s), 0.86 (6H, s).

Anti-inflammatory assays.

Materials. [5,6,8,11,12,14,15(n)-^{3}H] PGE_2 and [9,10-^{3}H]oleic acid were purchased from Amersham Biosciences (Barcelona, Spain). Inducible NO synthase specific polyclonal antiserum was purchased from Cayman Chem. (MI, USA). The peroxidase-conjugated goat anti-rabbit Immunoglobulin G (IgG) was purchased from Dako (Copenhagen, Denmark). The rest of reagents were from Sigma (MO, USA)

Assay of $sPLA_2$. $sPLA_2$ activity was assayed using [^{3}H]-oleate labeled membranes of *Escherichia coli*, following a modification of the method of Franson *et al.*[221,222] *E. coli* strain CECT 101 was grown for 6 to 8 h at 37 ºC in the presence of 5 μCi/mL [^{3}H]-oleic acid (specific activity 10 Ci/mmol) until the end

of the logarithmic phase. After centrifugation at 1,800 *g* for 10 min at 4 ºC, the membranes were washed, resuspended in PBS and autoclaved for 30 to 45 min. At least 95% of the radioactivity was incorporated into the phospholipid fraction. *Naja naja* venom (Group IA $sPLA_2$), porcine pancreatic (Group IB $sPLA_2$), human recombinant synovial (Group IIA $sPLA_2$), and bee venom (Group III $sPLA_2$) enzymes were used as sources of $sPLA_2$. Enzymes were diluted in 10 µL of 100 mM Tris-HCl, 1 mM $CaCl_2$ buffer pH 7.5, and preincubated at 37 ºC for 5 min with test compound or vehicle in a final volume of 250 µL. Incubation proceeded for 15 min in the presence of 20 µL of [^{3}H]oleic-*Escherichia coli* membranes and was terminated by addition of 100 µL ice-cold solution of 0.25% BSA in saline to a final concentration of 0.07% w/v. After centrifugation at 2,500 x g for 10 min at 4 ºC, the radioactivity in the supernatants was determined by liquid scintillation counting.

Culture of murine macrophage RAW 264.7. The mouse macrophage cell line RAW 264.7 (Cell Collection, Department of Animal Cell Culture, C.S.I.C., Madrid, Spain) was cultured in Dulbecco's modified Eagle's medium (DMEM) containing 2 mM L-glutamine, 100 U/mL penicillin, 100 µg/mL streptomycin and 10% foetal bovine serum. Cultures were maintained at 37 ºC in 5% CO2 (air: CO2, 95:5) humidified incubator. Cells were resuspended at a concentration of $1.5x10^6$ cells/mL.

Nitric oxide and PGE_2 production in RAW 264.7 macrophages. RAW 264.7 macrophages ($1.5x10^6$ cells/mL) were co-incubated in 96-well culture plate (200 µL) with 1 µg/mL of *Escherichia coli* [serotype 0111:B4] lipopolysaccharide (LPS) at 37 ºC for 20 h in the presence of test compounds or vehicle. Nitrite

concentration as reflection of NO release was assayed fluorometrically.[223] PGE_2 levels were determined in culture supernatants by radioimmunoassay.[224] The mitochondrial-dependent reduction of 3-(4,5-dimethylthiazol-2-yl)-2,5-diphenyltetrazolium bromide (MTT) to formazan,[225] was used to assess the possible cytotoxic effects of compounds (100% viability = 0.533 ± 0.010 at 492 nm).

Western blot assay of iNOS. Cellular lysates from RAW 264.7 (murine macrophages $1.5x10^6$ cell/mL) incubated for 18 h with LPS (1 μg/mL) were obtained with lysis buffer A (10 mM HEPES, pH 8.0, 1 mM EDTA, 1mM EGTA, 10 mM KCl, 1 mM dithiothreitol, 5mM NaF, 1 mM Na_3VO_4, 10mM Na_2MoO_4, 1 μg/mL leupeptin, 0.1 μg/mL aprotinin and 0.5 mM phenylmethyl sulfonyl fluoride). Following centrifugation (10,000 x g/15 min/4 ºC), supernatant protein was determined by the Bradford method[226] using bovine serum albumin (BSA) as standard. iNOS protein expression was studied in the total fraction Equal amounts of protein (25 μg) were loaded on 15% SDS-PAGE and transferred onto polyvinylidene difluoride membranes for 90 min at 125 mA. Membranes were blocked in PBS (0.02M pH 7.0)-Tween 20 (0.1%), containing 3% w/v unfatted milk and incubated with specific polyclonal antibody against iNOS (1/1,000). Finally, membranes were incubated with peroxidase-conjugated goat anti-rabbit IgG (1/10,000). The immunoreactive bands were visualized using an enhanced chemiluminescence system (Amersham Biosciences, Barcelona, Spain).

Statistical analysis. The results are presented as mean ± SEM represents the number of experiments. Inhibitory concentration 50% (IC_{50}) values were calculated from at least 4 significant concentrations (n=6). The level of statistical

significance was determined by analysis of variance (ANOVA) followed by Dunnett's *t*-test for multiple comparisons.[227]

Spectroscopic Data of Coscinolactams A and B

^{1}H NMR spectrum of coscinolactam A in CD_3OD at 700 MHz.

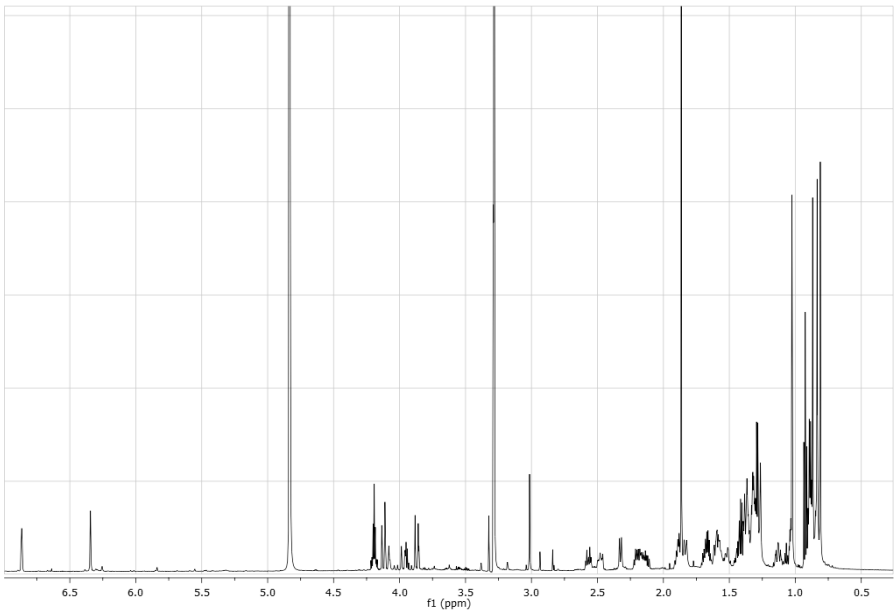

COSY spectrum of Coscinolactam A in CD_3OD at 700 MHz.

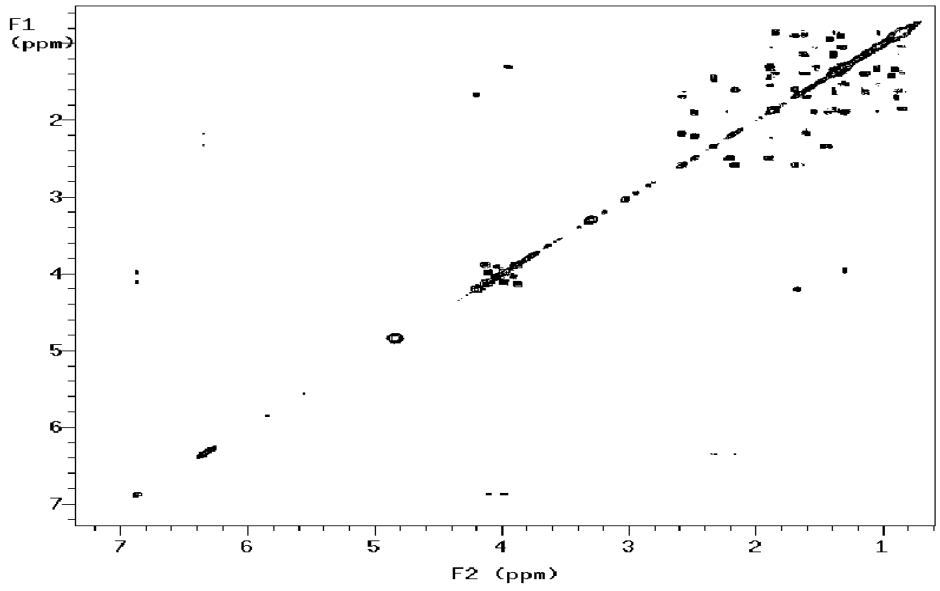

HSQC spectrum of Coscinolactam A in CD_3OD at 700 MHz.

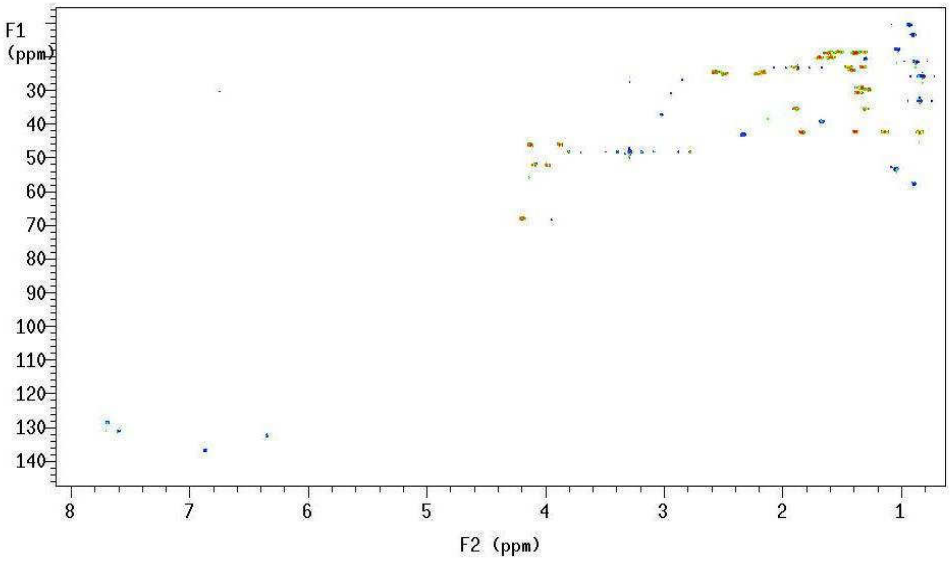

TOCSY spectrum of coscinolactam A in CD_3OD at 700 MHz.

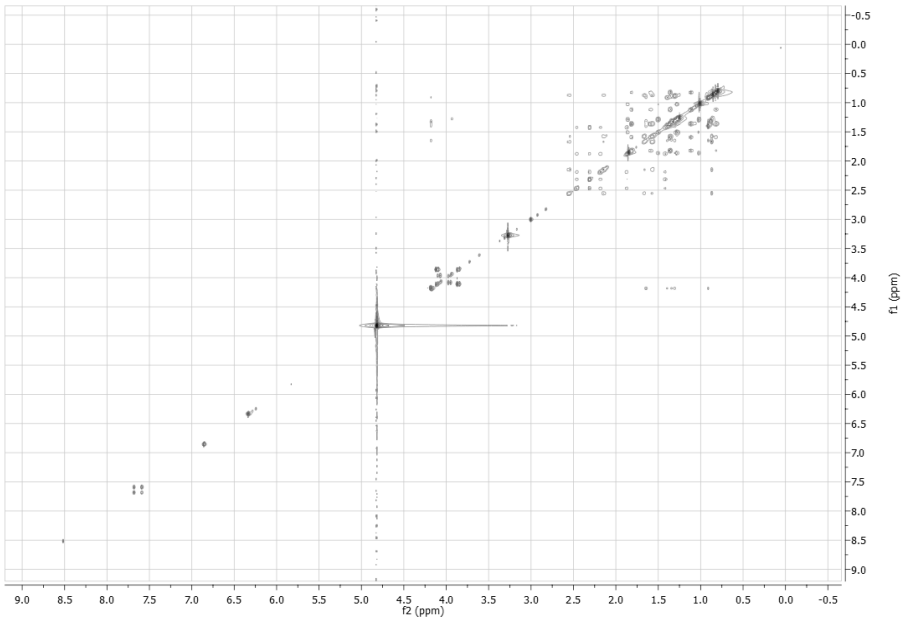

HMBC spectrum of Coscinolactam A in CD_3OD at 700 MHz.

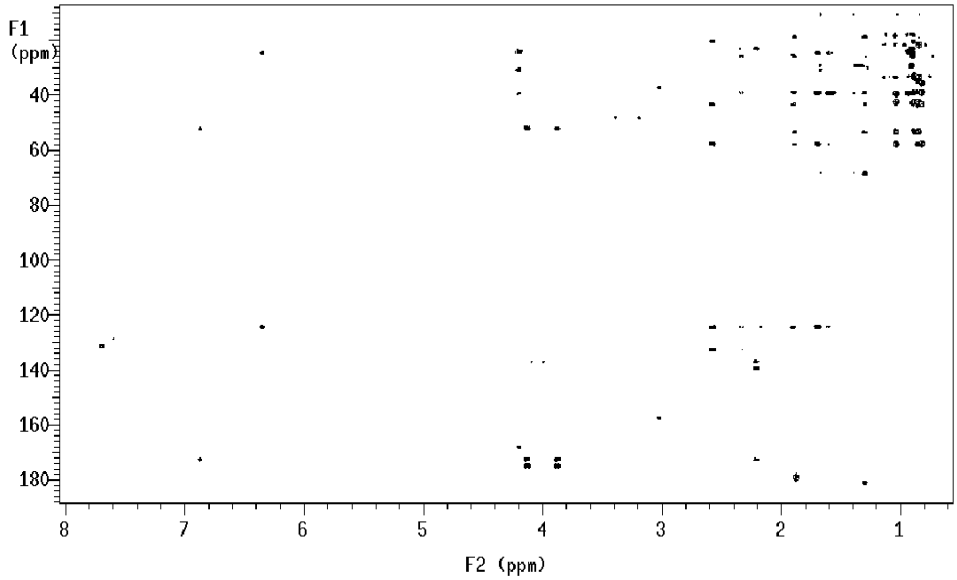

^1H NMR spectrum of coscinolactam B in CD_3OD at 700 MHz.

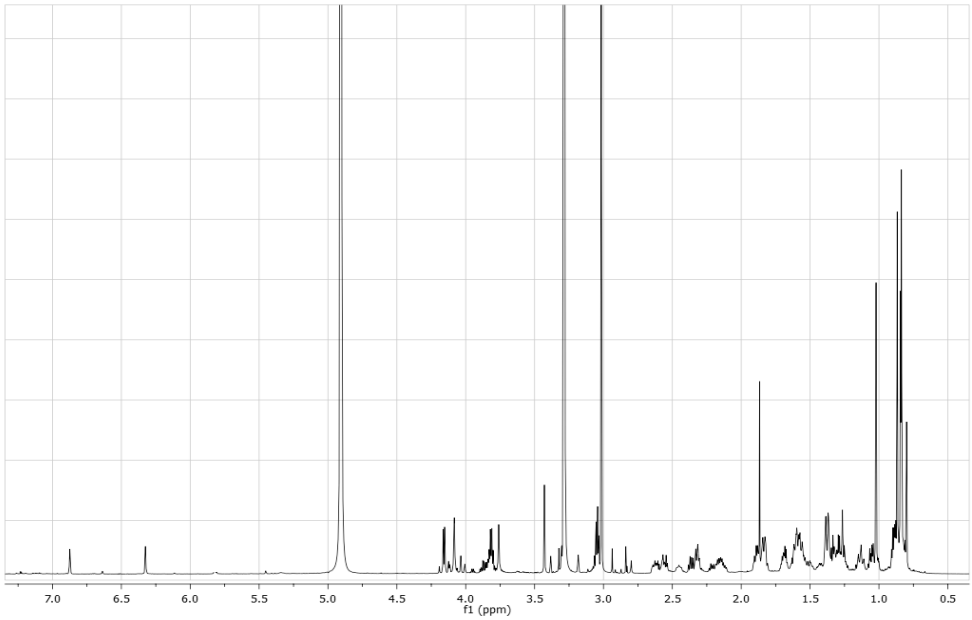

HSQC spectrum of coscinolactam B in CD_3OD at 700 MHz.

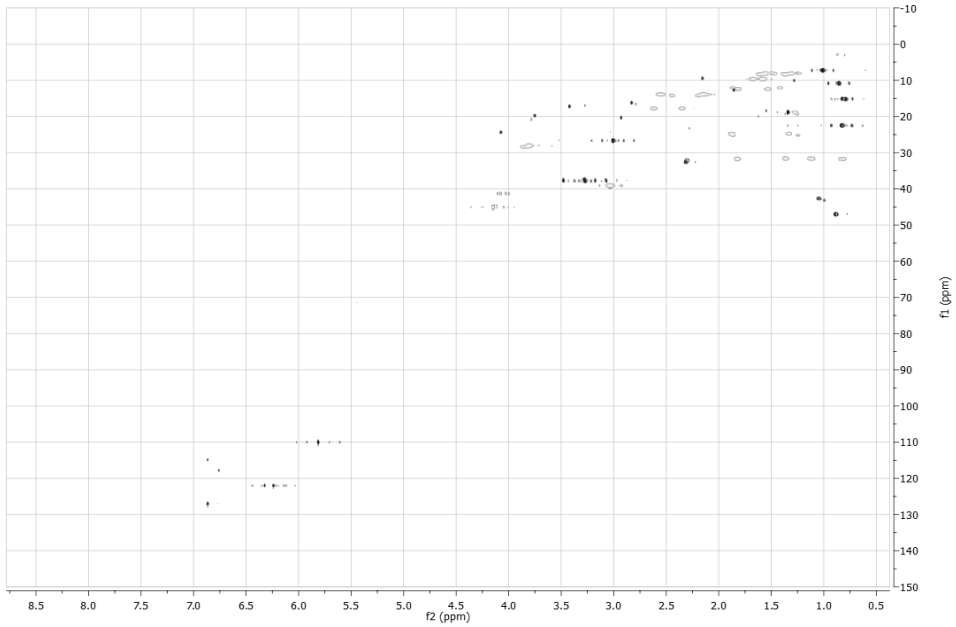

HMBC spectrum of coscinolactam B in CD_3OD at 700 MHz.

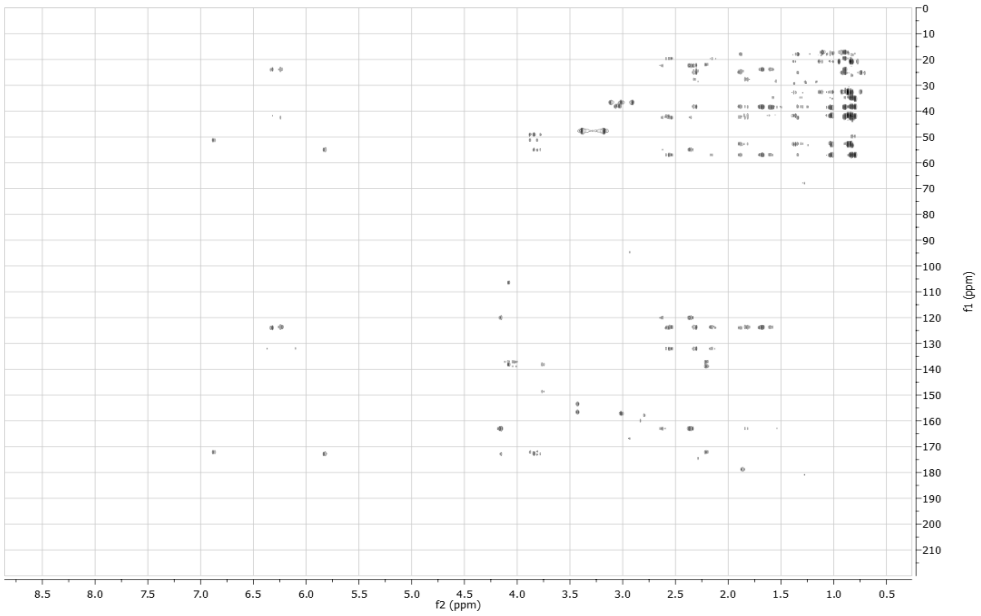

III. Experimental section of *Theonella swinhoei*

Sponge material and separation of individual. *Theonella swinhoei* (order Lithistida, family Theonellidae) was collected on the barrier reef of Vangunu Island, Solomon Islands, in July 2004. The samples were frozen immediately after collection and lyophilized to yield 207 g of dry mass. Taxonomic identification was performed by Prof. John Hooper of Queensland Museum, Brisbane, Australia, and reference specimens are on file (R3170) at the ORSTOM Centre of Noumea.

The lyophilized material (207 g) was extracted with methanol (3×1.7 L) at room temperature and the crude methanolic extract was subjected to a modified Kupchan's partitioning procedure as follows. The methanol extract was dissolved in a mixture of MeOH/H_2O containing 10% H_2O and partitioned against *n*-hexane. The water content (% v/v) of the MeOH extract was adjusted to 30% and partitioned against $CHCl_3$. The aqueous phase was concentrated to remove MeOH and then extracted with *n*-BuOH.

The *n*-BuOH extract (4 g) was chromatographed in two runs by DCCC using *n*-BuOH/Me_2CO/H_2O (3:1:5) in the descending mode (the upper phase was the stationary phase), flow rate 8 mL/min; 4 mL fractions were collected and combined on the basis of their similar TLC retention factors.

Fractions 2 and 3 (45.4 mg) were purified by HPLC on a C-18 column Macherey-Nagel Nucleodur 100-5 (5µ, 250 x 4.6 mm, 1.0 mL/min) using 32% MeOH/H_2O (isocratic mode) as eluent to give solomosterols A and B.

Fractions 8-13 (560 mg) were purified by HPLC on a reverse phase C-12 Jupiter Proteo C12 (Phenomenex, 4µ, 250 x 4.6 mm, 1.0 mL/min) eluting in isocratic mode with 59% MeOH/H_2O + 0.1% TFA to afford perthamides C-K.

Fractions 15-23 (256.6 mg) were purified by HPLC on a C-12 Jupiter Proteo column (Phenomenex, 4μ, 250 x 4.6 mm, 1.0 mL/min) with 20% MeOH/H_2O + 0.1% of TFA as eluent to give 44.3 mg of solomonamide A and B.

The chloroform-soluble material (5.83 g) was chromatographated by silica gel MPLC (Macherey-Nagel 200-400 mesh, eluting with CH_2Cl_2-MeOH 0-100%), the fractions were collected on the basis of their TLC retention times. Fraction 2 (88 mg) was purified by HPLC on a Nucleodur C18 column (5μ, Makerey Nagel, 250 x 7.8mm, 1.0 mL/min) with 95% MeOH/H_2O as eluent to give swinholide A (24.2 mg) and its structural analogue (compound **19**, 1.6 mg).

Characteristic data for Solomonsterols A and B

Characteristic data for each compound. Solomonsterol A (**6**): white amorphous solid; $[\alpha]_D^{25}$ +4.6 (*c* 0.8, methanol); ^1H and ^{13}C NMR data in CD_3OH given in Table 5; ESIMS: *m/z* 661.2 $[M\text{-}Na]^-$, 308.3 $[M\text{-}2Na]^{2-}$. HR ESIMS: calcd for $C_{24}H_{39}Na_2O_{12}S_3$: 661.1399; found 661.1415 $[M\text{-}Na]^-$.

Solomonsterol B (**7**): white amorphous solid; $[\alpha]_D^{25}$ +3.3 (*c* 0.1, methanol); ^1H and ^{13}C NMR data in CD_3OH given in Table 5 ESIMS: *m/z* 647.3 $[M\text{-}2Na]^-$, 301.2 $[M\text{-}2Na]^{2-}$. HR ESIMS: calcd for $C_{23}H_{37}Na_2O_{12}S_3$: 647.1243; found 647.1298 $[M\text{-}Na]^-$.

Quantitative Real-Time PCR. RAW264.7 macrophages and HepG2 cells were cultured as previously described. Cells were incubated with 10 and 50 μM of solomonsterols A and B for 24 hours. At the end of incubation cells were harvested and lysed with 1 mL TRIZOL reagent for RNA extraction (Invitrogen). Fifty ng template was added to the PCR mixture (final volume 25 μL) containing the following reagents: 0.2 μM of each primer and 12.5 μL of 2X SYBR Green qPCR master mix (Invitrogen, Milan, Italy). All reactions were performed in triplicate and the thermal cycling conditions were: 2 minutes at 95 °C, followed

by 40 cycles of 95 °C for 20 seconds, 55 °C for 20 seconds and 72 °C for 30 seconds in iCycler iQ instrument (Biorad, Hercules, CA). The mean value of the replicates for each sample was calculated and expressed as cycle threshold (C_T: cycle number at which each PCR reaction reaches a predetermined fluorescence threshold, set within the linear range of all reactions). The amount of gene expression was then calculated as the difference (ΔC_T) between the C_T value of the sample for the target gene and the mean C_T value of that sample for the endogenous control (GAPDH). Relative expression was calculated as $2^{-\Delta\Delta C}{}_{T.}$ All PCR primers were designed with PRIMER3-OUTPUT software using published sequence data from the NCBI database.[152]

Cell Based Luciferase Assay. To investigate their PXR-activating properties, solomonsterols A and B were tested in a cell based luciferase assay. Since PXR functions as an heterodimer with the retinoid-X-receptor (RXR), HepG2 cells were transfected with a PXR and RXR expressing vectors (pSG5-PXR and pSG5-RXR), with a reporter vector containing the PXR target gene promoter (CYP3A4 gene promoter) cloned upstream of the luciferase gene (pCYP3A4promoter-TKLuc) and with a β-galactosidase expressing vector as internal control of transfection efficiency (pCMV-β-gal). 24 hours post transfection the cells were stimulated 18 hours with the PXR ligand rifaximin 10 μM (as positive internal control) and with 50 μM of solomonsterols A and B**.** 5 μL of cell lysate was incubated with a substrate of luciferase gene (luciferase assay substrate - Promega) and the Relative Luciferase Units (RLU) were measured with the Glomax 20/20 luminometer (Promega). Luciferase activities were normalized for transfection efficiencies by dividing the relative light units by β-galactosidase activity expressed from cotransfected pCMV-βgal plasmid (RLU/β-gal).

Computational Details. To allow full exploration of the conformational space of solomonsterol A, molecular dynamics (MD) calculations were performed at 300K for 50ns using the AMBER force field (MacroModel software package)[228] to give 100 structures, each of which was minimized using the Polak-Ribier Conjugate Gradient algorithm (PRCG, 1000 steps, maximum derivative less than 0.05 kcal/mol). These calculations provided the lowest energy minimum conformer for solomonsterol A.

Docking of the minimized energy structure of solomonsterol A to the crystal structure of the human pregame-X-receptor in complex with hyperforin, pdb accession code 1M13) was carried out with the program Autodock Vina 1.0.3. Blind docking was carried out with an exhaustiveness value of 256. The binding affinities of the 9 output structures ranged from -10.0 kcal/mol to -8.7 kcal/mol.

Spectroscopic Data of Solomonsterols A and B

^{1}H NMR spectrum of solomonsterol A in CD_3OD at 700 MHz.

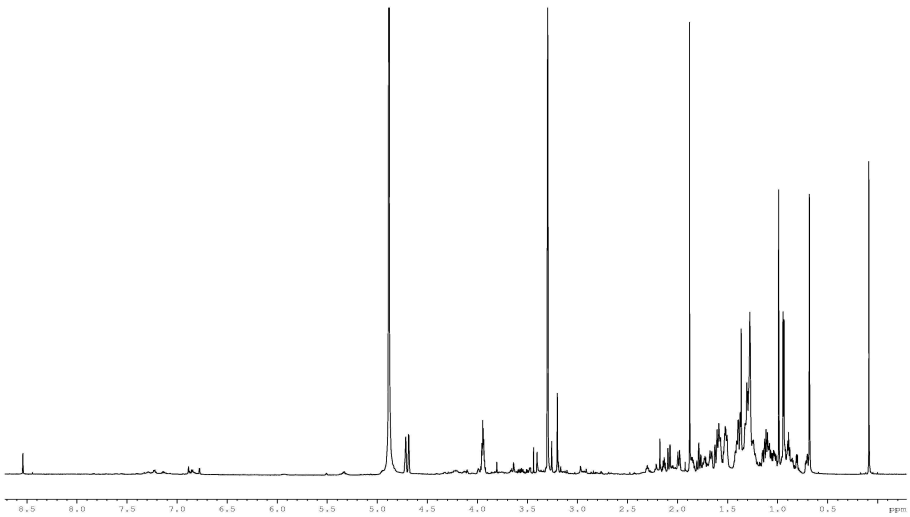

COSY spectrum of solomonsterol A in CD_3OD at 700 MHz.

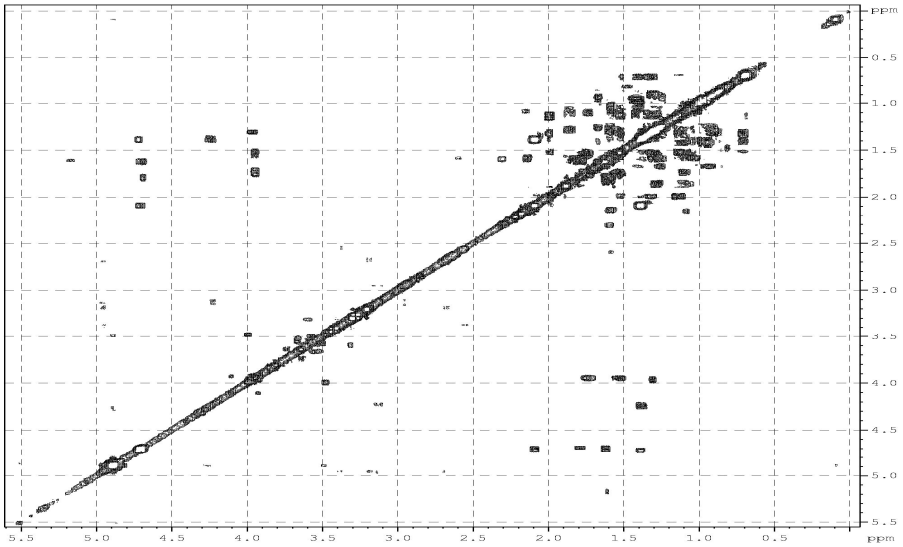

HSQC spectrum of solomonsterol A in CD_3OD at 700 MHz.

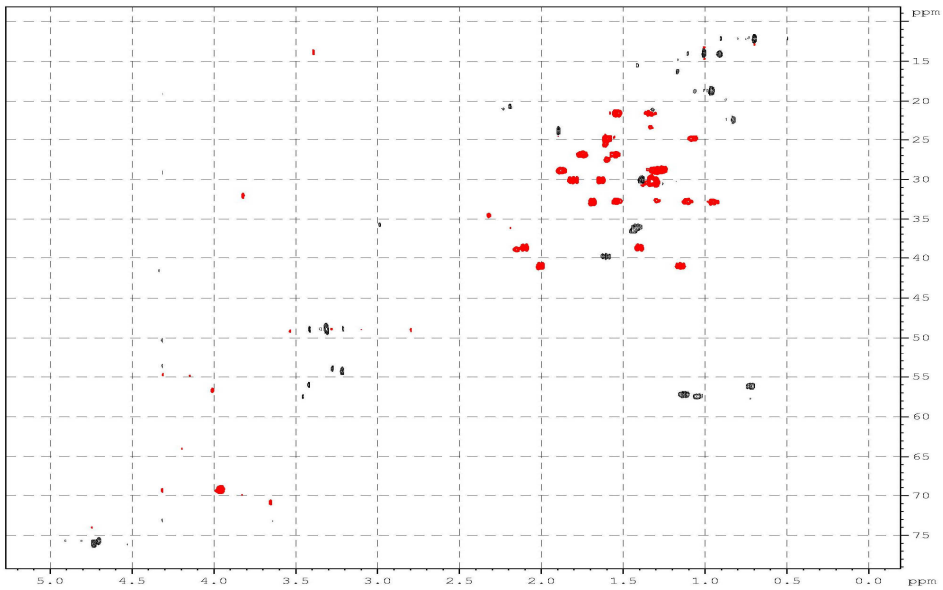

HMBC spectrum of solomonsterol A in CD_3OD at 700 MHz.

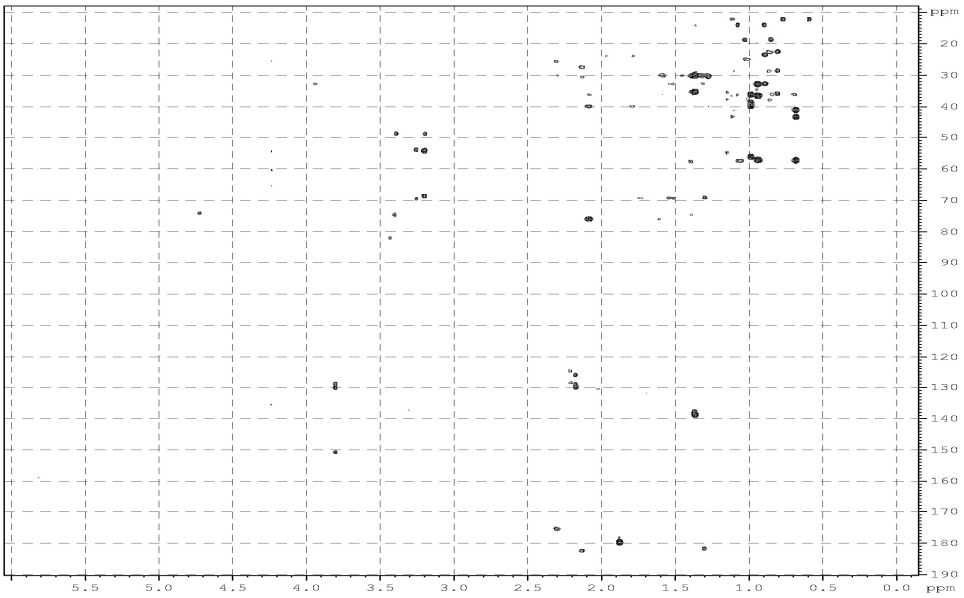

ROESY spectrum of solomonsterol A in CD_3OD at 700 MHz (200 msec).

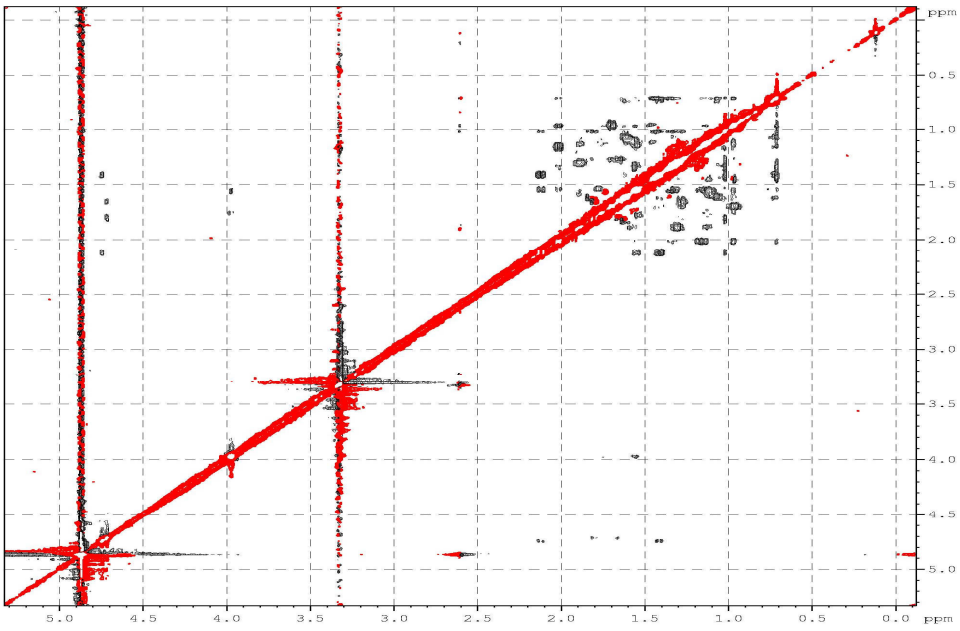

ROESY spectrum of solomonsterol A in CD_3OD at 700 MHz (400 msec).

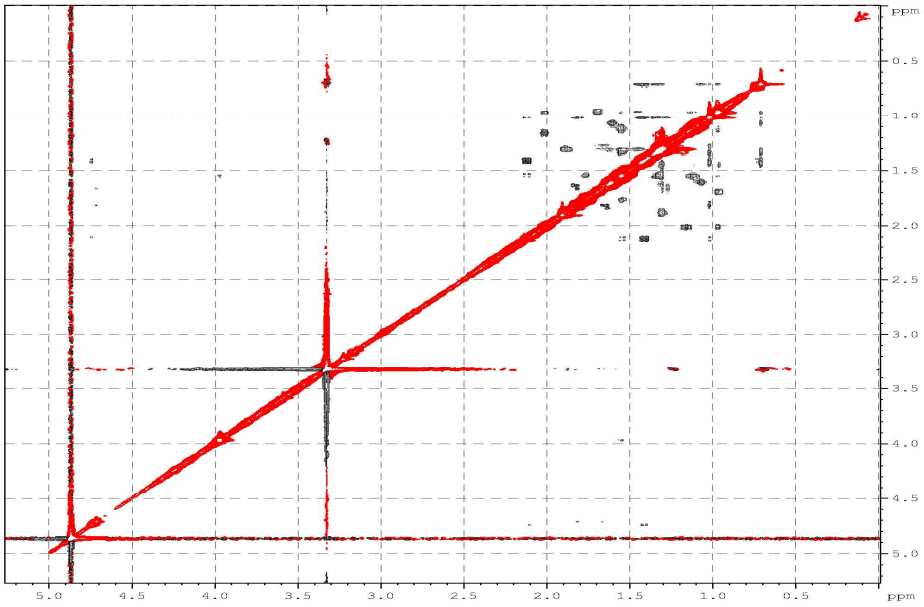

^1H NMR spectrum of solomonsterol B in CD_3OD at 700 MHz.

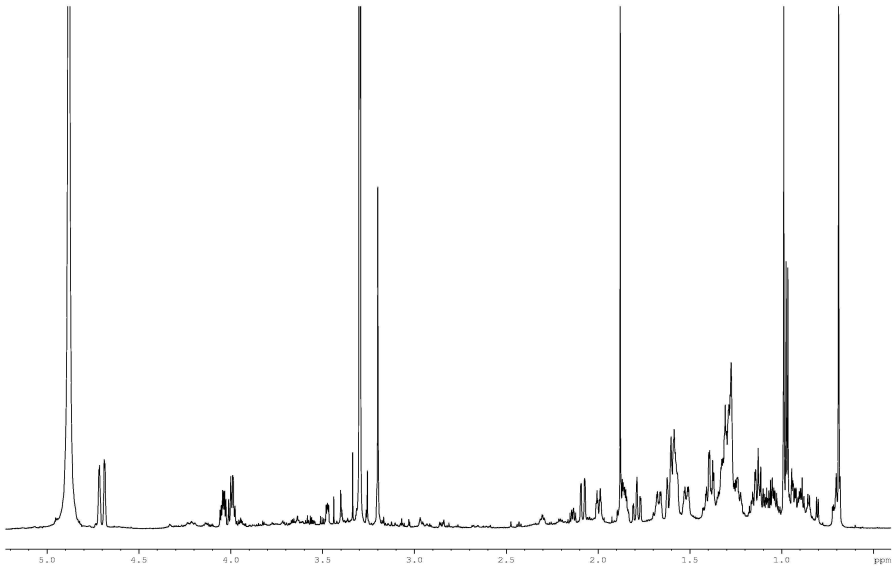

COSY spectrum of solomonsterol B in CD_3OD at 700 MHz.

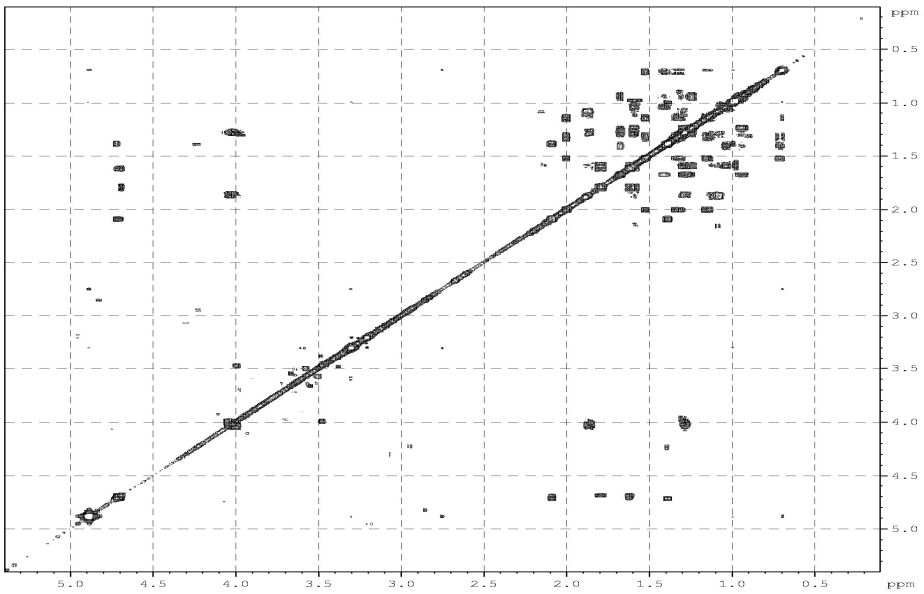

HSQC spectrum of solomonsterol B in CD_3OD at 700 MHz.

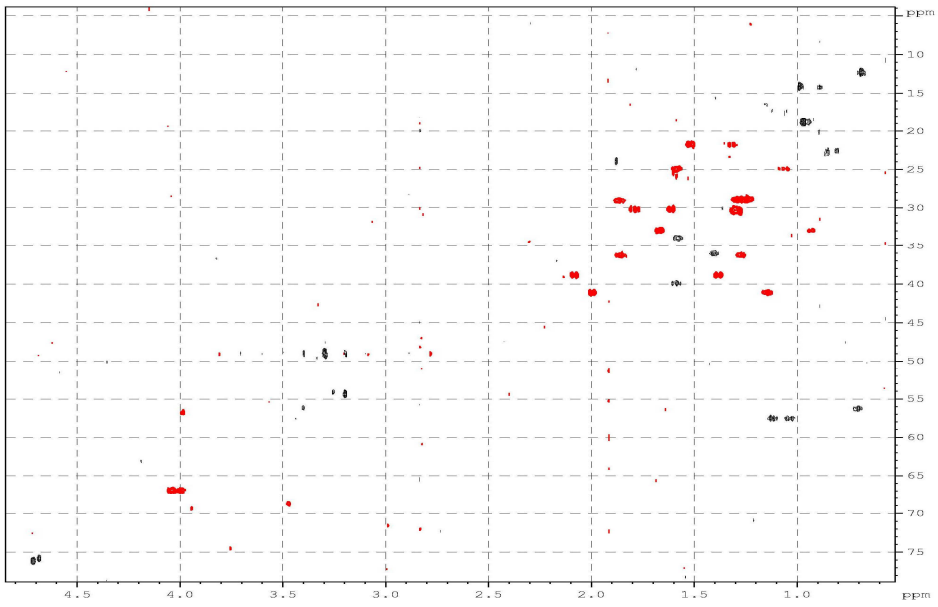

HMBC spectrum of solomonsterol B in CD_3OD at 700 MHz.

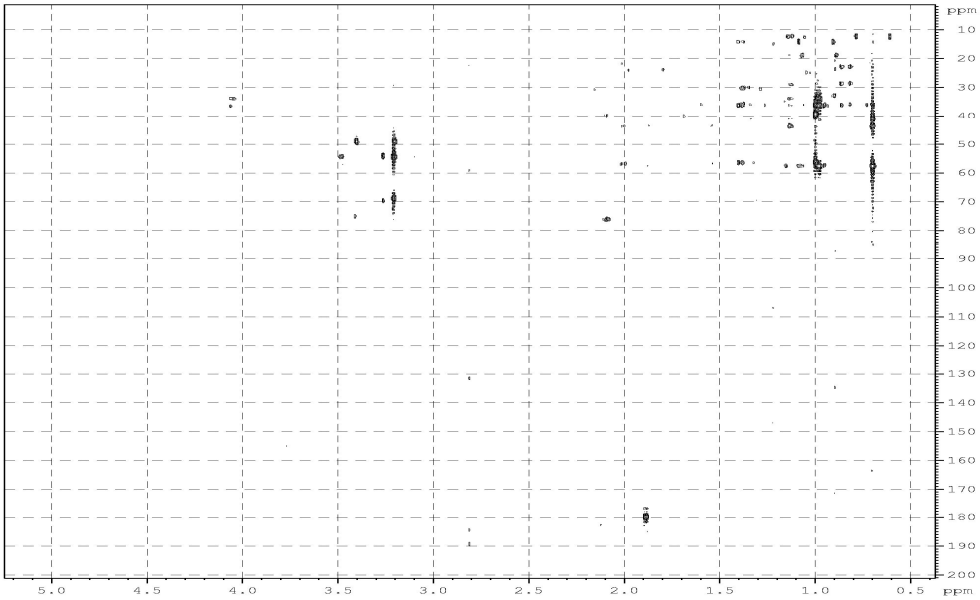

Characteristic data for Perthamides C-K

Perthamide C (8): white amorphous solid; $[\alpha]_D^{25}$ -6.3 (*c* 2.8, chloroform); ^{1}H and ^{13}C NMR data in DMSO-d_6 given in Table 6; HRMS (ESI): calcd for $C_{44}H_{65}N_{11}O_{18}S$: 1066.4242; found 1066.4106 $[M-H]^-$.

Perthamide D (9): White amorphous solid; $[\alpha]_D^{25}$ –4.1 (*c* 0.1, chloroform); HRMS (ESI): calcd for $C_{44}H_{65}N_{11}O_{17}S$: 1050.4353; found 1050.4302 $[M-H]^-$.

Perthamide E (10): white amporphous solid; ^{1}H and ^{13}C NMR data in DMSO-d_6 given in Table 6; HR-ESIMS: calcd for $C_{45}H_{67}N_{11}O_{18}S$ *m/z* 1080.4386; found 1080.4394 $[M-H]^-$.

Perthamide F (11): white amporphous solid; ^{1}H; HR-ESIMS: calcd for $C_{45}H_{67}N_{11}O_{17}S$ *m/z* 1064.4437; found 1064.4473 $[M-H]^-$.

Perthamide G (12): white amporphous solid; HR-ESIMS: calcd for $C_{43}H_{63}N_{11}O_{18}S$ *m/z* 1052.4146; found 1052.4237 $[M-H]^-$.

Perthamide H (13): white amporphous solid; ^{1}H; HR-ESIMS: calcd for $C_{44}H_{65}N_{11}O_{15}$ *m/z* 986.4662; found 988.4804 $[M-H]^-$.

Perthamide I (14): white amporphous solid; ^{1}H; HR-ESIMS: calcd for $C_{45}H_{67}N_{11}O_{15}$ *m/z* 1000.4823; found 1000.5003 $[M-H]^-$.

Perthamide J (15): white amporphous solid; ^{1}H; HR-ESIMS: calcd for $C_{44}H_{62}N_{10}O_{15}$ *m/z* 970.4396; found 970.4405 $[M-H]^-$.

Perthamide K (16): white amporphous solid; ^{1}H; HR-ESIMS: calcd for $C_{45}H_{64}N_{10}O_{15}$ *m/z* 984.4553; found 984.4635 $[M-H]^-$.

Amino Acid Analysis of perthamide C (8). For a large scale hydrolysis, a 12 mg sample of perthamide C dissolved in 6N HCl (3 mL) and heated at 130 °C for 12 h. The crude residue was fractionated by HPLC on the reversed-phase Phenomenex Hydro (4μ, 250 x 4.6 mm) column eluting with MeOH:H_2O 2:98,

(flow rate 0.5 mL/min) to give: NMeGly (t_r=4.8 min), ThrOMe (t_r=6.4 min), γ-MePro (t_r=7.6 min), *o*-Tyr (t_r=24.6 min).

γ-MePro**:** ^{1}H NMR (500 MHz, D_2O) δ 4.10 (1H, dd, *J* = 6.7, 5.1 Hz, H-2), 3.44 (1H, dd, *J* = 10.5, 7.6 Hz, H-5a), 2.90 (1H, t, *J* = 10.5 Hz, H-5b), 2.51 (1H, dt, *J* = 13.0, 7.0 Hz, H-3a), 1.60 (1H, dt, *J* = 13.0, 9.4 Hz, H-3b), 1.04 (3H, d, *J* = 6.6 Hz, Me-4).

Determination of the Absolute Configuration of Perthamide C and D.

Peptide Hydrolysis. Peptide samples (200 μg) were dissolved in degassed 6 M HCl (0.5 mL) in an evacuated glass tube and heated at 160 °C for 16 h. The solvent was removed *in vacuo* and the resulting material was subjected to further derivatisation.

LC-MS Analysis of Marfey's (FDAA) Derivatives. A portion of the hydrolysate mixture (800 μg) or the amino acid standard (500 μg) was dissolved in 80 μL of a 2:3 solution of TEA:MeCN and this solution was then treated with 75 μL of 1% 1-fluoro-2,4-dinitrophenyl-5-L-alaninamide (FDAA) in 1:2 MeCN:acetone. The vials were heated at 70 °C for 1 h, and the contents were neutralised with 0.2N HCl (50 μL) after cooling to room temperature. An aliquot of the L-FDAA derivative was dried under vacuum, diluted with MeCN-5% HCOOH in H_2O (1:1), and separated on a Proteo C18 (25 x 1.8 mm i.d.) column by means a linear gradient from 10% to 50% aqueous acetonitrile containing 5% formic acid and 0.05% trifluoroacetic acid, over 45 min at 0.15 mL/min. The RP-HPLC system was connected to the electrospray ion source by inserting a splitter valve and the flow going into the mass spectrometer source was set at a value of 100 μL/min. Mass spectra were acquired in positive ion detection mode (*m/z* interval of 320-900) and

the data were analysed using the suite of programs Xcalibur; all masses were reported as average values. Capillary temperature was set at 280 °C, capillary voltage at 37 V, tube lens offset at 50 V and ion spray voltage at 5 V.

Retention times (min) of FDAA-amino acids are given in parentheses: D-Asp (26.5), L-Asp (25.2), D-*allo*ThrOMe (37.3), L-*allo*ThrOMe (32.5), D-ThrOMe (39.8), L-ThrOMe (34.5) (2*S*,3*R*)-βOHAsp (24.0), (2*R*,3*S*)-βOHAsp (21.8), (2*S*,3*S*)-βOHAsp (18.0), (2*R*,3*R*)-βOHAsp (16.9), L-Phe (45.0), D-Phe (49.2).

The hydrolysate of perthamide C (**8**) contained: L-Asp (25.4), L-ThrOMe (34.5), (2*R*,3*S*)-βOHAsp (21.9).

The hydrolysate of perthamide D (**9**) contained: L-Asp (25.4), L-ThrOMe (34.5), (2*R*,3*S*)-βOHAsp (21.9), L-Phe (45.0).

To determine the absolute configuration of γ-MePro two aliquots of the hydrolysate mixture were derivatised with L- and D-FDAA, respectively and then they were subjected to LC-MS as described above. Retention times (min): L-FDAA- γ-MePro (37.7), D-FDAA- γ-MePro (39.8).

To determine the absolute configuration of *o*-Tyr in perthamide C, a stream of ozone in O_2 was bubbled through cooled solutions of pure amino acid residue (0.1 mg) in MeOH (0.5 mL) at -78 °C for 1 h. Hydrogen peroxide (35%, 10 drops) was added to the reaction mixture which was then allowed to stand at room temperature overnight. The solvent was removed under a stream of N_2 and the ozonolysis product was subjected to Marfey's derivatisation with L- FDAA and LC–MS analysis to obtain L-Asp (25.4 min).

Pharmacological Assays.

Mouse Paw Oedema. Male Swiss (CD-1; Harlan, Italy) weighing 28-30g were divided into groups (n=6 each group) and lightly anaesthetized with isoflurane. Each group of animals received subplantar injection of 50µl of carrageenan 1% (w/v) or 50µl of saline in the left hind paw. Paw volume was measured by using an hydropletismometer specially modified for small volumes (Ugo Basile, Comerio, Italy) immediately before the subplantar injection and 2, 4, 6, 24, 48, 72 and 96h thereafter. The same operator always performed the double-blind assessment of paw volume. The increase in paw volume was calculated as the difference between the paw volume measured at each time point and the basal paw oedema. Each group of animals received intraperitoneal administration of Perthamide C (0.1, 0.3, 1 mg/kg), Perthamide D (0.3 mg/kg) or vehicle (PEG). All drugs were administrated immediately before the injection of carrageenan and 24h thereafter.

Statistical analysis. Results were expressed as mean ± s.e.m. Statistical analysis was determined by one way ANOVA followed by Dunnett's test for multiple comparisons, using GraphPad Prism software (GraphPad Software Inc., San Diego, CA). Differences were considered statistically significant when $p < 0.05$.

Spectroscopic Data of Perthamide C-K

^{1}H NMR spectrum of Perthamide C (**8**) in DMSO-d_6 at 700 MHz.

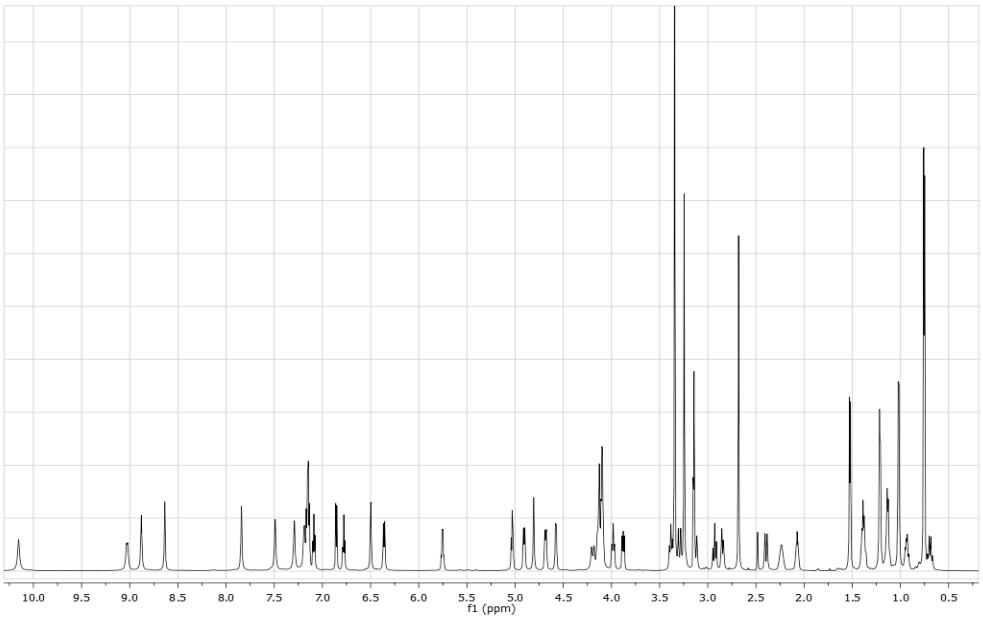

COSY spectrum of Perthamide C (**8**) in DMSO-d_6 at 700 MHz.

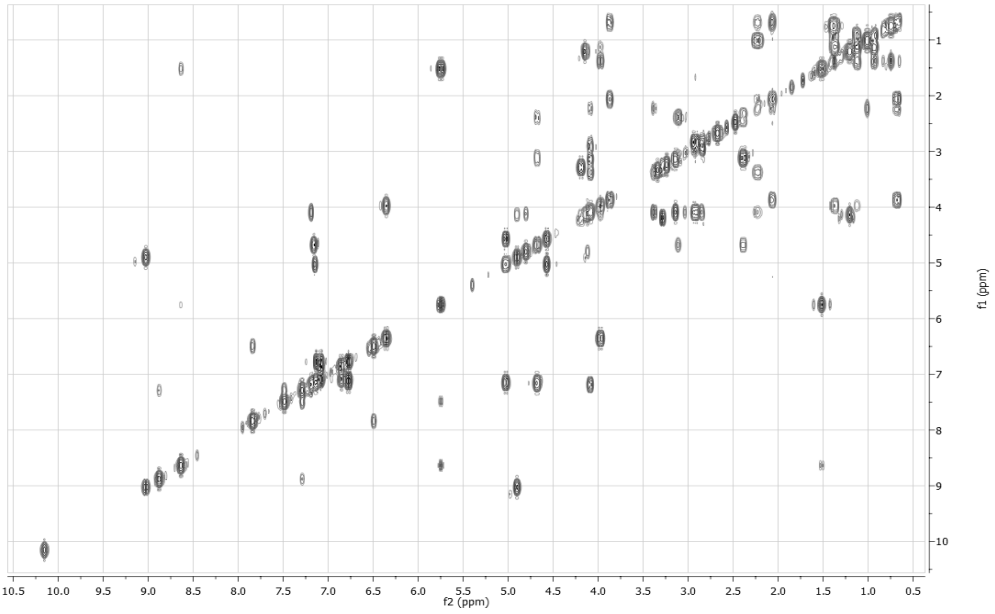

HSQC spectrum of Perthamide C (**8**) in DMSO-d_6 at 700 MHz.

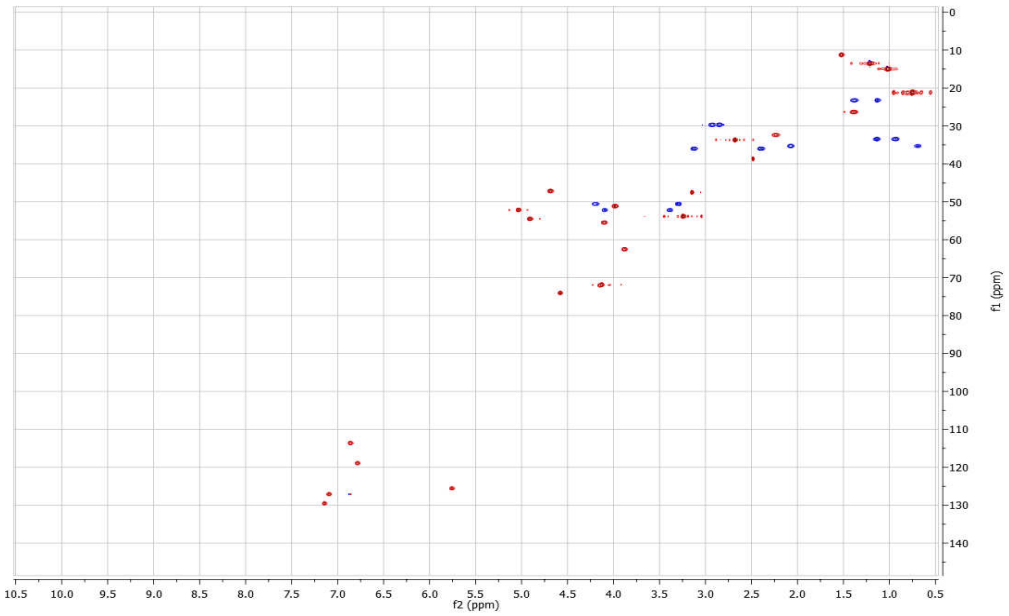

HMBC spectrum of Perthamide C (**8**) in DMSO-d_6 at 700 MHz.

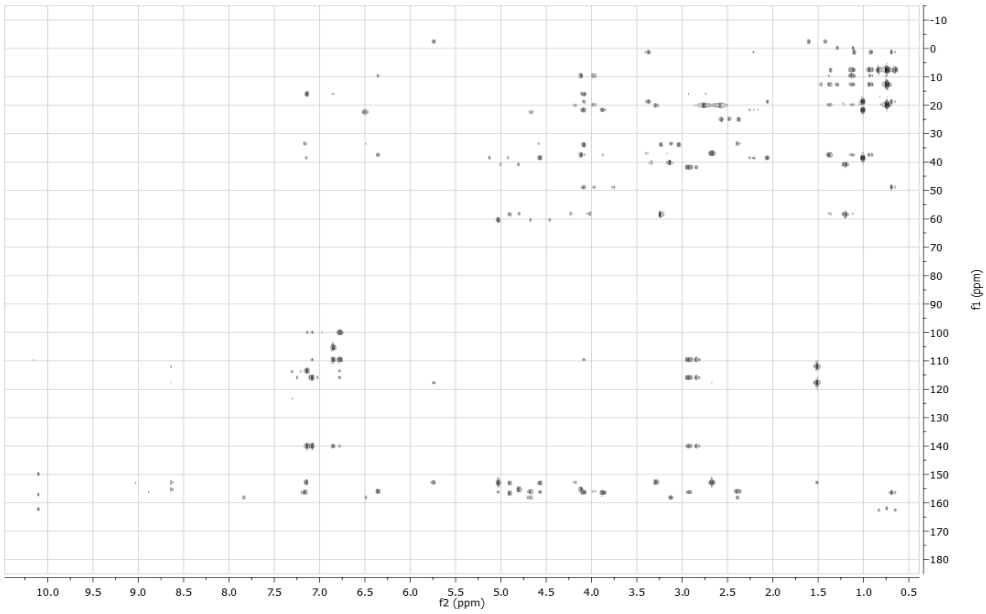

ROESY spectrum of Perthamide C (**8**) in DMSO-d_6 at 700 MHz (100 ms).

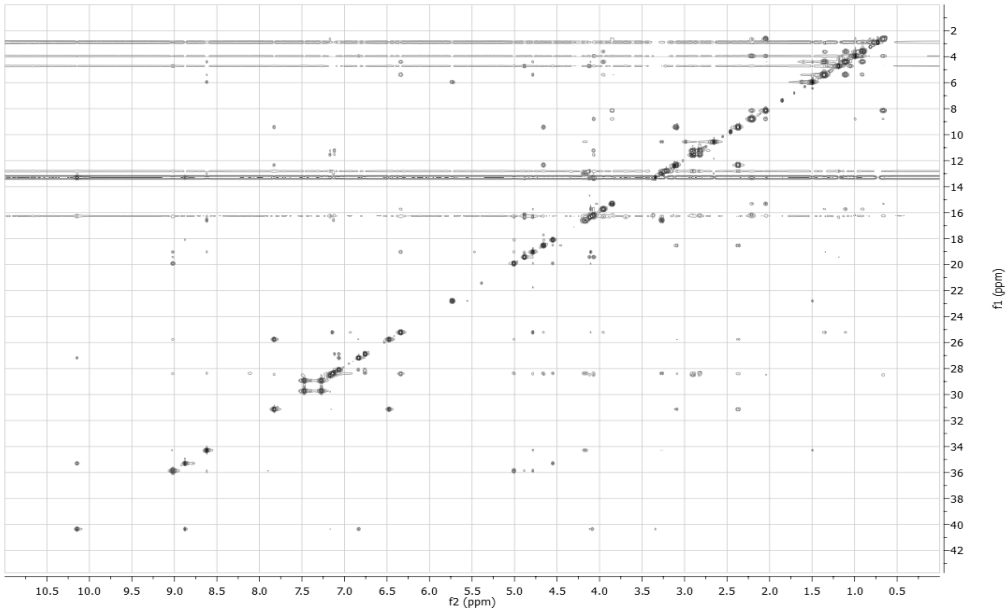

^{1}H NMR spectrum of Perthamide D (**9**) in DMSO-d_6 at 700 MHz.

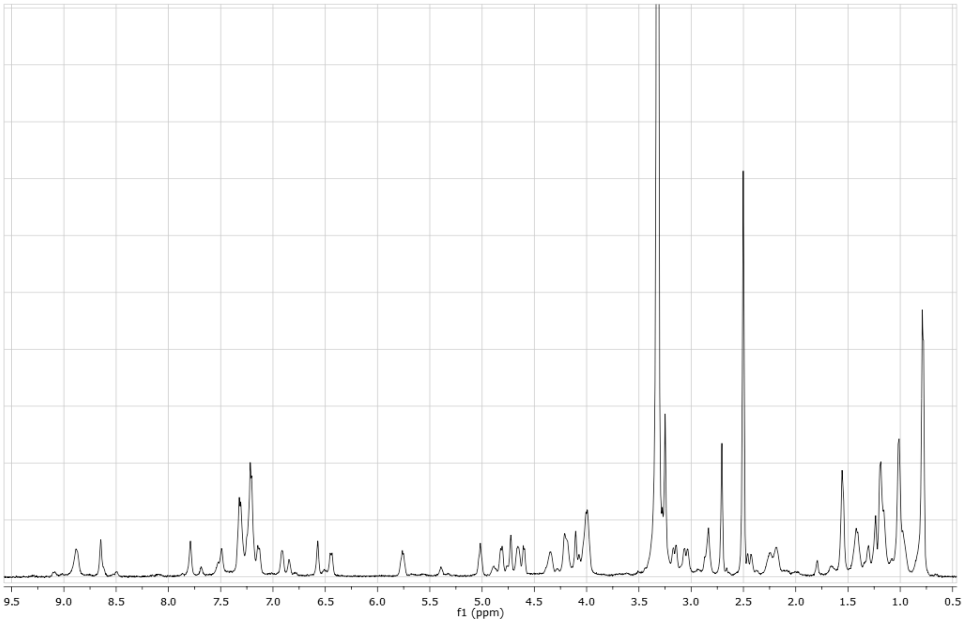

^{1}H NMR spectrum of Perthamide E (**10**) in DMSO-d_6 at 700 MHz.

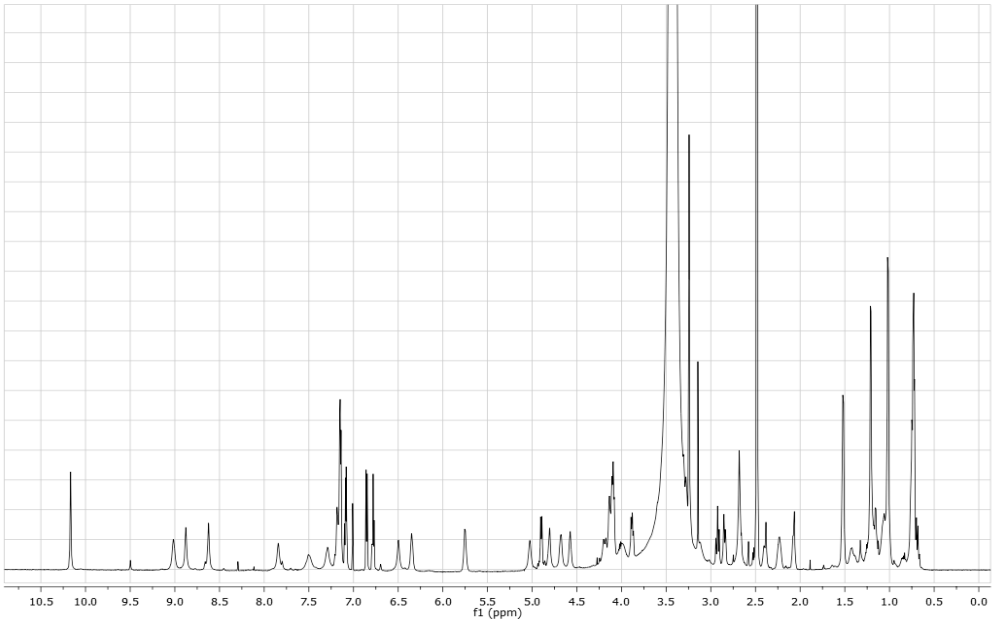

COSY spectrum of Perthamide E (**10**) in DMSO-d_6 at 700 MHz.

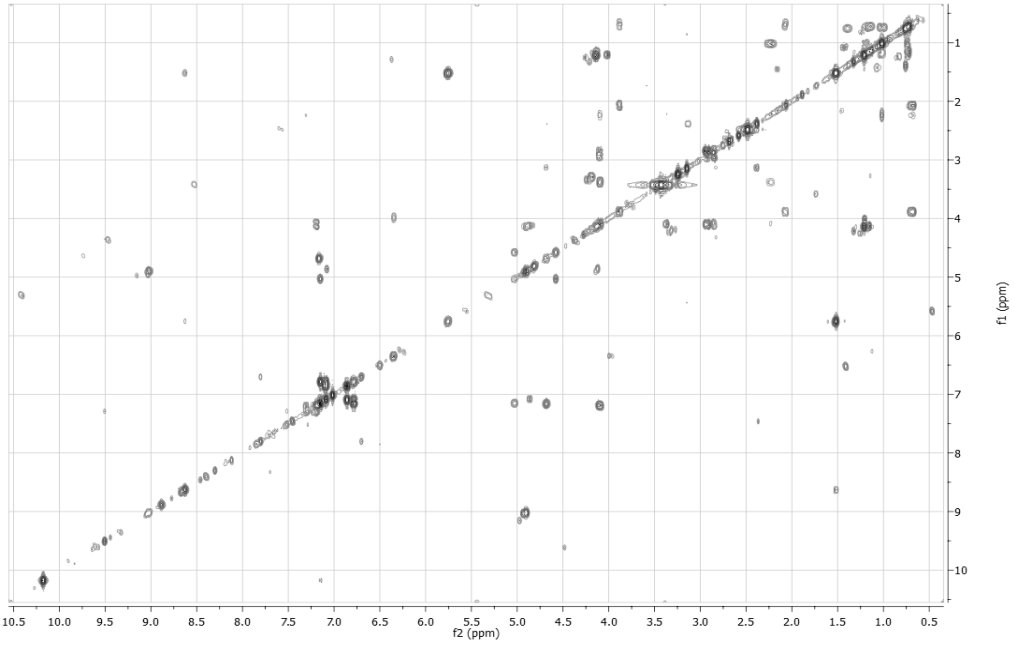

HSQC spectrum of Perthamide E (**10**) in DMSO-d_6 at 700 MHz.

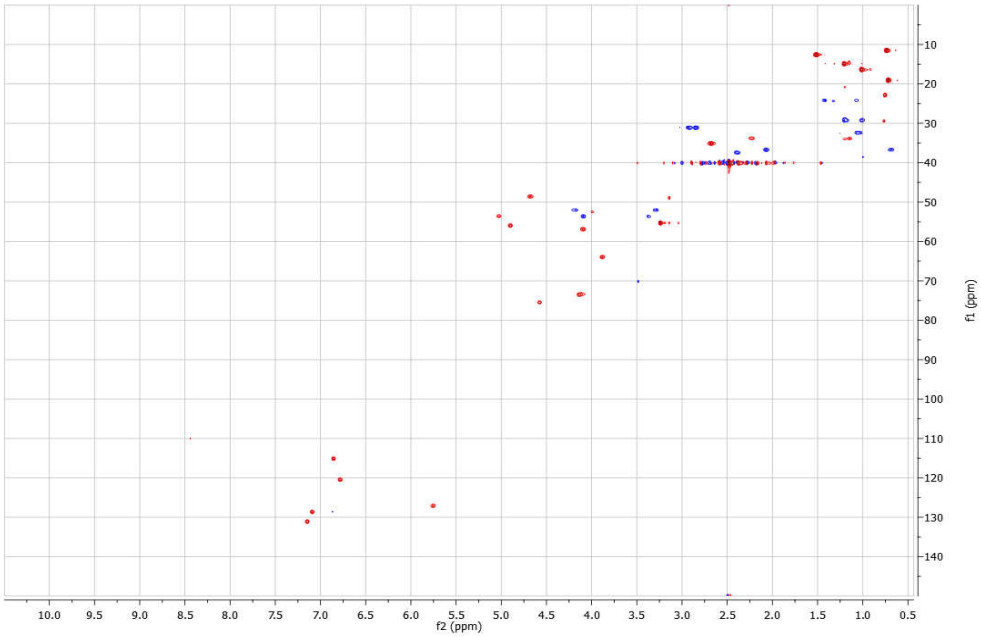

HMBC spectrum of Perthamide E (**10**) in DMSO-d_6 at 700 MHz.

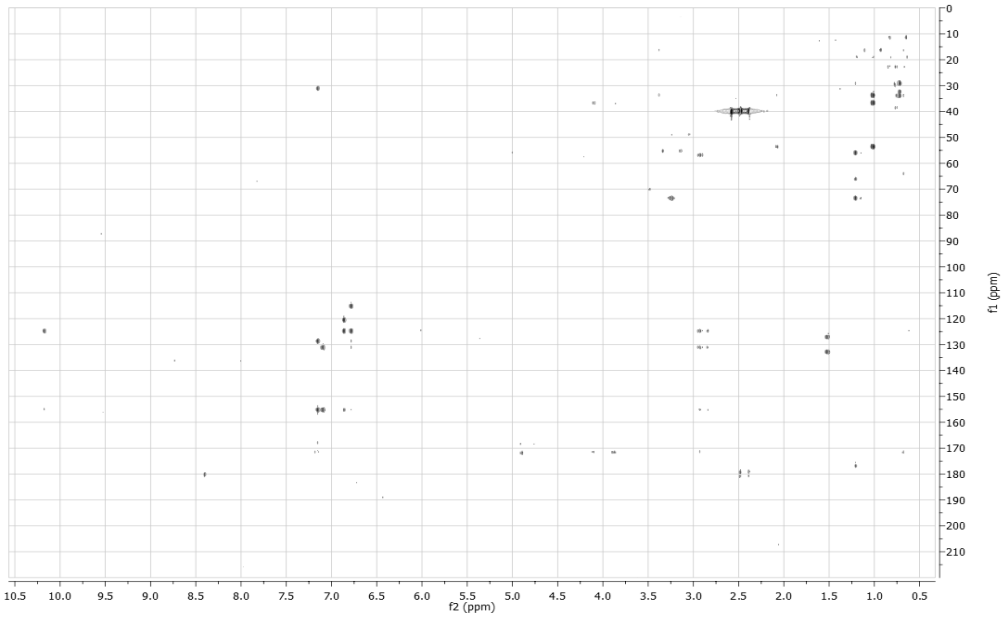

TOCSY spectrum of Perthamide E (**10**) in DMSO-d_6 at 700 MHz.

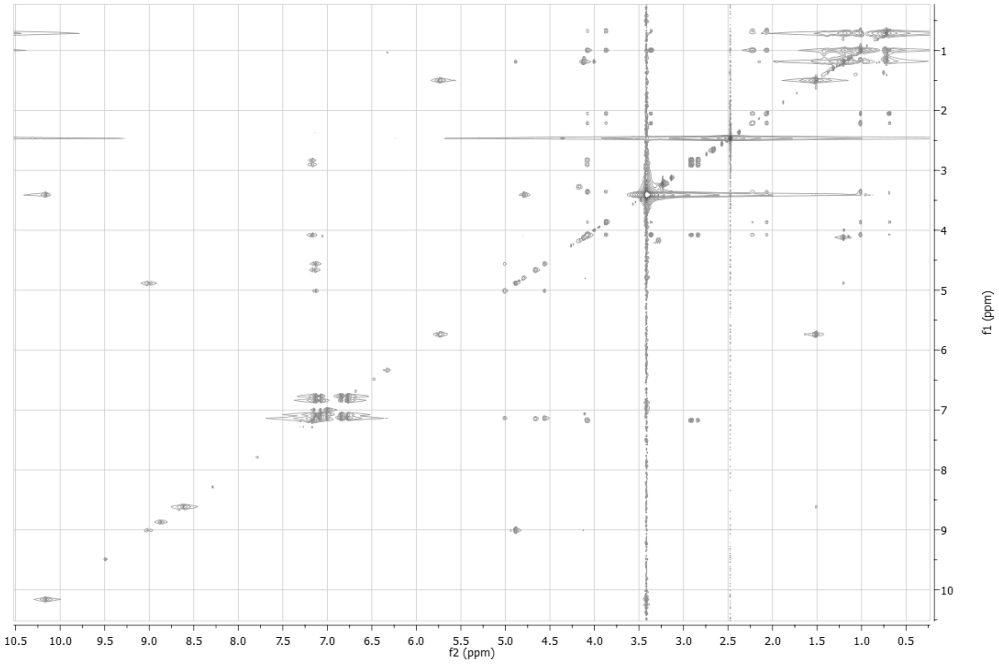

^{1}H NMR spectrum of Perthamide F (**11**) in DMSO-d_6 at 700 MHz.

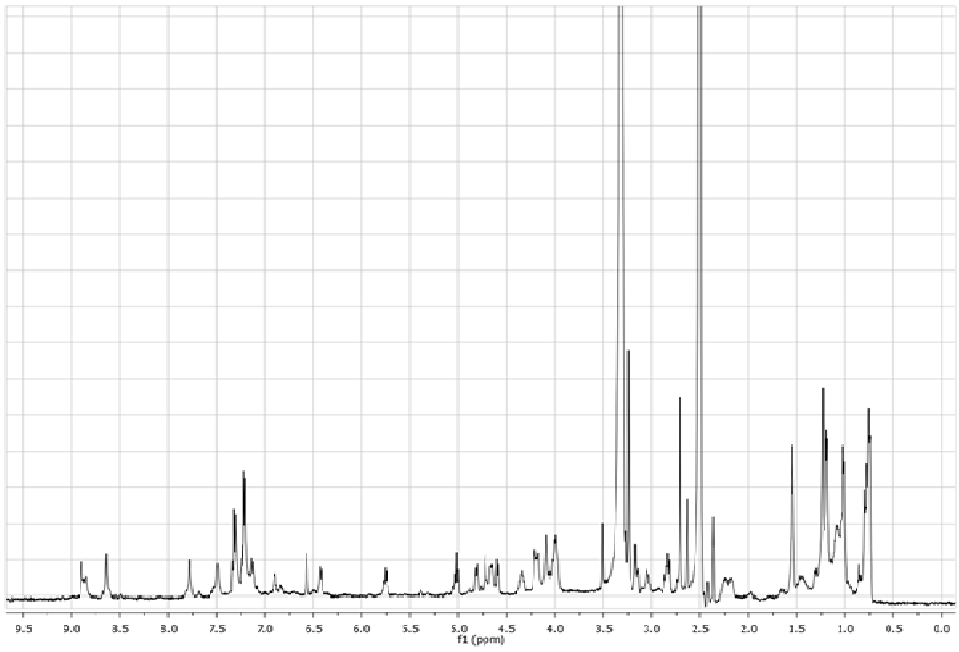

^{1}H NMR spectrum of Perthamide G (**12**) in DMSO-d_6 at 700 MHz.

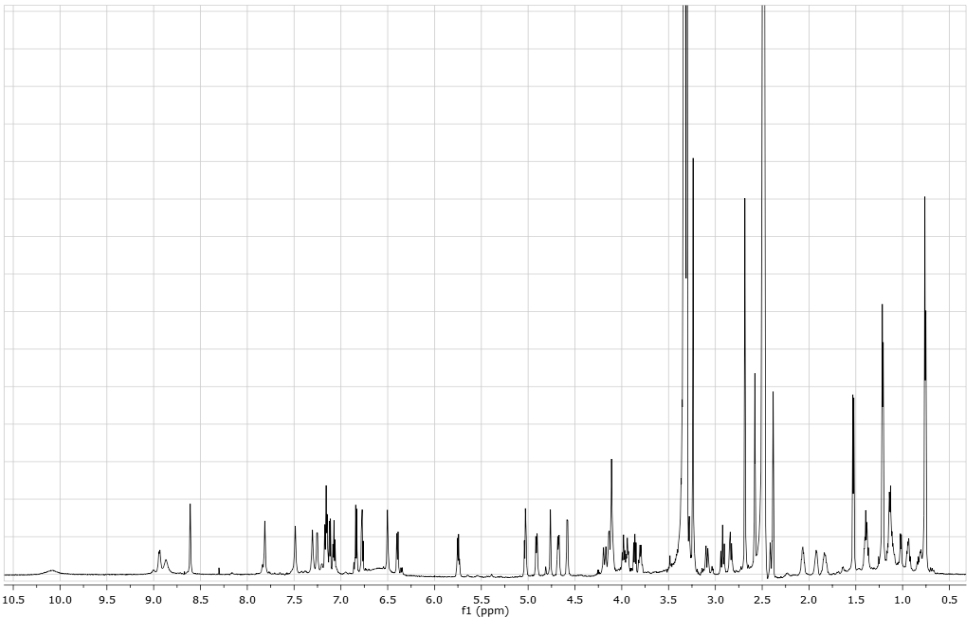

COSY spectrum of Perthamide G (**12**) in DMSO-d_6 at 700 MHz.

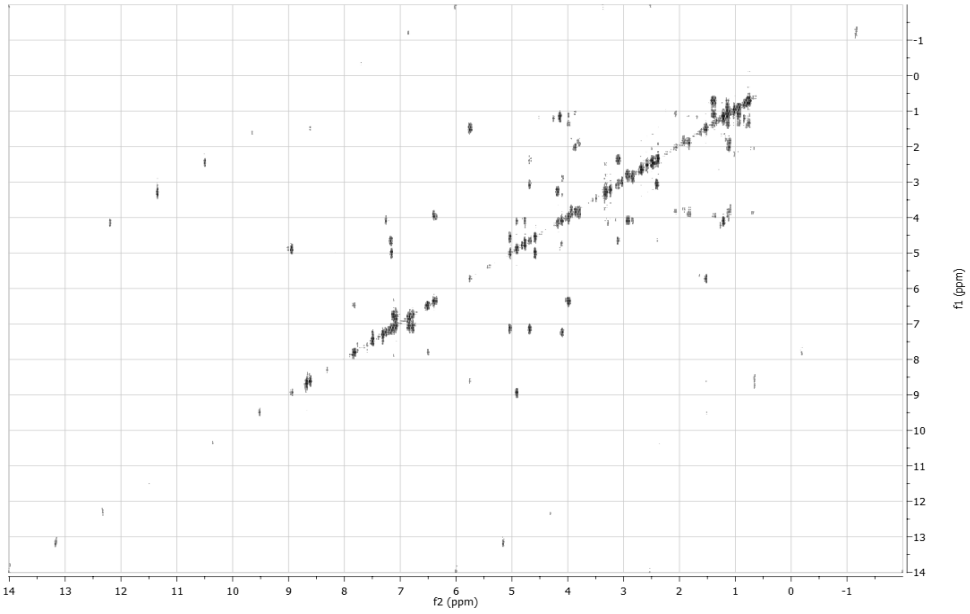

HSQC spectrum of Perthamide G (**12**) in DMSO-d_6 at 700 MHz.

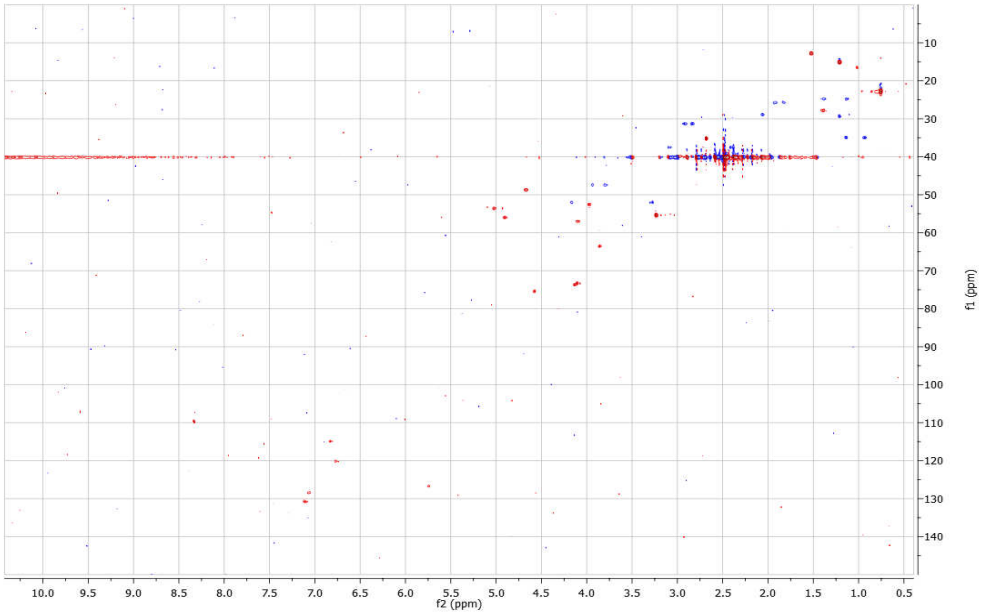

HMBC spectrum of Perthamide G (**12**) in DMSO-d_6 at 700 MHz.

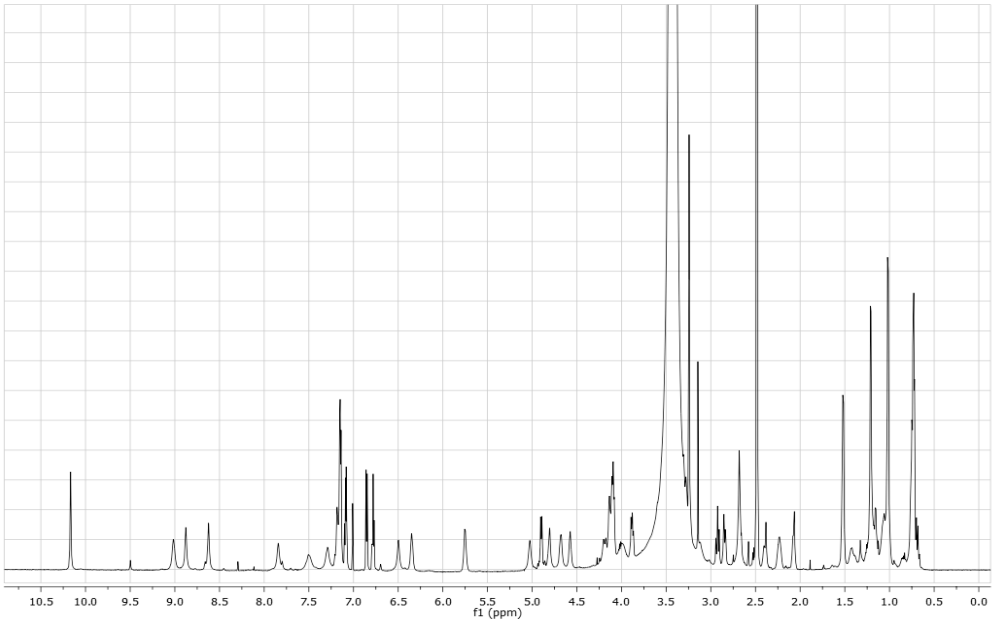

^{1}H NMR spectrum of Perthamide H (**13**) in DMSO-d_6 at 700 MHz.

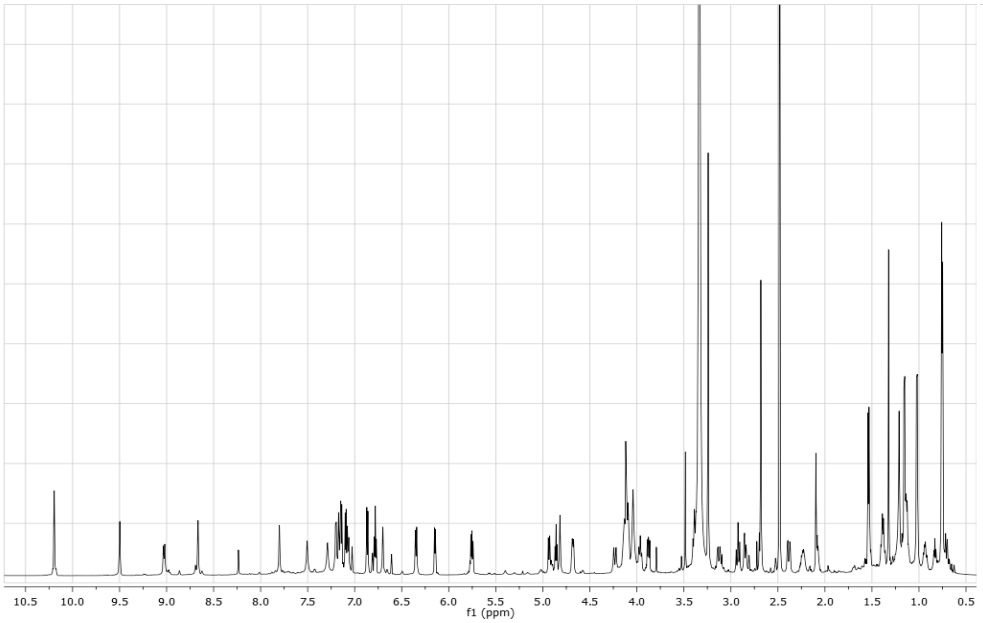

TOCSY spectrum of Perthamide H (**13**) in DMSO-d_6 at 700 MHz.

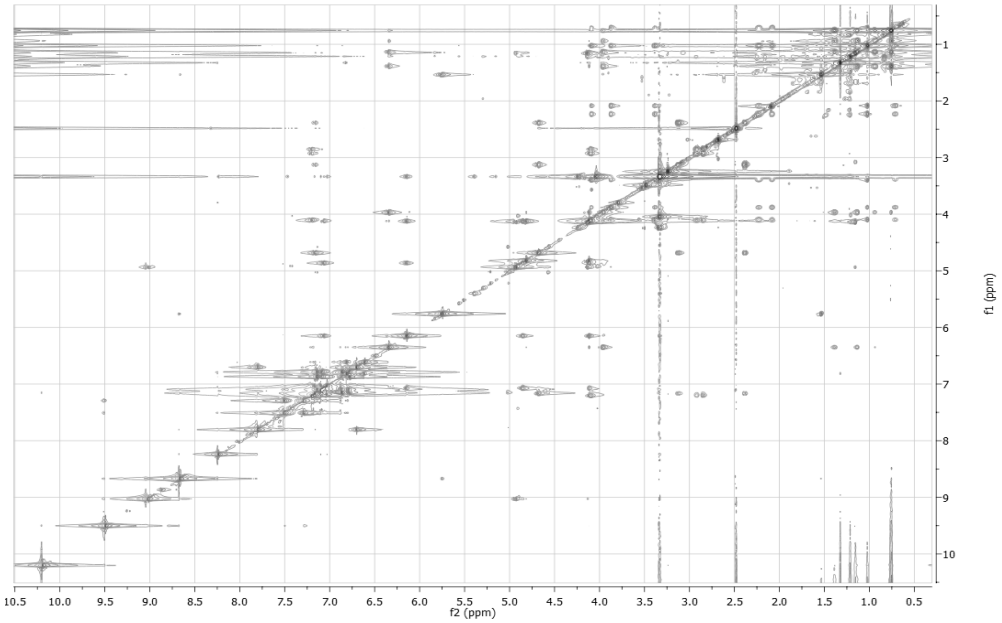

HMBCspectrum of Perthamide H (**13**) in DMSO-d_6 at 700 MHz.

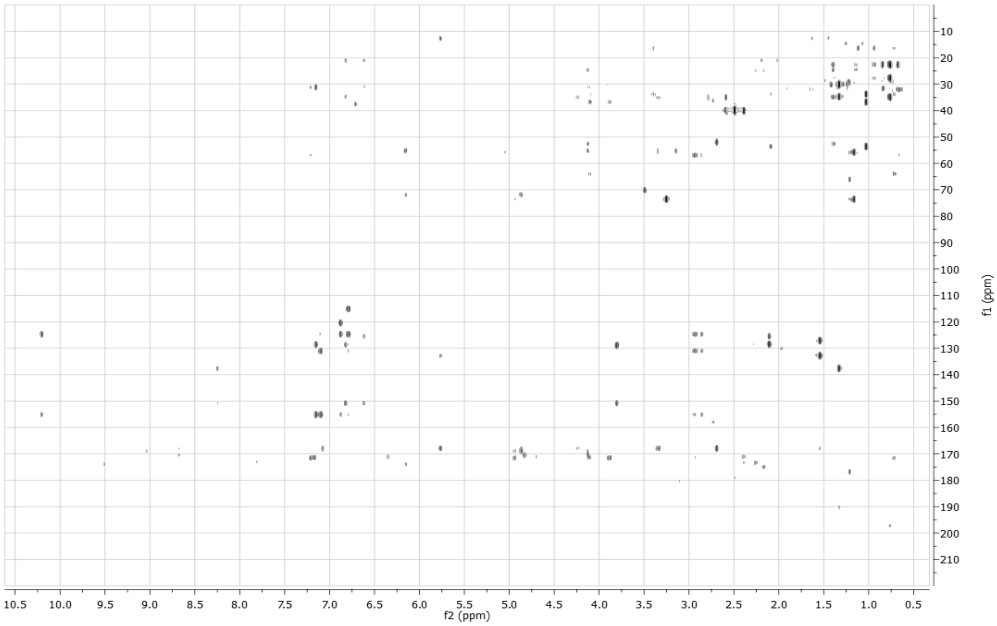

HSQC spectrum of Perthamide H (**13**) in DMSO-d_6 at 700 MHz.

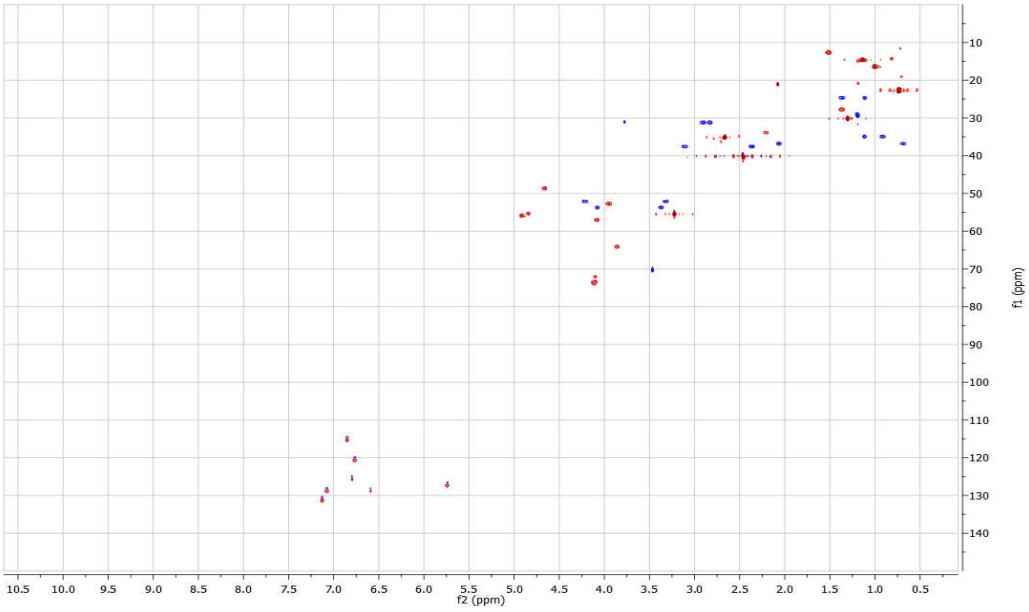

HMBC spectrum of Perthamide H (**13**) in DMSO-d_6 at 700 MHz.

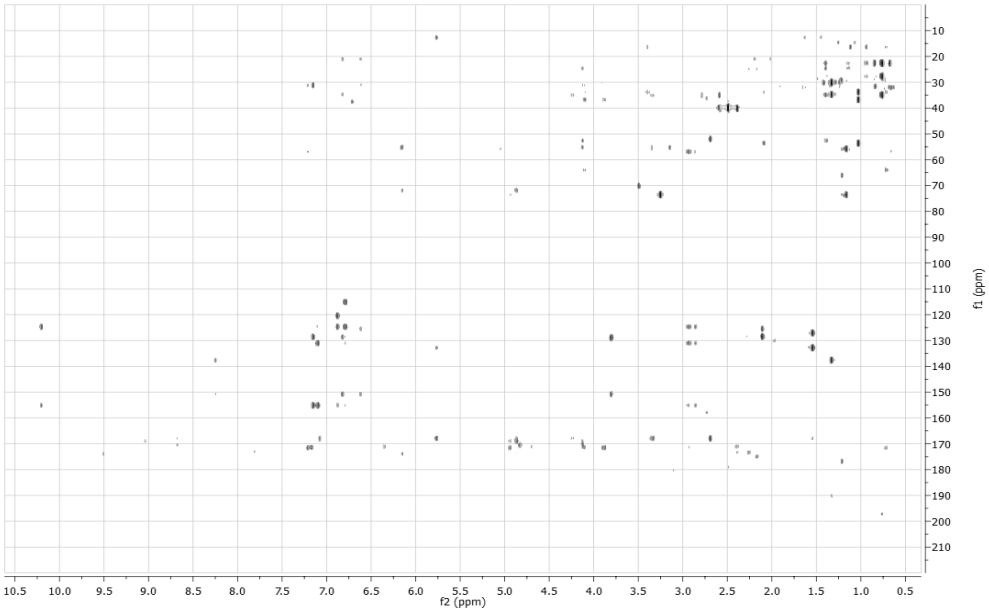

^{1}H spectrum of Perthamide I (**14**) in DMSO-d_6 at 700 MHz.

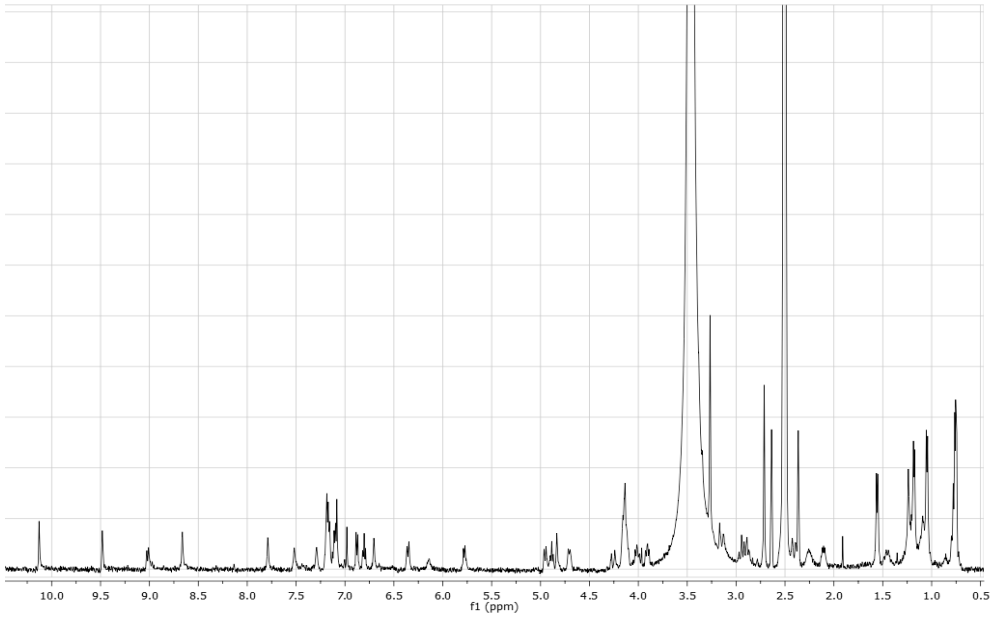

^{1}H NMR spectrum of Perthamide J (**15**) in DMSO-d_6 at 700 MHz.

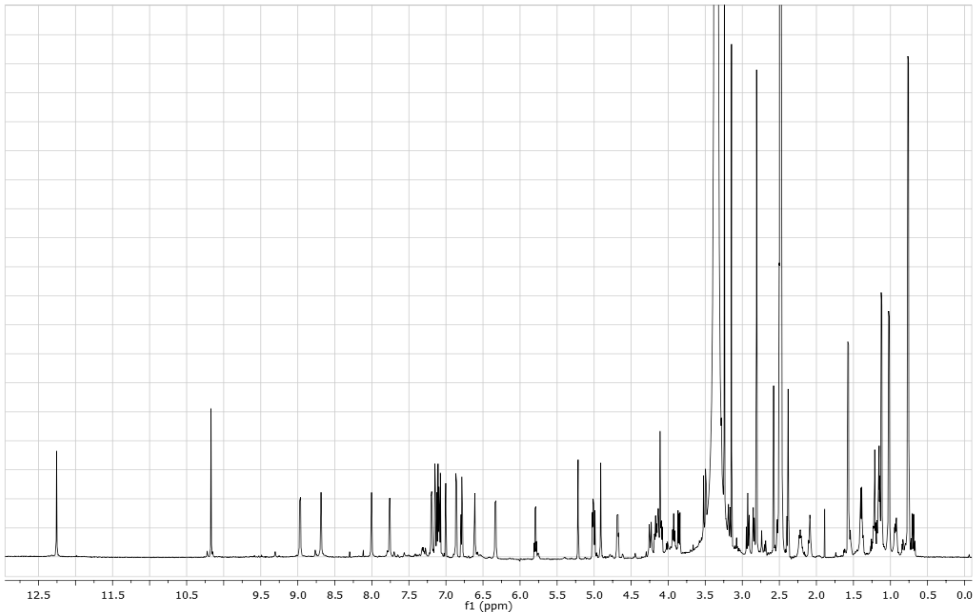

COSY spectrum of Perthamide J (**15**) in DMSO-d_6 at 700 MHz.

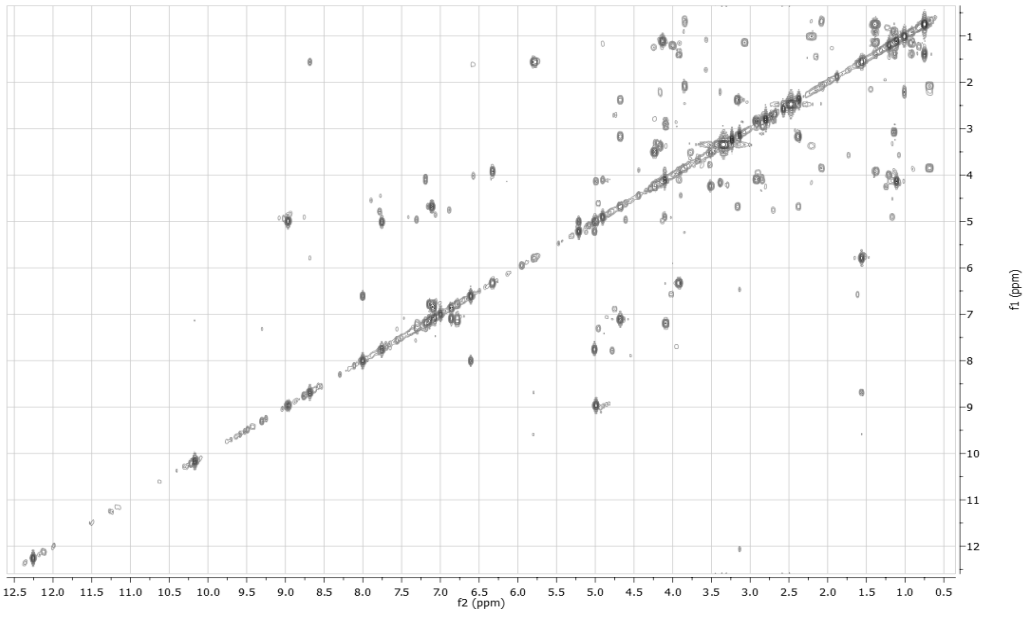

HSQC spectrum of Perthamide J (**15**) in DMSO-d_6 at 700 MHz.

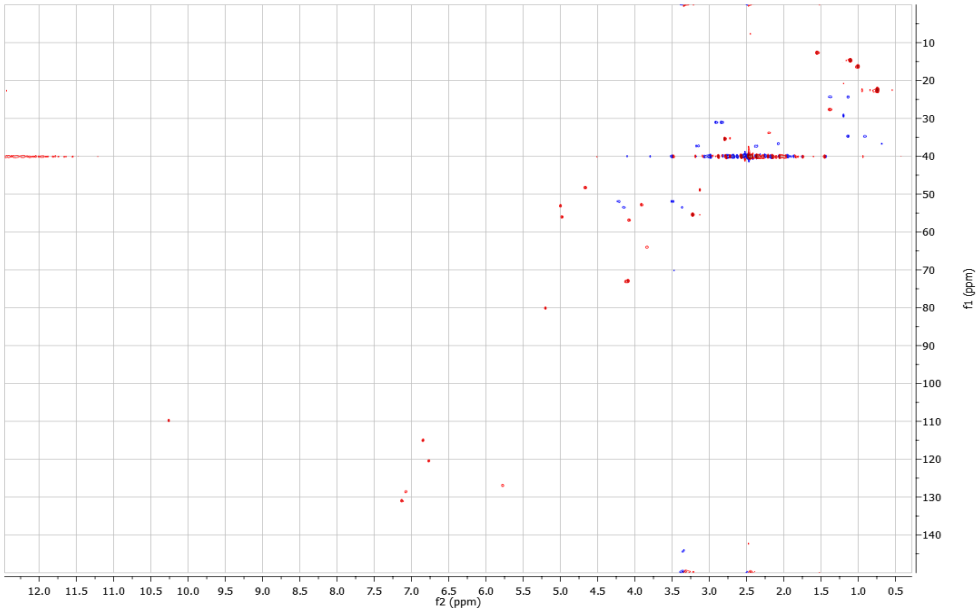

HMBC spectrum of Perthamide J (**15**) in DMSO-d_6 at 700 MHz.

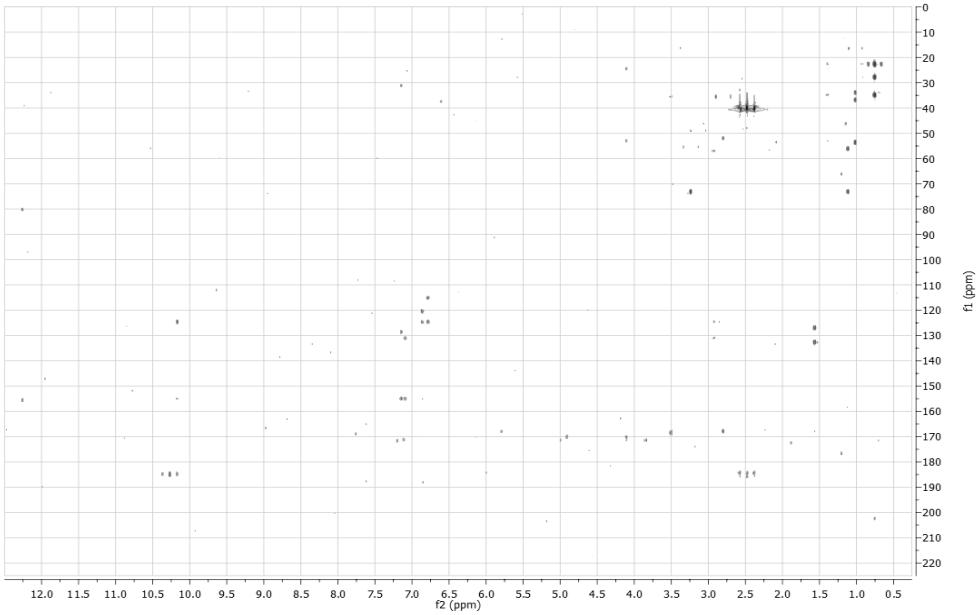

ROESY spectrum of Perthamide J (**15**) in DMSO-d_6 at 700 MHz.

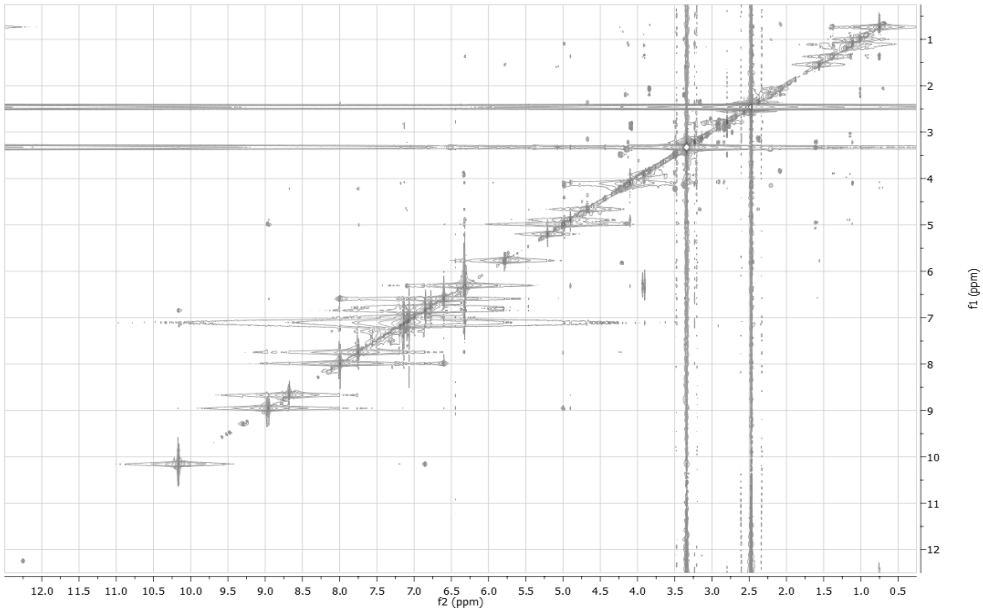

TOCSY spectrum of Perthamide J (**15**) in DMSO-d_6 at 700 MHz.

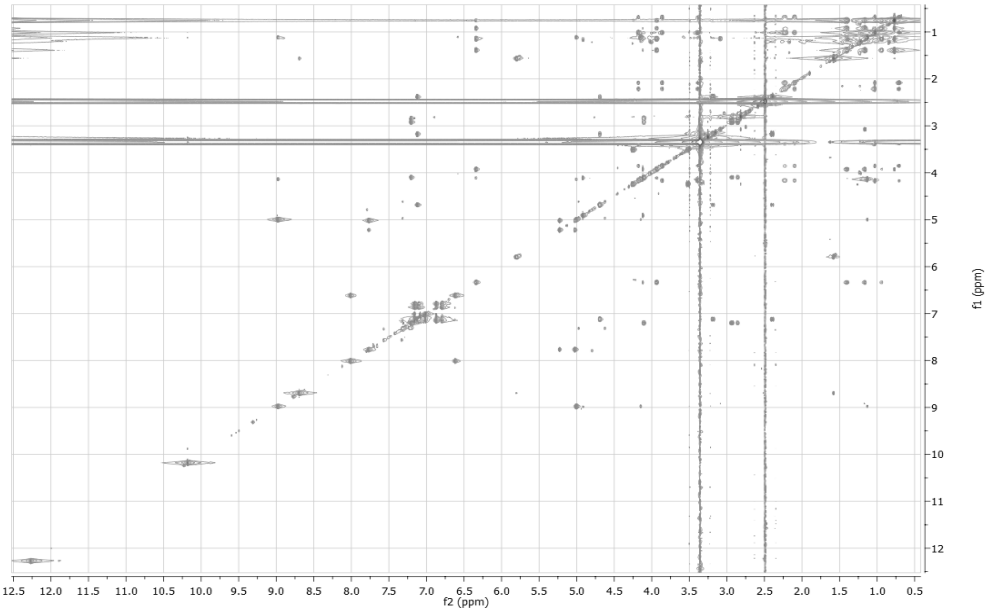

^{1}H spectrum of Perthamide K (**16**) in DMSO-d_6 at 700 MHz.

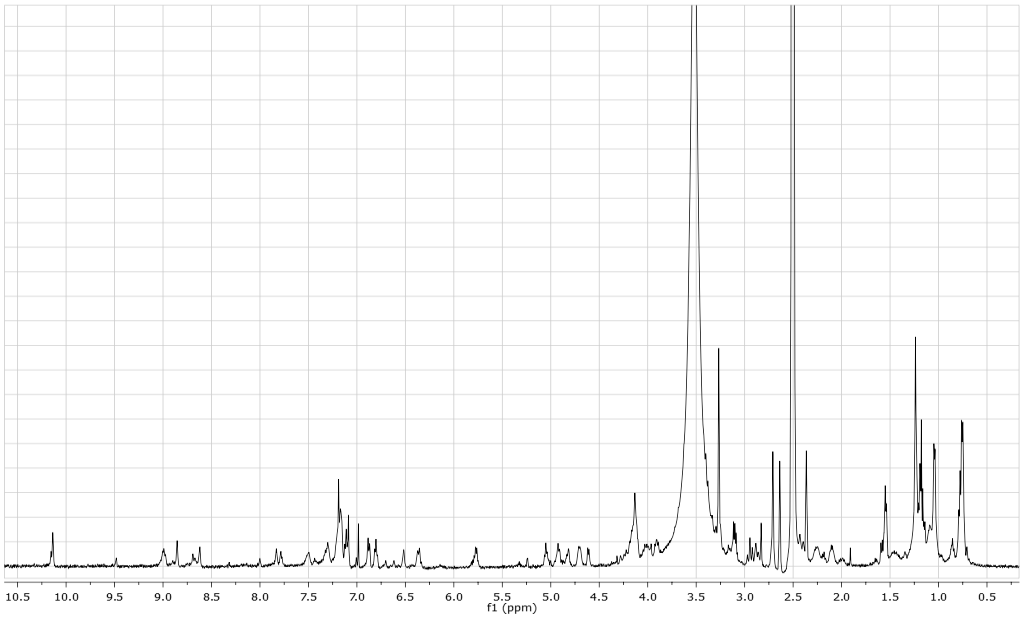

Characteristic data for Solomonamide A and B

Solomonamide A (**17**): white amorphous solid; $[\alpha]^{25}D$ +2.3° (*c* 0.17, CH_3OH); ^{1}H NMR and ^{13}C NMR data in DMSO-d_6 given in **Table 7**; positive HR ESIMS *m*/*z* 496.2018 $[M + H]^+$ (calcd for $C_{21}H_{30}N_5O_9$, 496.2044).

Solomonamide B (**18**): white amorphous solid; $[\alpha]_D^{25}$ +4.8 (*c* 0.28, CH_3OH); ^{1}H and ^{13}C NMR data in DMSO-d_6 given in **Table 8**; positive HR ESIMS *m*/*z* 480.2067 $[M + H]^+$ (calcd for $C_{21}H_{30}N_5O_8$, 480.2094).

LC–MS analysis of Marfey's (FDAA) derivatives. The hydrolysate mixture or the amino acid standards (100 μg) was dissolved in 80 μL of a 2:3 solution of TEA:MeCN and this solution was then treated with 75 μL of 1% 1-fluoro-2,4-dinitrophenyl-5-L-alaninamide (L-FDAA) in 1:2 MeCN:acetone. The vials were heated at 45 °C for 1 h, and the contents were neutralised with 0.2 N HCl (50 μL) after cooling to room temperature. An aliquot of the L-FDAA derivative was dried

under vacuum, diluted with MeCN-5% HCOOH in H_2O (1:1), and separated on a Proteo C18 (25x1.8 mm i.d.) column by means a linear gradient from 10% - 50% aqueous acetonitrile containing 5% formic acid and 0.05% trifluoroacetic acid, over 45 min at 0.15 mL/min. The RP-HPLC system was connected to the electrospray ion source by inserting a splitter valve and the flowgoing into the mass spectrometer source was set at a value of 100 µL/min. Mass spectra were acquired in positive ion detection mode (m/z interval of 320–900) and the data were analysed using the suite of programs Xcalibur; all masses were reported as average values. Capillary temperature was set at 280 °C, capillary voltage at 37 V, tube lens offset at 50 V and ion spray voltage at 5 V. Retention times (min) of FDAA-amino acids are given in parentheses: D-Ala (29.53), L-Ala (24.97), D-Ser (25.02), L-Ser (22.18)

The hydrolysate of solomonamide A contained: L-Ser (22.13) and D-Ala (29.68).

The hydrolysate of solomonamide B contained: L-Ser (22.2) and D-Ala (29.64).

Biological activity. Male Swiss (CD-1; Harlan, Italy) weighing 28–30 g were divided into groups (n¼6 each group) and lightly anaesthetized with isoflurane. Each group of animals received subplantar injection of 50 µL of carrageenan 1% (w/v) or 50 µL of saline in the left hind paw. Paw volume was measured by using an hydropletismometer specially modified for small volumes (Ugo Basile, Comerio, Italy) immediately before the subplantar injection and 2, 4, 6, 24, 48, 72 and 96 h thereafter. The same operator always performed the double-blind assessment of paw volume. The increase in paw volume was calculated as the difference between the paw volume measured at each time point and the basal paw oedema. Each group of animals received intraperitoneal administration of

solomonamide A (0.03, 0.1, 0.3 mg/kg) or vehicle (PEG). All drugs were administrated immediately before the injection of carrageenan and 24 h thereafter.

Statistical analysis. Results were expressed as mean_s.e.m. Statistical analysis was determined by one way ANOVA followed by Dunnett's test for multiple comparisons, using GraphPad Prism software (GraphPad Software Inc., San Diego, CA). Differences were considered statistically significant when $p<0.05$.

Spectroscopic Data of SolomonamideA and B

^{1}H spectrum of Solomonamide A (**17**) in DMSO-d_6 at 700 MHz.

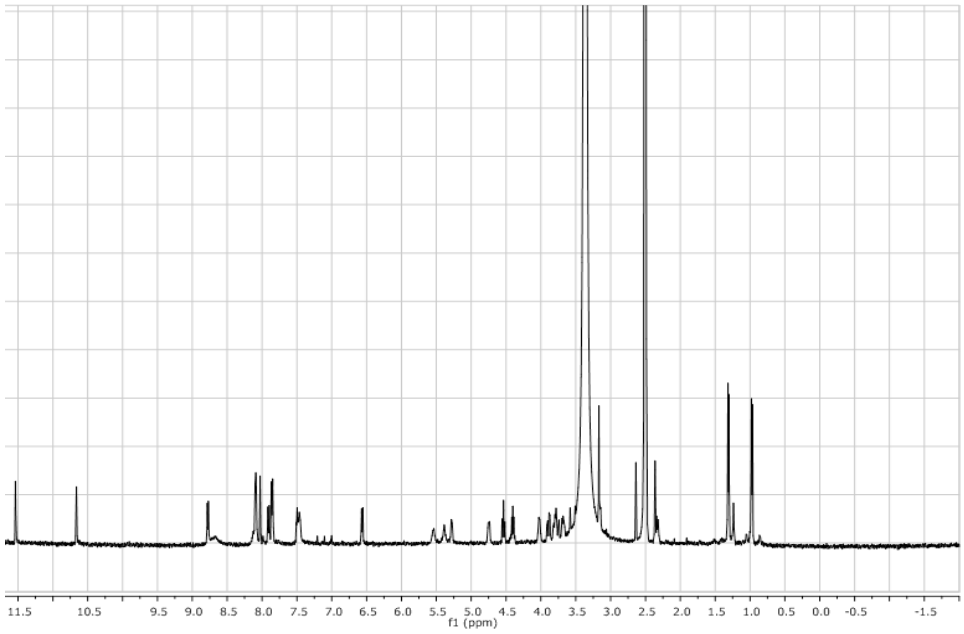

COSY spectrum of Solomonamide A (**17**) in DMSO-d_6 at 700 MHz.

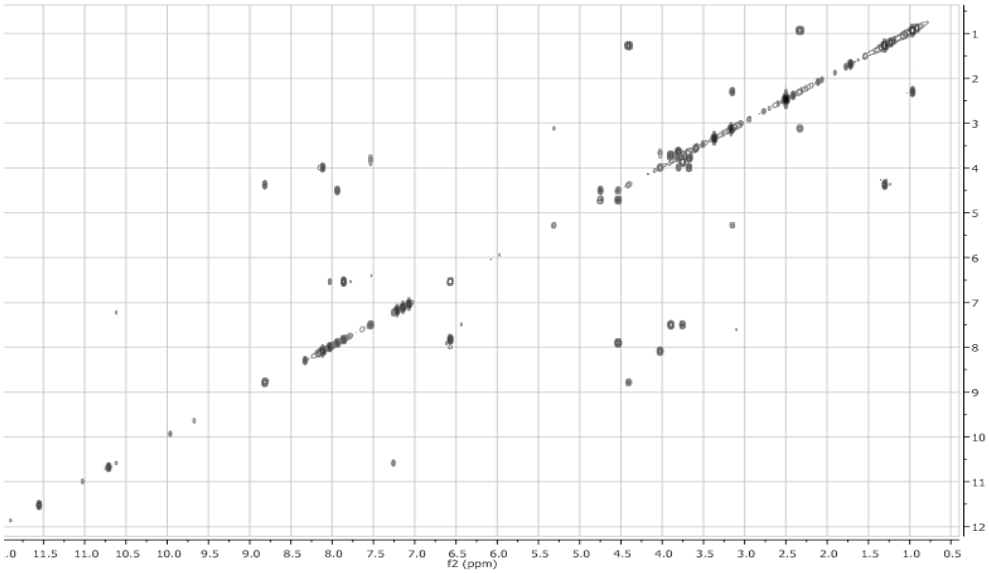

HSQC spectrum of Solomonamide A (**17**) in DMSO-d_6 at 700 MHz.

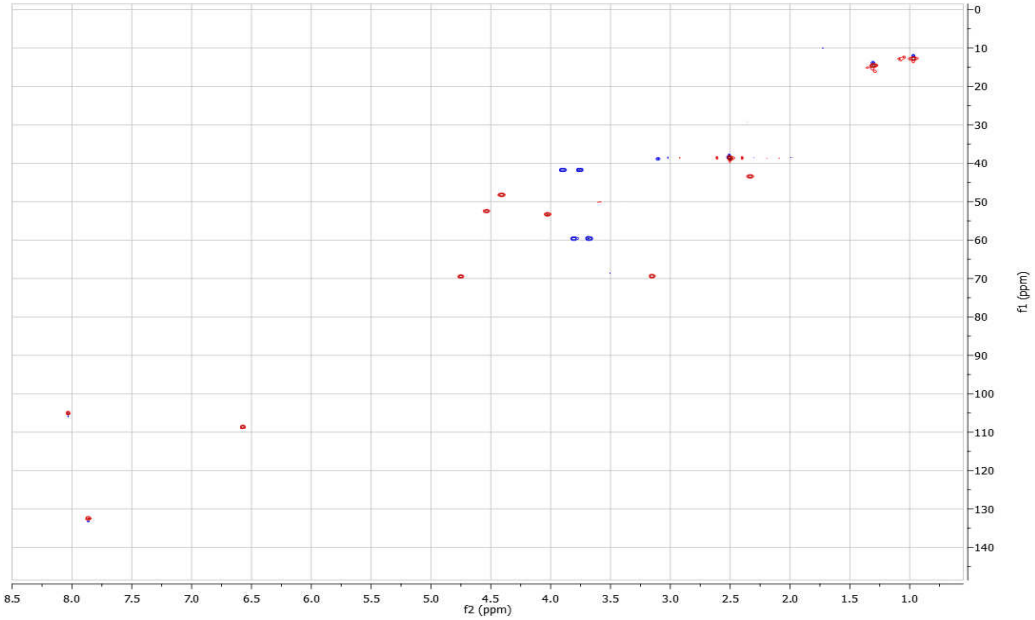

HMBC spectrum of Solomonamide A (**17**) in DMSO-d_6 at 700 MHz.

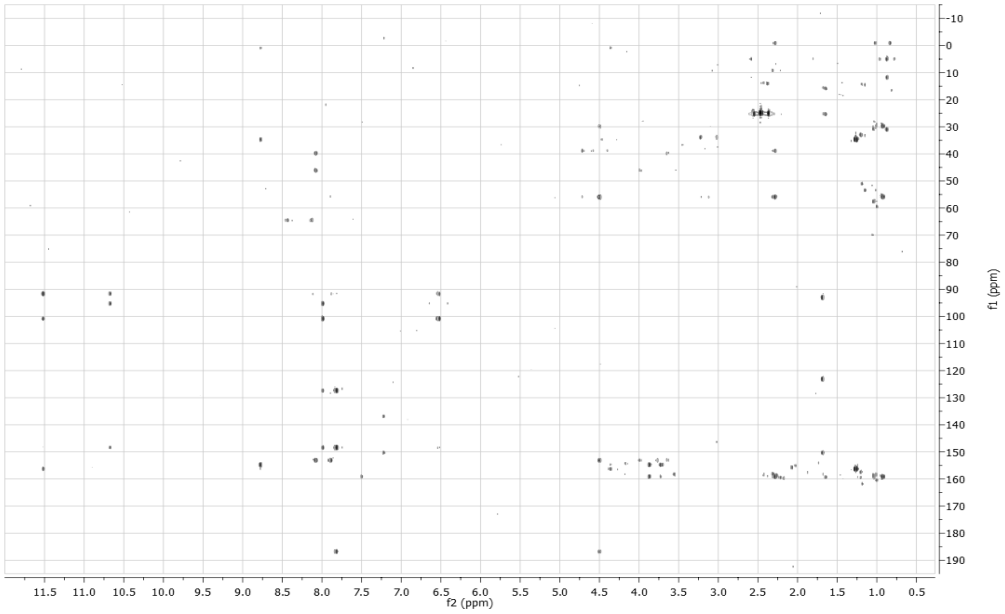

ROESY spectrum of Solomonamide A (**17**) in DMSO-d_6 at 700 MHz (200ms).

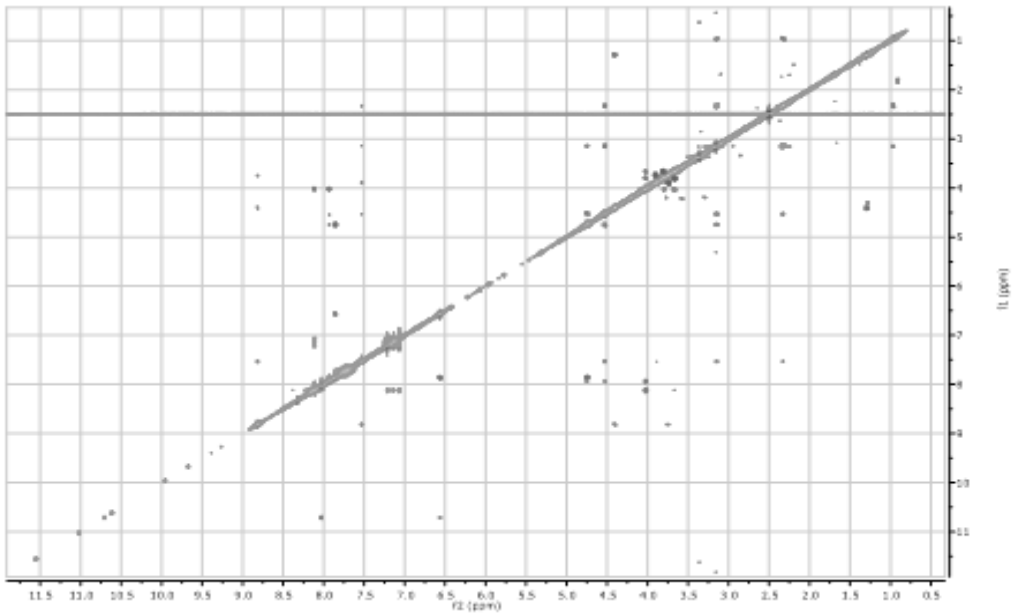

ROESY spectrum of Solomonamide A (**17**) in DMSO-d_6 at 700 MHz (500 ms).

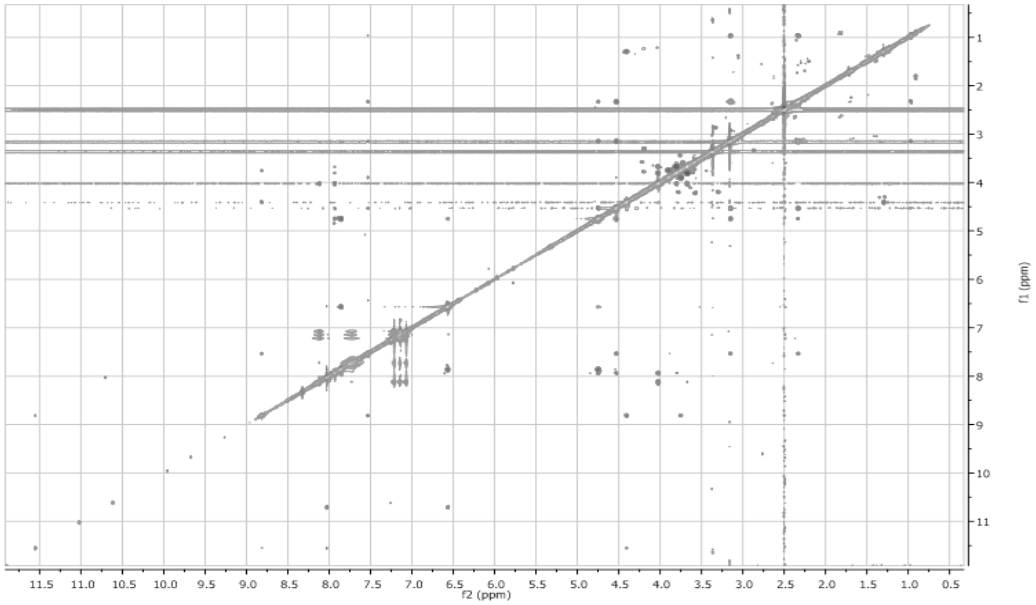

^{1}H spectrum of Solomonamide A (**17**) in DMSO-d_6 at 700 MHz.

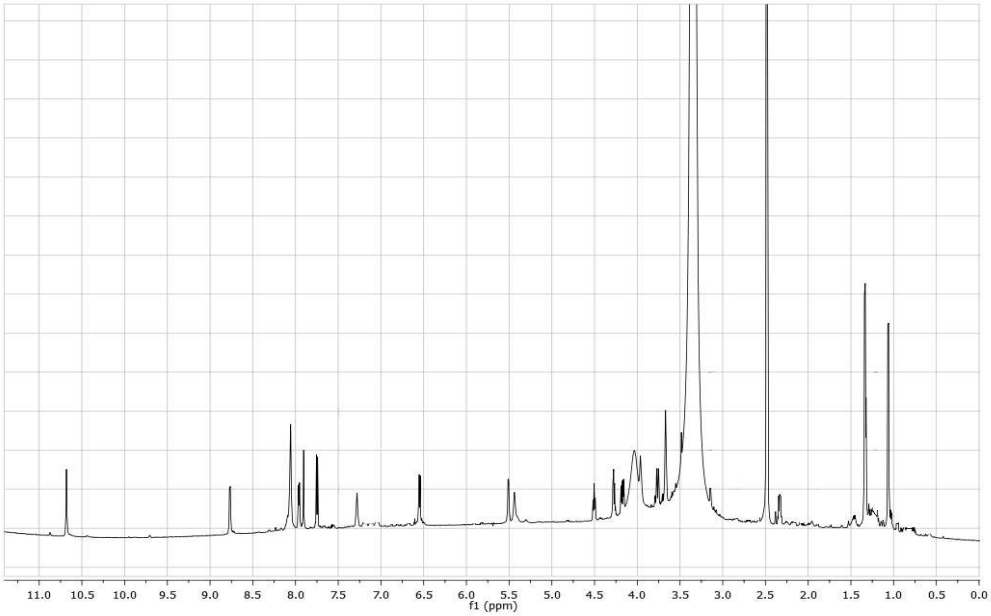

COSY of Solomonamide B (**18**) in DMSO-d_6 at 700 MHz.

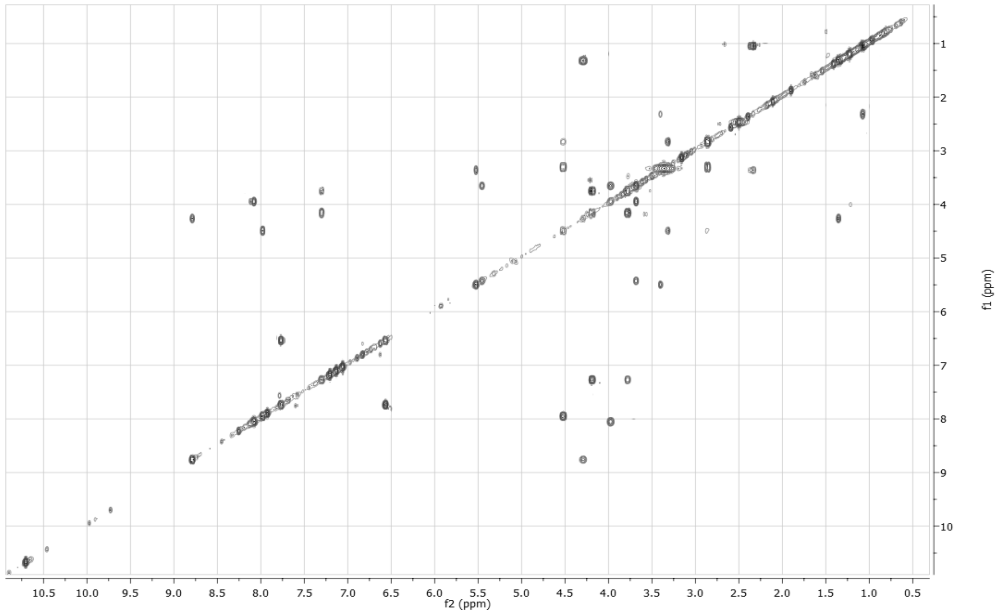

HSQC of Solomonamide B (**18**) in DMSO-d_6 at 700 MHz.

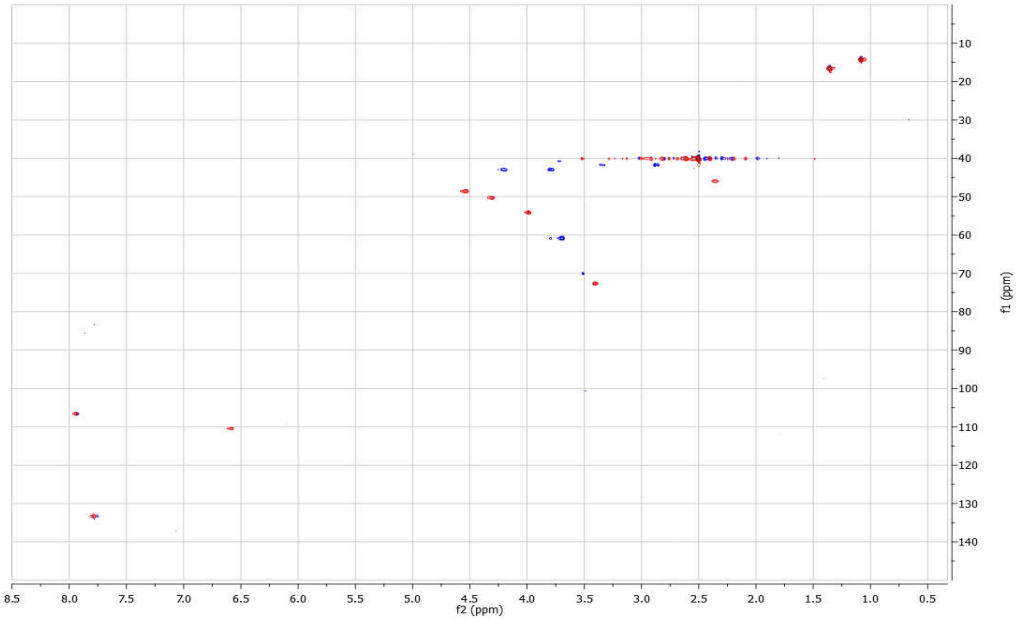

HMBC of Solomonamide B (**18**) in DMSO-d_6 at 700 MHz.

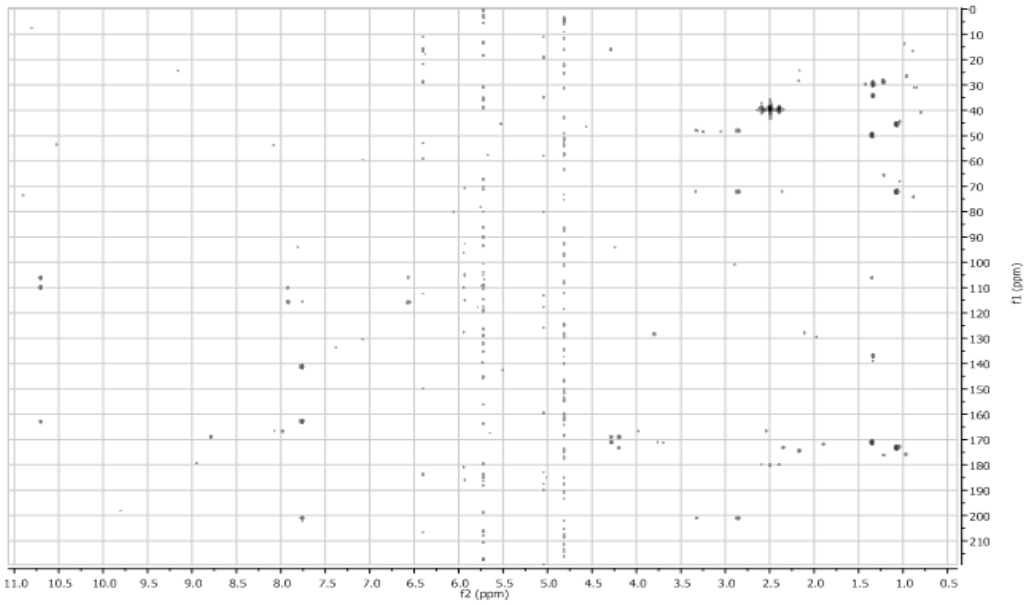

Characteristic data for swinholide A and Compound 19

Swinholide A: light yellow solid; ^{1}H NMR and ^{13}C NMR data in CD_3OD given in **Table 9**; positive ESIMS *m/z* 1408.9 $[M + Na]^+$.

Compound 19: light yellow solid; ^{1}H NMR and ^{13}C NMR data in CD_3OD given in **Table 9**; positive HR ESIMS *m/z* 1424.9 $[M+Na]^+$.

Spectroscopic Data of Swinholide A and Compound 19

^{1}H spectrum of Swinholide A in CD_3OD at 700 MHz.

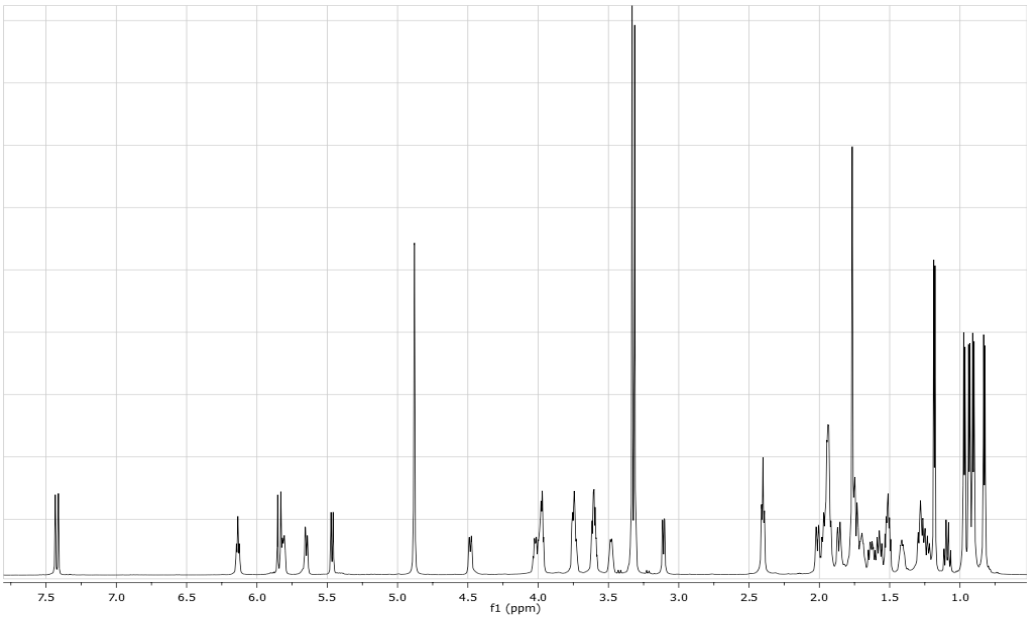

COSY spectrum of Swinholide A in CD_3OD at 700 MHz.

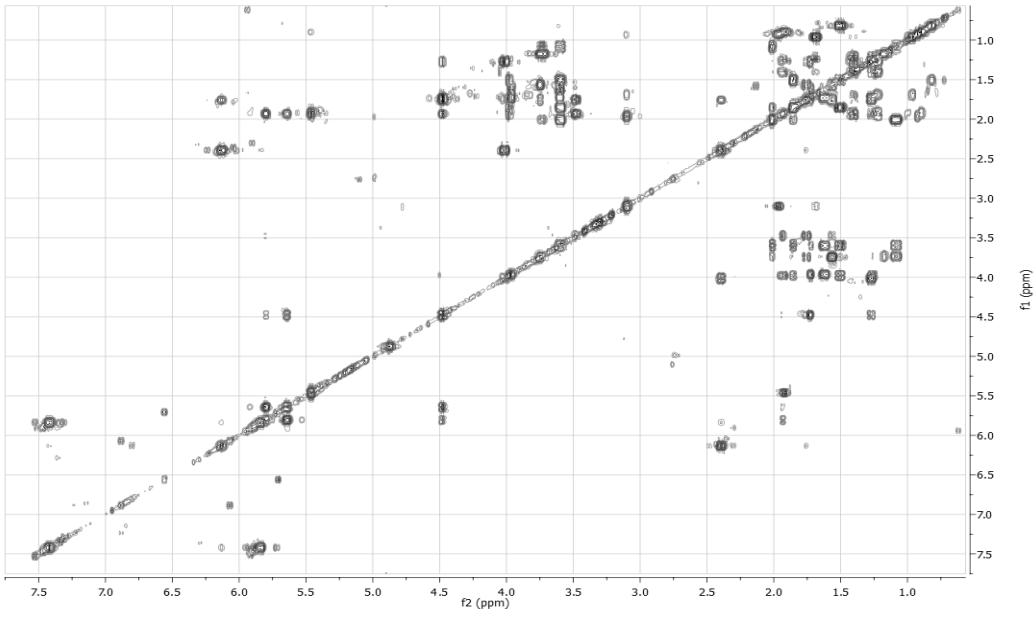

HSQC spectrum of Swinholide A in CD_3OD at 700 MHz.

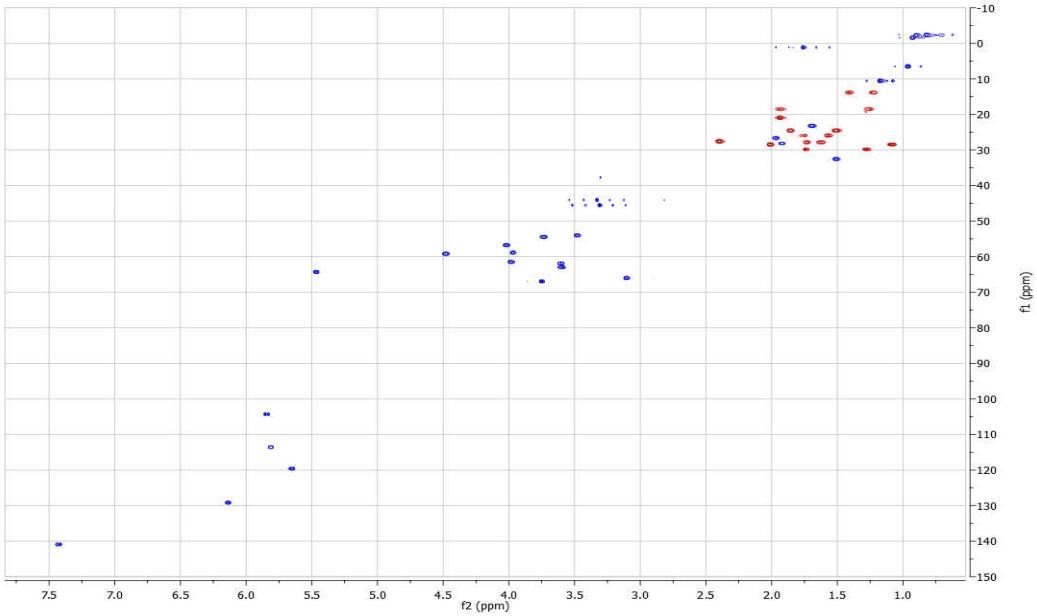

HMBC spectrum of Swinholide A in CD_3OD at 700 MHz.

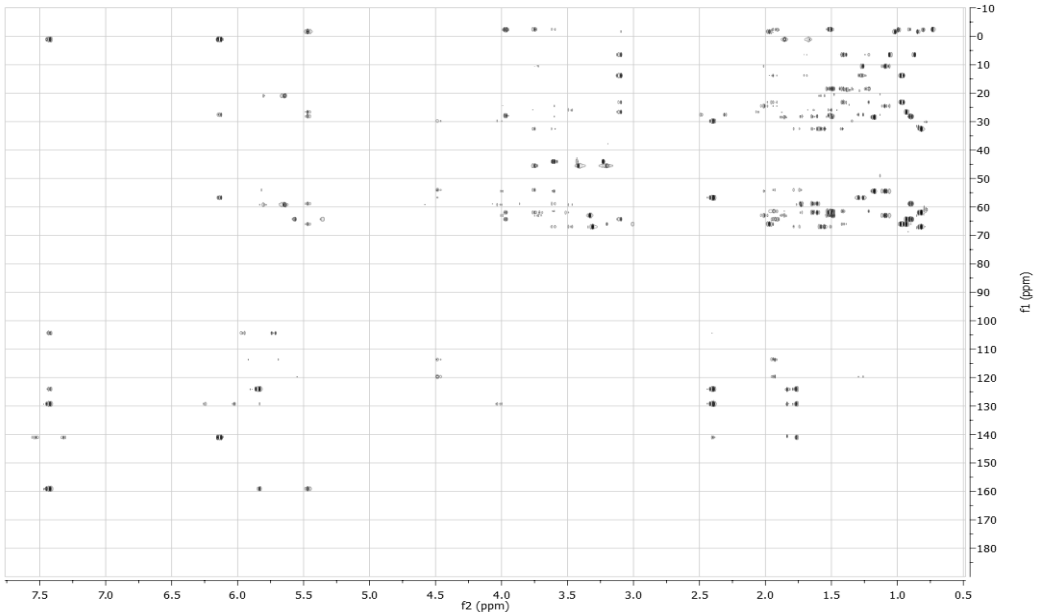

^{1}H spectrum of Compound **19** in CD_3OD at 700 MHz.

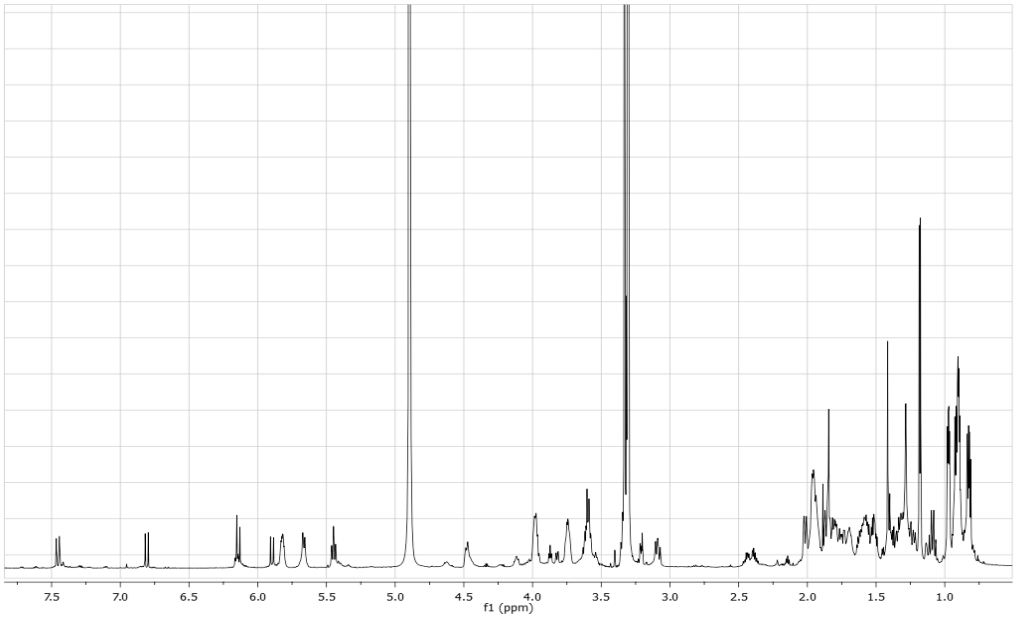

HSQC spectrum of Compound **19** in CD_3OD at 700 MHz.

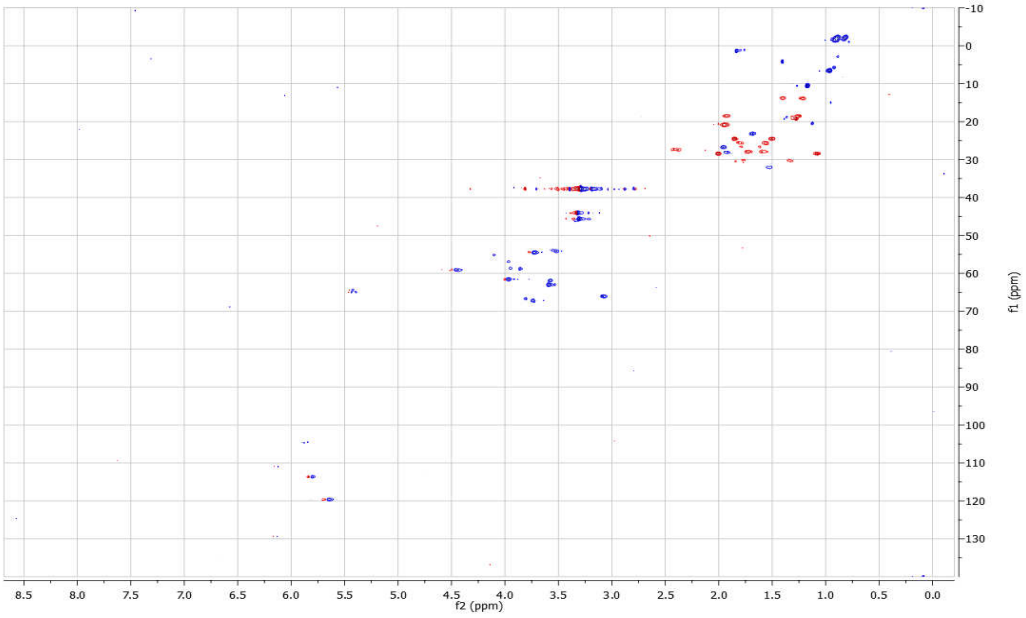

HMBC spectrum of Compound **19** in CD_3OD at 700 MHz.

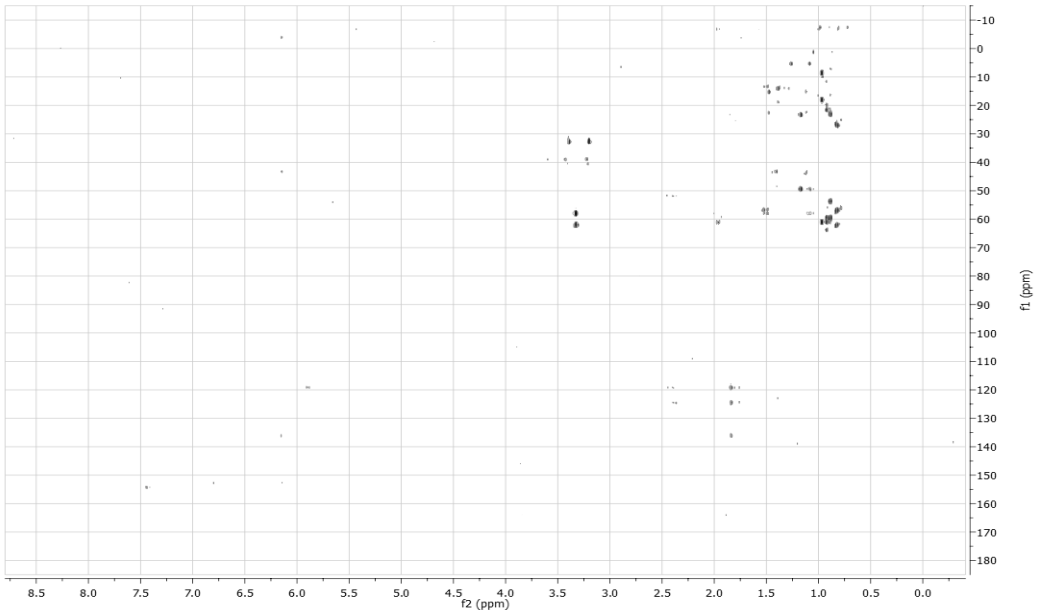

IV. Experimental section of *Cucumis melo*

Extraction and isolation. The powdered seeds (230 g) were extract with MeOH (1.5 L) at room temperature. The methanol extracts (4 g) were then subjected to Kupchan's partitioning methodology to give four extracts: *n*-hexane (910 mg), $CHCl_3$ (312 mg), *n*-BuOH (372 mg) and an aqueous residue (3.65 g). The *n*-BuOH extract was chromatographed by DCCC using *n*-BuOH-Me_2CO-H_2O (3:1:5) in the descending mode (the upper phase was the stationary phase), flow rate 8 ml min^{-1}; 4 ml fractions were collected and monitored by thin layer chromatography (TLC) on silica gel with *n*-BuOH-HOAc-H_2O (12:3:5) and $CHCl_3$-MeOH-H_2O (80:18:2). These fractions were then separated by reversed-phase HPLC (C_{18} μ-Bondapak 30 cm × 3.9 mm i.d.) with MeOH-H_2O (15:85) as eluent, to give pure compound **20** (1.4 mg), Tryptophan and Inosine. The purification by HPLC with MeOH-H_2O (1:9) as eluent, gave pure compound **21** (2 mg).

The $CHCl_3$ extract was chromatographed by DCCC using $CHCl_3$-MeOH-H_2O (7:13:8) in the ascending mode (the lower phase was the stationary phase), flow rate 8 ml min^{-1}; 4 ml fractions were collected and monitored by thin layer chromatography (TLC) on silica gel with $CHCl_3$-MeOH-H_2O (80:18:2). These fractions were then separated by reversed-phase HPLC (C_{18} μ-Bondapak 30 cm × 3.9 mm i.d.) with MeOH-H_2O (85:15) as eluent, to give pure compound **22** (2.3 mg) and with MeOH-H_2O (9:1) as eluent, to give pure compound **23** (1.5 mg) and unsaturated fatty acids.

Acid hydrolysis and sugars analysis. Compound **20** and apiin (0.5 mg each) were hydrolyzed with 2N CF_3CO_2H (2 ml) at 110° in a sealed tube for 8 h. After

cooling, the solution was diluted with H_2O (5 ml) and extracted with AcOEt (3 x 2 ml). The aqueous layer was evaporated to dryness under reduced pressure and the residue was reacted with 0.1 M L-cysteine methyl ester hydrochloride in anhydrous pyridine (200 µl) for 2 h at 80°.[193] 1-(Trimethylsilyl)imidazole in pyridine was added and the thiazolidine derivatives analyzed by GC.[194] D-apiose and D-glucose were confirmed in **20** by comparison of the retention time of their derivatives with those of apiine hydrolysate prepared in a similar way [D-apiose (t_R 5.22 min) and D-glucose (t_R 12.10 min)].

Characteristic data

Compound 20: (E)-4-hydroxycinnamyl alcohol 4-O-(2'-O-β-D-apiofuranosyl) (1''→2')-β-D-glucopyranoside. $[\alpha]^{25}_D$ -6.0 (*c* 0.14, MeOH); ^{1}H and ^{13}C NMR data (Table **10**); HRESIMS ($C_{20}H_{28}O_{11}$) *m/z* 467.1602 $(M + Na)^+$ [calcd. for $C_{20}H_{28}O_{11}Na$ 467.1529]

Compound 21: Benzyl O-β-D-glucopyranoside. FAB-MS (positive ion) *m/z* 293 $[M + Na]^+$;^{1}H NMR (500 MHz, CD_3OD): 7.42 (d, *J* = 7.5 Hz, H-2 and H-6), 7.33 (t, *J* = 7.5 Hz, H-3 and H-5), 7.28 (d, *J* = 7.5 Hz, H-4), 4.93 (d, *J* = 11.9 Hz, H-7), 4.67 (d, *J* = 11.9 Hz, H-7), 4.36 (d, *J* = 7.7 Hz, H-1'), 3.91 (dd, *J* = 11.9, 1.9 Hz, H-6'), 3.70 (dd, *J* = 11.9, 5.7 Hz, H-6'), 3.25-3.33 (H-2'-H5'). ^{13}C NMR (500 MHz, CD_3OD): 138.0 (C-1), 128.2 (C-3, C-5), 128.0 (C-2, C-6), 127.8 (C-4), 102.1 (C-1'), 77.7 (C-5'), 78.1 (C-3'), 74.9 (C-2'), 71.5 (C-4'), 70.5 (C-7), 61.7 (C-6').

Compound 22: 3,29-O-dibenzoylmultiflor-8-en-3α,7β,29-triol. ^{1}H NMR (500 MHz, CD_3OD): 8.00 (d, *J* = 7.5 Hz, H-3'' and H-7''), 7.95 (d, *J* = 7.5 Hz, H-3' and H-7'), 7.62 (t, *J* = 7.6 Hz, H-5''), 7.60 (t, *J* = 7.6 Hz, H-5'), 7.48 (t, *J* = 7.6

Hz, H-4'' and H-6''), 7.46 (t, *J* = 7.6 Hz, H-4' and H-6'), 4.85 (br s, H-3), 4.39 (t, *J* = 6.0 Hz, H-7), 4.11 (d, *J* = 10.5 Hz, H_2-29), 1.32 (s, CH_3-26), 1.18 (s, CH_3-28), 1.16 (s, CH_3-25), 1.14 (s, CH_3-30), 1.04 (s, CH_3-24), 1.01 (s, CH_3-27), 0.94 (s, CH_3-23). ^{13}C NMR (500 MHz, CD_3OD): 167.3 (C-29a), 166.3 (C-3a), 138.3 (C-8), 140.3 (C-9), 134.0 (C-4'/C-4''), 129.4 (C-3'/C-5', C-3''/C-5''), 130.0 (C-2'/C-6', C-2''/C-6''), 131.6 (C-1', C-1''), 78.8 (C-3), 73.7 (C-29), 70.6 (C-7), 45.2 (C-5), 43.8 (C-18),41.3 (C-14), 38.7 (C-10), 38.4 (C-13), 37.0 (C-4), 36.8 (C-16), 36.7 (C-22), 32.4 (C-20), 31.3 (C-6), 31.4 (C-17), 31.1 (C-28), 31.0 (C-12), 30.9 (C-1), 29.6 (C-19), 29.3 (C-30), 28.6 (C-21), 27.3 (C-26), 27.2 (C-23), 26.3 (C-15), 23.4 (C-2), 21.3 (C-24), 20.3 (C-25), 19.9 (C-11), 18.2 (C-27).

Compound 23: 3-O-p-amino-benzoyl-29-O-benzoylmultiflor-8-en-3α,7β,29-triol. ^{1}H NMR (500 MHz, CD_3OD): 8.01 (OPABA, H-3'' and H-7''), 7.90 (d, *J* = 7.5 Hz, H-3' and H-7'), 7.64 (t, *J* = 7.6 Hz, H-5'), 7.46 (t, *J* = 7.6 Hz, H-4' and H-6'), 6.64 (OPABA, H-4'' and H-6''), 4.85 br s (H-3), 4.39 (t, *J* = 6.0 Hz, H-7), 4.13 (d, *J* = 10.5 Hz, H_2-29), 1.32(s, CH_3-26), 1.18 (s, CH_3-28), 1.15 (s, CH_3-25), 1.14 (s, CH_3-30), 1.03 (s, CH_3-24), 1.01 (s, CH_3-27), 0.92 (s, CH_3-23).

Spectroscopic Data of Compound 20

^{1}H NMR spectrum of Compound **20** in CD_3OD at 700 MHz.

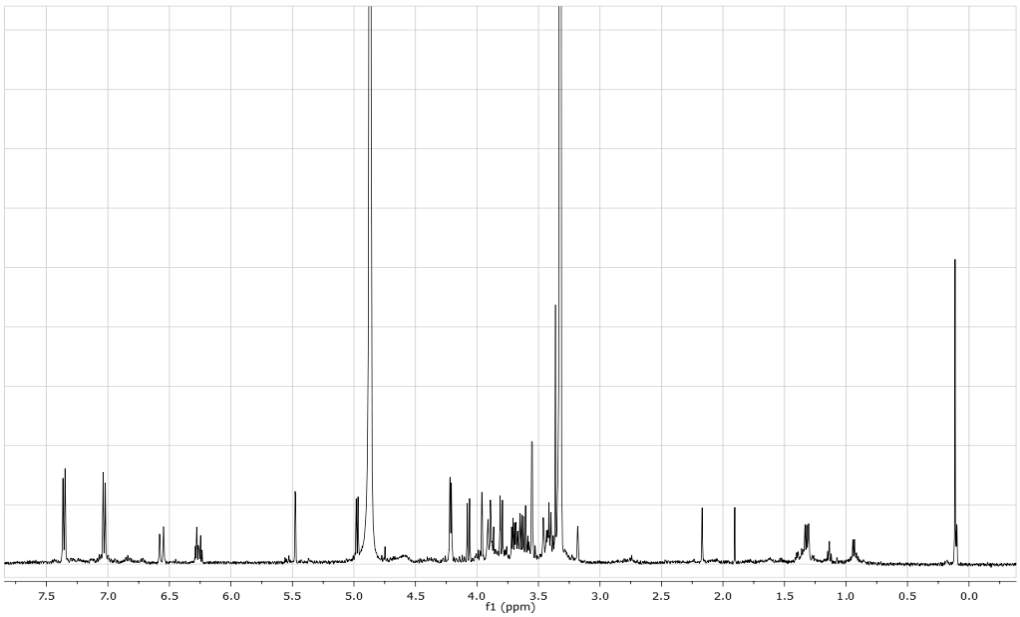

COSY spectrum of Compound **20** in CD_3OD at 700 MHz.

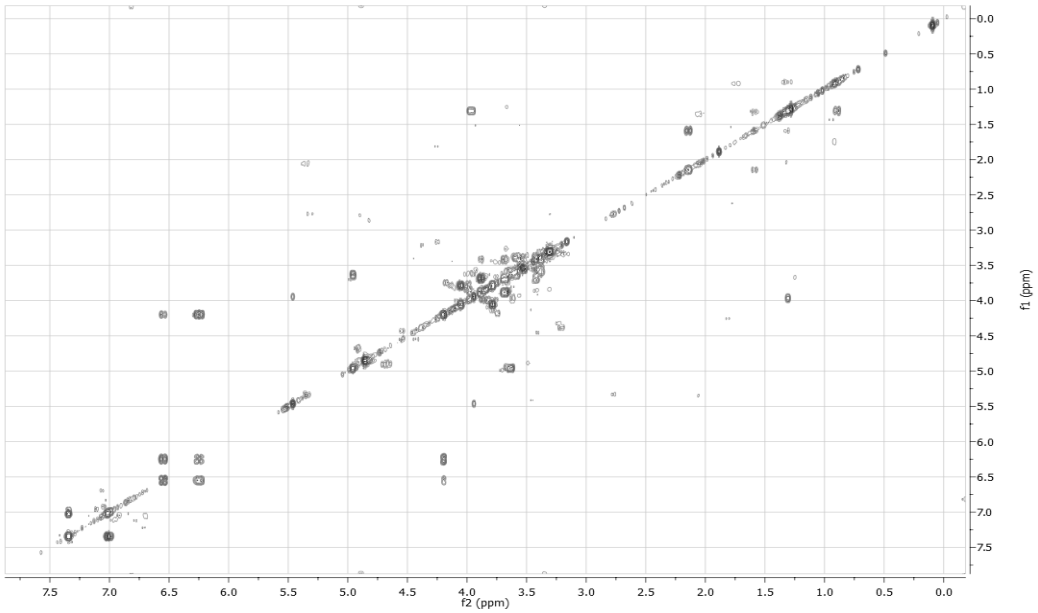

HSQC spectrum of Compound **20** in CD_3OD at 700 MHz.

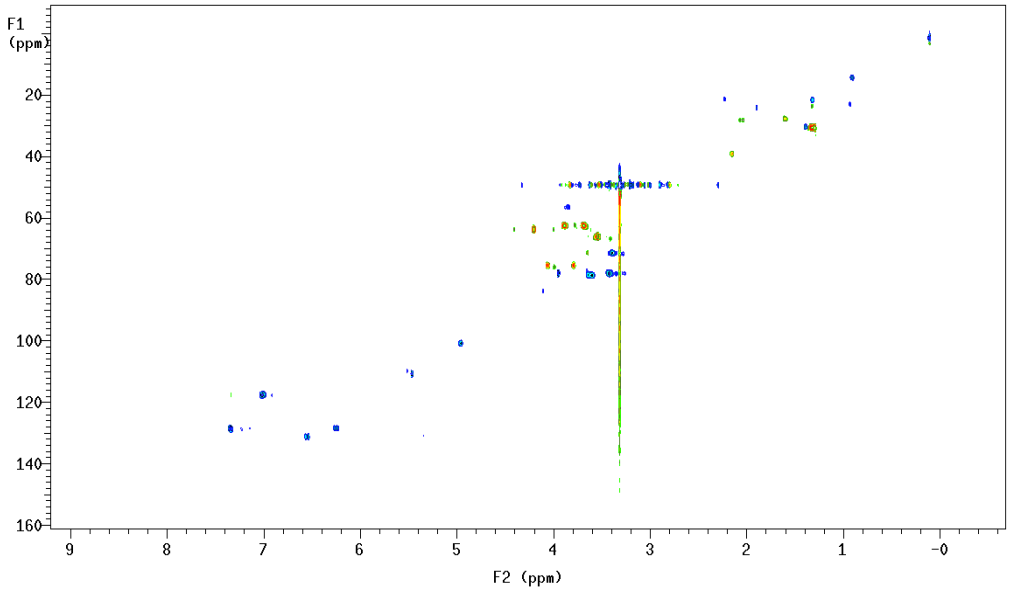

HMBC spectrum of Compound **20** in CD_3OD at 700 MHz.

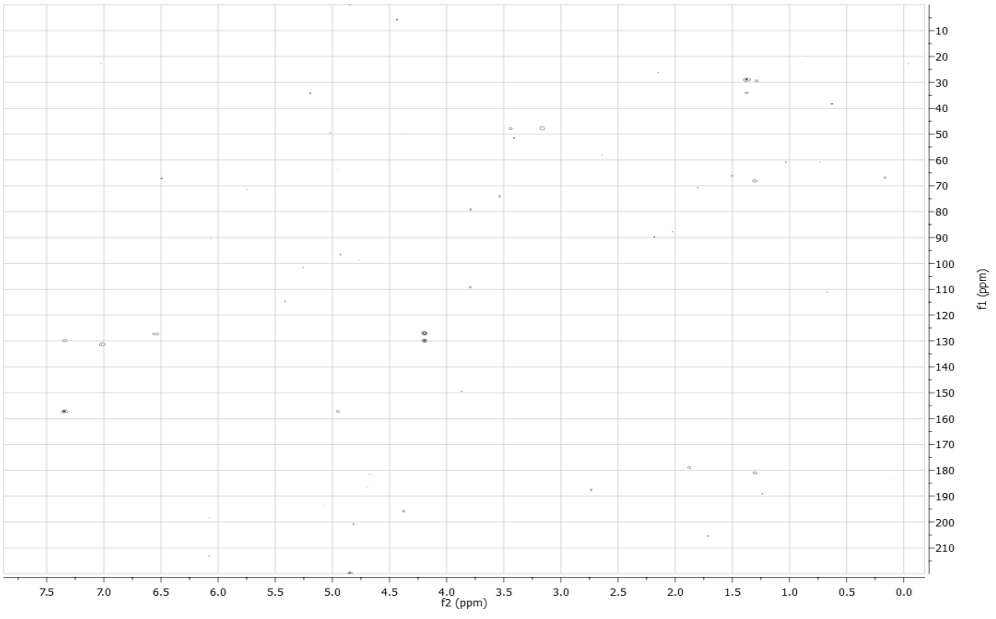

V. Experimental section of *Borrago officinalis*

Extraction and isolation. The flowers (300 g), deprived of stem, were crushed and subsequently extract with MeOH (1.5 L) at room temperature. The methanol extracts (10.8 g) were then subjected to Kupchan's partitioning methodology to give four extracts: *n*-hexane (760 mg), $CHCl_3$ (1.32 g), *n*-BuOH (1.71 g) and an aqueous residue (4.1 g). The *n*-BuOH extract was chromatographed by DCCC using *n*-BuOH-Me_2CO-H_2O (3:1:5) in the descending mode (the upper phase was the stationary phase), flow rate 8 ml min^{-1}; 4 ml fractions were collected and monitored by thin layer chromatography (TLC) on silica gel with *n*-BuOH-HOAc-H_2O (12:3:5). The fraction 8 was then separated by reversed-phase HPLC (C_{18} μ-Bondapak 30 cm × 3.9 mm i.d.) with MeOH-H_2O (1:9) as eluent, to give pure compound **24** (3.6 mg).

Acid hydrolysis and sugar analysis. Compound **24** (0.5 mg) was hydrolyzed with 2N CF_3CO_2H (2 mL) at 110° in a sealed tube for 8 h. After cooling, the solution was diluted with H_2O (5mL) and extracted with AcOEt (3 x 2 mL). The aqueous layer was evaporated to dryness under reduced pressure and the residue was reacted with 0.1M L-cysteine methyl ester hydrochloride in anhydrous pyridine (200 μL) for 1 h at 60°. 1-(Trimethylsilyl)imidazole in pyridine was added and the thiazolidine derivatives analyzed by GC.[193] The D configuration of glucose was confirmed by comparison of the retention time of D- and L- glucose derivatives with the hydrolysate prepared in a similar way (t_R 12.10 min).

Characteristic data of Compound 24: white amorphous solid; ^1H and ^{13}C NMR data in CD_3OD given in Table **11**; HR-ESIMS *m/z* 415.1534 $[M]^+$ (calcd. for $C_{19}H_{26}O_{10}$ 415.1526).

Spectroscopic Data of Compound 24

^{1}H spectrum of Compound **24** in CD_3OD at 500 MHz.

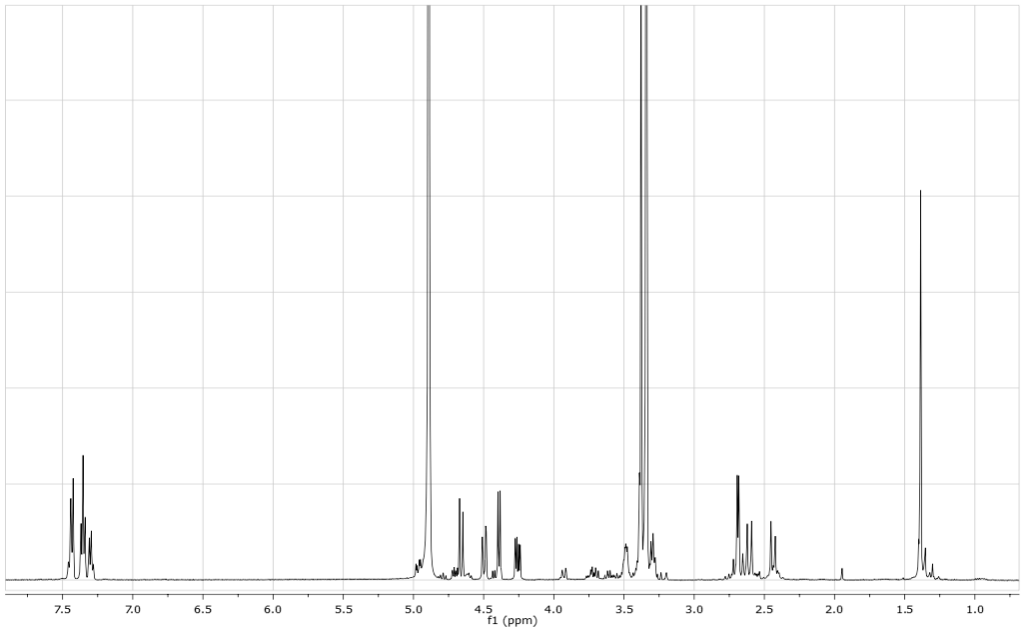

COSY of Compound **24** in CD_3OD at 500 MHz.

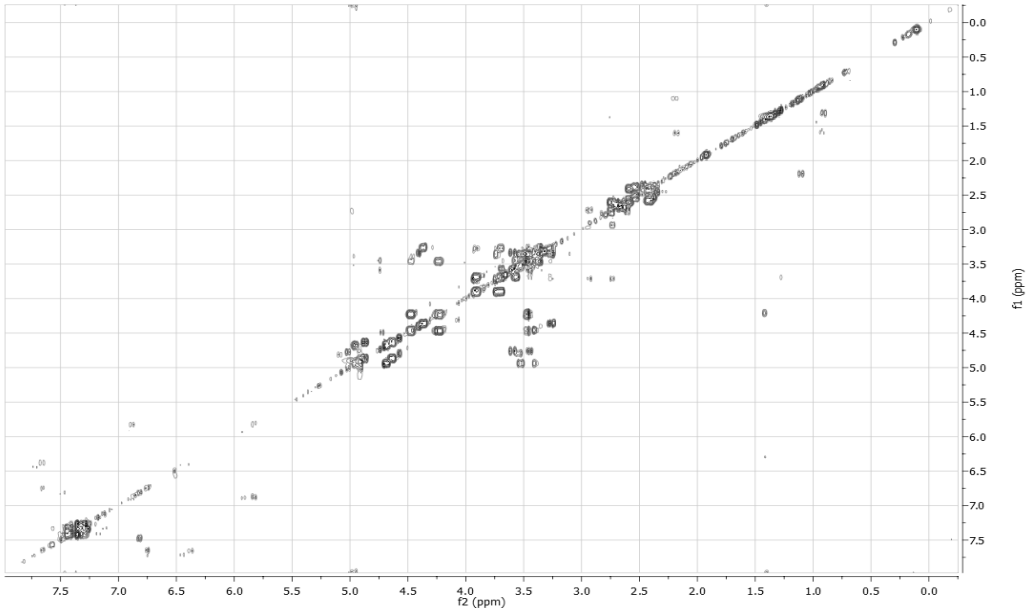

HMBC of Compound **24** in CD_3OD at 500 MHz.

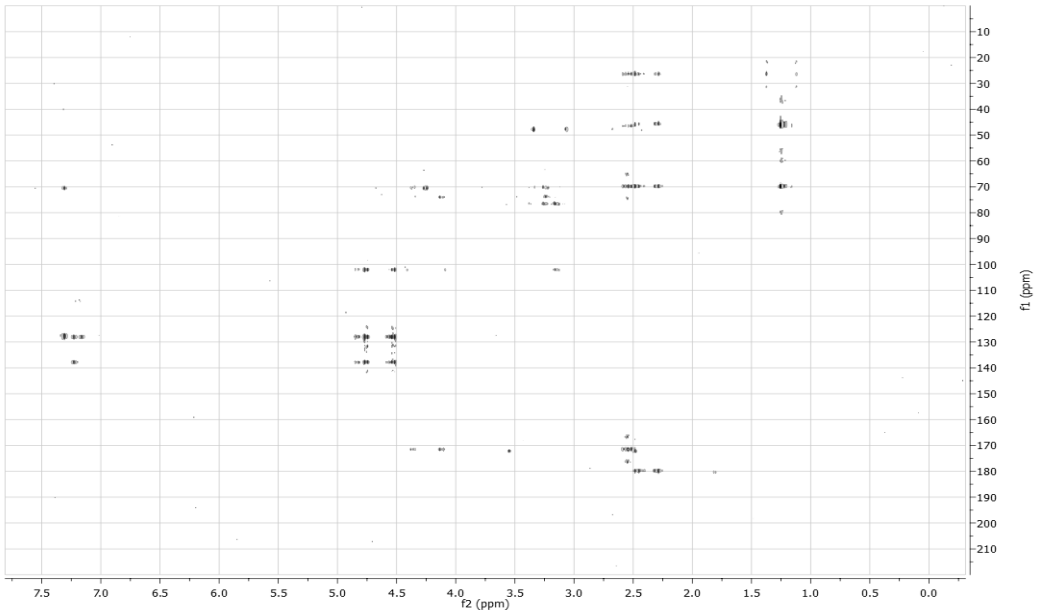

VI. Experimental section of *Ruscus aculeatus*

Extraction and isolation. Rhizomes (243.5 g) of *Ruscus aculeatus* were shaved and exhaustively extracted with MeOH (1.5 L) at room temperature. The methanol extracts (56 g) were then subjected to Kupchan's partitioning methodology to give four extracts: *n*-hexane (483.8 mg), $CHCl_3$ (3.7 g), *n*-BuOH (9.1 g) and an aqueous residue (36.2 g). The *n*-BuOH extract was chromatographed by DCCC using *n*-BuOH-Me_2CO-H_2O (3:1:5) in the descending mode (the upper phase was the stationary phase), flow rate 8 ml min^{-1}; 4 ml fractions were collected and monitored by thin layer chromatography (TLC) on silica gel with *n*-BuOH-HOAc-H_2O (12:3:5). The fractionas 8-11 were then separated by reversed-phase HPLC (Luna C_{18} Phenomenex, 5µ, 250 × 4.6 mm) with MeOH-H_2O (48:52) as eluent, to give pure compound **25** (4.3 mg, t_R=25.5 min), compound **26** (4.1 mg, t_R=25.5 min). The fractions 16-18 were purified in the same conditions to give compound **27** (16.6 mg, t_R=23 min).

Determination of the sugar absolute configuration of glucose. A solution of each isolated compounds **25** and **26** (1 mg) in 1N HCl (0.25 mL) was stirred at 80° C for 4 h. The hydrolysed was reacted with 0.1M L-cysteine methyl ester hydrochloride in anhydrous pyridine (200 µl) for 1 h at 60°. 1-(Trimethylsilyl)imidazole in pyridine was added and the thiazolidine derivatives analyzed by GC.[193]

Solvolysis of Compound 25. A solution (1 mg) of the compound 25 in a mixture of pyridine (125 mL) and dioxane (125 mL) was heated at 150° C for 3 h in a stoppered reaction vial. The residue was evaporated to dryness and purified by HPLC [Luna C_{18} (Phenomenex**,** 5µ, 250 × 4.6 mm)] with MeOH-H_2O (80%) as eluent.

Characteristic data

Compound 25: white amorphous solid; ^{1}H and ^{13}C NMR data in CD_3OD given in Table **12**; HR-ESIMS *m/z* 703.5130 $[M\text{-}Na]^-$.

Compound 26: white amorphous solid; ^{1}H and ^{13}C NMR data in CD_3OD given in Table **12**; HR-ESIMS *m/z* 701.4326 $[M\text{-}Na]^-$.

Compound 27: white amorphous solid; ^{1}H and ^{13}C NMR data in CD_3OD given in Table **13**; HR-ESIMS *m/z* 929.5682 $[M\text{-}H]^-$.

Spectroscopic Data of Compound 25 and 26

^{1}H NMR spectrum of Compound **25** in CD_3OD at 500 MHz.

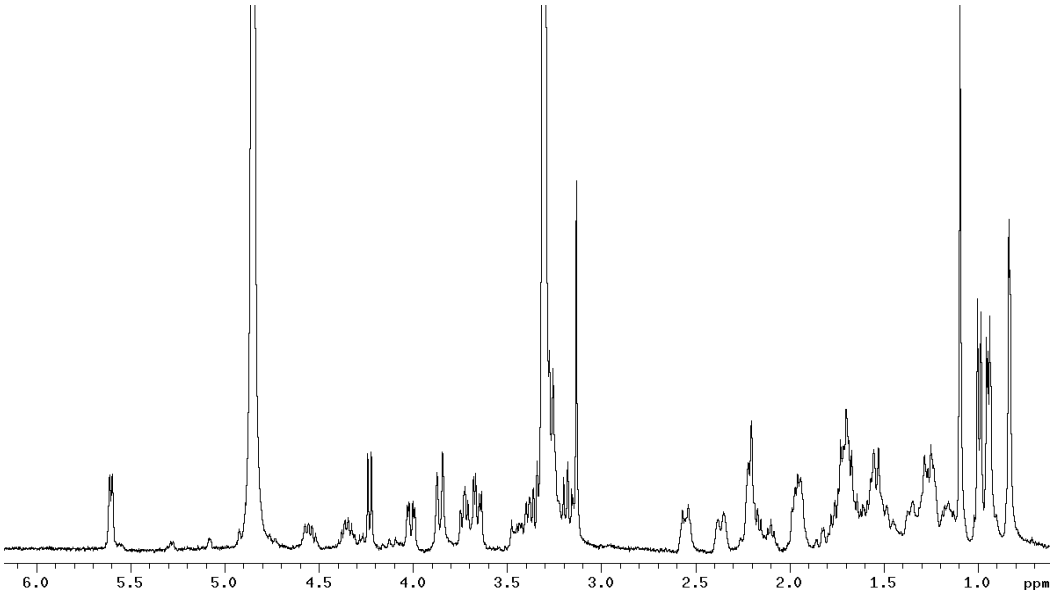

COSY spectrum of Compound **25** in CD_3OD at 500 MHz.

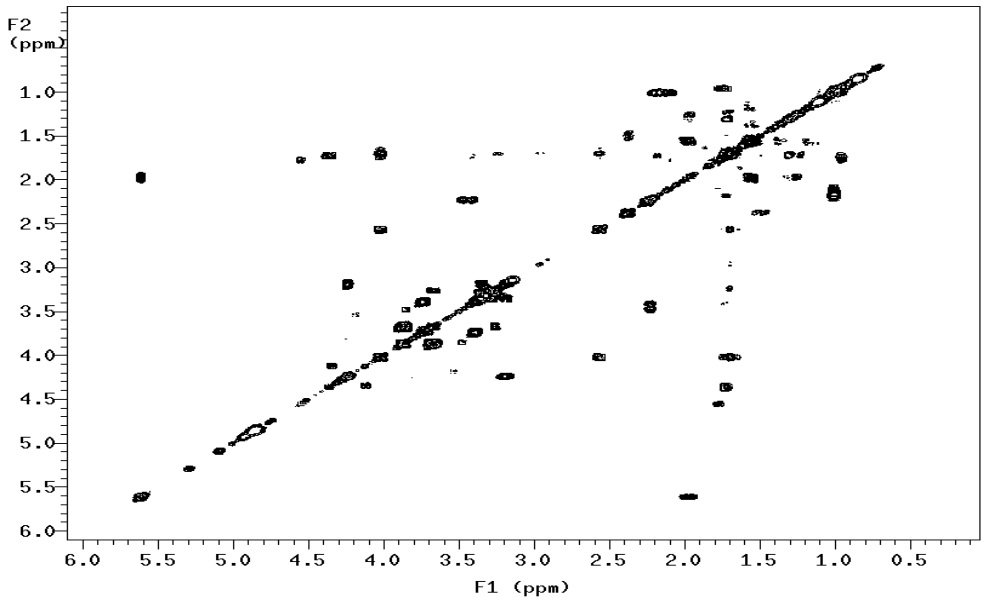

HSQC spectrum of Compound **25** in CD_3OD at 500 MHz.

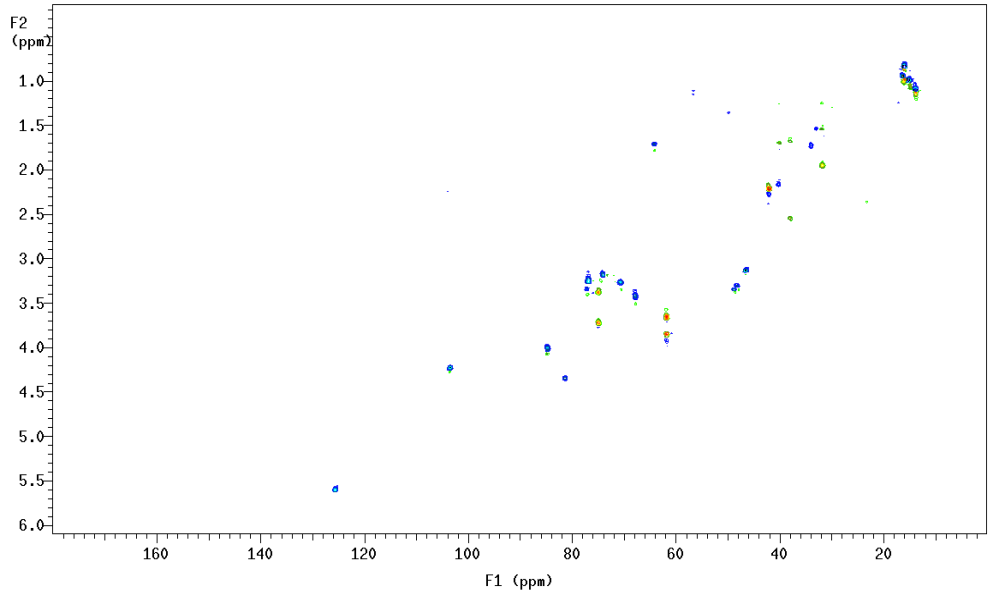

HMBC spectrum of Compound **25** in CD_3OD at 500 MHz.

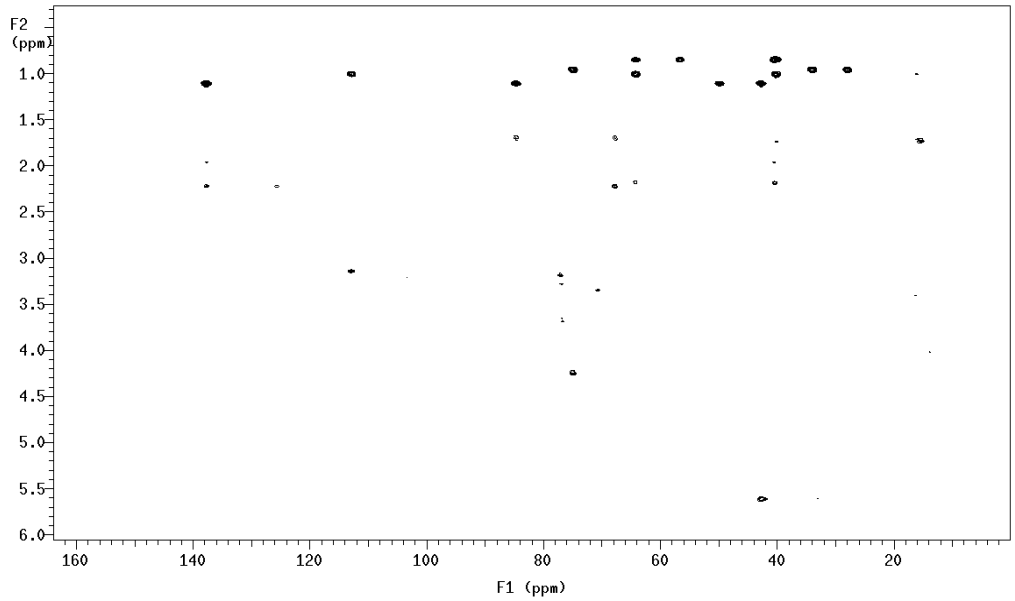

^1H NMR spectrum of Compound **26** in CD_3OD at 500 MHz.

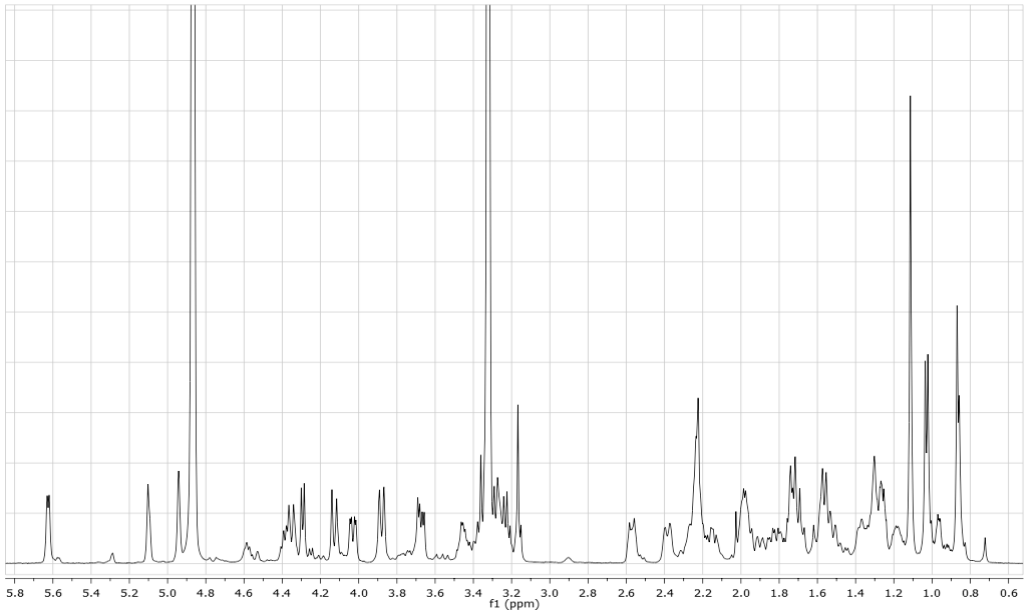

COSY spectrum of Compound **26** in CD_3OD at 500 MHz.

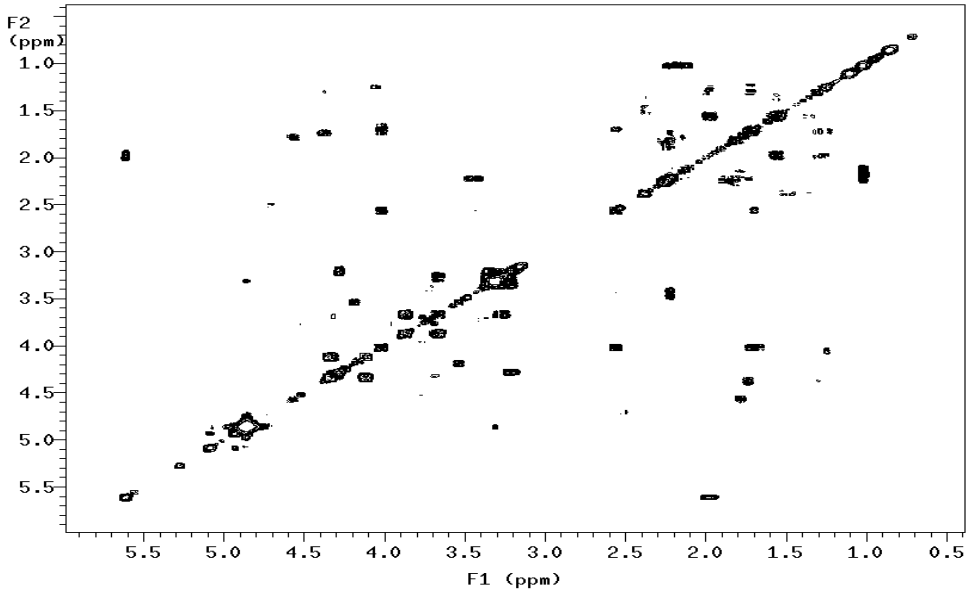

HSQC spectrum of Compound **26** in CD_3OD at 500 MHz.

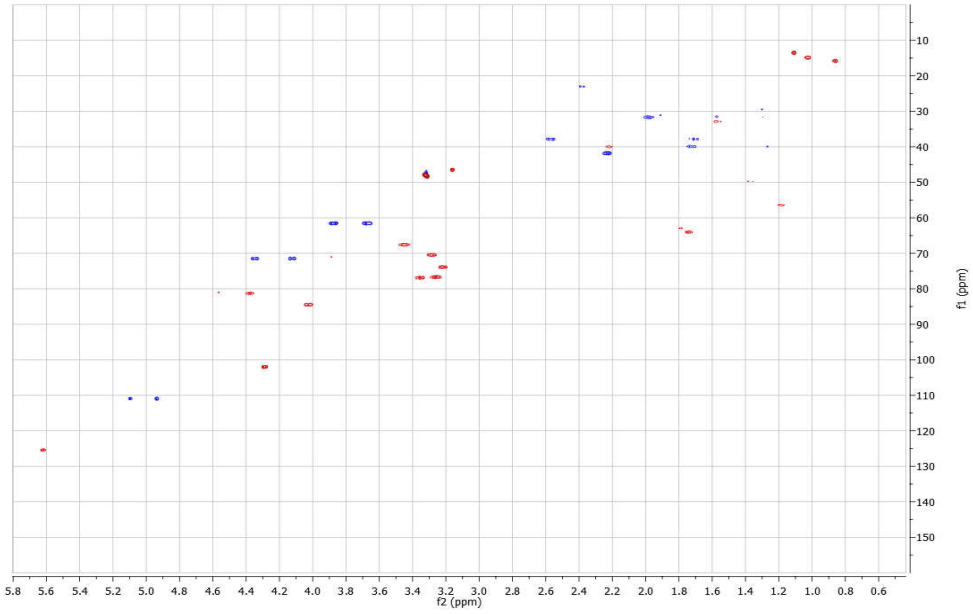

HMBC spectrum of Compound **26** in CD_3OD at 500 MHz.

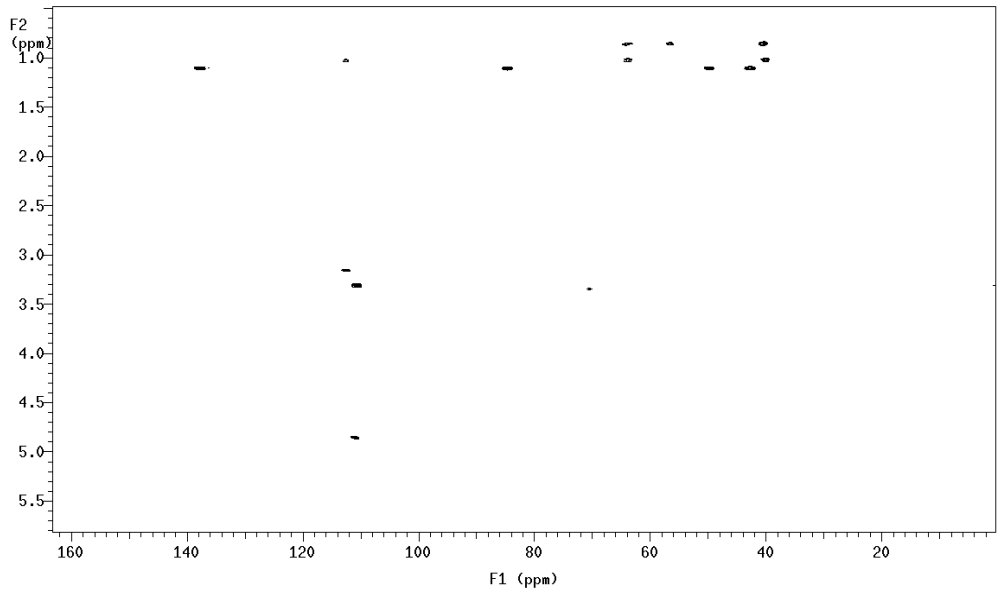

TOCSY spectrum of Compound **26** in CD_3OD at 500 MHz.

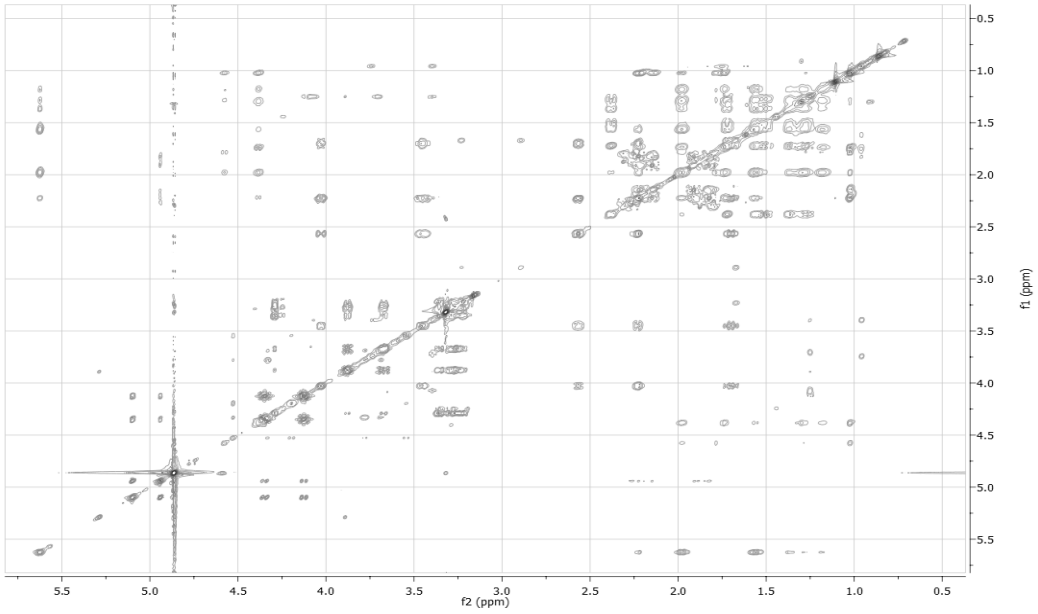

^{1}H NMR of Compound **27** in CD_3OD at 500 MHz.

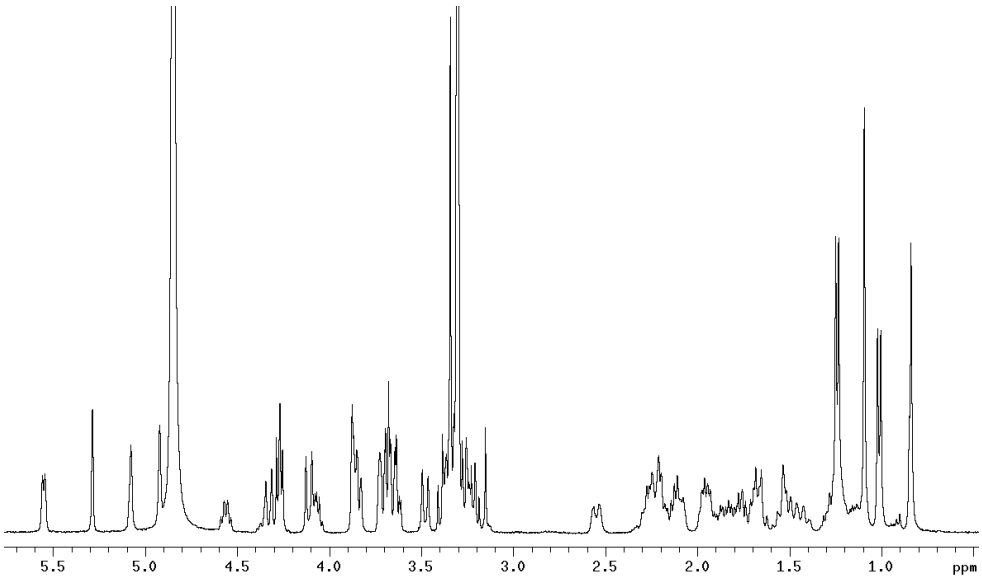

^{13}C NMR of Compound **27** in CD_3OD at 500 MHz.

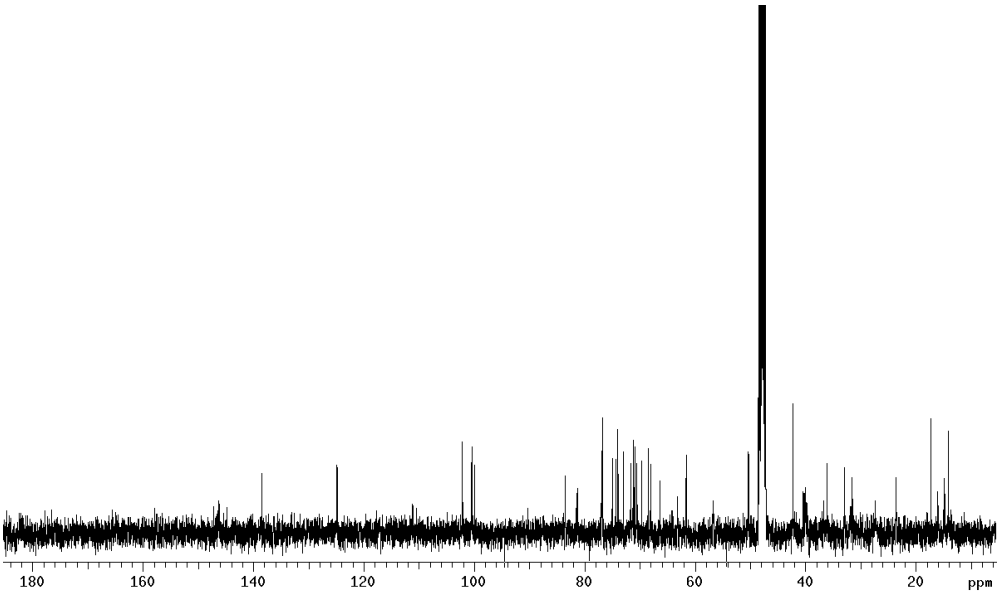

COSY of Compound **27** in CD_3OD at 500 MHz.

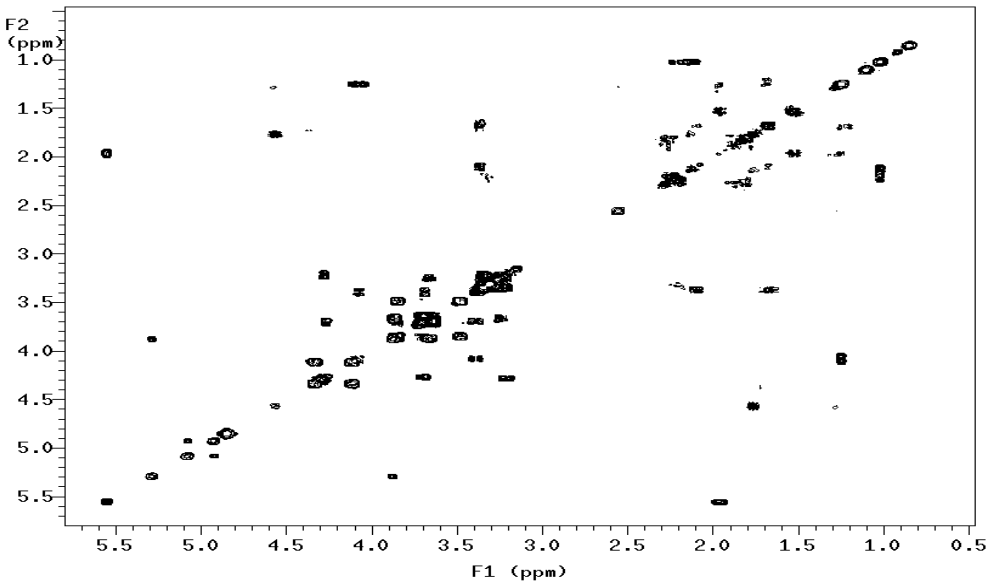

HSQC of Compound **27** in CD_3OD at 500 MHz.

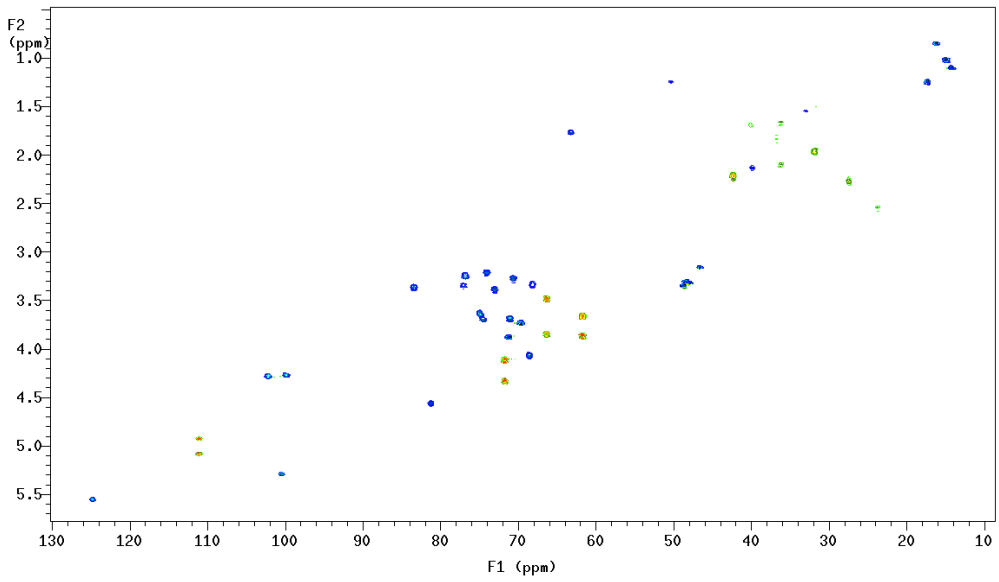

HSQC-TOCSY of Compound **27** in CD_3OD at 500 MHz.

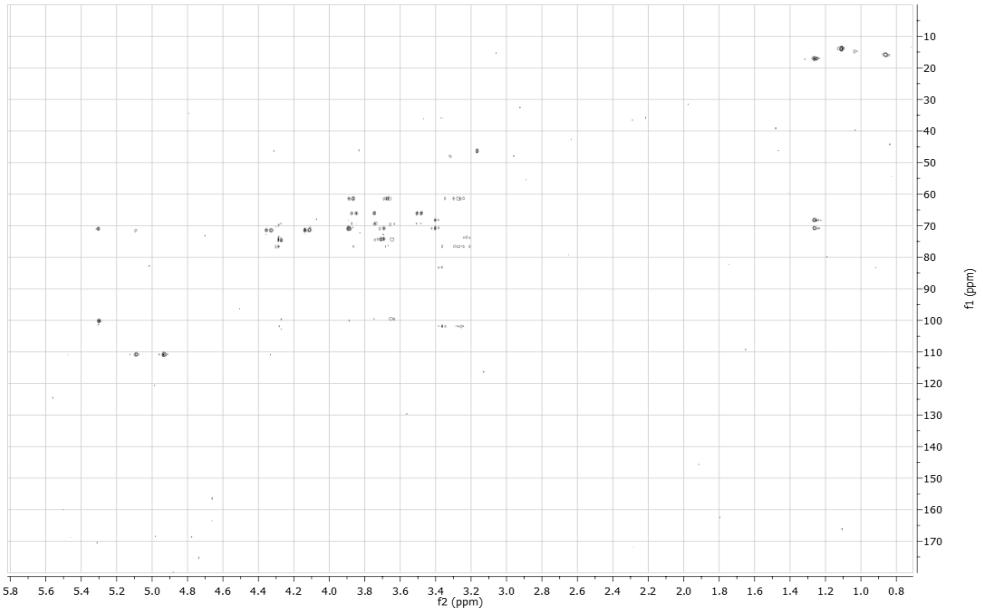

HMBC of Compound **27** in CD_3OD at 500 MHz.

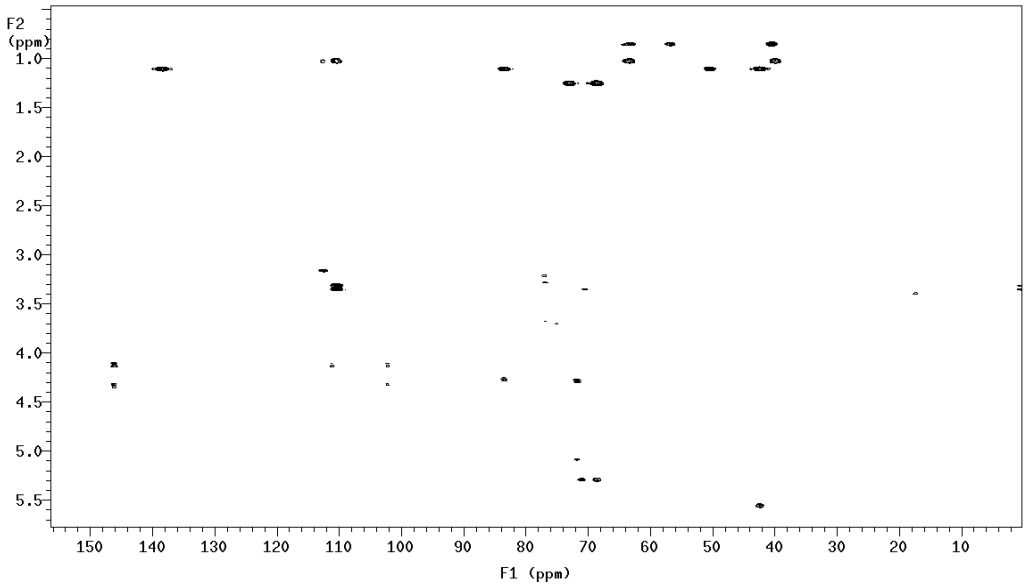

TOCSY of Compound **27** in CD_3OD at 500 MHz.

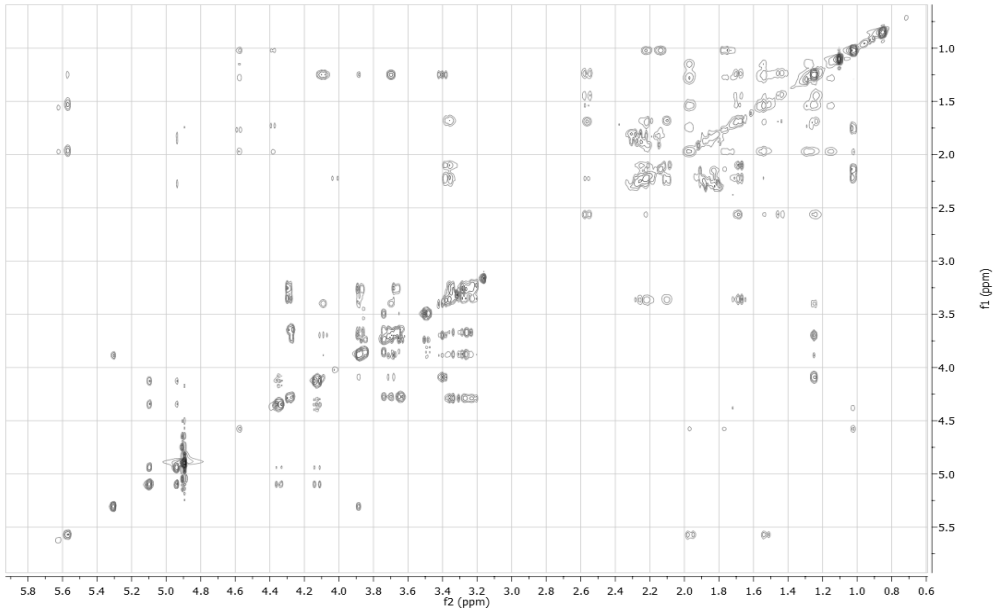

ROESY of Compound **27** in CD_3OD at 500 MHz.

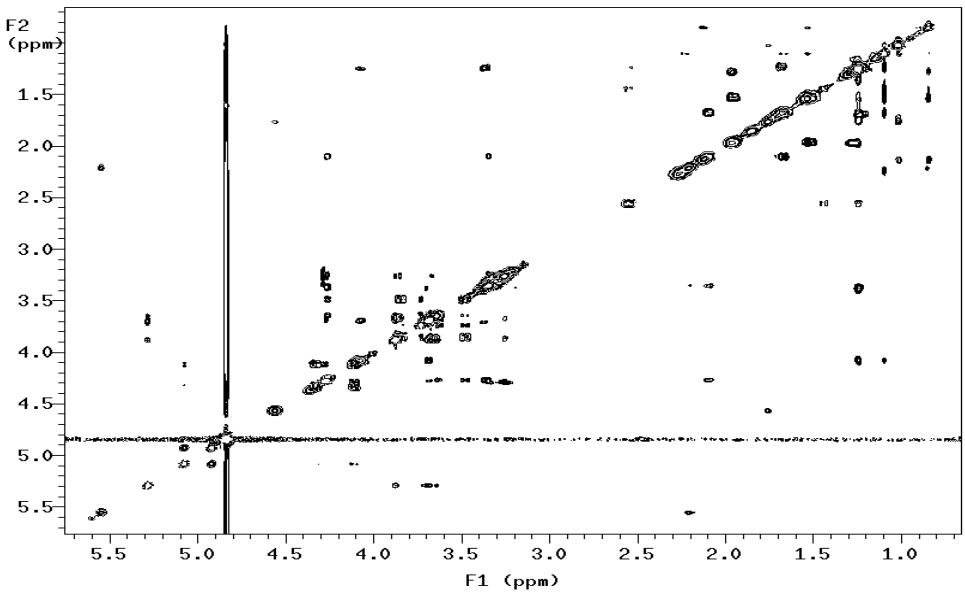

References

1) Cragg, G.M.; Grothaus, P.G.; Newman, D. J. *Chem. Rev.*, **2009**, *109*, 3012–3043.

2) Kupchan S. M., Britton R. W., Ziegler M. F., Sigel C. W. *J. Org. Chem*., **1973**, *38*, 178.

3) Hostettmann, K.; Hostettmann, M.; Marston**,** A. *Natural products report*, **1984**, 471-481.

4) Jamali, F.; Mehahvar, R.; Pautto, F.M. *J. Pharm. Sci*., **1989**, *78*, 685

5) Karplus, M. *J. Chem. Phys.*, **1959**, 11.

6) Derome, A.E. Modern NMR techniques for chemistry research; Pergamon Press: Oxford, **1987**, 98.

7) Neuhaus, D.; Williamson, M. The Nuclear Overhause Effect in structural and conformational analysis; VCH publisher, Inc.: New York Weinheim Cambridge, **1989.**

8) Matsumori, N.; Kaneno, D.; Murata, M.; Nakamura, H.; Tachibana, K. *J. Org.Chem*., **1999**, 64, 866.

9) Griesenger, C.; Sorensen, O. W.; Ernst, R. R. *J. Am. Chem. Soc*., **1985**, *107*, 6394.

10) Mueller, L. *J. Magn. Reson*., **1987**, *72*, 191.

11) Biamonti, C.; Rios, C. B.; Lyons, B. A.; Montelione, G. T. *Adv. Biophys. Chem*., **1994**, *4*, 51.

12) Kurz, M.; Schmieder, P.; Kessler, H. *Angew. Chem. Int. Ed. Engl.*, **1991**, *30*, 1329.

13) Wollborn, U.; Leibfritz, D. *J. Magn. Reson*., **1992**, *98*, 142.

14) Zhu, G.; Live, D.; Bax, A. *J. Am. Chem. Soc*., **1994**, *116*, 8370.

15) Zhu, G.; Bax, A. *J. Magn. Reson*., **1993**, Ser. A 104, 353.

16) Boyd, J.; Soffe, N.; John, B.; Plant, D.; Hurd, R. *J. Magn. Res*., **1992**, *98*, 660.

17) Davis, A. L.; Keeler, J.; Lane, E. D.; Moskau, D. *J. Magn. Reson*., **1992**, *98*, 207.

18) Bifulco, G.; Bassarello, C.; Riccio, R.; L. Gomez-Paloma. *Org. Lett*., **2004**, *6*, 1025-1028.

19) Hohenberg, P.; Kohn, W. *Phys. Rev*., **1964**, *136*, B864-B871.

20) Kohn, W.; Sham, L. *J. Phys. Rev*., **1965**, *140*, A1133-A1138.

21) Hohemberg, P.; Kohn, W. *Phys. Rev*., **1964**, *136*, B864-B861.

22) Kohn, W; Sham, L.J. *Phis. Rev*., **1965**, *140*, A1133-A1138.

23) Barone, G.; Gomez-Paloma, L.; Duca, D.; Silvestri, A.; Riccio, R.; Bifulco, G. *Chem. Eur. J*., **2002**, *64*, 3233-3239.

24) Barone, G.; Duca, D.; Silvestri, A.; Gomez-Paloma, L.; Riccio, R.; Bifulco, G. *Chem. Eur. J*., **2002**, *64*, 3240-3245.

25) Bassarello, C.; Cimino, P.; Gomez-Paloma, L.; Riccio, R.; Bifulco, G. *Tetrahedron*, **2003**, 59, 9555-9562.

26) Marfey, P. *Carlsberg Res. Commun*., **1984**, *49*, 591-596.

27) Fujii, K.; Harada, K. et al. *Anal. Chem*., **1997**, *69*, 3346-3352.

28) Bergquist, P.R., The Porifera, in *Invertebrate Zoology*, Anderson, D.T., Ed., Oxford University Press, Melbourne, **1998**, 2.

29) Bewley, C.A.; Holland, N.D.; Faulkner, D.J. *Experientia*, **1996**, *52*, 716-722.

30) Faulkner, D. *J. Nat. Prod. Rep*., **2000,** *17*, 1-6.

31) Kashman, Y.; Groweiss, A.; Shmueli, U. *Tetrahedron Lett.*, **1980**, *21*, 3629-3632.

32) D'Auria, M.V.; Gomez-Paloma, L.; Minale, L.; Zampella, A.; Verbist, J.F.; Roussakis, C.; Debitus, C. *Tetrahedron*, **1993**, *49*, 8645-8657.

33) D'Auria, M.V.; Gomez-Paloma, L.; Minale, L., Zampella, A.; Verbist, J.F.; Roussakis, C.; Debitus, C.; Patissou, J. *Tetrehedron*, **1994**, *50*, 4829-4834.

34) Carbonelli, S.; Zampella, A.; Randazzo, A.; Debitus, C.; Gomez-Paloma, L.; *Tetrahedron*, **1999**, *55*, 14665-14674.

35) Zhang, X.; Minale, L.; Zampella, A.; Smith, C.D.; *Cancer Research*, **1997,** *57*, 3751-3758.

36) Bassarello, C.; Bifulco, G.; Zampella, A.; D'Auria, M.V.; Riccio, R.; Gomez-Paloma, L.; *Eur. J. Org. Chem*., **2001**, *39*, 39-44.

37) Kitagawa , I.; Kobayashi, M.; Katori, T.; Yamashita, M.; Tanaka, J.; Doi, M.; Ishida, T.J. *Am Chem Soc*, **1990**, 112, 3710-3712.

38) Kobayashi, M.; Tsukamoto, S.;Tanabe, A.;Sakai, T.;Ishibashi, M.J.;, T.J. *Chem. Soc. Perkin trans.*, **1991**, 1, *112*, 2379-2389.

39) El Saye, K.A.; Yousaf, M.; Hamann, M.T.; Avery, M.A.; Kelly, M.; Wipf, P. *J. Nat. Prod.* **2002**, *65*, 1547–1553.

40) Kohmoto, S.; Mcconnell, O.J.; Wright, A.; Cross, S. *Chemistry Lett*., **1987**, *16*, 1687-1690

41) Garcia, M.O.; Rodriguez, A.D. *Tetrahedron*, **1990**, *46*, 4, 1119-1124

42) De Rosa, S.; De Stefano, S. *J. Org. Chem.*, **1988**, *53*, 5020-5023

43) Lederer, E. *Quart. Rev.* **1969**, *23*, 453.

44) Idler, D. R.; Wiseman, P. M.; Safe, L. M. *Steroids*, **1970**, *16*, 451.

45) Ferezon, J. P.; Devys, M.; Allois, J. P.; Barbier, M. *Phytochemistry*, **1974**, *13*, 593.

46) Fattorusso, E.; Magno, S.; Mayol, L.; Santacroce, C.; Sica, D. *Tetrahedron*, **1975**, 31, 1715–6.

47) Ker, .G.; Kerr, S.L.; Pettit, G.R.; Herald, D.L.; Groy, T.L.; Djerassi C. *J. Org. Chem.*, **1991**, *52*, 58–62.

48) Aiello, A.; Fattorusso, E.; Menna, M.; Carnuccio, R.; Iuvone, T. *Steroids*, **1995**, *60*, 666–73.

49) Carballera, N.; Thomson, J.E.; Ayanoglu, E.; Djerassi, C. *J. Org. Chem.*, **1986**, *51*, 2751–6.

50) Hahn, S.; Stoilov, I.L.; Raedersdorff, D.; Djerassi, C. *J. Am. Chem. Soc.*, **1988**, *110*, 8117–24.

51) Lam, W.K.; Hahn, S.; Ayanoglu,E.; Djerassi, C. *J. Org. Chem.*, **1989**, *54*, 3428–32.

52) Djerassi C, Lam WK. *Acc. Chem. Res*., **1991**, *24*, 69–75

53) Capon, R.J.; Faulkner, D.J. *J. Org. Chem.*, **1985**, *50*, 4771–3.

54) Burgoyne, D.L.; Andersen, R.J,; Allen, T.M. *J. Org. Chem.*, **1992**, *57*, 525–8.

55) Kerr, R.G.; Kerr, S.L.; Malik, S.; Djerassi, C. *J. Am. Chem. Soc.,* **1992**, *114*, 299 –303.

56) Giner, J.L. *Chem Rev,* **1993**, *93*, 1735–52

57) Fusetani, N.; Matsunaga, S.; Konosu, S. *Tetrahedron Lett.*, **1981**, *21*, 1985-8.

58) Perkel. *The Scientist*, **2003**, 17, 6.

59) Mootz et al. *Chembiochem*, **2002**, *3*, 490-504.

60) Von Dohren, Kaufer et al. *Chembiochem*, **2006**, *7*, 612-622

61) Matsunaga, S.; Fusetani, N.; Konosu, S. *Tetrahedron Lett*., **1984**, *25*, 5165-5168.

62) Zampella, A.; D'Auria, M. V.; Gomez-Paloma, L.; Casapullo, A.; Minale, L.; Debitus, C.; Henin, Y. *J. Am. Chem. Soc*., **1996**, *118*, 6202-6209.

63) Trevisi, L.; Bova, S.; Cargnelli, G.; Danieli. Betto, D.; Floreali, M.; Germinarlo, E.; D'Auria, M.V.; Luciani, S. *Biochem. Biophys. Res. Commun*., **2000**, *279*, 219-222.

64) Trevisi, L.; Cargnelli, G.; Ceolotto, G.; Papparella, I.; Semplicini, A.; Zampella, A.; D'Auria, M.V.; Luciani, S. *Biochemical Pharmacology*., **2004**, *68*, 1331-1338.

65) Kimura, J.; Ishizuka, E.; Nakao, Y.; Yoshida, W. Y.; Scheuer, P. J.; Kelly-Borges, M. *J. Nat. Prod.*, **1998**, *61*, 248-250.

66) Kimura, J.; Hyosu, M. *Chem. Lett*., **1999**, 61-62.

67) Fu, X.; Ferreira, M. L. G.; Schmitz, F. J.; Kelly, M. *J. Nat. Prod.*, **1999**, *62*, 1190-1191.

68) Capelle, N.; Braekman, J. C.; Daloze, D.; Tursch, B. *Bull. Soc. Chim. Belg.*, **1980**, *89*, 399-404.

69) Cimino, G.; Morrone, M.; Sodano, G. *Tetrahedron Lett*., **1982**, *23*, 4139-4142.

70) Li, C.-J.; Schmitz, F. J.; Kelly-Borges, M. *J. Nat. Prod.*, **1998**, *61*, 546-547.

71) Li, C.-J.; Schmitz, F. J.; Kelly-Borges, M. *J. Nat. Prod.*, **1999**, *62*, 287-290.

72) Kimura, J.; Ishizuka, E.; Nakao, Y.; Yoshida, W.; Y.; Scheuer, P. J.; Kelly-Borges, M. *J. Nat. Prod*., **1998**, *61*, 248-250.

73) Fu, X.; Ferreira, M. L. G.; Schmitz, F. J.; Kelly-Borges, M. *J. Nat. Prod*., **1999**, *62*, 1190-1191.

74) Carr, G.; Raszek, M.; Van Soest, R.; Matainaho, T.; Shopik, M. L.; Holmes, C. F. B.; Andersen, R. J. *J. Nat. Prod*., **2007**, *70*, 1812-1815.

75) Shin, D.-S.; Lee, T.-H.; Lee, H.-S.; Shin, J.; Oh, K.-B. *FEMS Microbiol. Lett*., **2007**, *272*, 43-47;

76) Lee, H.-S.; Lee, T.-H.; Yang, S. H.; Shin, H. J.; Shin, J.; Oh, K.-B. *Bioorg. Med. Chem. Lett.*, **2007**, *17*, 2483-2486.

77) Loukaci, A.; Le Saout, I.; Samadi, M.; Leclerc, S.; Damiens, E.; Meijer, L.; Debitus, C.; Guyot, M. *Bioorg. Med. Chem.*, **2001**, *9*, 3049-3054.

78) Manes, L. V.; Naylor, S.; Crews, P.; Bakus, G. J. *J. Org. Chem*., **1985**, *50*, 284-286;

79) Manes, L. V.; Crews, P.; Kernan, M. R.; Faulkner, D. J.; Fronczek, F. R.; Gandour, R. D. *J. Org. Chem*., **1988**, *53*, 570-575.

80) Nicholas, G. M.; Eckman, L. L.; Newton, G. L.; Fahey, R. C.; Ray, S.; Bewley, C. A *Bioorg. & Med. Chem*., **2003**, *11*, 601-608.

81) De Marino, S.; Festa, C.; D'Auria, M.V.; Bourguet-Kondracki, M.L.; Petek, S.; Debitus, C.; Andres, R.M.; Terencio, M.C.; Paya, M.; Zampella, A. *Tetrahedron*, 2009, 65, 2905-2909.

82) H. Khan, A. Zaman, G.L. Chetty, A.S. Gupta and S. Dev, *Tetrahedron Lett.*, **1971**, 12, 4443–4446.

83) Kobayashi, J.; Sekiguchi, M.; Shigemori, H.; Ohsaki, A. *Tetrahedron Lett*., **2000**, *41*, 2939-2943.

84) Kobayashi, J.; Sekiguchi, M.; Shimamoto, S.; Shigemori, H.; Ohsaki, A. *J. Nat. Prod*., **2000**, *63,* 1576-1579.

85) Mori, D.; Kimura, Y.; Kitamura, S.; Sakagami, Y.; Yoshioka, Y.; Shintani, T.; Okamoto, T.; Ojika, M. *J. Org. Chem*., **2007**, *72*, 7190-719

86) Schevitz, R. W.; Bach, N. J.; Carlson, D. G.; Chirgadze, N. Y.; Clawson, D. K.; Dillard, R. D.; Draheim, S. E.; Hartley, L. W.; Jones, N. D.; Mihelich, E. D.; Olkowski, J. L.; Snyder, D. W.; Sommers, C.; Wery, J. P. *Nat. Struct. Biol*., **1995**, *2*, 458-432.

87) Wegerski, C. J.; Hammond, J.; Tenney, K.; Matainaho, C.; Crews, P. *J. Nat. Prod*., **2007**, *70*, 89-94.

88) Ratnayake, A. S.; Davis, R.A.; Harper, M.K.; Veltri, C. A.; Andjelic, C.D.; Barrows, L.R.; Ireland, C.M. *J. Nat. Prod*., **2005**, *68*, 104-107.

89) Kho, E.; Imagawa, D.K.; Rohmer, M.; Kashman, Y.; Djerassi, C. *J. Org. Chem*., **1981**, *46*, 1836-1839.

90) Hamada, T.; Sugawara, T.; Matsunaga, S.; Fusetani, N. *Tetrahedron Let*., **1994**, *35*, 609-612.

91) Hamada, T.; Matsunaga, S.; Yano, G.; Fusetani, N. *J. Am. Chem. Soc*., **2005**, *127*, 110–118.

92) Fusetani, N.;Warabi, K.; Nogata, Y.; Nakao, Y.; Matsunaga, S.; Van Soest, R. R. M. *Tetrahedron Lett*., **1999**, *40*, 4687–4690.

93) Araki, T.;Matsunaga, S.; Fusetani,N. *Biosci. Biotechnol. Biochem*., **2005**, *69*, 1318–1322.

94) Fusetani, N.; Matsunaga, S.; Matsumoto, H.; Takebayashi, Y. *J. Am. Chem. Soc.*, **1990**, *112*, 7053–7054.

95) Nakao, Y.; Matsunaga, S.; Fusetani, N. *Bioorg. Med. Chem*., **1995**, *3*, 1115–1122.

96) Nakao, Y.; Oku, N.; Matsunaga, S.; Fusetani, N. *J. Nat. Prod*., **1998**, *61*, 667–670.

97) Kobayashi, J.; Sato, M.; Murayama, T.; Ishibashi, M.; Walchi, M. R.; Kanai, M.; Shoji, J.; Ohizumi, Y. *J. Chem. Soc. Chem. Commun*., **1991**, 1050–1052.

98) Fusetani, N.; Sugawara, T.; Matsunaga, S.; Hirota, H. *J. Am. Chem. Soc*., **1991**, *113*, 7811–7812.

99) Roy, M. C.; Ohtani, I. I.; Tanaka, J.; Higa, T.; Satari, R. *Tetrahedron Lett.*, **1999**, *40*, 5373–5376.

100) Kobayashi, J.; Sato, M.; Ishibashi, M.; Shigemori, H.; Nakamura, T.; Ohizumi, Y. *J. Chem. Soc. Perkin Trans*., **1991**, 1, 2609–2611.

101) Itagaki, F.; Shigemori, H.; Ishibashi, M.; Nakamura, T.; Sasaki, T.; Kobayashi, J. *J. Org. Chem*., **1992**, *57*, 5540–5542.

102) Kobayashi, J.; Itagaki, F.; Shigemori, H.; Takao, T.; Shimonishi, Y. *Tetrahedron*, **1995**, *51*, 2525–2532.

103) Uemoto, H.; Yahiro, Y.; Shigemori, H.; Tsuda, M.; Takao, T.; Shimonishi, Y.; Kobayashi, J. *Tetrahedron*, **1998**, *54*, 6719–6724.

104) Tsuda, M.; Ishiyama, H.; Masuko, K.; Takao, T.; Shimonishi, Y.; Kobayashi, J. *Tetrahedron*, **1999**, *55*, 12543–12548.

105) Bonnington, L. S.; Tanaka, J.; Higa, T.; Kimura, J.; Yoshimura, Y.; Nakao, Y.; Yoshida, W. Y.; Scheuer, P. J. *J. Org. Chem.*, **1997**, *62*, 7765–7767.

106) Chill, L.; Kashman, Y.; Schleyer, M. *Tetrahedron*, **1997**, *53*, 16147–16152.

107) Matsunaga, S.; Fusetani, N.; Hashimoto, K.; Walchli, M. *J. Am. Chem. Soc*., **1989**, *111*, 2582–2588.

108) Kobayashi, M.; Kanzaki, K.; Katayama, S.; Ohashi, K.; Okada, H.; Ikegami, S.; Kitagawa, I. *Chem. Pharm. Bull*., **1994**, *42*, 1410–1415.

109) Kitagawa, I.; Kobayashi, M.; Lee, N. K.; Shibuya, H.; Kawata, Y.; Sakiyama, F. *Chem. Pharm. Bull.,* **1986**, *34*, 2664–2667.

110) Clark, D. P.; Carroll, J.; Naylor, S.; Crews, P. *J. Org. Chem*., **1998**, *63*, 8757–8764.

111) Araki, T.; Matsunaga, S.; Nakao, Y.; Furihata, K.; West, L.; Faulkner, D. J.; Fusetani, N. *J. Org. Chem*., **2008**, *73*, 7889–7894.

112) Ford, P. W.; Gustafson, K. R.; McKee, T. C.; Shigematsu, N.; Maurizi, L. K.; Pannell, L. K.; Williams, D. E.; Dilip de Silva, E.; Lassota, P.; Allen, T. M.; Van Soest, Rob; Andersen, R. J.; Boyd, M. R. *J. Am. Chem. Soc*., **1999**, *121*, 5899–5909.

113) Okada, Y.; Matsunaga, S.; van Soest, R. W. M.; Fusetani, N. *Org. Lett*., **2002**, *4*, 3039–3042.

114) Ratnayake, A. S.; Bugni, T. S.; Feng, X.; Harper, M. K.; Skalicky, J. J.; Mohammed, K. A.; Andjelic, C. D.; Barrows, L. R.; Ireland, C. M. *J. Nat. Prod*., **2006**, *69*, 1582–1586.

115) Bewley, C. A.; Faulkner, D. J. *J. Org. Chem*., **1994**, *59*, 4849–4852.

116) Schmidt, E. W.; Bewley, C. A.; Faulkner, D. J. *J. Org. Chem*., **1998**, *63*, 1254–1258.

117) Bewley, C.A.; Faulkner, D.J. *Angew. Chem. Int. Ed*., **1998**, *37*, 2162-2178.

118) Andrianasolo, E. H.; Gross, H.; Goeger, D.; Musafija-Girt, M.; McPhail, K.; Leal, R. M.; Mooberry, S. L.; Gerwick, W. H. *Org. Lett*., **2005**, *7*, 1375-1378.

119) Piel, J.; Butzke, D.; Fusetani, N.; Hui, D.; Platzer, M.; Wen, G.; Matsunaga, S. *J. .Nat. Prod*., **2005**, *68*, 472-479.

120) Fusetani, N.; Sugawara, T.; Matsunaga, S. *J. Am. Chem. Soc*., **1991**, *113*, 7811-7812.

121) Tsukamato, S.; Matsunaga, S.;Fusetani, N.; Toh-E, A. *Tetrahedron*, **1999**, *55*, 13697-13702.

122) Gabant, M.; Schmitz-Afonso, I.; Gallard, J.-F.; Menou, J.-L.; Laurent, D.; Debitus, C.; Al-Mourabit, A. *J. Nat. Prod*., **2009**, *72*, 760-763.

123) Di Girolamo, J. A.; Li, Xing-Cong; J., Melissa R.; Clark, A. M.; Ferreira, D. *J. Nat. Prod*., **2009**, *72*, 1524-1528.

124) Guzii, A. G.; Makarieva, T. N.; Denisenko, V. A.; Dmitrenok, P. S.; Burtseva, Y. V.; Krasokhin, V. B.; Stonik, V. A. *Tetrahedron Lett*., **2008**, *49*, 7191-7193.

125) Boonlarppradab, C.; Faulkner, D. J. *J. Nat.Prod*., **2007**, *70*, 846-848.

126) Koehn, F.E.; Gunasekera, M.; Cross, S.S. *J. Org. Chem*., **1991**, *56*, 1322-1325.

127) Sun, H.H.; Cross, S.S.; Gunasekera, M.; Koehn, F.E. *Tetrahedron*, **1991**, *47*, 1185- 1190.

128) Yang, S.W.; Chan, T.M.; Pomponi, S.A.; Chen, G.; Loebenberg, D.; Wright, A.; Patel, M.; Gullo, V.; Pramanik, B.; Chu, M. *J. Antib*., **2003**, *56*, 186-189.

129) Nakatsu, T.; Walker, R. P.; Thompson, J. E.; Faulkner, D. J. *Experientia*, **1983**, *39*, 759-761.

130) Gunasekera, S. P.; Sennett, S. H.; Kelly-Borges, M.; Bryant, R. W. *J. Nat.Prod*., **1994**, *57*, 1751-1754.

131) Fujita, M.; Nakao, Y.; Matsunaga, S.; Seiki, M.; Itoh, Y.; van Soest, R. W. M.; Heubes, M.; Faulkner, D. J.; Fusetani, N. *Tetrahedron*, **2001**, *57*, 3885-3890.

132) Aoki, S.; Naka, Y.; Itoh, T.; Furukawa, T.; Rachmat, R.; Akiyama, S.-i.; Kobayashi, M. *Chem. Pharm. Bull*., **2002**, *50*, 827-830.

133) Yang, S.-W.; Buivich, A.; Chan, T.-M.; Smith, M.; Lachowicz, J.; Pomponi, S. A.; Wright, A. E.; Mierzwa, R.; Patel, M.; Gullo, V.; Chu, M. *Bioorg. Med. Chem. Lett*., **2003**, *13*, 1791-1794.

134) Whitson, E. L.; Bugni, T. S.; Chockalingam, P. S.; Concepcion, G. P.; Harper, M. K.; He, M.; Hooper, J. N. A.; Mangalindan, G. C.; Ritacco, F.; Ireland, C. M. *J. Nat. Prod*., **2008**, *71*, 1213-1217.

135) D'Auria, M. V.; Riccio, R.; Minale, L.; La Barre, S.; Pusset J. *J. Org. Chem*., **1987**, *52*, 3947-3952.

136) Gutíerrez, M.; Capson, T. L.; Guzmán, H. M.; Gonzalez, J.; Ortega-Barría, E.; Quiñoá, E.; Riguera, R. *J. Nat. Prod*., **2006**, *69*, 1379–1383.

137) Ciavatta, M. L.; Lopez G., M. P.; Manzo, E.; Gavagnin, M.; Wahidulla, S.; Cimino, G. *Tetrahedron Lett*., **2004**, **45**, 7745-7748.

138) Lorenzo, M.; Cueto, M.; D'Croz, L.; Mate, J. L.; San-Martin, A.; Darias, J. *Eur. J. Org. Chem*., **2006**, 582-585.

139) Yan, X.-H.; Liu, H.-L.; Guo, Y.-W. *Steroids*, **2009**, *74*, 1061-1065.

140) Makarieva, T. N.; Stonik, V. A.; Dmitrenok, A. S.; Krosokhin, V. B.; Svetashev, Vassilii I.; Vysotskii, M. V. *Steroids*, **1995**, *60*, 316-320.

141) Ballantine, J. A.; Williams, K.; Burke, B. *Tetrahedron Lett*., **1977**, 1547-1550.

142) Guella, G.; Pietra, F. *Hel*v. *Chim. Acta*, **1988**, *71*, 62–71.

143) Corgiat, J. M.; Scheuer, P. J.; Steiner, J. L. Rios; Clardy, J. *Tetrahedron*, **1993**, *49*, 1557-1562

144) Fattorusso, E.; Taglialatela-Scafati, O.; Petrucci, F.; Bavestrello, G.; Calcinai, B.; Cerrano, C.; Di Meglio, P.; Ianaro, *Org. Lett*., **2004**, *6*, 1633-1635.

145) Wang, G.-Y.-S.; Crews, P. *Tetrahedron Lett*., **1996**, *37*, 8145-8146.

146) Li1, H., Shinde, P. B.; Lee, H. J.; Yoo, E. S.; Lee, C.-O.; Hong, J.; Choi, S. H.; Jung, J. H. *Arch. Pharm. Res*., **2009***, 32 (6),* 857-862.

147) Mandeau, A.; Debitus, C.; Aries, M.-F.; David, B. *Steroids*, **2005**, *70*, 873-878.

148) Youssef, D. T.; Ibrahim, A. K.; Khalifa S. I.; Mesbah, M. K.; Mayer A. M.; van Soest R. W. *Nat. Prod. Commun*., **2010**, *5,* 27-31.

149) Rock K. L.; Latz E.; Ontiveros F.; Kono H. *Annu. Rev. Immunol*., **2010**, *28*, 321-342.

150) Ma, X.; Shah, Y. M.; Guo, G. L.; Wang, T.; Krausz, K. W.; Idle, J. R.; Gonzalez, F. J. *J. Pharmacol. Exp. Ther*., **2007**, *322*, 391-398.

151) Fiorucci, S.; Cipriani, S.; Baldelli, F.; Mencarelli, A. *Prog. Lipid Res*., **2010**, *49*, 171-185.

152) Mencarelli, A.;, Migliorati, M.; Barbanti, M.;, Cipriani, S.; Palladino, G.; Distrutti, E.; Renga, B.; Fiorucci, S. *Biochem. Pharmacol*. Epub ahead of print **2010** Sep.8.

153) Shah, Y. M.; Ma, X.; Morimura, K.; Kim, I.; Gonzalez, F. J. *Am. J. Physiol. Gastrointest. Liver Physiol*., **2007**, *292*, 1114-1122.

154) Trott, O.; Olson, A. J. *J. Comput. Chem*., **2010**, *31*, 455-461.

155) Ekins, S.; Kortagere, S.; Iyer, M.; Reschly, E. J.; Lill, M. A.; Redinbo, M. R.; Krasowski, M. D. *PLoS Comput. Biol*., **2009**, *5*, e1000594.

156) Gulavita, N. K.; Pomponi, S. A.; Wright, A. E.; Yarwood, D.; Sills, M. A. *Tetrahedron Lett*., **1994**, *35*, 6815-18.

157) Festa, C.; De Marino, S.; Sepe, V.; Monti, M.C.; Luciano, P.; D'Auria, M.V.; Debitus, C.; Bucci, M.; Vellecco, V.; Zampella, A. *Tetrahedron*, 2009, 65, 10424-10429.

158) Karam, L.R.; Simic, M.G. *J. Biol. Chem*., **1990**, *265*, 11581.

159) Ming, D.; Wie, W.; Nuran, E.; Yinfa, M. *J. Chrom*., **2004**, *803*, 321-329.

160) Bui, H. T. N.; Jansen, R.; Pham, H. T. L.; Mundt, S. *J. Nat. Prod*., **2007**, *70*, 499.

161) Zampella, A.; Sepe, V.; Luciano, P.; Bellotta, F.; Monti, M.C.; D'Auria, M.V., Jepsen, T.; Petek, S.; Adeline, M.T.; Laprèvote,O.; Aubertin, A.M.; Debitus, C. *J. Org. Chem*., **2008**, *73*, 5319–5327

162) Murphy, A. C.; Mitova, M. I; Blunt, J. W. ; Munro M. H. G. *J. Nat. Prod*., **2008,** *71,* 806–809.

163) Easton, C. J.; Hutton, C. A.; Roselt, P. D.; Tiekink, E. R. T. *Tetrahedron*, **1994**, *50*,7327–7330.

164) Sepe, V.; D'Auria, M.V.; Bifulco, G.; Ummarino; R., Zampella, A. *Tetrahedron*, **2010**, *66*, 7520-7526

165) Posadas, I.; Bucci, M.; Roviezzo, F.; Rossi, A.; Parente, L.; Sautebin, L.; Cirino, G.Br. *J. Pharmacol*., **2004**, *142*, 331–338.

166) Renner, M. K.; Shen, Y. C.; Cheng, X. C.; Jensen, P. R.; Frankmoelle, W.; Kauffman, C. A.; Fenical, W.; Lobkovsky, E.; Clardy, J. *J. Am. Chem. Soc*., **1999**, *121*, 11273- 11276.

167) Trischman, J. A.; Tapiolas, D. M.; Jensen, P. R.; Dwight, R.; Fenical, W.; McKee, T. C.; Ireland, C. M.; Stout, T. J.; Clardy, J. *J. Am. Chem. Soc*., **1994**, *116*, 757-758

168) Moore, B. S.; Trischman, J. A.; Seng, D.; Kho, D.; Jensen, P. R.; Fenical, W. *J. Org. Chem*., **1999**, *64*, 1145-1150.

169) Randazzo, A.; Bifulco, G.; Giannini, C.; Bucci, M.; Debitus, C.; Cirino, G.; Gomez-Paloma, L. *J. Am. Chem. Soc*., **2001**, *123*, 10870-10876.

170) Blodig, W.; Doyle, W. A.; Smith, A. T. Winterhalter, K.; Choinowski, T.; Piontek. K..*Biochemistry*, **1998,** *37*, 8832-8838.

171) Wang, Y., Wyllie, S.G., Leach, D.N. Chemical changes during the development and ripening of the fruit of Cucumis melo (Cv. Makdimon). *J. Agric. Food Chem*., **1996,** 44, 210–216.

172) Hernandez-Gomez, L.F.; Ubeda-Iranzo, J.; Garcia-Romero, E.; Briones-Pérez, A. *Food Chem*., **2005**, *90*, 115-125.

173) Villanueva, M.J.; Tenorio, M.D.; Esteban, M.A.; Mendoza, M.C. *Food Chem*., **2004**, *87*, 179-185.

174) Duke, J.A. and Ayensu, E.S. *Medicinal Plants of China,* **1985** ISBN 0-9177256-20-4.

175) Teotia, M.S. and Ramakrishna, P. *J. Food. Sci. Technol*., **1984**, *21*, 332-337.

176) Lal, S.D. and Lata, K. *Econ. Bot*., **1980**, *34*, 273-275.

177) Abdalbasit, M.; Bertrand, M. *Journal of Food Lipids*, **2008**, *15*, 56-67.

178) Yanty, N.A.M.; Lai, O.M.; Osman, A.; Long, K.; Ghazali, H.M. *J. of Food Lipids*, **2008**, *15*, 42-55.

179) De Marino, S.; Festa, C.; Zollo, F.; Iorizzi, M. *Phytochemistry Letters*, 2009, 2, 130-133.

180) Lei, Y.; Wu, Li-J.; Shi, H.M.; Tu, P.F. *Helv. Chem. Acta*, **2008**, *91*, 495-500.

181) Ishii, T.; Yanagisawa, M. *Carbohydr. Res*., **1998**, *313*, 189-192.

182) Nakano, K.; Nishizawa, K.; Takemoto, I.; Murakami, K.; Takaishi, Y.;Tomomatsu, T. *Phytochemistry*, **1989**, *28*, 301-303.

183) Williams, P.J.; Strauss, C.R.; Wilson, B.; Massy-Westropp, R.A. *Phytochemistry*, **1983**, *22*, 2039-2041.

184) Wu, T.; Cheng, X-M.; Bligh, A.S.W.; Chou, G-X.; Wang, Z-T.; Bashall, A.; Brandford-White, C. *Helv. Chem. Acta*, **2005**, *88*, 2617-2623.

185) Appendino, G.; Jakupovic, J.; Belloro, E.; Marchesini, A. *Phytochemistry*, **1999**, *51*, 1021-1026.

186) Appendino, G.; Jakupovic, J.; Belloro, E.; Marchesini, A. *Fitoterapia*, **2000**, *71*, 258-263

187) Syed Rahmatullah, M.S.K.; Shukla, V.K.S.; Mukherjee, K.D. *JAOCS,* **1994**, *71*, 6, 563-567.

188) Horrobin, D.F. The Regulation of prostaglandin biosynthesis by the manipulation of essential fatty acid metabolism., *Rev. Pure Appl. Pharmacol*., **1983**, *4*, 339,383.

189) Herrmann, M.; Joppe, H.; Schmaus, G. *Phytochemistry*, **2002**, 60, 399-402.

190) Dodson, C.D. *J. Nat. Prod*., **1986**, *49*, 727.

191) Larson, K.M.; Roby, M.R.; Stermitz, F.R. *J. Nat. Prod*., **1984,** *47*, 4, 747-745.

192) Gerard, J., The Hystory of Plants, 1597, edited by Marcus Woodward, 1927, and published by Senate, Studio Editions Ltd. London, **1994**, 185-186

193) Hara S, Okabe H, Mihashi K. *Chem. Pharm. Bull*., **1987**; *35*, 501-506.

194) Bognar, R.; Somogyl, L.; Gyorgydeak, Z.; *Liebigs Ann. Chem*. **1970**, 738, 68–78.

195) Struijs, K.; Vincken, J.P., Verhoef, R. et al. *Phytochemistry*, **2007**, *68*, 1227-1235.

196) Kamel-Eldin, A.; Peerlkamp, N.; Johnsson, P.; Andersson, R; Andersson, R.E.; Lundgren, L.N.; Aman, P. *Phytochemistry*, **2001**, *58*, 587-590.

197) Berg, D. *Fortschr. Medizin*, **1990**, *108*, 473-476.

198) Bouskela, E.; Cyrino, F. Z.; Marcelon, G. *J. Cardio*V*asc. Pharmacol*., **1994**, *24*, 281-285.

199) Facino, R. M.; Carini, M.; Stefani, R.; Aldini, G.; Saibene, L. *Arch. Pharm*., 1**995**, *328*, 720-724.

200) Capra, C. *Fitoterapia*, **1972**, *43*, 99-113.

201) Cluzan, R. V.; Alliot, F.; Ghabboun, S.; Pacot, M. *Lymphology*, **1996**, *29*, 29-35.

202) Tarayre, J. P.; Lauressergues, H. *Ann. Pharm. Fr*., **1979**, *37*, 191-198.

203) Balandrin, M.F.; Waller, G.R.; Yamasaki, K.; Eds.; Plenum Press: New York, **1996**, 1-4.

204) Lacalle-Dubois, M.A.; Wagner, H. Elsevier Science: Amsterdam, The Netherlands, **2000**, Vol.21, 633-687.

205) Bouskela, E.; Cyrino , F.; Marcelon, G. *J. Cardiovasc. Pharmacol*., 1**993**, *22*, 225.

206) Bouskela, E.; Cyrino, F.; Marcelon, G. *J. Cardiovasc. Pharmacol*., **1993**, *22*, 221.

207) Bouskela, E.; Cyrino, F.; Bougaret S. *Clin. Hemorheol. Microcirc*., **1997**, *17*, 351.

208) Facino, R.M.; Carini, M.; Stefani, R.; Aldini, G.; Saibene, L. *Arch Pharm* (Weinheim Ger.), **1995**, 328, 720.

209) Mimaki, Y.; Kuroda, M.; Kameyama, A.; Yokosuka, A.; Sashida, Y. *J. Nat. Prod.,* **1998**, 61, 1279.

210) Mimaki, Y.; Kuroda, M.; Yokosuka, A.; Sasahida, Y. *Chem. Pharm. Bull*., **1998**, *46*, 879.

211) Mimaki, Y.; Kuroda, M.; Yokosuka, A.; Sashida, Y. *Phytochemistry*, **1999**, *51*, 689

212) Agrawal, P.K. *Phytochemistry*, **1992**, *31*, 3307-3330.

213) Corea, G.; Fattorusso, E., Lanzotti, V. *J. Nat. Prod.*, **2003**, *66*, 1405-1411.

214) Pretsch, E.; Buhlmann, P.; Affolter, C. Spinger Verlag: Berlin, Germany, **2000**, 203-237.

215) Corea, G.; Fattorusso, E.; Lanzotti, V.; Capasso, R.; Izzo, A.A. *J. Agric. Food Chem*., **2005**, *53*, 935-940.

216) Dong, M.; Feng, X.; Wang, B.; Wu, L.; Ikejima, T. *Tetrahedron*, **2001**, *57*, 3307-3330.

217) Higuchi, Y.; Kubota, T.; Kawasaki, T.; Pandey, V.B.; Singh, J.P.; Shah, A.H. *Phytochemistry*, **1984**, 23*,* 2597.

218) Ahmad, V.U.; Ghazala, U.S.; Ali, M.S. *Phytochemistry*, **1993**, *33*, 453.

219) Oulad-Ali, A.; Guillaume, D.; Belle, R.; David, B.; Anton, R. *Phytochemistry*, **1996**, *42*, 895-897.

220) Sang, S.; Lao, A.; Wang, H.; Chen, Z. *J. Nat. Prod*., **1999**, 62, 1028-1029.

221) Franson, R.; Patriarca, P.; Elsbach, P. *J. Lipid. Res*., **1974**, *15*, 380-388.

222) Payá, M.; Terencio, M. C.; Ferrándiz M. L.; Alcaraz, M. J.. *Br. J. Pharmacol*., **1996**, *117*, 1773-1779.

223) Misko, T. P.; Schilling, R. J.; Salvemini, D.; Moore, W. M.; Currie, M. G. *Anal. Biochem*., **1993**, *214*, 11-16.

224) Hoult, J. R.; Moroney, M. A.; Payá, M. *Methods Enzymol*., **1994**, *234*, 443-454.

225) Gross, S. S.; Levi, R. *J. Biol. Chem*., **1992**, *267*, 25722-25729.

226) Bradford M. M. *Anal. Biochem*., **1976**, *7*, 248-54.

227) Dunnet, C.W. *Biometrics*, **1964,** *20*, 482-491.

228) Mohamadi, F.; Richards, N. G.; Guida, W. C.; Liskamp, R.; Lipton, M.; Caufield, C.; Chang, G.; Hendrickson, T.; Still, W. C. *J. Comput. Chem.,* **1990**, *11*, 440-467.

Acknowledgements

Among all the people who have been around during my work with this thesis I would like to acknowledge:

Professor Franco Zollo, my tutor, for his exceptional generous support, academic guidance and advice;

Professors Maria Valeria D'auria and Angela Zampella, that with their knowledge and love for the chemistry, have always been pillars of support for all my research work;

Dr. Simona De Marino, I don't know what I would do without her help and encouragement;

Dr. Valentina Sepe and Raffaella Ummarino, for their time, patience and useful suggestions;

All the the members of laboratories "N22" and "N23", past and present.

For non-scientific reasons I would like to thank some people making my life more than just a quest for scientific answers:

My dad, Antonio, and mom, Clara, who motivate me to keep going with their love;

My brothers, Ettore and Federico, and Marina, for their support although the distance;

All my friends and my Naples coresidents, for their companionships and friendships;

And last but not least I am indebted to my boyfriend, Antonio, for him love, encouragement and patience throughout the entire process.

Above all, thanks to Lord Jesus Christ for his indescribable gifts.